Stochastic processes and disordered systems : around Brownian motion

Mathieu Delorme

THÈSE DE DOCTORAT

de l'Université de recherche Paris Sciences Lettres – PSL Research University

Préparée à l'École normale supérieure

Processus stochastiques et systèmes désordonnés

Autour du mouvement Brownien

Stochastic processes and disordered systems, around Brownian motion

École doctorale n°564
Physique en Île-de-France

Spécialité : Physique

Composition du Jury :

M. KRUG Joachim
University of Cologne
Rapporteur

M. KRAPIVSKY Paul
Boston University
Rapporteur

M. WIESE Kay
École normale supérieure
Directeur de thèse

M. TEXIER Christophe
Université Paris-Sud
Membre du Jury

M. SIRE Clément
Université Paul Sabatier
Président du Jury

M. MALLICK Kirone
CEA Saclay
Membre du Jury

Soutenue par Mathieu DELORME
le 02 novembre 2016

Dirigée par **Kay WIESE**
et **Pierre LE DOUSSAL**

ENS ÉCOLE NORMALE SUPÉRIEURE | PSL RESEARCH UNIVERSITY PARIS

Remerciements

Je tiens à remercier en tout premier lieu Kay Wiese, mon directeur de thèse, sans qui cette thèse n'aurait évidemment pas pu voir le jour. Je lui suis reconnaissant aussi bien pour m'avoir initié aux questions qui sont au cœur de cette thèse, que pour avoir su me motiver et m'enthousiasmer tout au long de ces trois années de travail. J'espère que je saurai conserver de lui cette persévérance face à un calcul difficile, cette rigueur dans la vérification et ce souci de clarté dans les explications. Cette thèse doit aussi beaucoup à Pierre Le Doussal pour sa co-direction, et avec qui j'aurai eu le plaisir de découvrir la renormalisation fonctionelle et les questions qui lui sont liées. Les collaborations avec Alberto Rosso et Tridib Sadhu ont aussi largement contribuées au contenu scientifique de cette thèse. L'école d'été de Beg Rohu, et le workshop du KITP de Santa-Barbara auquel j'ai pu participer, auront été des moments forts de ces années de thèse. Je tiens à remercier leurs organisateurs respectifs.

Je remercie aussi les thésards du Laboratoire de Physique Théorique dont j'ai eu le plaisir de croiser la route. Tout d'abord Alexander, qui aura été d'une aide très précieuse pour mes premiers pas dans le monde de la recherche, et plus particulièrement des systèmes désordonnés. Puis Thomas, Thimothée, Antoine, Antoine et Thibaud pour avoir toujours su maintenir une ambiance chaleureuse et motivante au sein de notre bureau. La qualité de vie au LPT doit aussi beaucoup à la bienveillance logistique et administrative de Viviane Sebille et Sandrine Patacchini.

Et enfin bien sûr, un grand merci à Joachim Krug et Paul Krapivksy d'avoir accepté de relire ma thèse, ainsi qu'à Kirone Mallick, Clément Sire et Christophe Texier qui me font l'honneur d'être dans le jury de cette soutenance.

Contents

Chapter 1
Introduction

1.1 Statistical physics and disordered systems

This thesis takes place in the large context of the study of disordered systems from a statistical physics point of view. The general idea of statistical physics is to use a probabilistic description of a system and its interaction with the environment, and study the properties which emerge at large scales (typically when the number of degrees of freedom becomes very large). The most interesting properties, at least from a theoretical point of view, are the ones that do not depend on the details of the probabilistic description, but only on some global settings: symmetries, spatial dimension, decreasing of correlations, existence of large moments for a distribution, etc. A well-known example of such an emerging large-scale property is formalized mathematically with the central limit theorem. It states that the average of a large number of random variables converges (after proper rescaling) to a Gaussian variable, as soon as the variables are independent (or at least weakly correlated), and distributed with the same distribution for which the second moment exists, i.e. large fluctuations are not too probable.

A physical system is usually defined with the specification of the possible configurations, the configuration space, and the energy of the system in each of these configurations, the energy landscape. When the system has a large number of degrees of freedom (for example if the system is a gas with many particles), it is usually not possible to determine its exact configuration, or to describe its exact dynamics, due to thermal fluctuations.

In such a situation, the statistical physics approach consists in defining macroscopic states of the system as probability distributions over the configuration space, which depend only on a few parameters (e.g. the temperature of the system). This means that when the system is in a given macroscopic state, we do not know its exact configuration (the positions and velocities of all particles in gas for example), only the probability for it to be in each configuration. This allows us to makes the link between the microscopic description of a system and the phenomenological laws of thermodynamics which govern its macroscopic properties. Ideas of statistical physics have also inspired other fields of science who deal with collective phenomenon, chaos, etc.

Standard statistical physics is a very successful theory, but not all systems can be described with a simple energy landscape. Disordered system, in the context of statistical physics, means that even the energy of each configuration is described by a probabilistic approach. For example, to study the transport of electrons in a metal, one needs to take into account that the energy of a given configuration for the electrons depends on the impurities and the defects of the metal lattice. These are hard to describe exactly, but can be modeled efficiently by a probabilistic approach, stating for example that the impurities are uniformly distributed in the sample. In

this case, the density of impurities remains the only parameter of the model, compared to all the spatial positions of the defects needed to define a deterministic energy landscape.

At non-zero temperature, the study of a disordered system involves two levels of randomness: the energy landscape (i.e. the energy level of each configuration) is itself a random object, and for each realisation of this landscape the state of the system is defined by a probability distribution, depending on this energy landscape. The random energy model (REM), developed by Derrida in [1], is a good toy model to understand the ideas of disordered systems.

At low temperatures, the equilibrium thermodynamics of a system is governed by configurations with the lowest energies, and by the energy barriers between them. In disordered systems, due to the randomness of the energy landscape, characterizing these low energy configurations is difficult. This generally leads to the existence of lots of metastable states, i.e. configurations with an energy level close to the minimal energy one (which is the equilibrium state at zero temperature), but far away in configuration space. Finding the statistical properties of the equilibrium state or the metastable states in a disordered system (which are random objects) are difficult questions, and can be viewed as a special case of extreme-value statistics, which will be defined later in this introduction.

It is important to note that sometimes, even if a deterministic description of a system is possible, it can be more interesting to try to understand it using a probabilistic approach, as the microscopic details of the energy landscape can be irrelevant to the properties studied. A probabilistic approach can lead to exact predictions with simpler derivations. It is also possible that a deterministic solution of a problem, with very strong dependence on initial conditions (or other parameters) has no practical use.

Ideas from statistical physics of disordered systems are now used in a wide range of contexts: combinatorial optimisation, neural networks, error-correcting codes, financial markets, protein-folding problems, and more.

1.2 Probability theory and stochastic processes

We now briefly introduce some concepts of probability which are used in this thesis. The main objects of probability theory are random variables. These are the mathematical formalisations of experiments with several possible outcomes, for which it is not possible to predict the result, but only give probabilities for the possible outcomes. Typical examples are the result of flipping a coin or rolling a dice. These are also historical examples, as probability theory started with the study of games of chance, and gambling.

If X designs a random variable, and A a subset of the possible outcomes, we will denote the probability that the event A happens as $\mathrm{Prob}(X \in A)$, which is a number between 0 and 1.

When X takes its values in $\mathbb{R}$ (for example, the temperature of the day with arbitrary precision), the probability of any event depending on X can be expressed in terms of the probability density function of X, which we denote $\mathcal{P}(x) := \partial_x \mathrm{Prob}(X < x)$. X is said to be a Gaussian variable with mean μ and variance σ^2 if it has the density

$$\mathcal{P}(x) = \frac{1}{\sigma\sqrt{2\pi}} e^{-\frac{(x-\mu)^2}{2\sigma^2}} \ . \tag{1.1}$$

In this thesis, we denote average quantities with respect to some random variable X using a bracket notation: $\langle f(X) \rangle$. In the case of a Gaussian variable as defined above, this gives for the first two moments

$$\langle X \rangle := \int_{-\infty}^{\infty} \mathrm{d}x \, x\mathcal{P}(x) = \mu \ , \ \langle (X-\mu)^2 \rangle := \int_{-\infty}^{\infty} \mathrm{d}x \, (x-\mu)^2 \mathcal{P}(x) = \sigma^2 \ . \tag{1.2}$$

For more details on the mathematical formalism of probability theory, and its various applications, we refer to the good introduction of W. Feller [2].

In physics, when the random variable is the microscopic configuration q of a thermodynamical system at temperature T, its law (i.e. the probability to be in each configuration which define the macroscopic state) is constructed from the Boltzmann weight $w_q = e^{-\frac{E(q)}{T}}$, where $E(q)$ is the energy of the configuration q (which can also be random in the case of a disordered system). To obtain a well-defined probability law, we need it to be normalised to one (if we sum over all the possible configurations). This naturally leads to the introduction of the partition function of the system

$$Z = \sum_q e^{-\frac{E(q)}{T}} \ , \tag{1.3}$$

such that the probability to be in configuration q is w_q/Z. While appearing here solely as a normalisation constant, the partition function is a powerful tool to compute various quantities on a thermodynamical system. For example, in this thesis we will be able to extract extreme value statistics using a formulation of the problem in terms of a partition function.

A particular class of random variables are stochastic (or random) processes. Formally, it is a collection of random variables, indexed by a unidimensional parameter, discrete or continuous, which we interpret as a time. The existence of this parameter allows us to have an object with more structure and look, for example, at a dynamical situation. The regularity (continuity, differentiability) of a stochastic process is a subtle question and in this thesis we use derivatives even if the mathematical definition of these are sometimes unclear.

There are various ways to define a random process; stochastic differential equations, Markov chain, random walk. These can be effective models for out-of-equilibrium situations, either transient or stationary, where a system evolves in contact with a random environment. It allows us to go beyond equilibrium statistical physics and study diffusion or transport phenomena, relaxation to the equilibrium and aging. As in the equilibrium case, the randomness of the microscopic dynamic can have different physical origins, and is usually only an effective description which try to capture the relevant ingredients of the true microscopic dynamics. For a more detailed discussion on the possibilities and the limitations of stochastic processes to model physical situations, we refer to the book of Van Kampen [3].

1.2.1 Random walks and Brownian motion

The simplest stochastic process one can construct is the symmetric random walk. It is defined with a discrete time and and represents a particle, or a walker, evolving on the (vertical) real axis. At each time step, the particle either goes up by one unit, or down by the same quantity, with equal probability. Furthermore the increments are independent (as given by successive coin toss). The value of a random walk, i.e. the position of the particle at discrete time n, denoted X_n, is constructed from a sequence of independent and identically distributed (i.i.d.) variables δX_1, δX_2, δX_3,... as

$$X_n = \sum_{k=1}^{n} \delta X_k, \quad \text{and} \quad X_0 = 0 \ . \tag{1.4}$$

For the standard random walk described above, the distribution of the X_k is defined by $\text{Prob}(\delta X_k = 1) = \text{Prob}(\delta X_k = -1) = 1/2$. Random walks have a lot of interesting properties, as we will see through this thesis. One is the possibility to construct a continuous process from it, defined as the scaling limit

$$B_t = \lim_{\delta t \to 0} \sqrt{2D\delta t} X_{\lfloor t/\delta t \rfloor} \ . \tag{1.5}$$

We denote $\lfloor x \rfloor$ the floor of x (the largest interger smaller than x). B_t is the well-known Brownian motion, or Wiener process, which we defined here with an arbitrary diffusive constant D. It was formalized by Einstein in [4] as an effective probabilistic description for the dynamics of a particle suspended in a gas or liquid, as observed by Brown in 1827. Physically, the movement of the particle is due to the large number of collisions with the molecules of its environment, and the diffusive constant D is then related to the molecular, discrete, nature of matter and the Avogadro number.

The existence of the scaling limit (1.5) , where time scales with δt while space scales with $\sqrt{\delta t}$, allowing us to define a continuous process is very similar to the central limit theorem mentioned above. The resulting process B_t is Gaussian and does not depend, apart from the diffusive constant D, on the distribution of δX_k, as long as the second moment $\langle \delta X_k^2 \rangle$ is finite. The covariance of a Brownian motion is given by

$$\langle X_t X_s \rangle = 2D \min(t, s) \ . \tag{1.6}$$

The limit (1.5) can also be viewed as a physical experiment where the resolution does not allow us to observe the microscopic dynamics (i.e. the discretness of the evolution). This means that large-time properties of random walks falling in the universality class of the Brownian motion (i.e. its increments are independent and have a finite second moment) can be studied using Brownian motion as an effective model. We will see in the next sections some of the strong properties of Brownian motion. These are useful both to use Brownian motion as a starting point to understand physical systems, but also to construct models which go beyond Brownian motion by relaxing some of the hypothesis used in its construction.

1.2.2 Markov processes

One of the interesting properties of Brownian motion, which is natural from its construction as a scaling limit of a random walk, cf. Eq. (1.5), is that it is a process without memory. More precisely, the evolution of the process after time t does not depend on how the process arrived to its current value X_t. This property is called Markov property, and any process with this property is called a Markov process.

In analogy with quantum mechanics, it is common to define the propagator $P(x_2, t_2|x_1, t_1)$ of a real valued random process, which is the probability density function for the process X_t to be at position x_2 at time t_2, knowing that the process was in x_1 at time t_1. In the case of a Markov process, this propagator is very important, as it allows us to construct any probability density of the process (and then, any observables on the process). If the process is starting from the origin, i.e. $X_{t=0} = 0$, this gives for $t_1 < t_2 < t_3$

$$\mathcal{P}(X_{t_1} = x_1, X_{t_2} = x_2, X_{t_3} = x_3) = P(x_3, t_3|x_2, t_2)P(x_2, t_2|x_1, t_1)P(x_1, t_1|0, 0) \ , \tag{1.7}$$

and the formula can obviously be generalized to an arbitrary number of points, and to processes with values in a larger-dimensional space, e.g. $X_t \in \mathbb{R}^d$. From this, it is clear that the knowledge of the starting point, or its distribution if it is random, and the propagator completely define a Markovian process.

The propagator of a Markov process also has the following property, sometimes referred as Chapman-Kolmogorov equation

$$P(x_2, t_2|x_1, t_1) = \int_{-\infty}^{\infty} \mathrm{d}x \, P(x_1, t_1|x, t)P(x, t|x_2, t_2) \quad \text{for any} \quad t \in (t_1, t_2) \ . \tag{1.8}$$

On top of these important properties, other tools commonly used in statistical physics are restricted to Markov processes. To cite a few, we have the master equation and the Fokker-Planck equation. This last one consists in writing the evolution of the probability density function for the position of the process as a deterministic partial differential equation. All this makes Markov processes suitable for exact analytic calculations, and explains why they are so commonly used in the physics (and other science) literature. The Markov property is also very useful when dealing with numerical simulations of a random process, as it allows one to store only the current value of the process. Monte-Carlo simulations are an important example of a numerical method based on the Markov property. For more details on the properties of Markov process, as well as a lot of their applications, we refer to [3] and [5].

While we have introduced the Markov property using Brownian motion as an example, it is important to note that the independence of the increments is not a necessary condition for a process to be Markovian (but it is sufficient). For example, an Ornstein–Uhlenbeck [6] process is a Markov process with correlated increments.

In physical situations, or in other fields where stochastic processes play an important role, one may encounter situations where the history dependence is primordial [7, 8, 9]. This means that constructing a model using a Markov process is not possible. Then, many of the standard methods, both to construct and study the model, fail, and results are usually derived case by case. In the first part of this thesis we consider an important class of non-Markovian processes: the fractional Brownian motion. This is the object of chapters 2 and 4.

1.2.3 The three Levy's arcsine laws

Another striking property of Brownian motion is the existence of the three *arcsine laws*. They state that for a Brownian motion B_t, with $0 < t < 1$ and $B_0 = 0$, three observables Y have the same cumulative distribution function (1.9), the *arcsine distribution*, equivalent to the probability density (1.10),

$$\text{Prob}(Y < y) = \frac{2}{\pi} \arcsin(\sqrt{y}) \tag{1.9}$$

$$\Leftrightarrow \quad \mathcal{P}(y) = \frac{1}{\pi\sqrt{y(1-y)}} \ . \tag{1.10}$$

The observables in question are (see Fig. 1.1)

1. First arcsine law: The time that the process B_t is positive, (red in Fig. 1.1),

$$t_+ := \int_0^1 \Theta(B_t)\, \mathrm{d}t \ . \tag{1.11}$$

2. Second arcsine law: The last time the process is at its initial position, (blue in Fig. 1.1),

$$t_{\text{last}} := \sup\{t \in [0,1], B_t = 0\} \ . \tag{1.12}$$

3. Third arcsine law: The time at which the process B_t achieves its maximum (which is almost surely unique), (green in Fig. 1.1)

$$t_{\max} := t, \text{ s.t. } B_t = \sup\{B_s, s \in [0,1]\} \ . \tag{1.13}$$

The historical derivation of these results is by P. Lévy [10]. While these laws are well-studied for Brownian motion, with many derivations and generalisations to constrained Brownian motion

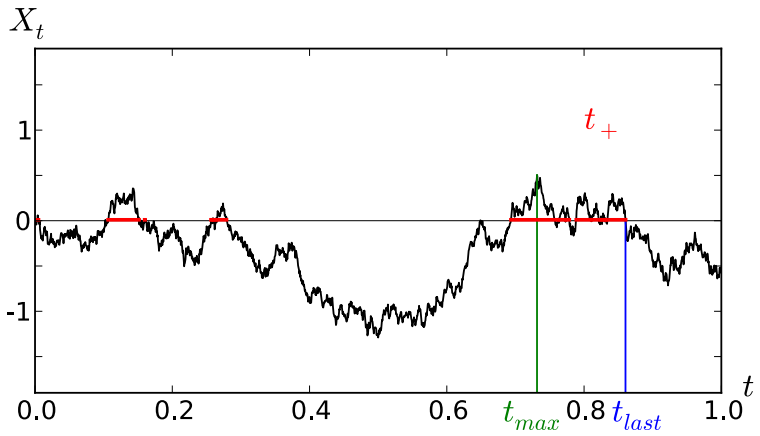

Figure 1.1: The three random variables following the arcsine distribution: $t_{\max}$, in green, is the time where the process achieves its maximum. t_{last}, in blue, is the last time the process is at its starting value $X_0 = 0$. Finally, t_+, in red, is the time spend in the positive half space, which is the sum of the red intervals.

(see for example [11]), little is known about their generalization to other random processes, especially in the non-Markovian case. The random acceleration process was investigated recently [12, 13]. Chapters 2 and 3 of this thesis give a new generalization of these laws to an important class of non-Markovian processes, namely fractional Brownian motions. These new results contain scaling properties (i.e. the asymptotic behavior of probabilities) which were already conjectured from the persistence exponent (defined in section 1.2.5) and non-trivial predictions in the bulk. This gives, in most cases, different distributions for Levy's observables which we were able to compare with great precision to numerical simulations.

1.2.4 Anomalous diffusion and self-similarity

As we have seen in the previous section, cf. 1.2.1, a large class of stochastic processes behave at large times like a standard Brownian motion, and as a consequence the second moment of the position of the particle grows linearly with time: $\langle X_t^2 \rangle \sim t$. This is the signature of a diffusion process.

This universality is due to the fact that Brownian motion is the only *continuous* process with *stationary*, *independent* and *Gaussian* increments. In physical situations, these properties of the increment are usually verified only on a large enough time scale, but this explains why this standard diffusion is very commonly seen in nature.

However, there are also interesting situations where experimental data show a non-linear growth of the second moment, $\langle X_t^2 \rangle \sim t^\alpha$, which is a phenomenon usually referred as anomalous diffusion. The case where $\alpha > 1$ is referred to as super-diffusion, while $\alpha < 1$ corresponds to sub-diffusion. To model such a situation, and obtain an anomalous diffusive process, at least one of the three fundamental hypotheses of Brownian motion has to be removed. This gives three main classes of anomalous diffusive process:

- heavy tails of the increments (Levy-flight process) or heavy tails in the waiting time between increments for continuous-time random walks (CTRW); these processes are *non-Gaussian*.

- time dependence of the diffusion constant, which means in the discrete settings that the

distribution of the increments is time dependent: the process has *non-stationary* increments.

- long-range correlations between increments: the process is *non-Markovian*.

These mathematical properties leading to anomalous diffusion can have various physical origins. CTRW is a good model for diffusion on a disordered substrate, where the particle may be trapped for long times in a specific site. Long-range correlations appear naturally when dealing with spatially extended systems and trying to write an effective dynamics of a single degree of freedom. For an extensive review on anomalous diffusion from a statistical physics point of view, we refer to [14]. Other studies on anomalous diffusion can be found in [15, 16, 17, 18].

Anomalous diffusion can be a consequence of a stronger property (but equivalent in the case of a Gaussian process): self-similarity with index H, an exponent that we will refer as the Hurst exponent, cf. 1.3. A stochastic process X_t is called H-self-similar if rescaling time by $\lambda > 0$ and space by λ^{-H} leaves the distribution of the process invariant:

$$\lambda^{-H} X_{\lambda t} \overset{\text{law}}{=} X_t \ . \tag{1.14}$$

This property is stronger than anomalous diffusion in the sense that the growth of every moment, and not only the second one, is governed by the same exponent H: $\langle X_t^n \rangle \sim t^{nH}$. The Brownian motion is self-similar of index $1/2$. For an introduction to self-similar processes, we refer to [19].

Self-similarity, also known as scale invariance, is an important notion of statistical physics which appears also in other contexts [20]. Self-similar geometric objects are the well known fractals [21, 22], and critical phenomena, or phase transitions, usually lead to a divergence of the typical length scale, leaving a large window of scale invariance for the system between its microscopic scale and its macroscopic one.

1.2.5 Extreme-value statistics and persistence

When dealing with random objects, the first and most natural questions to ask are related to averaged quantities or typical behavior. These questions are obviously an important step in understanding and comparing stochastic models to experiments or data, but there are also situations were the interest lies in the extremes or rare events. As we already mentioned in section 1.1, the physics of disordered systems at low temperatures is governed by the states with a (close to) minimal energy in the random energy landscape. In other contexts, extreme weather conditions are of large importance in the dimensioning of infrastructures such as dams and bridges. More generally, extreme-value questions appear naturally in many optimization problems.

The simplest and first case studied for these extreme-value statistics (EVS) was the distribution of the maximum of N independent and identically distributed (i.i.d.) random variables, which is now well understood in the large-N limit thanks to the classification of the Fisher-Tippett-Gnedenko theorem: Depending on the initial distribution of the variables, the rescaled maximum follows either a Weibull, Gumbel or Fréchet distribution. These results are reviewed in [23] within a mathematical approach. For a physical presentation of the extreme value statistics, its links with statistical physics of disordered system, and more specifically the replica-trick, we refer to [24]. Another physical interpretation of EVS in the context of depinnig of a particle in disorder, where the three limiting distributions are relevant, can be found in [25].

The case of strongly correlated variables is a natural extension to this problem, as many physically relevant situations present deviations from the i.i.d. case. Lots of results were derived

for random walks and Brownian motion [26], the free energy of a directed polymer on a tree [27], path length on trees [28] or hierarchically correlated variables [29]. The distribution of the largest eigenvalue is also a central question in random matrix theory [30, 31]. A very interesting case of a 1D Hamiltonian with disorder is studied in Ref. [32], where the transition between a strongly localised phase to a delocalised one corresponds in the EVS language to "breaking of the Gumble universality class": In the localised phase, the eigenvalues of the Hamiltonian are independent while the delocalisation induces level correlations, leading to a new result for the ordered statistics of correlated variables, obtained explicitly in Ref. [33].

As we will see in more details in section 1.3.5, Pickands and later Piterbarg were able to derive interesting results for the extreme-value distribution of generic Gaussian processes, leading to the introduction of the universal Pickands constants. This will be introduced in more details in section 1.3.5.

Extreme-values statistics is also closely linked to other interesting observables one can define on a stochastic process. A natural quantity one can investigate is the distribution of the time it takes to reach a certain level, known as the hitting time. If for simplicity we choose this level to be 0, the probability that a continuous process X_t did not reach 0 up to time T (i.e. the hitting time is larger than T) is called the survival probability, usually defined with a fixed starting point $x > 0$:

$$S(T, x) = \text{Prob}(X_t > 0 \ , \ \forall t \in [0, T] \, | X_0 = x) \ . \tag{1.15}$$

The asymptotic properties of this object have motivated lots of work. In many cases of interest the large-T behavior of the survival probability has an algebraic decay, independent of x and with an exponent θ, called the persistence exponent

$$S(T, x) \underset{T \to \infty}{\sim} T^{-\theta} \ . \tag{1.16}$$

This exponent is non trivial and difficult to compute in many situations, even for a simple diffusion with random initial conditions [34]. An extensive review of these questions, in the context of statistical physics, can be found in [35]. For a mathematical approach of some other recent developments, we refer to [36]. All these objects are notably difficult to investigate in the case of non Markovian processes. Some other studies in this case can be found in Ref. [37, 38, 39, 12].

To make the link with the previous section, it is useful to note that if $X(t)$ is a self-similar process of index H, one can construct a stationary process $\tilde{X}(s)$ by defining

$$\tilde{X}(s) := e^{-Hs} X(e^s) \ . \tag{1.17}$$

This duality is at the basis of several studies of the persistence exponent, where the algebraic decay of the survival probability of the self-similar process is transformed to an exponential decay in the stationary process. This is used in [40, 41, 34, 42, 43, 44, 45].

For example, if we apply the transformation (1.17) to the standard Brownian motion B_t, we obtain a Gaussian process $\tilde{B}(s)$ with correlator

$$\left\langle \tilde{B}(s_1) \tilde{B}(s_2) \right\rangle = \exp\left(-\frac{1}{2} |s_1 - s_2| \right) \ , \tag{1.18}$$

which is nothing but an Ornstein–Uhlenbeck process [6].

Another natural extension of the extreme-values statistic is to look at extreme values not defined relative to a fixed threshold, but relative to the previous extremes of the process. This leads to the statistics of records, with many new interesting questions. The notion of records has taken a large importance in the last decades, and it is quite common to see sports performance or climate change to cite a few, analyzed in terms of records. Some recent studies on this topic can be found in [46, 47, 48, 49, 50].

1.3 Fractional Brownian motion (fBm)

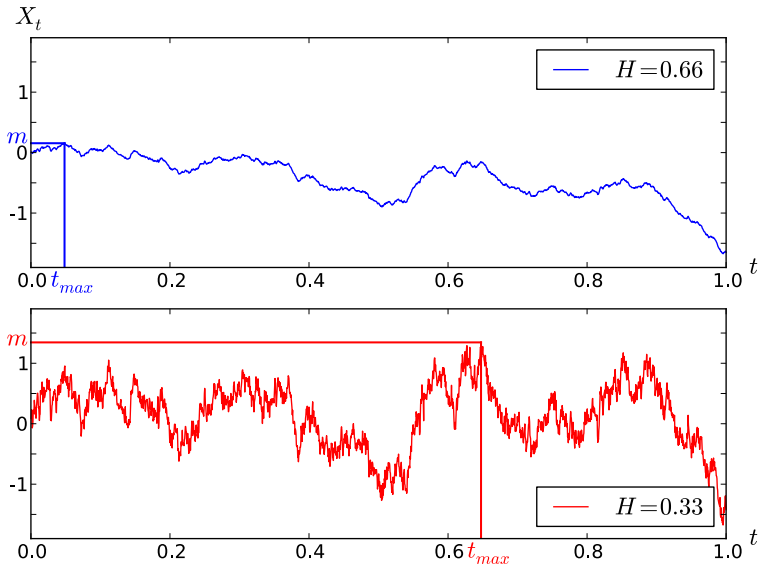

Figure 1.2: Two realisations of fBm paths for different values of H, generated using the same random numbers for the Fourier modes in the Davis and Harte procedure [51]. Some of the observables studied in this thesis, the maximum value m and the time when it is reached $t_{\max}$, are represented.

1.3.1 Definition and properties

Fractional Brownian motion is a generalization of standard Brownian motion, introduced previously in section 1.2.1. It has two of the main properties of standard Brownian motion, namely, it is a Gaussian process X_t and its increments are stationary, i.e. the distribution of $X_t - X_s$ depends only on the time difference $t - s$. However, relaxing the condition of independence of the increments (so the process can be non-Markovian) allows the process to be self-similar of arbitrary index H (between 0 and 1), contrary to the fixed value of 1/2 for the standard Brownian case. Following the historical introduction of Mandelbrot and Van Ness in [52], the self-similarity index H of a fBm is called the Hurst exponent.

As a Gaussian process, a fBm X_t is defined via its mean $\langle X_t \rangle = 0$ and covariance function (or 2-point correlation function)

$$\langle X_t X_s \rangle = |s|^{2H} + |t|^{2H} - |t-s|^{2H} \ . \tag{1.19}$$

This constraints the process X_t to start at 0, $X_0 = 0$, but we can also consider a fBm Y_t starting at a non-zero value $y = Y_0$, simply defined as $Y_t = X_t + y$, with X_t as above. As we said, the case $H = 1/2$ correspond to standard Brownian motion; there the covariance function (1.19) reduces to $\langle X_t X_s \rangle = 2\min(s,t)$ and it is the only value of H where the process is Markovian. The correlations of the increments are given by

$$\langle \partial_t X_t \, \partial_s X_s \rangle = 2H(2H-1)|t-s|^{2(H-1)}. \tag{1.20}$$

For $H > 1/2$ they are positively correlated, whereas for $H < 1/2$ they are anti-correlated. As we can see in Fig. 1.2, this makes the paths of a fBm with H small very rough, while for large

H, the paths are more smooth. Mathematically this is formalized via Hölder continuity: the fBm paths X_t are almost surely Hölder-continuous of any order less than H.

The stationarity of the increments can be checked from the covariance (1.19) by computing the second moment

$$\langle (X_t - X_s)^2 \rangle = 2|t-s|^{2H} \ , \tag{1.21}$$

and as $X_t - X_s$ is a centered Gaussian variable, it proves that its full distribution depends only on $|t-s|$.

In order for the process X_t to be well-defined, its covariance function (1.19) has to be a continuous and positive-definite function. This constraints the possible values of H, namely $0 < H \leq 1$. To see this, we can look at the covariance matrix of the process taken at time $t_1 = 1$ and $t_2 = 2$:

$$\left(\langle X_i X_j \rangle\right)_{ij} = \begin{pmatrix} 2 & 2^{2H} \\ 2^{2H} & 2^{2H+1} \end{pmatrix} \tag{1.22}$$

The diagonal terms are always positive, while the determinant $2^{2H+2} - 2^{4H}$ is negative if $H > 1$. This implies that one of its eigenvalues is negative. This is not possible for a Gaussian covariance matrix.

The limiting case $H = 1$ is a linear process with a single degree of freedom, its Gaussian random slope X: $X_t = Xt$. In the other limit, when $H \to 0$, the correlations become logarithmic, and there is no unique definition of a limiting process corresponding to $H = 0$. Log-correlated Gaussian fields are an active topic of research, both in the mathematics and physics community. Recent work can be found in Refs. [53, 54].

The study of the extreme-value statistics for fractional Brownian processes started with Sinai [55], and led few years later to the derivation of the persistence exponent (1.16) for the fBm by Molchan [56] : $\theta = 1 - H$, a very non trivial result cited by Nourdin in [57] as one of the most beautiful results about fBm. In the physical literature, this result was guessed a few years earlier using heuristical arguments by Krug et al [40, 58]. Note that this topic is not closed, as the error terms, i.e. bounds on the subleading corrections in the rigorous proofs of Eq. (1.16) for the fBm seems still far from optimal. Aurzada gave a recent improvement in this direction [59], as well as an extension to moving boundaries in [60]. In this thesis, chapter 2, various observables related to extreme-value statistics for fBm are considered, and their distributions are computed with a perturbative approach around standard Brownian motion. This allows us to check some scaling behavior involving the persistence θ and go beyond.

And finally, we note that even if it will not be used in this thesis, the links between fBm and stochastic integration is an active topics in the mathematical community. It is for example possible to define fBm as the integration of a deterministic kernel with respect to a standard Brownian motion. Stochastic equations defined with a fractional Brownian noise (the formal derivative of a fBm) are also interesting for various reasons, and difficult from a theoretical point of view, due to the lack of the Martingale property. All these directions of studies are well presented in the book of Nourdin [57].

1.3.2 History and applications

The history of fractional Brownian motion started with a study by Kolmogorov [61], even if the model was not clearly defined. Then, Hurst showed while studying the Nil river, as well as other hydrological systems, that long range dependence is a key factor to understand statistics of certain time series, notably via the introduction of the rescaled range observable [62]. This led Mandelbrot and Van Ness to name after him the parameter of their model of self-invariant

Gaussian process with stationary increments, the fractional Brownian motion, defined in its final form in [52].

Interestingly, several processes commonly used in physics, mathematics, and computer science belong to the fBm class. For example, it was recently proven that the dynamics of a tagged particle in single-file diffussion, cf. [63, 64, 65], has at large times the fBm covariance function (1.19) with Hurst exponent $H = 1/4$. Experimental realisations of single-file diffusion can be found in [66, 67].

Anomalous diffusion, already discussed in section 1.2.4, is another interesting property of fractional Brownian motion. The fact that the index of self-similarity H of a fBm is a free parameter allows us to model situations where the second moment grows non-linearly with time: $\langle X_t^2 \rangle = 2t^{2H}$, both for super diffusion and sub-diffusion.

Other applications of fBm can be found: diffusion of a marked monomer inside a polymer [17, 68, 69, 70], polymer translocation through a pore [17, 71, 72, 73], finance (fractional Black-Scholes, fractional stochastic volatility models, and their limitations) [74, 75, 76], telecommunication and network [77], granular materials [78], in top of the historical application to hydrology [79, 80].

Let us now discuss how extended Markovian systems lead to a non-Markovian dynamics when a single degree of freedom is considered. As a simple example we consider the Edwards-Wilkison dynamics for an interface (or a polymer) parametrized by a function h of x, which evolves with time according to the dynmaics

$$\partial_t h(x,t) = \Delta_x h(x,t) + \xi(x,t) \ . \tag{1.23}$$

This is a first-order differential equation with respect to time. The random noise ξ is uncorrelated in the t direction and Gaussian. This implies that the evolution of the whole system is Markovian.

If we now choose a specific point x_0, and look at the evolution of $h_{x_0}(t) = h(x_0,t)$, the Markovian nature is lost. This can be derived by first looking at (1.23) in Fourier domain:

$$(\partial_t + q^2)\hat{h}(q,t) = \hat{\xi}(q,t) \ . \tag{1.24}$$

where the noise has now correlations $\langle \hat{\xi}(q,t)\hat{\xi}(q',t') \rangle = 2\pi\delta(q+q')\delta(t-t')$, assuming that the initial noise $\xi(x,t)$ is uncorrelated in both x and t directions, and that space is unidimensional. For each values of q, the equation (1.24) now reduces to the evolution equation of an Ornstein-Uhlenbeck process [6] and allows us to express the correlations of the solutions in Fourier variables, assuming we start with flat initial conditions $h(x, t=0) = 0$, and $t_1 < t_2$:

$$\langle \hat{h}(q_1,t_1)\hat{h}(q_2,t_2) \rangle = \frac{1 - e^{-2q_1^2 t_1}}{2q_1^2} e^{-q_2^2(t_2-t_1)} (2\pi)\delta(q_1+q_2) \ . \tag{1.25}$$

This expression is not symmetric with respect to $q_1 \leftrightarrow q_2$ because of the time ordering ($t_1 < t_2$). After two inverse Fourier transformations, which reduce to a simple integration over q, we can obtain the correlations of the process at a point x_0:

$$\begin{aligned} \langle h_{x_0}(t_1) h_{x_0}(t_2) \rangle &= \frac{1}{2\pi} \int_q \frac{1 - e^{-2q^2 \min(t_1,t_2)}}{2q^2} e^{-q^2|t_2-t_1|} \\ &= \frac{1}{2\sqrt{\pi}} \left(\sqrt{t_1+t_2} - \sqrt{|t_1-t_2|} \right) \ . \end{aligned} \tag{1.26}$$

We see here the appearance of a non-trivial diffusion exponent : $\langle h_{x_0}(t)^2 \rangle \sim t^{1/2}$. But this process is not self-affine due to the initial conditions. However, if we look at the large-time behavior of

this process, the correlation function of its increments becomes exactly the correlation function of a fBm, Eq. (1.19), with Hurst exponent $H = \frac{1}{4}$, as shown in [40]. This can be interpreted as follows for a very large polymer (with $L^2 >> t$, where L is the number of monomer): At large times, the polymer is in an equilibrium thermal state, and has forgotten its initial condition. Thus if we start with a polymer in thermal equilibrium, each of its monomers will perform a fBm with Hurst exponent 1/4.

Depending on the space dimension, the elasticity kernel (the Laplacian term in Eq. (1.23)), and the spatial correlations of the noise, fBm with other values of the Hurst exponent can emerge from this simple dynamic [40, 70]. The emergence of non-Markovian random processes and in particular of a fBm process is an important motivation for this thesis.

1.3.3 Numerical simulations

The absence of Markov property makes simulations of fractional Brownian motion less straightforward that for a standard Brownian motion. Various methods have been developed depending on the objective: exact or approximated, with a fixed total length or not, etc. For a good presentations of these, and a lot of details, we refer to [51] and [81].

In this thesis, we test most of our analytical results on fBm with numerical simulations. The nature of observables we investigate gives a fixed length to the paths we need to generate (cf. the three arcsine laws). In this situation, the Davis and Harte algorithm is the most suited, as it is exact (cf. section 2.I) and fast, path with N discrete points are generated in a time of order $N \ln(N)$.

1.3.4 Fractional Brownian bridges

When studying random processes X_t in a time interval $[0, T]$, quite generally the initial value X_0 is known, and the endpoint X_T is itself a random variable determined by the random process. On the other hand, there are also cases when one knows the endpoint X_T. These processes are referred to as *bridges*. Fractional Brownian motion bridges, with an endpoint chosen as $X_1 = 0$, are presented on Fig. 1.3 for different values of H.

Bridges are useful building blocks in constructing more complicated observables; we will see an application of this idea when looking at the positive time of a process, cf. section 3.2. They are also commonly used in constructing refinements of random walks, e.g. for financial modeling [82]. Finally, they appear as the difference from the asymptotic limit in the construction of the empirical distribution function [83].

For a Brownian motion bridge ($H = 0.5$) terminating at its starting point after time T,i.e. $X_0 = X_T = 0$ both $t_{\max}$ and t_+ corresponding to the observables of the first and third arcsine laws and defined in section 1.2.3, have a uniform distribution [10]

$$\mathcal{P}^{\text{bridge}}_{H=1/2}(t_{\max}) = \mathcal{P}^{\text{bridge}}_{H=1/2}(t_+) = \frac{1}{T} \ . \tag{1.27}$$

This is in contrast to the case of a Brownian motion with a free endpoint corresponding to the Arcsine law given in (1.10):

$$\mathcal{P}^{\text{free}}_{H=1/2}(t = t_{\max}) = \mathcal{P}^{\text{free}}_{H=1/2}(t = t_+) = \frac{1}{\pi\sqrt{t(T-t)}} \ . \tag{1.28}$$

These two results, as well as a way to interpolate between them can be found in Ref. [11]. For the maximum value m, on the interval $[0, T]$, the probability distributions of the bridge case

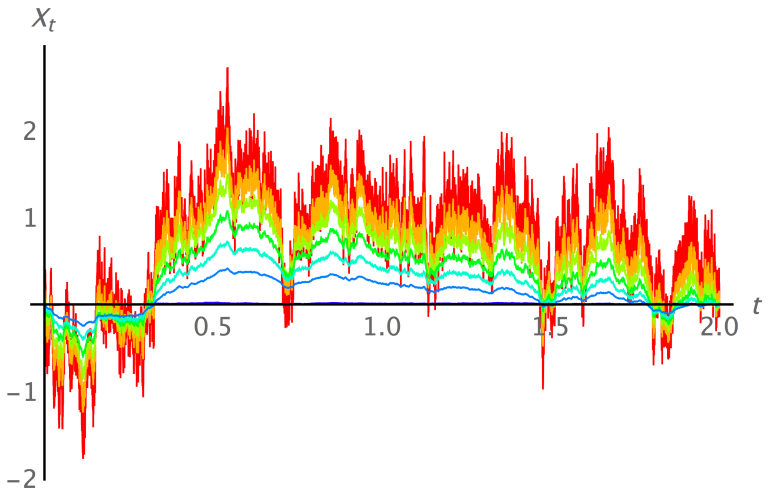

Figure 1.3: Examples of fBm bridges for different values of H, generated from the same random numbers using the Davis and Harte procedure [51]. $H = 0.25$ in red (outmost curves) to $H = 0.875$ in blue (innermost), with increments of 1/8.

also differ from the free case:

$$\mathcal{P}^{\text{bridge}}_{H=1/2}(m) = \frac{2m}{T} e^{-\frac{m^2}{T}} \Theta(m) \ , \tag{1.29}$$

$$\mathcal{P}^{\text{free}}_{H=1/2}(m) = \frac{e^{-\frac{m^2}{4T}}}{\sqrt{\pi T}} \Theta(m) \ . \tag{1.30}$$

In chapter 4, we extend these results to the case of a fBm, giving the expression of the distribution of t_+, $t_{\max}$ and m in an expansion in $\varepsilon = H - \frac{1}{2}$.

1.3.5 Pickands constants

The properties, and particularly the asymptotics, of the distribution of the maximum of Gaussian processes has been well studied in the mathematical and physical literature [84, 43, 44]. For X_t a stationary centered Gaussian process, whose covariance function verifies, for some $\alpha > 0$ and $C > 0$, the short time asymptotic

$$r(t) = \langle X_s X_{t+s} \rangle = 1 - C|t|^\alpha + o(|t|^\alpha) \ , \tag{1.31}$$

Pickands proved in [85] the following asymptotic:

$$\text{Prob}\left(\max_{t\in[0,T]} X_t > u \right) \simeq C^{\frac{1}{\alpha}} \mathcal{H}_\alpha T u^{\frac{2}{\alpha}} \frac{e^{-u^2}}{\sqrt{2\pi} u} \quad \text{when} \quad u \to \infty \ . \tag{1.32}$$

This asymptotic probability is proportional to T, as the events corresponding to large value of the maximum are localized in time, and can appear anywhere in the interval $[0, T]$. The constant C can be absorbed via a rescaling of time. This yields several non-trivial predictions: first the dominant term in this asymptotic is Gaussian, which is quite intuitive and follows the Borell lemma [86]. But this also predicts the power law prefactor $u^{2/\alpha}$ and its universal amplitude, which is now known as the Pickands constants $\mathcal{H}_\alpha$. It is important to note that these constants depend only on α, and not on the precise nature of the process X_t, which gives this results a

strong universality. In his seminal paper, Pickands gives the expression of these constants in term of a fBm X_t of Hurst exponent $H = \alpha/2$:

$$\begin{aligned}\mathcal{H}_\alpha &= \lim_{T\to\infty} \frac{1}{T} \int_0^\infty \mathrm{d}m\, e^m \,\mathrm{Prob}\left(\max_{t\in[0,T]} \chi_t > m\right) \\ &= \lim_{T\to\infty} \frac{1}{T} \left\langle e^{\max_{t\in[0,T]} \chi_t} \right\rangle \qquad \text{with} \quad \chi_t := X_t - |t|^\alpha \ . \end{aligned} \tag{1.33}$$

This result has been extended by Piterbarg in 1978, where he relaxed the stationarity condition to arrive at an even more universal statement. The hypothesis are now the following: X_t is a continuous Gaussian process defined for $t \in [0, T]$, with a unique time $t_0 \in (0, T)$ of maximal variance, which we normalise to one for simplicity:

$$\langle X_t^2 \rangle < 1 \quad \forall t \neq t_0 \quad \text{and} \quad \langle X_{t_0}^2 \rangle = 1 \ . \tag{1.34}$$

We suppose that close to t_0, the squared variance verifies

$$\langle X_t^2 \rangle = 1 - a|t - t_0|^\beta + o\left(|t - t_0|^\beta\right) \quad \text{when} \quad t \to t_0, \tag{1.35}$$

and the covariance

$$\langle X_t X_s \rangle = 1 - |t - s|^\alpha + o\left(|t - s|^\alpha\right) \quad \text{when} \quad s, t \to t_0 \ , \tag{1.36}$$

which defines two exponents $\alpha > 0$ and $\beta > 0$ and a constant $a > 0$. In this situation, and contrary to the stationary case, the large values of the maximum are always reached close to t_0, which naturally remove the dependence on T in the asymptotics. If $\alpha > \beta$, which means that the concentration of the variance is stronger than the decay of the correlations, it reduces to the same asymptotic as a single Gaussian variable, namely

$$\mathrm{Prob}\left(\max_{t\in[0,T]} X_t > u\right) \simeq \frac{e^{-\frac{u^2}{2}}}{\sqrt{2\pi}u} \quad \text{when} \quad u \to \infty \ . \tag{1.37}$$

The most interesting case corresponds to $\beta > \alpha$, when both the correlations and the variance matter, and we have the following asymptotic, cf. [84],

$$\mathrm{Prob}\left(\max_{t\in[0,T]} X_t > u\right) \simeq \frac{2\mathcal{H}_\alpha \Gamma(\frac{1}{\beta})}{\beta a^{1/\beta}} u^{\frac{2}{\alpha}-\frac{2}{\beta}} \frac{e^{-\frac{u^2}{2}}}{\sqrt{2\pi}u} \quad \text{when} \quad u \to \infty \ . \tag{1.38}$$

The Pickands constants (1.33) appear again, which makes it a central quantity in the study of Gaussian processes. For the derivation of these results, (1.32), (1.37) and (1.38), and some other important concepts in the study of Gaussian process, and particularly their extremes, we refer to [84]. In a more physical context, the Pickands constants and the related theorem presented here were used in the study of fluctuating interfaces in [87]. More recent developments on this topic can be found in [88, 89, 90, 91]

The question of how to compute the Pickands constants remains. Despite its importance in the previously mentioned theorem, and up to now, only two of the values of $\mathcal{H}_\alpha$ are known analytically:

$$\mathcal{H}_1 = 1 \qquad \text{and} \qquad \mathcal{H}_2 = \frac{1}{\sqrt{\pi}} \ . \tag{1.39}$$

The first value, when $\alpha = 1$, can be computed because the fBm of Hurst exponent $H = \alpha/2 = 1/2$ reduces to a standard Brownian motion. The second value corresponds to the case where the

fBm is simply an affine process, i.e. a straight line of random slope. For other values of α the question is still open, and only some bounds exist [92].

This give numerical simulations a particular importance in the study of Pickands constants. However, straightforward simulation, using the original definition of Eq. (1.33), is quite unstable as the convergence to the large-T limit is slow ($T^{-1/2}$ in the case $\alpha = 1$) and the variance of the observable $e^{\max z_t}$ is large [93]. Recently, Dieker and Yakir [94] gave a new representation for Pickands constants, more suitable to numerical simulations, especially for $\alpha \geq 1$. The results obtained in their article seem to be the best estimation up to date for Pickands constant. The new expression of Pickands constant they built and used is

$$\mathcal{H}_\alpha = \left\langle \frac{e^{\max_{t\in\mathbb{R}} \chi_t}}{\int_{-\infty}^{\infty} \mathrm{d}t e^{\chi_t}} \right\rangle \ , \tag{1.40}$$

with the same process χ_t as defined in Eq. (1.33).

In chapter 5 we will extand our study of fractional Brownian motion to introduce drift. This allows us to study observables related to the process z_t and we will be able to expend the value of Pickands constant arround its known value at $\alpha = 1$, leading to a new exact result for the Pickands constants with α close to 1:

$$\mathcal{H}_\alpha = 1 - \gamma_E(1-\alpha) + O(1-\alpha)^2 \ . \tag{1.41}$$

1.4 Elastic interfaces in disordered media

1.4.1 Generical ideas

Elastic interfaces are a simple model of disordered systems where the system studied is an interface, i.e. a line or a surface in usual experimental situations, which have some form of elastic energy and thus tend to remain flat. In order to treat this with a simple mathematical formulation, we assume that the interface can be described as a function, usually called displacement or position, $u(x)$ with $x \in \mathbb{R}^d$. d is the internal dimension of the interface: $d = 1$ for a line, $d = 2$ for a surface, etc. This description excludes overhangs and dislocations from the discussion. To simplify notation, we will also write variables as indices: $u_x := u(x)$.

If we consider the equilibrium situation, the energy of the system can be written as the sum of two terms:

$$E[u_x] = \frac{c}{2}\int_x (\nabla_x u_x)^2 + \int_x V(u_x, x) \ . \tag{1.42}$$

The first one expresses the elastic energy (in the case of standard short-ranged elasticity) which is locally proportional to the curvature of the surface, and c is the elastic constant. The second term models the interaction of the interface with a quenched (i.e. which does not change with time) disordered environment. This is a random field, the extension of random processes when the parameter is a multidimensional variable, depending both on the internal variable x and the position of the interface u_x at this point. For simplicity, we assume that this random field is Gaussian and has two-point correlation function of the form

$$\langle V(u,x)V(u',x')\rangle = R(u-u')\delta^d(x-x') \ . \tag{1.43}$$

Considering uncorrelated disorder in the x direction is natural when we look at situation where the interface is rough, i.e.

$$\left\langle (u_x - u_y)^2 \right\rangle \sim |x-y|^{2\zeta} \ , \tag{1.44}$$

with $\zeta < 1$, such that the elasticity dominates over disorder at small scale.

For the model to be well defined, it is usual to add a confining term to the energy of the interface, for example in the form of a quadratic potential $\frac{m^2}{2}(u_x - w)^2$, such that the position of the interface remains bounded, as in any realistic situation. The curvature of the potential is m and w is its center.

Understanding the zero temperature behavior of this model is linked to the research of the minimal energy $E_{\text{tot}} = E[u_x] + \frac{m^2}{2}(u_x - w)^2$, as a function of w, over all the possible configurations $x \mapsto u_x$ of the interface. This is a good example of extreme-value statistics problems appearing in the statistical physics of disordered system. This also has an interesting mapping to Burgers equation with random initial conditions [41].

It is possible to consider an overdamped dynamics (out of equilibrium) for the same model (i.e. the inertia of the interface is negligible) at zero temperature, with some friction coefficient η. The displacement of the interface is now a function of the time t and space x, and denoted u_{xt}. Its evolution can be modeled with a stochastic differential equation, which writes

$$\eta \partial_t u_{xt} = c\nabla_x^2 u_{xt} + F(u_{xt}, x) + m^2(w_t - u_{xt}) \ . \tag{1.45}$$

The random force is related to the random potential of the static model by $F(u, x) = \partial_u V(u, x)$, but it is also possible to consider a dynamics which does not have a static equivalent (when the force is non-potential). It is then useful to introduce the force force correlator Δ

$$\big\langle F(u, x)F(u', x')\big\rangle = \Delta(u - u')\delta^d(x - x') \ . \tag{1.46}$$

The last term of Eq. (1.45) is the confining potential already introduced in the static case, and acts as a driving for the interface if its center w_t is time dependent. To model a non-zero temperature dynamics, we simply need to add a white noise (both in t and x) to Eq. (1.45), but this case will not be considered in this thesis, and its analytical treatment is very hard.

As we will see, this simple model of elastic interfaces exhibits a lot of complex features due to the competition between elasticity (which tends to flatten the interface) and the disorder (which tends to make it rough). In the dynamical situation and for generic disorder, the motion consists in avalanches, i.e. bursts of movement localized in time, between which the interface is pinned, i.e. blocked by the disorder. We refer to [95] for a more detailed introduction on elastic interfaces in disordered media.

1.4.2 Some applications and experimental realisations

Consider a 2D Ising box, with an external field imposed on two opposite boundaries represented on figure 1.4. As in a typical metallic sample, the lattice contains impurities: some missing spins (denoted by a circle) and some random-field disorder for some other vertex, i.e. vertex where the sign of the spin is imposed by an external field (denoted by a bold sign on the figure). The boundary conditions (with a different sign on each side) generate typical configurations where the spins are separated into two domains. The interface between these two domains, represented by a dotted line on the figure, is a good example of an elastic object as the interaction between spins gives an energy proportional to the surface. In the continuous limit, such a magnetic sample is then well analyzed with the model presented in the previous section, where the random potential V represents the impurities of the metalic lattice. And varying the strength of the external field is equivalent to a driving of the interface.

The crackling electromagnetic signal emitted when slowly magnetizing a ferromagnet, corresponding to the growth of one of the magnetic domain into the other and observed by H.

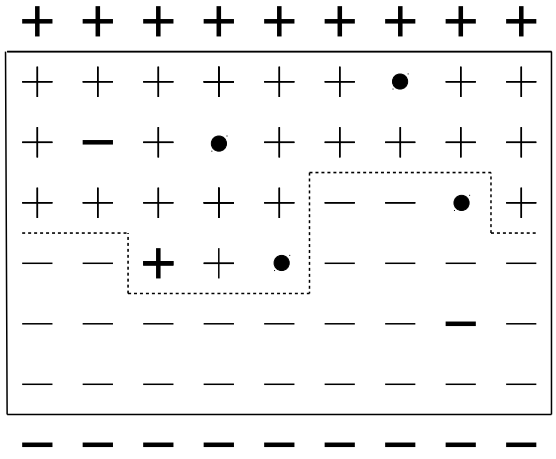

Figure 1.4: A 2D Ising box, with a domain wall (dashed line) in the presence of disorder (bold signs for random-field disorder and dots for missing spin) and opposite boundary conditions at the top and bottom of the box.

Barkhausen in 1919 [96], can then be understood as the avalanches of an interface under quasi-static driving. For more recent experiments related to magnetic domain walls and their dynamics we cite [97, 98], and [99] is a good review of the concepts involved.

Other examples of systems described using the model of an elastic interface slowly driven in a random medium are: fluid contact lines [100], crack fronts in fracture [101, 102], strike-slip faults in geophysics [103], fronts of chemical reaction in porous media, and many more [104, 105]. Note that some of these experimental setups present interfaces with long-range elasticity, which requires to change the Laplacian term in (1.45) to an non-local operator.

The model of elastic interfaces in random media, which allows us to investigate systems developing rough surfaces and avalanche dynamics, is then important both conceptually and in applications.

1.4.3 Functional renormalisation

The full model (1.45) of an interface of internal dimension d in presence of realistic short-ranged disorder, i.e. $\Delta(u)$ in Eq. (1.46) decays to 0 for large u, is difficult to treat analytically and requires methods such as the Functional Renormalization Group (FRG) [106, 107, 108]. The idea is first to define the effective disorder correlator,

$$\Delta_{\text{eff}}(w_1 - w_2) = \langle F(u_x(w_1), x) F(u_x(w_2), x) \rangle \ , \tag{1.47}$$

where $u_x(w)$ is the equilibrium configuration in the static case, or the left-most metastable configuration in the dynamic case, given that the confining potential is centered in w. The FRG follows its flow as the curvature of the confining potential m is sent to 0, in order to study the large scale properties of the model. The limit of $m \to 0$ allows the interface to explore larger and larger portions of the disorder to find its most favorable position (i.e. the lowest energy configuration in the equilibrium case).

When the dimension d of the interface is larger than a critical value, $d > d_{\text{uc}}$, this effective disorder correlator flows to zero, i.e. the disorder becomes irrelevant and the interface is flat at large scales. Note that $d_{\text{uc}} = 4$ for short-ranged elasticity and $d_{\text{uc}} = 2$ for long-ranged elasticity.

Using standard ideas of renormalisation theory, it is possible to compute the effective disorder correlator at large scale for $d \leq d_{\rm uc}$ in a perturbative expansion in $\epsilon = d_{\rm uc} - d$. One of the key features of this effective disorder correlator (both for the statics and the dynamics) is the existence of a cusp at $u = 0$, i.e. $\Delta'_{\rm eff}(0^+) \neq 0$ even if the microscopic disorder is smooth [108]. This is important both for the theoretical treatment of the model (as it gives a non analytical field theory) and for its physical interpretation, as this cusp is directly related to the existence of metastable states and avalanches.

Once the effective disorder correlator is known, several observables can be investigated. For details on the functional renormalisation formalism and some of its recent applications, we refer to [109, 110, 111, 112, 113, 114].

1.4.4 The mean field model and the Brownian force model

A simpler version of the model presented in Eq. (1.45) is the so-called Brownian force model (BFM) introduced in [112, 115, 116, 117]. The BFM is defined with the dynamical equation (1.45) by choosing the disordered forces $F(u, x)$ as independent (in the x direction) Brownian motions, i.e.

$$\langle F(u,x)F(u',x')\rangle = 2\min(u,u')\delta^d(x-x') \tag{1.48}$$

This model is not stationary in the u direction (as the correlator is not a function of $u - u'$), contrary to what we expect from a realistic model, but it is very interesting in several respects: first it is exactly solvable, and several avalanche observables have been calculated, as discussed in chapter 6 or in [95]. Second, it was shown recently [115, 117] to be the appropriate mean-field theory (i.e. $d \geq d_{\rm uc}$) for the space-time statistics of the velocity field $\dot{u}_{xt}$ (i.e. the derivative with respect to time t of the displacement field u_{xt}) in a single avalanche for d-dimensional interfaces close to the depinning transition as it reproduces the main feature of the effective disorder of a realistic model: its cusp, cf. previous section.

Remarkably, when considering the dynamics of the center of mass of the interface, it reproduces the results of the simpler ABBM model (in reference to its authors Alessandro, Beatrice, Bertotti and Montorsi), a toy model for a single degree of freedom (a particle), introduced long ago on a phenomenological basis to describe the Barkhausen experiments presented earlier [118, 119] and much studied since [97, 120, 116]. Last but not least, the BFM is an exact fixed point of the flow equations of the FRG [116], and it is stable, even for $d < d_{\rm uc}$, but it requires a quite unphysical infinite range correlator for the disordered force. On the other hand, it is also the starting point for the calculation of avalanche observables beyond mean-field, i.e. for realistic short-ranged correlated disorder forces, as it corresponds in the field theory language to the resummation of all tree diagrams [115, 117].

The key property which makes the BFM (and the ABBM) model solvable is that the disorder is taken to be a Brownian random force landscape. Since it can be shown that under monotonous forward driving the interface always moves forward (Middleton's theorem [121]), the resulting equation of motion for the velocity field is Markovian, and amenable to exact methods, as presented in chapter 6.

Despite being exactly solvable, the explicit calculation of avalanche observables in the BFM requires solving a non-linear *instanton equation* and performing Laplace inversions, which is not always an easy task. Global avalanche properties, such as the probability distribution function (PDF) of global size S, of duration, and of velocity have been obtained for arbitrary driving [95]. Detailed space time properties however are more difficult. In Ref. [117] a finite wave-vector observable was calculated, demonstrating an asymmetry in the temporal shape. More recently, in Ref. [122], the joint PDF of the local avalanche size at all points was obtained for the BFM, and from that, the spatial shape of an avalanche in the limit of large aspect ratio S/ℓ^4 was derived,

where ℓ is the spatial extension of an avalanche, i.e. the range of points which move during an avalanche. This is an important observable accessible in experiments, but not well studied up to now. Even the fact that an avalanche has a finite extent, instead of an exponentially decaying tail in its spatial extension is a non-trivial result, which up to now was only proven for very large avalanches in the BFM.

In this thesis, chapter 6, we show that this extension is indeed finite in the BFM, and we give its distribution, in agreement with the exponent we can extract from scaling arguments. We also calculate further distributions of observables for the BFM which contain information about local properties, such as the joint density of global and local avalanches. We consider various protocols, where the interface is either driven uniformly in space or at a single point; in the latter case we identify new universal exponents characterizing the small scale behavior of the avalanche distribution, which are gathered in table 6.1.

Chapter 2

Extreme-value statistics of fractional Brownian motion

2.1 Presentation of the chapter

This chapter is based on joint work by K. J. Wiese and myself, published in two articles [123, 124]. Large portions of these articles have been used with only minor changes. We study here the extreme-value statistics of a fBm, a generalisation of Brownian motion presented in section 1.3 of the introduction. The structure is as follows: Section 2.2 introduces the path-integral formulation of the extreme-value statistics, followed by its perturbative expansion around the markovian case, with $\varepsilon = H - 1/2$ as a small parameter and where H is the Hurst exponent of the process. This defines the main integrals to be calculated, for which we give a diagrammatic representation. As the calculations are rather tedious, they are relegated to appendix 2.C.

Section 2.3 presents our results: We start by recalling scaling relations in section 2.3.1, before introducing our most general formula, the probability to start at $m_1 > 0$, to reach the minimum $x_0 \approx 0$ at time time t, and to finish at time $T > t$ in $m_2 > 0$. This allows us to derive several simpler results: First the distribution of times when the maximum is achieved, for a Brownian known as the *third arcsine law* (section 2.3.3). Second, the distribution of the value of this maximum. And third, the joint distribution of maximum, and the time when this maximum is taken.

Extensive numerical simulations for different values of H test these analytical predictions in section 2.4 and give very good agreement with the analytical prediction, even far from the expansion point $H = 1/2$.

Conclusions of this chapter are given in Section 2.5, followed by several appendices: Appendix 2.A gives details on the perturbation expansion. Appendix 2.B reviews useful results from [125], including a new derivation of the latter. Appendix 2.C calculates the main new, and most difficult, contribution. Appendix 2.D gives details on the corrections to the third Arcsine Law, while for the attained maximum and its cumulative distribution this is done in appendices 2.E and 2.F. Appendix 2.G gives a list of used inverse Laplace transforms. Finally, in appendix 2.H is verified that the second cumulant is correctly reproduced, and appendix 2.I presents the algorithm used to generate samples in numerical simulations.

2.2 Perturbative approach to fractional Brownian motion

2.2.1 Path integral formulation and the action

Following the ideas of [126, 127, 42, 125], we start our study of the extreme-value statistics of the fBm with a path-integral Z^+ from which several distributions will be deduced,

$$Z^+(m_1,t_1;x_0;m_2,t_2) = \int_{X_0=m_1}^{X_{t_1+t_2}=m_2} \mathcal{D}[X]\,\Theta[X]\,\delta(X_{t_1}-x_0)\,e^{-S[X]}\ . \tag{2.1}$$

It sums over all paths X_t, weighted by their probability $e^{-S[X]}$, starting at $X_0 = m_1 > 0$, passing through x_0 (close to 0) at time t_1, and ending in $X_{t_1+t_2} = m_2 > 0$, while staying positive for all $t \in [0, T = t_1 + t_2]$, as it is schematically represented in Fig. 2.1. The latter is enforced by the product of Heaviside functions $\Theta[X] := \prod_{s=0}^{t_1+t_2} \Theta(X_s)$. This positivity constraint is necessary to get information on the extreme-value statistics as it selects paths with a minimum value which is larger than the barrier. It is also what renders calculations difficult (computing a Gaussian integral on a constrained domain is non-trivial). This path integral depends on the Hurst exponent H through the action.

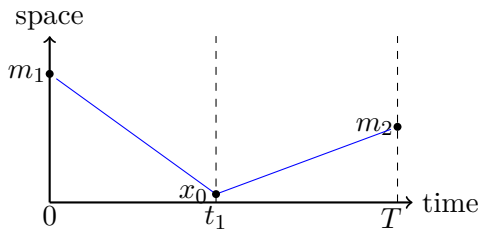

Figure 2.1: Schematic representation of the paths contributing to Z^+

Since the fBm X_t is a Gaussian process, the action $S[X]$ can (at least formally) be constructed from the covariance function of X_t,

$$S[X] = \frac{1}{2}\int_{t_1,t_2} X_{t_1} G(t_1,t_2) X_{t_2}\ . \tag{2.2}$$

Here $\langle X_{t_1} X_{t_2}\rangle = G^{-1}(t_1,t_2)$, with the covariance given in Eq. (1.19). This, however, is not enough to evaluate the path integral (2.1), since it is not evident how to implement the product of Θ-functions. Following the formalism of Ref. [125], we use standard Brownian motion as a starting point for a perturbative expansion, setting $H = \frac{1}{2} + \varepsilon$ with ε a small parameter; then the action at first order in ε is (we refer to the appendix of Ref. [125] for the derivation)

$$S\,[X] = \frac{1}{4D_{\varepsilon,\tau}}\int_0^T \dot{X}_{\tau_1}^2 \mathrm{d}\tau_1 - \frac{\varepsilon}{2}\int_0^{T-\tau}\mathrm{d}\tau_1 \int_{\tau_1+\tau}^T \mathrm{d}\tau_2\, \frac{\dot{X}_{\tau_1}\dot{X}_{\tau_2}}{|\tau_2-\tau_1|} + O(\varepsilon^2)\ . \tag{2.3}$$

The time τ is a regularization cutoff for coinciding times (a UV cutoff). We will see that it has no impact on the distribution of observables which can be extracted from the path integral. One can also introduce discrete times spaced by τ, as in [125].

The first term of Eq. (5.7), which we denote $S_0[X]$, is the action for standard Brownian motion, with a rescaled diffusion constant

$$D_{\varepsilon,\tau} = 1 + 2\varepsilon[1+\ln(\tau)] + O(\varepsilon^2) \simeq (\mathrm{e}\tau)^{2\varepsilon}. \tag{2.4}$$

It is a dimensionful constant, as fBm and standard Brownian motion do not have the same *time dimension*. The second term, which we denote $S_1[X]$, is the first correction to the action. It is non-local in time, which implies that the process is non-Markovian (even if we neglect $O(\varepsilon^2)$ terms). We check this expansion of the action in appendix 2.H, where we compute the covariance of the process from a path integral, and recover Eq. (1.19) at first order in ε.

As we will see in section 2.3, this path integral $Z^+(m_1,t_1;x_0;m_2,t_2)$, in the limit of $x_0 \to 0$, encodes a plethora of information about the maximum of the process: both distributions of the maximal value m of the process , denoted $\mathcal{P}_H^T(m)$ and of the time $t_{\max}$ when this maximum is reached, denoted $\mathcal{P}_H^T(t)$, can be extracted from it, as well as the joint distribution of this two observables. Further, the same distributions in the case of a fBm bridge can be extracted, but this will be the object of chapter 4.

It is important to note that the limit of $x_0 \to 0$ is non-trivial, as it forces the process to go close to an absorbing boundary which leads to non-trivial scaling involving the persistence exponent θ, as defined in Eq. (1.16).

2.2.2 The order-0 term

Having expressed the perturbative expansion of the action, the main task is to compute the path integral (2.1), at first order in ε, and in the limit of small x_0. Expanding the exponential of the action in (2.1),

$$e^{-S[X]} = e^{-S_0[X]}\left(1 - S_1[X] + ...\right) \ , \tag{2.5}$$

allows us to compute the path integral perturbatively in the non-local interaction $S_1[X]$, defined as the second term of Eq. (2.3),

$$S_1[X] = -\frac{\varepsilon}{2}\int_0^{T-\tau} \mathrm{d}\tau_1 \int_{\tau_1+\tau}^{T} \mathrm{d}\tau_2 \, \frac{\dot{X}_{\tau_1}\dot{X}_{\tau_2}}{|\tau_2-\tau_1|} \ . \tag{2.6}$$

This gives

$$Z^+(m_1,t_1;x_0;m_2,t_2) = Z_0^+(m_1,t_1;x_0;m_2,t_2) + \varepsilon Z_1^+(m_1,t_1;x_0;m_2,t_2) + O(\varepsilon^2) \ . \tag{2.7}$$

Z_0^+ is the term with no non-local interaction, while εZ_1^+ is the term with one interaction (it is proportional to ε because the non-local interaction itself has an amplitude of order ε). Formally, the order-0 term is

$$Z_0^+(m_1,t_1;x_0;m_2,t_2) = \int_{X_0=m_1}^{X_{t_1+t_2}=m_2} \mathcal{D}[X]\,\Theta[X]\,\delta(X_{t_1}-x_0)\,e^{-S_0[X]} \ , \tag{2.8}$$

where S_0 is the action of a standard Brownian motion,

$$S_0[X] = \frac{1}{4D_{\varepsilon,\tau}}\int_0^t \dot{X}_{\tau_1}^2 \mathrm{d}\tau_1 \ . \tag{2.9}$$

Since Brownian motion is a Markov process, this action is local in time. It allows us to write the path integral as a product,

$$\begin{aligned} Z_0^+(m_1,t_1;x_0;m_2,t_2) &= \int_{X_0=m_1}^{X_{t_1}=x_0} \mathcal{D}[X]\Theta[X]e^{-S_0[X]} \int_{X_{t_1}=x_0}^{X_T=m_2} \mathcal{D}[X]\Theta[X]e^{-S_0[X]} \\ &= P_0^+(m_1,x_0,t_1)P_0^+(x_0,m_2,t_2) \ . \end{aligned} \tag{2.10}$$

In the second line, the constraint $\delta(X_{t_1} - x_0)$ is enforced by the boundary conditions of the path integral. In the last line, we expressed each path integral in terms of the propagator $P_0^+(x_1, x_2, t)$ of standard Brownian motion, constraint to the positive half space. Its formal definition is

$$P_0^+(x_1, x_2, t) = \partial_{x_1} \text{Prob}(X_{t+t_0} < x_1 \text{ and } X_s > 0,\ \forall s \in [t_0, t_0 + t]\,|X_{t_0} = x_2) \tag{2.11}$$

The expression of this propagator is obtained using the fact that the increments of a Brownian motion is Gaussian, and its Markovian nature allows to enforce the positivity constraint using the method of images. This gives

$$P_0^+(x_1, x_2, t) = \frac{1}{\sqrt{4\pi D t}} \left(e^{-\frac{(x_1 - x_2)^2}{4Dt}} - e^{-\frac{(x_1 + x_2)^2}{4Dt}} \right) \underset{x_1 \to 0}{\simeq} x_1 x_2 \frac{e^{-\frac{x_2^2}{4Dt}}}{\sqrt{4\pi D^3 t^3}} , \tag{2.12}$$

for an arbitrary diffusive constant D. We now use that the diffusive constant is $D_{\varepsilon,\tau} = 1 + O(\varepsilon)$. This allows us to express the path integral (2.1) at leading order in ε, and in the limit of small x_0, as

$$Z_0^+(m_1, t_1; x_0; m_2, t_2) \underset{x_0 \to 0}{\simeq} x_0^2 \frac{m_1 m_2 e^{-\frac{m_1^2}{4t_1} - \frac{m_2^2}{4t_2}}}{4\pi t_1^{3/2} t_2^{3/2}} + O(\varepsilon) . \tag{2.13}$$

Before going to the order ε calculation, let us briefly discuss how we recover known results for Brownian motion from the expression 2.13. If we integrate Z_0^+ over m_1 and m_2 in the limit of $x_0 \to 0$, we select all paths reaching a minimum over $[0, t_1 + t_2]$ of value equal to 0 and at time t_1, without any constraint on the starting and ending points (apart that they are larger than the minimum value 0). Due to translation invariance, this is equivalent to a process with fixed starting value equal to 0, and an arbitrary minimum value (smaller than 0). The distribution of the time at which such a minimum is reached is known as one the arcsine laws, discussed in the introduction 1.2.3. We recover it here,

$$\mathcal{P}^T_{H=\frac{1}{2}}(t_{\max} = t) = \lim_{x_0 \to 0} \frac{1}{x_0^2} \int_{m_1, m_2 > 0} Z_0^+(m_1, t; x_0; m_2, T - t) = \frac{1}{\pi \sqrt{t(T - t)}} , \tag{2.14}$$

as given in Eq. (1.10) apart that we did not fixe the length of the time interval to 1.

To include the order-ε term in the diffusive constant to get the full result for Z_+ at order ε, we use Eq. (2.4) expanded in ε,

$$Z_0^+ \underset{x_0 \to 0}{\simeq} x_0^2 \frac{m_1 m_2 e^{-\frac{m_1^2}{4t_1} - \frac{m_2^2}{4t_2}}}{4\pi t_1^{3/2} t_2^{3/2}} \times \left\{ 1 + \varepsilon \left[1 + \ln(\tau) \right] \left(\frac{m_1^2}{2t_1} + \frac{m_2^2}{2t_2} - 6 \right) \right\} + O(\varepsilon^2) . \tag{2.15}$$

It is interesting to note that the order-ε term appearing here can also be computed from the result (2.13) as

$$2[1 + \ln(\tau)](t_1 \partial_{t_1} + t_2 \partial_{t_2}) Z_0^+ . \tag{2.16}$$

2.2.3 The first-order terms

To go beyond Brownian motion and include non-Markovian effects, i.e. interactions non-local in time, we need to compute the first-order correction in the expansion (2.7), which is called Z_1^+ and reads

$$Z_1^+(m_1, t_1; x_0; m_2, t_2) = \frac{1}{2} \int_0^{T-\tau} \mathrm{d}\tau_1 \int_{\tau_1 + \tau}^{T} \mathrm{d}\tau_2 \int_{X_0 = m_1}^{X_T = m_2} \mathcal{D}[X] \frac{\dot{X}_{\tau_1} \dot{X}_{\tau_2}}{|\tau_2 - \tau_1|} \delta(X_{t_1} - x_0)\, \Theta[X]\, e^{-S_0[X]} . \tag{2.17}$$

As before, we denote $T = t_1 + t_2$. To compute Z_1^+, we decompose it into three terms, distinguished by their time ordering. Denote Z_α^+ the part where $\tau_1 < \tau_2 < t_1$, Z_β^+ the part where $t_1 < \tau_1 < \tau_2$, and Z_γ^+ the term where $\tau_1 < t_1 < \tau_2$. Then

$$Z_1^+(m_1,t_1;x_0;m_2,t_2) = Z_\alpha^+(m_1,t_1;x_0;m_2,t_2) + Z_\beta^+(m_1,t_1;x_0;m_2,t_2) + Z_\gamma^+(m_1,t_1;x_0;m_2,t_2)\ . \tag{2.18}$$

In the first term, the *interaction* affects only the process in the time interval $[0,t_1]$, and there is no coupling with the process on the time interval $[t_1, t_1+t_2]$. This leads, as shown in appendix 2.A, to a factorized expression for Z_α^+,

$$Z_\alpha^+(m_1,t_1;x_0;m_2,t_2) = P_1^+(m_1,x_0,t_1)P_0^+(x_0,m_2,t_2)\ . \tag{2.19}$$

Here $P_1^+(m,x_0,t)$ is the order-ε correction to the propagator of fBm in the half space (i.e. constrained to remain positive). This object, which we need in the limit of $x_0 \to 0$, was studied and computed in Ref. [125]. The result is recalled in appendix 2.B, and recalculated using more efficient technology developed here. The second term is similar to the first, swapping the two time intervals,

$$Z_\beta^+(m_1,t_1;x_0;m_2,t_2) = P_0^+(m_1,x_0,t_1)P_1^+(x_0,m_2,t_2)\ . \tag{2.20}$$

The third term, Z_γ^+, is more complicated as the interaction couples the two time intervals $[0,t_1]$ and $[t_1, T = t_1+t_2]$. We can still take advantage of locality in time of the action S_0 to write the path integral (2.17), with time integrals restricted to $0 < \tau_1 < t_1 < \tau_2 < T$, as a product of simpler path integrals:

$$\begin{aligned} &Z_\gamma^+(m_1,t_1;x_0;m_2,t_2) \\ &= \frac{1}{2}\int_0^{t_1}\mathrm{d}\tau_1 \int_{t_1}^{T}\frac{\mathrm{d}\tau_2}{\tau_2-\tau_1}\int_{x_1,x_2>0}\int_{X_0=m_1}^{X_{\tau_1}=x_1}\mathcal{D}[X]\Theta[X]e^{-S_0[X]}\int_{X_{\tau_1}=x_1}^{X_{t_1}=x_0}\mathcal{D}[X]\Theta[X]\dot{X}_{\tau_1}e^{-S_0[X]} \\ &\qquad\times\int_{X_{t_1}=x_0}^{X_{\tau_2}=x_2}\mathcal{D}[X]\Theta[X]e^{-S_0[X]}\int_{X_{\tau_2}=x_2}^{X_T=m_2}\mathcal{D}[X]\Theta[X]\dot{X}_{\tau_2}e^{-S_0[X]}\ . \end{aligned} \tag{2.21}$$

In this expression, all path integrals can be expressed in terms of the bare propagator P_0^+; we refer to appendix 2.A for how to deal with the terms containing $\dot{X}$. We have not written the cut-off τ as there are no short-time divergences that need to be regularized (contrary to the terms Z_α^+ and Z_β^+). The structure of the time integrals, which are products of convolutions, suggests to use Laplace transforms (with respect to the time variables: $t_1 \to s_1$, $t_2 \to s_2$). This, and the identity

$$\frac{1}{\tau_2-\tau_1} = \int_{y>0} e^{-y(\tau_2-\tau_1)} \tag{2.22}$$

give us a simple form for the double Laplace transform of Z_γ^+, which we will denote with a tilde (for details see appendix 2.A),

$$\begin{aligned} &\tilde{Z}_\gamma^+(m_1,s_1;x_0;m_2,s_2) \\ &\quad= 2\int_{x_1,x_2,y>0}\tilde{P}_0^+(m_1,x_1;s_1)\,\partial_{x_1}\tilde{P}_0^+(x_1,x_0;s_1+y)\tilde{P}_0^+(x_0,x_2;s_2+y)\,\partial_{x_2}\tilde{P}_0^+(x_2,m_2;s_2)\ . \end{aligned} \tag{2.23}$$

The Laplace-transformed constrained propagator appearing in this expression is

$$\tilde{P}_0^+(x_1,x_2;s) = \int_0^\infty \mathrm{d}t\, e^{-st}P_0^+(x_1,x_2,t) = \frac{e^{-\sqrt{s}|x_1-x_2|} - e^{-\sqrt{s}(x_1+x_2)}}{2\sqrt{s}} \underset{x_1\to 0}{\simeq} x_1 e^{-\sqrt{s}x_2}\ . \tag{2.24}$$

The Laplace transformation gives another simplification: the space dependence is now exponential in the propagator, as compared to the Gaussian form of $P_0^+(x_1, x_2, t)$, which renders the space integrations elementary. (Without the Laplace transform, already the first space integration gives an error-function, and the remaining integrations are highly non-trivial). Nevertheless, the final result for $Z_\gamma^+(m_1, t_1; x_0; m_2, t_2)$ is complicated, and requires to compute the three integrals in Eq. (2.23), and two inverse Laplace transformations. These steps are performed in appendix 2.C.

2.2.4 Graphical representation and diagrams

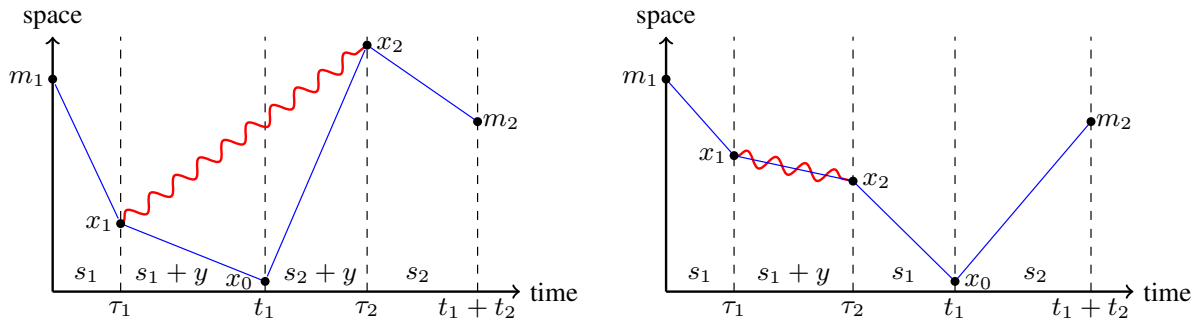

Figure 2.2: Left: Graphical representation of the contribution Z_γ^+ to the path-integral $Z^+(m_1, t_1; x_0; m_2, t_2)$ given in Eq. (2.1). The red curve represents the non-local interaction in the action, second line of Eq. (5.7), while blue lines are bare propagators. We also indicate the Laplace variable which appears in each time slice in Eq. (2.23). Right: Graphical representation of Z_α^+

It is useful to give a diagrammatic representation for the terms of the perturbative expansion. We denote bare propagators (2.24) with a solid blue lines. The interaction between two points (τ_1, x_1) and (τ_2, x_2) is represented in red. As can be seen from Eq. (2.23), it acts as $2\partial_{x_1}$ on the propagator starting at x_1, $2\partial_{x_2}$ on the propagator starting at x_2; it also translates the Laplace variable of each time slice between these two points by $+y$. The space variables x_1, x_2 and the *interaction* variable y (which has the inverse dimension of time) have to be integrated from 0 to ∞. In case of divergences, the integration has to be cut off with a large-y cutoff (cf. appendix 2.G for the link between the short time cutoff τ and the large y cutoff).

The contribution of Z_γ^+ is computed in detail in Appendix 2.C, and represented in Figure 2.2 (left), together with the contribution Z_α^+(right).

2.3 Analytical Results

We recall here some known scaling results about extremal properties of the fBm. We then show how our perturbative expansion, and the computation of $Z^+(m_1, t_1; x_0; m_2, t_2)$, allows us to obtain analytical results on the distributions beyond these scaling arguments.

2.3.1 Scaling results

We review the links between the survival probability, defined in Eq. (1.15) and the related persistence exponent θ (1.16), to the extreme value observables we investigate here. We recall that for fractional Brownian motion with Hurst exponent H it was shown that $\theta = 1 - H$ [56, 59].

To understand the link of $S(T,x)$ with the maximum distribution for fBm, we use self affinity of the process X_t to write $\mathcal{P}_H^T(m)$ as

$$\mathcal{P}_H^T(m) = \frac{1}{\sqrt{2}T^H} f_H\left(y = \frac{m}{\sqrt{2}T^H}\right) . \tag{2.25}$$

Here f is a scaling function depending on H. The survival probability is related to the maximum distribution by

$$S(T,x) = \int_0^x P^T(m)\,\mathrm{d}m = \int_0^{\frac{x}{\sqrt{2}T^H}} f_H(y)\,\mathrm{d}y . \tag{2.26}$$

This states that due to translational invariance a realisation of a fBm starting at x and remaining positive is the same as a realisation starting at 0 and having a minimum larger than $-x$. Finally, the symmetry $x \to -x$ (for a fBm starting at $X_0 = 0$) gives the correspondence between minima and maxima. These considerations allow us to predict the scaling behavior of $\mathcal{P}_H^T(m)$ at small m from the large-T behaviour of $S(T,x)$ [56],

$$f(y) \underset{y\to 0}{\sim} y^\alpha \;\Leftrightarrow\; S(T,x) \sim T^{-(\alpha+1)H} , \tag{2.27}$$

and finally

$$\mathcal{P}_H^T(m) \underset{m\to 0}{\sim} m^{\frac{\theta}{H}-1} = m^{\frac{1}{H}-2} . \tag{2.28}$$

For the distribution of the time at which the maximum is achieved we can estimate the behavior close to the origin by assuming that small values of the maximum are reached close to the origin. Starting with

$$\mathcal{P}_H^T(m)\mathrm{d}m = \mathcal{P}_H^T(t)\mathrm{d}t , \tag{2.29}$$

and using scaling, $m \sim t^H$, we obtain

$$\mathcal{P}_H^T(t) \sim P_H^T(m)\frac{\mathrm{d}m}{\mathrm{d}t} \sim \left(t^H\right)^{\frac{1}{H}-2} t^{H-1} \sim t^{-H} . \tag{2.30}$$

This should be valid when $t \to 0$ (or $m \to 0$). By time reversal symmetry $t \to T - t$, we also have

$$\mathcal{P}_H^T(t) \underset{t\to T}{\sim} (T-t)^{-H} . \tag{2.31}$$

2.3.2 The complete result for $Z^+(m_1,t_1;x_0;m_2,t_2)$

We present here the final result for Z^+, defined in Eq. (2.1), at order ε. This path integral was first expanded, cf. Eq. (2.7), by treating the non-local term in the action (5.7) perturbatively. The first term Z_0^+ of this expansion is given in Eq. (2.15), while the second term Z_1^+ was split into three contributions Z_α^+, Z_β^+ and Z_γ^+, see Eq. (2.18). The first two terms can be obtained explicitly from (2.89), while the third one is computed in appendix 2.C, the result being split between (2.102), (2.117) and (2.133).

In order to display a compact form, we choose $T \equiv t_1 + t_2 = 1$ (which is equivalent to rescaling m_1 and m_2 by T^{-H} and t_1 and t_2 by T^{-1}) and introduce new rescaled (dimensionless) variables,

$$y_1 = \frac{m_1}{\sqrt{2}t_1^H} , \qquad y_2 = \frac{m_2}{\sqrt{2}t_2^H} \tag{2.32}$$

$$t_1 = \vartheta , \qquad t_2 = 1 - \vartheta . \tag{2.33}$$

In these new variables, the final result is

$$Z^+(m_1,t_1;x_0;m_2,t_2) \underset{x_0\to 0}{\simeq} x_0^{2-4\varepsilon}\frac{y_1y_2\exp\left(-\frac{1}{2}y_1^2-\frac{1}{2}y_2^2\right)}{2\pi\left[\vartheta(1-\vartheta)\right]^{2H}}\times \tag{2.34}$$
$$\left\{1+\varepsilon\left[\mathcal{I}(y_1)\left(1+\sqrt{\frac{1-\vartheta}{\vartheta}}\frac{y_2}{y_1}\right)+\mathcal{I}(y_2)\left(1+\sqrt{\frac{\vartheta}{1-\vartheta}}\frac{y_1}{y_2}\right)+\frac{(1-y_2^2)\,\mathcal{I}(\sqrt{1-\vartheta}y_1)}{\sqrt{\vartheta(1-\vartheta)}y_1y_2}\right.\right.$$
$$+\frac{(1-y_1^2)\,\mathcal{I}(\sqrt{\vartheta}y_2)}{\sqrt{\vartheta(1-\vartheta)}y_1y_2}-\frac{\mathcal{I}\left(\sqrt{1-\vartheta}y_1+\sqrt{\vartheta}y_2\right)}{\sqrt{\vartheta(1-\vartheta)}y_1y_2}+2\frac{(1-\vartheta)y_1^2+\vartheta y_2^2-1}{\sqrt{\vartheta(1-\vartheta)}y_1y_2}$$
$$\left.\left.+(y_1^2-2)\big(\ln(2y_1^2)+\gamma_{\mathrm{E}}\big)+(y_2^2-2)\big(\ln(2y_2^2)+\gamma_{\mathrm{E}}\big)-4-2\gamma_{\mathrm{E}}\right]\right\}+O(\varepsilon^2)\ .$$

The special function $\mathcal{I}$ appearing in this expression is

$$\mathcal{I}(z)=\frac{z^4}{6}\,{}_2F_2\left(1,1;\frac{5}{2},3;\frac{z^2}{2}\right)+\pi(1-z^2)\mathrm{erfi}\left(\frac{z}{\sqrt{2}}\right)-3z^2+\sqrt{2\pi}e^{\frac{z^2}{2}}z+2\ , \tag{2.35}$$

where erfi is the imaginary error function, defined from the error function as $\mathrm{erfi}(z)=-i\,\mathrm{erf}(iz)$.

2.3.3 The third arcsine law: Distribution of the time when the maximum is reached

To simplify the result (2.34), we can extract from it distributions of a single observable. We start with the probability distribution $\mathcal{P}_H^T(t)$ of $t_{\max}$, the time when the fBm achieves its maximum. For Brownian motion, $H=1/2$, this distribution is well known as the third arcsine law, because the cumulative distribution involves the arcsin function, cf. Eq. (1.9),

$$\mathcal{P}_{\frac{1}{2}}^T(t_{\max}=t)=\frac{1}{\pi\sqrt{t(T-t)}}\ ,\ \text{for } t\in[0,T]\ . \tag{2.36}$$

Until now, only scaling properties were known for this distribution in the general case [18], as recalled in Eq. (2.30).

The path integral (2.1), in the limit of $x_0\to 0$, selects paths which go through $x_0\approx 0^+$ at time t_1 while staying positive. This means that we sum over paths reaching their minimum (in the interval $[0,t_1+t_2]$, and which is almost surely unique) at t_1, starting at m_1 and ending at m_2. This is equivalent to summing over paths starting at 0, reaching their minimum with value $-m_1$ at time t_1, and ending in m_2-m_1. Integrating over m_1 and m_2 finally gives the sum over all paths reaching their minimum in t_1, independent of the value of this minimum, and the end point. Up to a normalization, this is the probability distribution of $t_{\min}$. By symmetry, this is the same as the distribution of $t_{\max}$. Formally, it reads

$$\mathcal{P}_H^T(t_{\max}=t)=\lim_{x_0\to 0}\frac{1}{Z^{\mathrm{N}}(x_0,T)}\int_{m_1,m_2>0}Z^+(m_1,t;x_0;m_2,T-t)\ . \tag{2.37}$$

The normalization Z^{N} depends on x_0 and T. It ensures that $\mathcal{P}_H^T(t)$ is normalized; it can be expressed in terms of the path integral Z^+ as

$$Z^{\mathrm{N}}(x_0,T)=\int_0^T\mathrm{d}t\int_{m_1,m_2>0}Z^+(m_1,t;x_0;m_2,T-t)\ . \tag{2.38}$$

At order 0, starting from Eq. (2.13) and integrating over m_1 and m_2 allows us to recover Eq. (2.36) with normalisation $Z^{\mathrm{N}}(x_0,T)=x_0^2$.

For the order-ε correction, the integrations over m_1 and m_2 are lengthy. This is done in appendix 2.D. It allows us to write an ε-expansion for the distribution of $t_{\max}$ in the form

$$\mathcal{P}^T_{H=\frac{1}{2}+\varepsilon}(t) = \mathcal{P}^T_{\frac{1}{2}}(t) + \varepsilon\, \delta\mathcal{P}^T(t) + O(\varepsilon^2)\ . \tag{2.39}$$

The result (2.146) reads

$$\delta\mathcal{P}^T(t) = \frac{1}{\pi\sqrt{t_1 t_2}}\left\{\sqrt{\frac{t_1}{t_2}}\left[\pi - 2\arctan\left(\sqrt{\frac{t_1}{t_2}}\right)\right] + \sqrt{\frac{t_2}{t_1}}\left[\pi - 2\arctan\left(\sqrt{\frac{t_2}{t_1}}\right)\right] - \ln(t_1 t_2) + \text{cst}\right\}\ , \tag{2.40}$$

where $t_1 = t$ and $t_2 = T - t$. It takes a simple form if we exponentiate this order-ε correction,

$$\boxed{\mathcal{P}^T_H(t_{\max} = t) = \frac{1}{\pi[t(T-t)]^H}\ \exp\left(\varepsilon\, \mathcal{F}\left(\vartheta = \frac{t}{T}\right)\right) + O\left(\varepsilon^2\right).} \tag{2.41}$$

The term $\ln(t_1 t_2) = \ln\big(t(T-t)\big)$ in $\delta P^T(t)$ gives the expected change, from Eq. (2.30) and (2.31), in the scaling form of the Arcsine law, $\sqrt{t(T-t)} \to [t(T-t)]^H$. The regular part (with a finite limit when $t \to 0$ and $t \to T$) induces a non-trivial change in the shape,

$$\boxed{\mathcal{F}(\vartheta) = \sqrt{\frac{\vartheta}{1-\vartheta}}\left[\pi - 2\arctan\left(\sqrt{\frac{\vartheta}{1-\vartheta}}\right)\right] + \sqrt{\frac{1-\vartheta}{\vartheta}}\left[\pi - 2\arctan\left(\sqrt{\frac{1-\vartheta}{\vartheta}}\right)\right] + \text{cst}\ .} \tag{2.42}$$

The time reversal symmetry $t \to T - t$ (corresponding to $\vartheta \to 1 - \vartheta$) is explicit and the constant ensures normalization. The contribution of $\mathcal{F}(\vartheta)$ to the probability that the maximum is attained at time t is quite noticeable, as shown in Fig. 2.3.

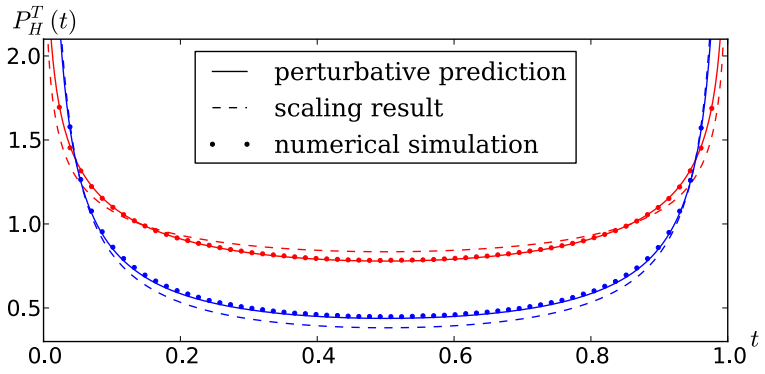

Figure 2.3: Distribution of $t_{\max}$ for $T = 1$ and $H = 0.25$ (red) or $H = 0.75$ (blue) given in Eq. (2.41) (plain lines) compared to the scaling ansatz, i.e. $\mathcal{F} = \text{cst.}$ (dashed lines) and numerical simulations (dots). For $H < 0.5$ realisations with $t_{\max} \approx T/2$ are less probable (by about 10%) than expected from scaling. For $H > 0.5$ the correction has the opposite sign.

2.3.4 The distribution of the maximum

We now present results for the distribution of the maximum $\mathcal{P}^T_H(m)$. For standard Brownian motion

$$\mathcal{P}^T_{\frac{1}{2}}(m) = \frac{e^{-\frac{m^2}{4T}}}{\sqrt{\pi T}}\ , \qquad m > 0\ . \tag{2.43}$$

On the other hand, the scaling results presented in 2.3.1 predict that for any H, $\mathcal{P}_H^T(m)$ behaves at small scale as $m^{1/H-2}$, as given in Eq. (2.28).

Using our path integral, we can go further. Similarly to the distribution of $t_{\max}$, the distribution of the maximum m itself can be extracted from Z^+, defined in Eq. (2.1),

$$\mathcal{P}_H^T(m) = \lim_{x_0\to 0} \frac{1}{Z^{\mathrm{N}}} \int_0^T \mathrm{d}t \int_{m_2>0} Z^+(m,t;x_0;m_2,T-t) \ . \tag{2.44}$$

The details of these computations (integrations over t and m_2) are given in appendix 2.E. Its ε-expansion, recast in exponential form, leads to the scaling form of Eq. (2.25), with

$$f_H(y) = \sqrt{\frac{2}{\pi}} e^{-\frac{y^2}{2}}\, e^{\varepsilon[\mathcal{G}(y)+\mathrm{cst}]} + O(\varepsilon^2) \ . \tag{2.45}$$

The constant term ensures normalization. Figure 2.4 shows the form of this scaling function for different values of H, as well as a *first comparison* to numerical simulations. The function $\mathcal{G}$ involves a combination of special functions denoted $\mathcal{I}$ in Eq. (2.35) , and logarithmic terms,

$$\mathcal{G}(y) = \mathcal{I}(y) + (y^2-2)[\gamma_{\mathrm{E}} + \ln(2y^2)] \ . \tag{2.46}$$

It has a different asymptotics for small and large y,

$$\mathcal{G}(y) \sim \begin{cases} -2\ln(y) & \text{for } y\to\infty \\ -4\ln(y) & \text{for } y\to 0 \end{cases} . \tag{2.47}$$

The second line implies that $P_H^T(m) \sim m^{-4\varepsilon}$ when $m\to 0$, which is consistent (at order ε) with the scaling result (2.28), $\frac{1}{H}-2 = -4\varepsilon + O(\varepsilon^2)$. Formulas (2.45)-(2.47) also predict the distribution at large m. It is known that the leading behavior of $P_H^T(m)$ is Gaussian, which can be formalized as

$$\lim_{y\to\infty} \frac{\ln\big(f_H(y)\big)}{y^2} = -\frac{1}{2} \ . \tag{2.48}$$

This is a direct consequence of an important theorem in the theory of Gaussian processes, the *Borell inequality* [86]. It states that for any Gaussian process X_t the cumulative distribution of its maximum value over the interval $[0,T]$, $m = \sup_{t\in[0,T]} X_t$, verifies

$$\mathrm{Prob}(m>u) \le \exp\left(-\frac{(u-\langle m\rangle)^2}{2\sigma^2}\right) \ , \tag{2.49}$$

where $\langle m\rangle$ and $\sigma^2 = \sup_{t\in[0,T]}\langle X_t^2\rangle$ are assumed to be finite. Specifying this to fBm with $T=1$ allows us to derive Eq. (2.48). A proof of this theorem and a derivation of its implications for fBm can be found in Ref. [57].

Our result (2.45) goes further, and gives the subleading term in the large-m (and equivalently large-y) regime, a power law with exponent $-2\varepsilon + O(\varepsilon^2)$. It can be written as

$$\lim_{y\to\infty} \frac{\ln\Big(f_H(y)\exp(\frac{y^2}{2})\Big)}{\ln(y)} = -2\varepsilon + O(\varepsilon^2) \ . \tag{2.50}$$

Comparison of our full prediction (i.e. not only the asymptotics) with numerical simulations of the fBm are presented in the next section 2.4.

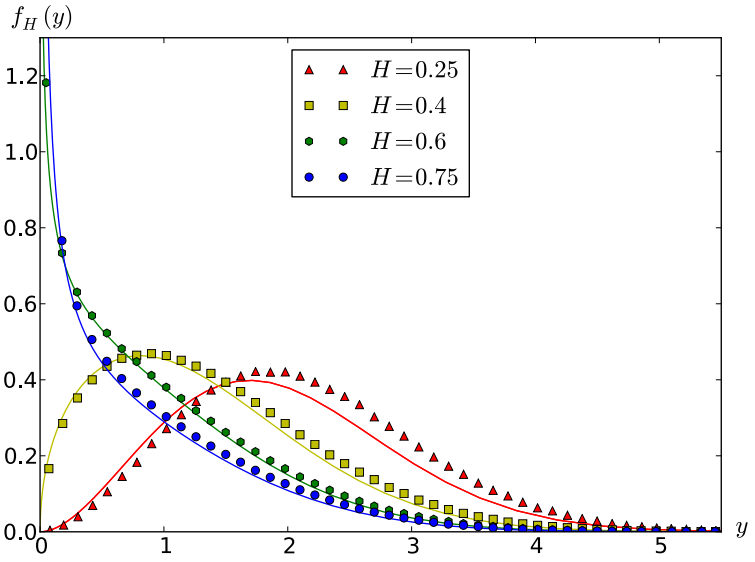

Figure 2.4: Scaling function $f_H(y)$ for the distribution of the maximum, as defined in Eq. (2.25), for different values of H: $H = 0.25$ in red, $H = 0.4$ in yellow, $H = 0.6$ in green, and $H = 0.75$ in blue. The plain lines represent the analytic prediction from our perturbative theory (at first order in ε) given in Eq. (2.45); the symbols are results from numerical simulations, cf. section 2.4.

2.3.5 Survival probability

The survival probability $S(x,T)$ is defined as the probability for a process X_t to stay positive up to time t, while starting at $X_0 = x$,

$$S(x,t) := \text{prob}\left(X_t > 0,\ \forall t \in [0,T] \,|\, X_0 = x\right) \ . \tag{2.51}$$

As before, scaling properties of the fBm allow us to write this as a function of $y = \frac{x}{\sqrt{2}T^H}$. As mentioned, the survival probability is the cumulative distribution of the maximum value, and reads

$$S(y) = \int_0^y \mathrm{d}u\, f_H(u) \ , \tag{2.52}$$

with f_H defined in Eq. (2.25). Similarly to the other distributions, we can compute its ε-expension and recast it into an exponential form to get

$$S(y) = \mathrm{erf}\left(\frac{y}{\sqrt{2}}\right) \exp\left(\varepsilon \frac{\mathcal{M}(y)}{\mathrm{erf}\left(\frac{y}{\sqrt{2}}\right)}\right) + O(\varepsilon^2) \ . \tag{2.53}$$

The function $\mathcal{M}(y)$ is

$$\begin{aligned}\mathcal{M}(y) = &\sqrt{\frac{8}{\pi}} y\, {}_2F_2\left(\frac{1}{2},\frac{1}{2};\frac{3}{2},\frac{3}{2};-\frac{y^2}{2}\right) - \sqrt{\frac{2}{\pi}} e^{-\frac{y^2}{2}} y^3\, {}_2F_2\left(1,1;\frac{3}{2},2;\frac{y^2}{2}\right) \\ &+ \sqrt{2\pi} e^{-\frac{y^2}{2}} y\, \mathrm{erfi}\left(\frac{y}{\sqrt{2}}\right) - \left[\mathrm{erf}\left(\frac{y}{\sqrt{2}}\right) + \sqrt{\frac{2}{\pi}} e^{-\frac{y^2}{2}} y\right]\left[\ln\left(2y^2\right) + \gamma_{\mathrm{E}}\right] \ .\end{aligned} \tag{2.54}$$

Some details of its derivation are given in appendix 2.F and thos result is plotted on Fig. 2.5.

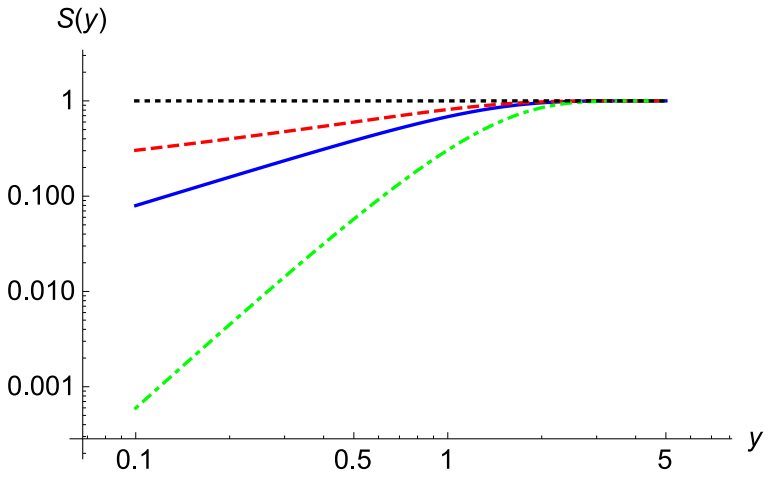

Figure 2.5: The survival probability $S(y)$ for $H = 1/2$ (blue solid line), $H = 0.75$ (red, dashed), $H = 0.25$ (green, dot-dashed), and asymptotics $S(y) = 1$ (black, dotted), in a log-log plot.

2.3.6 The joint distribution for $t_{\max}$ and m

The result (2.34) was obtained by considering paths starting at $X_0 = m_1 > 0$ with an absorbing boundary at $x = 0$ constraining the process to stay positive, as can be seen from the path-integral definition (2.1). Using translational invariance, and the symmetry $x \leftrightarrow -x$ of the fBm, we can reinterpret this as the sum over paths starting at $X_0 = 0$, reaching their maximum (over the interval $[0, T = t_1 + t_2]$) of value m_1 at time t_1, and ending in $X_T = m_1 - m_2 < m_1$.

The integral over m_2 is then, in the limit $x_0 \to 0$ and up to a normalisation factor Z^{N}, the joint probability density for a fBm to have a maximum value $m = m_1$ at a time $t = t_{\max} = t_1$ over the interval $[0, T]$; this we can write as

$$\mathcal{P}_H^T(m,t) = \lim_{x_0 \to 0} \frac{1}{Z^{\mathrm{N}}} \int_0^\infty \mathrm{d}m_2 \, Z^+(m,t;x_0;m_2,T-t) \; . \tag{2.55}$$

We recall the result for Brownian motion that we recover for $\varepsilon = 0$,

$$\mathcal{P}_{\frac{1}{2}}^T(m,t) = \frac{m e^{-\frac{m^2}{4t}}}{2\pi t^{3/2}\sqrt{T-t}} \; . \tag{2.56}$$

To simplify the ensuing discussion, we now consider the conditional probability

$$\mathcal{P}_H^T(m|t) := \frac{\mathcal{P}_H^T(m,t)}{\int_{m>0} \mathcal{P}_H^T(t,m)} = \frac{\mathcal{P}_H^T(m,t)}{\mathcal{P}_H^T(t)} \; . \tag{2.57}$$

Interestingly, in the case of the Brownian motion, we can make a change of variables $m \to \upsilon := m/\sqrt{2t}$ such that this conditional distribution function becomes independent of t (or equivalently, independent of $\vartheta = t/T$)

$$\mathcal{P}_{\frac{1}{2}}^T(m|t) = m\frac{e^{-\frac{m^2}{4t}}}{2t} = \frac{1}{\sqrt{2t}} \upsilon e^{-\frac{\upsilon^2}{2}} = \frac{\mathrm{d}\upsilon}{\mathrm{d}m} \mathcal{P}_{\frac{1}{2}}(\upsilon|\vartheta) \tag{2.58}$$

with

$$\mathcal{P}_{\frac{1}{2}}(\upsilon|\vartheta) = \upsilon e^{-\frac{\upsilon^2}{2}} \; . \tag{2.59}$$

For $H \neq \frac{1}{2}$, this independence is broken, and the result at order ε can be written as

$$\mathcal{P}_{H=\frac{1}{2}+\varepsilon}(\upsilon|\vartheta) = \upsilon e^{-\frac{\upsilon^2}{2}} e^{\varepsilon \mathcal{G}(\upsilon|\vartheta)} + O(\varepsilon^2) \ , \tag{2.60}$$

where now $\upsilon = \frac{m}{\sqrt{2}t^H}$ (to keep υ a dimensionless variable).

The non-trivial correction $\mathcal{G}(\upsilon|\vartheta)$ is obtained from the result (2.34) as

$$\mathcal{G}(y_1|\vartheta) = \int_{y_2>0} y_2 e^{-\frac{y_2^2}{2}} [...] \ , \tag{2.61}$$

where [...] are the terms in the square brackets of Eq. (2.34).

While we can integrate Eq. (2.34) over y_1 and y_2 to obtain the probability that the maximum is attained at time t, we were in general not able to analytically integrate it solely over y_2, due to the presence of the term $\mathcal{I}(\sqrt{1-\vartheta}y_1 + \sqrt{\vartheta}y_2)$. An exception are the two limiting cases $\vartheta = 0$ and $\vartheta = 1$, for which

$$\mathcal{G}(\upsilon|0) = (\upsilon^2 - 2)[\gamma_{\rm E} + \ln(2\upsilon^2)] + \frac{(3-\upsilon^2)[\mathcal{I}(\upsilon) - 2]}{1-\upsilon^2} + \frac{2\sqrt{2\pi}}{\upsilon}\left[1 - \upsilon^2 - \frac{e^{\frac{\upsilon^2}{2}} \operatorname{erfc}\left(\frac{\upsilon}{\sqrt{2}}\right)}{1-\upsilon^2}\right] \ , \tag{2.62}$$

$$\mathcal{G}(\upsilon|1) = (\upsilon^2 - 2)[\gamma_{\rm E} + \ln(2\upsilon^2)] + \mathcal{I}(\upsilon) - 2 \ . \tag{2.63}$$

Note that $\mathcal{P}_H(\upsilon|1)$ is also the conditional probability that a fBm path, starting at $x_0 \ll 1$, and having survived up to time T has final position $m = \sqrt{2}\upsilon T^H$. This reproduces Eqs. (9)-(10) of Ref. [125].

The asymptotic behaviors for small υ are

$$\mathcal{P}_H(\upsilon|\vartheta) \sim \upsilon^{\frac{1}{H}-1} \simeq \upsilon^{1-4\varepsilon} + O(\varepsilon^2) \tag{2.64}$$

For large υ, the situation is more complicated. For the two limiting cases the behavior is consistent with

$$\mathcal{P}_H(\upsilon|0) \sim \upsilon^{1+2\varepsilon} \mathrm{e}^{-\upsilon^2/2 - \sqrt{8\pi}\upsilon\varepsilon} + O(\varepsilon^2) \ , \tag{2.65}$$

$$\mathcal{P}_H(\upsilon|1) \sim \upsilon^{1-2\varepsilon} \mathrm{e}^{-\upsilon^2/2} + O(\varepsilon^2) \ . \tag{2.66}$$

It would be interesting to understand this behaviour from scaling arguments.

The conditional probability (2.60) is plotted on figure 2.6 for various value of H, supplemented by results obtained via numerical integration of Eq. (2.61) for $\vartheta = 0.1$, 0.5, and 0.9. It varies smoothly as a function of ϑ.

2.4 Numerical Results

To validate the perturbative approach presented in this thesis, we tested our analytical results with direct numerical simulations of fBm paths. The discretized fBm paths are generated using the Davis and Harte procedure as described in [51] (and references therein). The idea is to take advantage of the stationarity of the increments and use fast-Fourier transformations to compute efficiently the square root of its covariance function. This method is exact, i.e. the samples generated have exactly the covariance function given in Eq. (1.19), and is adapted to situations where the length of the path to generate is fixed. Other simulation techniques exist, reviewed in Ref. [128].

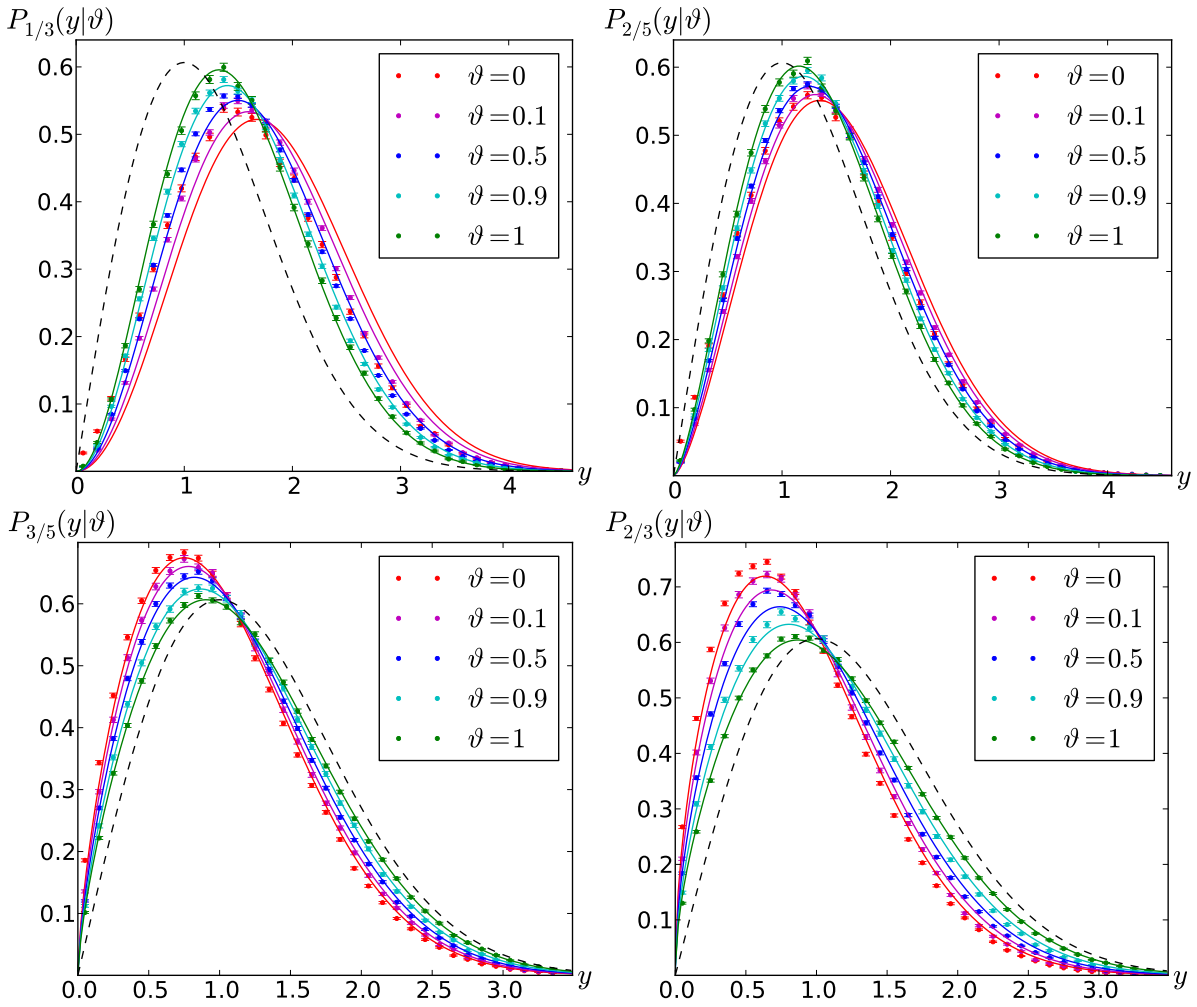

Figure 2.6: The conditional probability $\mathcal{P}_H(y|\vartheta)$ for various values of H and ϑ. Top left $H = \frac{1}{3}$, top right $H = \frac{2}{5}$, bottom left $H = \frac{3}{5}$ and bottom right $H = \frac{2}{3}$. The plain curves are the analytical prediction (2.60), where the scaling functions are given analytically for the two extremal cases, $\vartheta = 0$ and $\vartheta = 1$ cf. Eqs. (2.62)-(2.63); for $0 < \vartheta < 1$ the curves are obtained via numerical integration. The predicted spread of the curves (which collapse for $H = \frac{1}{2}$ to Eq. (2.56), plotted in black dashes) is well reproduced in the numerics, both for $\varepsilon > 0$ and $\varepsilon < 0$. For $\vartheta \to 1$ the agreement with numerics is remarkable, while for ϑ close to zero, we see significant deviations. These deviations may be due to both discretisation effects and ε^2 corrections (they have the same sign for both $\varepsilon > 0$ and $\varepsilon < 0$).

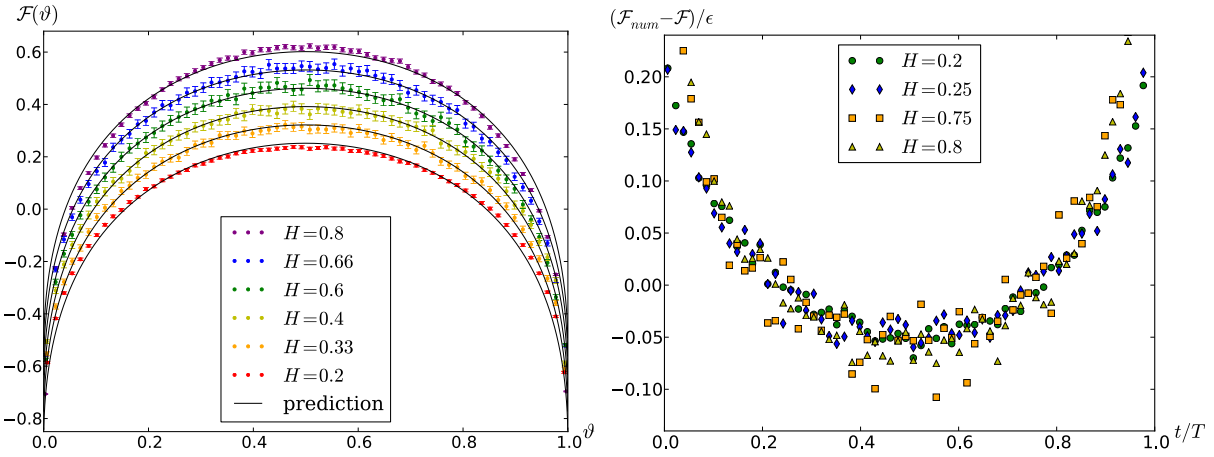

Figure 2.7: Left: Numerical estimation of $\mathcal{F}$ for different values of H on a discrete system of size $N = 2^{12}$, using 10^8 realizations. Plain curves represent the theoretical prediction (2.42), vertically translated for better visualization. Error bars are 2σ estimates. Note that for $H = 0.6$, $H = 0.66$ and $H = 0.8$ the expansion parameter ε is positive, while for $H = 0.4$, $H = 0.33$ and $H = 0.2$ it is negative. Right: Deviation for large $|\varepsilon|$ between the theoretical prediction (2.42) and the numerical estimations (2.67), rescaled by ε as in Eq. (2.68). These curves collapse for different values of H, allowing for an estimate of the $O(\varepsilon^2)$ correction to $\mathcal{P}_H^T(t)$, as written in Eq. (2.69).

2.4.1 The third arcsine Law

For the distribution of $t_{\max}$, we want to test our analytical results given in Eqs. (2.41)-(2.42). Fig. 2.3 shows the good agreement between theory and numerics. To perform a more precise comparison, we extract from the numerically computed distribution $P_{\rm num}^{T,H}(t)$ an estimation $\mathcal{F}_{\rm num}^{\varepsilon}$ of the function $\mathcal{F}$ as

$$\mathcal{F}_{\rm num}^{\varepsilon}\left(\frac{t}{T}\right) := \frac{1}{\varepsilon}\ln\left(\mathcal{P}_{\rm num}^{T,H}(t)\times[t(T-t)]^H\right) . \tag{2.67}$$

This function should converge, as $\varepsilon \to 0$, to the theoretical prediction (2.42). Obviously, statistical errors become relevant in this limit due to the factor of ε^{-1}, while for larger ε we expect to see deviation due to order-ε^2 (and larger) corrections, which are not taken into account in our analytical computations. As can be seen on Fig. 2.7, our numerical and analytical results are in *remarkable* agreement for all values of H studied, both for ε *positive* and *negative*. This means in particular that even for large values of ε ($H = 0.8$ or $H = 0.2$ in the cases studied here), the order-ε correction is large as compared to higher-order corrections.

The precision of our simulations allows us to numerically investigate these subleading $O(\varepsilon^2)$ corrections, extracted as follows,

$$\mathcal{F}_2^{\varepsilon}(\vartheta) = \frac{1}{\varepsilon}\left[\mathcal{F}_{\rm num}^{\varepsilon}(\vartheta) - \mathcal{F}(\vartheta)\right] = \frac{1}{\varepsilon^2}\ln\left(\frac{\mathcal{P}_{\rm num}^{T,H}(t)[t(T-t)]^H}{e^{\varepsilon\mathcal{F}(\vartheta)}}\right) . \tag{2.68}$$

This is shown in Fig. 2.7 (right). The collapse of the curves for different values of ε (once rescaled by ε^{-1}), suggests that there exists a function $\mathcal{F}_2(\vartheta)$, which would be the limit as $\varepsilon \to 0$ of $\mathcal{F}_2^{\varepsilon}(\vartheta)$, such that the probability distribution can be written as

$$\mathcal{P}_{H=\frac{1}{2}+\varepsilon}^T(t) = \frac{e^{\varepsilon\mathcal{F}(\vartheta)+\varepsilon^2\mathcal{F}_2(\vartheta)}}{[t(T-t)]^H} + O(\varepsilon^3) . \tag{2.69}$$

Our estimation of $\mathcal{F}_2$ is plotted on figure 2.7 (right). Our perturbative approach and its diagrammatic representation allows us to write the integrals needed to compute $\mathcal{F}_2$ analytically; this, however, is left for future work. This numerical study of the ε^2-order corrections is also used to compare $t_{\max}$ and t_+ distributions in figure 3.5.

2.4.2 The distribution of the maximum

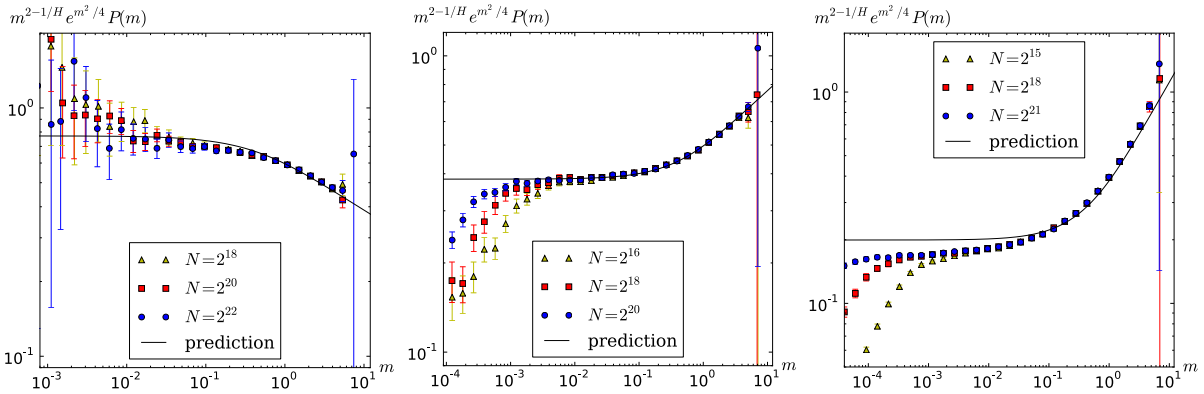

Figure 2.8: Middle: The combination (2.71) for $H = 0.6$. The plain line is the analytical prediction $\exp(\varepsilon[\mathcal{G}(m/\sqrt{2}) + 4\ln m] + \text{cst})$ of the distribution of the maximum without its small-scale power law and large-scale Gaussian behavior. The symbols are numerical estimations for $T = 1$ of the same quantity $m^{2-1/H}\exp(m^2/4)P^{T=1,H}_{\text{num}}(m)$ for different sample sizes. At small scale discretization errors appear. At large scales the statistics is poor due to the Gaussian prefactor. For the four decades in between theory and numerics are in very good agreement. Left: *ibid* for $H = 0.4$. Right *ibid* for $H = 0.75$. In all cases, the large scale-behavior on both plots is consistent with $m^{2\varepsilon}$.

For the distribution of the maximum we rewrite formula (2.45) such that the small-m behavior reproduces the exact scaling result (2.28) without changing the result at ε-order,

$$f_H(y) = \sqrt{\frac{2}{\pi}} y^{\frac{1}{H}-2} e^{-\frac{y^2}{2}} e^{\varepsilon[\mathcal{G}(y)+4\ln y+\text{cst}]} + O(\varepsilon^2)\ . \tag{2.70}$$

To extract the non-trivial contribution from numerical simulations, we study for $T = 1$ (see Fig. 2.8)

$$m^{2-\frac{1}{H}} e^{\frac{m^2}{4}} \mathcal{P}^{1,H}_{\text{num}}(m) = e^{\varepsilon\left[\mathcal{G}\left(\frac{m}{\sqrt{2}}\right)+4\ln m+\text{cst}\right]} + O(\varepsilon^2)\ . \tag{2.71}$$

The left-hand side is evaluated from the normalized binned distribution of the maximum for each fBm path, denoted $\mathcal{P}^{1,H}_{\text{num}}(m)$. The right-hand side is the analytical result; the constant term is evaluated by numerical integration such that $f_H(y)$, given in Eq. (2.70), is normalized to 1.

The sample size N (i.e. lattice spacing $\mathrm{d}t = N^{-1}$) of the discretized fBm used for this numerical test is important, as the samples recover Brownian behavior for m smaller than a cutoff of order N^{-H}. This can be understood by assuming that the typical value of the first discretized point $X_{1/N}$ is of order N^{-H}; thus for $m \ll N^{-H}$,

$$P^{1,H}_{\text{num}}(m) \sim \text{prob}(X_{1/N} = m) \sim m^0 \tag{2.72}$$

Far small H the system size necessary to obtain the asymptotic behavior at small scale is very large, so we focus our tests on $H > 0.4$. Figure 2.8 presents results for $H = 0.4$, $H = 0.6$ and

$H = 0.75$, without any fitting parameter. As predicted, convergence to the small-scale behavior is quite slow. For example, in the $H = 0.6$ plot the convergence to the small-scale behavior is somewhere between 10^{-1} and 10^{-2} (in dimensionless variables where we rescaled the total time to $T = 1$). This might lead to a wrong numerical estimation of the persistence exponent or other related quantities, if the crossover to the large-scale behavior is not properly taken into account. At large scales, the numerical data on Fig. 2.8 grow as $m^{2\varepsilon}$, consistent with the prediction (2.50).

As stated, for $H < 0.5$ the numerical simulations do not allow us to investigate the small-scale behavior of the distribution, as can be seen for $H = 0.4$ on figure 2.8. Nevertheless, the agreement with the theoretical prediction is good in the crossover region and in the beginning of the tail. The numerical prefactor of the small-scale power law is also very sensitive to numerical errors (and probably to ε^2-corrections) due to a vanishing probability when $m \to 0$ for $H < 0.5$, as can be seen in Fig. 2.4.

2.5 Conclusions

To conclude this chapter, we presented a perturbative approach for the extreme-value statistics of fractional Brownian motion. This allows to derive the first analytical results for generic values of H in the range $0 < H < 1$, beyond scaling relations. The main, and most general result is the joint probability of the value of the maximum and the time when this maximum is reached, conditioned on the value of the end point, as given in Eq. (2.34). From this, we extracted simpler result, as the unconditioned distribution of the value of the maximum, as well as distribution of the time when this maximum is reached. These two distributions have non-trivial features, which we compared to numerical simulations. The remarkable agreement of the simulations with our predictions is a valuable check of our method. It also shows that the perturbative approach gives surprisingly good results, even far form the expansion point $H = \frac{1}{2}$.

2.A Details on the perturbative expansion

We explicit here details on the steps transforming Eq. (2.21) into Eq. (2.23). We have to deal with terms of the form

$$\begin{aligned}\int_{X_0=x_1}^{X_t=x_2}\mathcal{D}[X]\Theta[X]\dot{X}_0 e^{-S_0[X]} &= \lim_{\delta\to 0}\int_{X_0=x_1}^{X_t=x_2}\mathcal{D}[X]\Theta[X]\frac{X_\delta - x_1}{\delta}e^{-S_0[X]}\\ &= \lim_{\delta\to 0}\int_0^\infty \mathrm{d}x\frac{x-x_1}{\delta}P_0^+(x_1,x,\delta)P_0^+(x,x_2,t-\delta)\\ &= \lim_{\delta\to 0}\int_0^\infty \mathrm{d}x\, 2\partial_x P_0^+(x_1,x,\delta)P_0^+(x,x_2,t-\delta)\\ &= \int_0^\infty \mathrm{d}x\,\delta(x-x_1)2\partial_x P_0^+(x,x_2,t)\\ &= 2\partial_{x_1}P_0^+(x_1,x_2,t)\ .\end{aligned} \tag{2.73}$$

We first introduced a discretized version of the derivative, then expressed the path integral in terms of propagators, did an integration by parts and finally took the limit of $\delta\to 0$.

With this result we can express every path integral in Eq. (2.21) in terms of the bare propagator $P_0^+(x_1,x_2,t)$,

$$\begin{aligned}Z_\gamma^+(m_1,t_1,x_0,t_2,m_2) = \frac{1}{2}\int_{t_1}^T d\tau_2\int_0^{t_1}d\tau_1\int_{x_1,x_2>0}\frac{1}{\tau_2-\tau_1}P_0^+(m_1,x_1,\tau_1)\\ \times\, 2\partial_{x_1}P_0^+(x_1,x_0,t_1-\tau_1)\,P_0^+(x_0,x_2,\tau_2-t_1)\,2\partial_{x_2}P_0^+(x_2,m_2,T-\tau_2)\ .\end{aligned} \tag{2.74}$$

We now use the identity $\frac{1}{\tau_2-\tau_1}=\int_{y>0}e^{-y(\tau_2-\tau_1)}$, and perform two Laplace transformations ($t_1\to s_1$ and $t_2\to s_2$). It is important to note that the time integrals are in general divergent at small times, thus we introduced a short-time cutoff τ in the action, cf. Eq. (5.7). The short-time cutoff τ corresponds to a large-y cutoff $\Lambda = e^{-\gamma_\mathrm{E}}/\tau$. This value is imposed by the following equality, valid for all $T>0$, in the limit of $\Lambda\to\infty$ and $\tau\to 0$:

$$\int_0^T \mathrm{d}t\int_0^\Lambda e^{-yt}\mathrm{d}y = \ln(T\Lambda)+\gamma_\mathrm{E}+O(e^{-T\Lambda})\overset{!}{=}\ln\left(\frac{T}{\tau}\right)=\int_\tau^T\frac{1}{t}\,\mathrm{d}t\ . \tag{2.75}$$

To simplify the computations, we introduce new time variables,

$$T_1=\tau_1,\ T_2=t_1-\tau_1,\ T_3=\tau_2-t_1,\ T_4=t_1+t_2-\tau_2\ . \tag{2.76}$$

This gives

$$\begin{aligned}\tilde{Z}_\gamma^+(s_1,s_2) = 2\int\limits_{t_1,t_2>0}e^{-s_1t_1-s_2t_2}\int\limits_{t_1}^{t_1+t_2}\mathrm{d}\tau_2\int\limits_0^{t_1}\mathrm{d}\tau_1\int\limits_0^\Lambda\mathrm{d}y\,e^{-y(\tau_2-\tau_1)}\,P_0^+(t_1)\,\partial P_0^+(\tau_1-t_1)\,P_0^+(\tau_2-t_1)\\ \times\,\partial P_0^+(t_1+t_2-\tau_2)\\ = 2\int_0^\Lambda\mathrm{d}y\int_{T_i>0}e^{-(T_1+T_2)s_1}e^{-(T_3+T_4)s_2}e^{-(T_2+T_3)y}\,P_0^+(T_1)\,\partial P_0^+(T_2)\,P_0^+(T_3)\,\partial P_0^+(T_4)\ .\end{aligned} \tag{2.77}$$

The space dependence (i.e. x_0, x_1, x_2 dependence) is omitted for notational clarity. The successive integrations over time variables transform this expression into a product of Laplace-transformed propagators with different Laplace variables,

$$\begin{aligned}\tilde{Z}_\gamma^+(m_1,s_1;x_0;m_2,s_2) = 2\int_0^\Lambda\mathrm{d}y\int_{x_1,x_2>0}\tilde{P}_0^+(m_1,x_1,s_1)\,\partial_{x_1}\tilde{P}_0^+(x_1,x_0,s_1+y)\\ \times\,\tilde{P}_0^+(x_0,x_2,s_2+y)\,\partial_{x_2}\tilde{P}_0^+(x_2,m_2,s_2)\ .\end{aligned} \tag{2.78}$$

This is the formula given in the main text in Eq. (2.23), apart that here we made explicit the large-y cutoff. As we will see, there is no large-y divergence here, which render the cutoff irrelevant. The other time orderings, corresponding to Z^+_α and Z^+_β, have a similar structure. For Z_α, this gives

$$Z^+_\alpha(m_1,t_1,x_0,t_2,m_2) = \frac{1}{2}\int_{\tau_1}^{t_1}\mathrm{d}\tau_2\int_0^{t_1}\mathrm{d}\tau_1 \int\limits_{x_1,x_2>0} \frac{P^+_0(m_1,x_1,\tau_1)\,2\partial_{x_1}P^+_0(x_1,x_2,\tau_2-\tau_1)\,2\partial_{x_2}P^+_0(x_2,x_0,t_1-\tau_2)\,P^+_0(x_0,m_2,t_2)}{\tau_2-\tau_1}\,. \tag{2.79}$$

This term is represented diagrammatically in Fig. 2.2 (right); computing the double Laplace transform gives

$$\tilde{Z}^+_\alpha(m_1,s_1;x_0;m_2,s_2) = \left[2\int_0^\Lambda \mathrm{d}y \int_{x_1,x_2>0} \tilde{P}^+_0(m_1,x_1,s_1)\,\partial_{x_1}\tilde{P}^+_0(x_1,x_2,s_1+y)\,\partial_{x_2}\tilde{P}^+_0(x_2,x_0,s_1)\right]\tilde{P}^+_0(x_0,m_2,s_2)\,. \tag{2.80}$$

In this case, the integrations affect only the first three propagators. The term in square brackets is the correction to the constrained propagator from m_1 to x_0, with Laplace variable s_1. This object was at the center of Ref. [125]; the results are recalled in the next appendix. Similarly for Z_β, after the Laplace transformations, the integrations affect only the last three propagators, giving

$$\tilde{Z}^+_\beta(x_0,s_1;x_0;m_2,s_2) = \tilde{P}^+_0(m_1,x_0,s_1)\left[2\int_0^\Lambda \mathrm{d}y \int_{x_1,x_2>0} \tilde{P}^+_0(x_0,x_1,s_2)\,\partial_{x_1}\tilde{P}^+_0(x_1,x_2,s_2+y)\,\partial_{x_2}\tilde{P}^+_0(x_2,x_0,s_2)\right]\,. \tag{2.81}$$

2.B Recall of the results for $Z^+_1(m,t)$

In Ref. [125], the propagator $Z^+(m,t)$ for fBm, conditioned to start at $x_0 \approx 0^+$, to remain positive, and to finish in m at time t was computed at order ε. For standard Brownian motion, this conditioned propagator is

$$Z^+_0(m,t) = \lim_{x_0\to 0}\frac{1}{x_0}P^+_0(x_0,m,t) = \frac{m e^{-\frac{m^2}{4t}}}{2\sqrt{\pi}t^{3/2}}\,. \tag{2.82}$$

The term x_0^{-1} is the normalisation (i.e. one divides by the conditional probability). The order-ε correction of this propagator is given in Eq. (51) of [125],

$$\begin{aligned} Z^+_1(m,t) =& Z^+_0(m,t)\left[\left(\frac{m^2}{2t}-2\right)\left(\ln(m^2)+\gamma_\mathrm{E}\right)+\mathcal{I}\left(\frac{m}{\sqrt{2t}}\right)+\ln(t)-2\gamma_\mathrm{E}\right] \\ =& Z^+_0(m,t)\left[\mathcal{I}(z)+z^2\left(\ln(2z^2)+\gamma_\mathrm{E}\right)+(z^2-1)\ln(t)-4\ln(z)-4\gamma_\mathrm{E}\right]\,. \end{aligned} \tag{2.83}$$

This result assumes a proper normalisation of Z^+_1 such that x_0 and $\ln(x_0)$ terms cancel, i.e. the limit $x_0 \to 0$ is well-defined, and the integral over m is equal to unity. We introduced $z := m/\sqrt{2t}$, and $\mathcal{I}$ is the combination of special functions defined in Eq. (2.35), and recalled in Eq. (2.167).

We can also use the diagrammatic rules introduced in section 2.2.4 to compute the Laplace-transformed correction to this propagator (without conditioning). This corresponds to the diagram represented in Fig. 2.2 (right) without the slice on the right,

$$\tilde{P}_1^+(x_0,m,s) = 2\int_0^\Lambda \mathrm{d}y \int_{x_1,x_2>0} \tilde{P}_0^+(x_0,x_1,s)\partial_{x_1}\tilde{P}_0^+(x_1,x_2,s+y)\partial_{x_2}\tilde{P}_0^+(x_2,m,s)\ . \tag{2.84}$$

This is the term appearing in the square brackets in Eqs. (2.80) and (2.81). The integrations over space can be done, giving the following integral, rescaling $y \to us$, and setting $m = 1$ for simplicity:

$$\tilde{P}_1^+(x_0,1,s) = \frac{1}{\sqrt{s}}\int_0^{\Lambda/s}\frac{\mathrm{d}u}{u^2}\Bigg\{ \left[(\sqrt{s}-1)\,u-2\right] e^{-\sqrt{s}}\sinh(\sqrt{s}x_0) - x_0 u\sqrt{s}\,e^{-\sqrt{s}}\cosh(\sqrt{s}x_0) \tag{2.85}$$

$$+ 2\sqrt{u+1}\left[e^{-\sqrt{s}\sqrt{u+1}}\cosh(\sqrt{s(u+1)}x_0) - e^{-\sqrt{s}(\sqrt{u+1}+x_0)} - e^{-\sqrt{s}(x_0\sqrt{u+1}+1)} + e^{-\sqrt{s}(x_0+1)}\right]\Bigg\}.$$

This is a logarithmically diverging integral at large u, which makes the UV cutoff necessary, cf. Appendix 2.A where we explicit the link between the y cutoff Λ and the time cutoff τ). Doing the integration over u, and then taking the limit $x_0 \to 0$ as well as expressing the cutoff Λ in term of τ gives

$$\frac{1}{x_0}\tilde{P}_1^+(x_0,m,s) \underset{x_0\to 0}{\simeq} e^{m\sqrt{s}}\left(m\sqrt{s}+1\right)\mathrm{Ei}\left(-2m\sqrt{s}\right) - e^{-m\sqrt{s}}\left(m\sqrt{s}+1\right)\ln(m\sqrt{s}) \tag{2.86}$$

$$+ m\sqrt{s}e^{-m\sqrt{s}}\left[\ln\left(\frac{m^2}{2\tau}\right)-1\right] + e^{-m\sqrt{s}}\left[\ln\left(\frac{\tau^2}{2x_0^4}\right) - 3\gamma_{\mathrm{E}} + 4\right]\ .$$

This expression in Laplace variables for the correction to the propagator is a new result (in [125], a more complicated transformation was used to derive Eq. (2.83)). The inverse Laplace transform can be done, using Eqs. (2.174)-(2.177) for the complicated terms,

$$\frac{P_1^+(x_0,m,t)}{P_0^+(x_0,m,t)} \underset{x_0\to 0}{\simeq} \mathcal{I}(z) + z^2\left[\ln(2z^2)+\gamma_{\mathrm{E}}\right] + (z^2-1)\left[\ln\left(\frac{t}{\tau}\right)-1\right] + \ln\left(\frac{\tau^2}{4x_0^4z^4}\right) - 4\gamma_{\mathrm{E}} + 2\ . \tag{2.87}$$

We still need to correct this with the rescaling of the diffusion constant, i.e. taking into account the order-ε correction in Eq. (2.12) given the expression of the diffusive constant (2.4). This gives

$$2t\partial_t P_0^+(x_0,m,t)[1+\ln(\tau)] = P_0^+(x_0,m,t)(z^2-3)[1+\ln(\tau)]. \tag{2.88}$$

A check of consistency is that this cancels all dependence on τ, and we find for the propagator at order ε,

$$P^+(x_0,m,t) \underset{x_0\to 0}{\simeq} \tag{2.89}$$

$$P_0^+(x_0,m,t)\Big\{1+\varepsilon\Big[\mathcal{I}(z)+z^2\left(\ln(2z^2)+\gamma_{\mathrm{E}}\right)+(z^2-1)\ln(t)-\ln\left(4x_0^4z^4\right)-4\gamma_{\mathrm{E}}\Big]\Big\}+O(\varepsilon^2)\ .$$

This propagator, integrated over m, reads, both in time and Laplace variables

$$\begin{aligned}
&\int_0^\infty \mathrm{d}m\,\tilde{P}_1^+(x_0,m,s) \underset{x_0\to 0}{\simeq} \frac{x_0}{\sqrt{s}}\left(3-3\gamma_{\mathrm{E}}-\ln(4s\tau)+\ln\left(\frac{\tau^2}{x_0^4}\right)\right)\ ,\\
&\int_0^\infty \mathrm{d}m\,P_1^+(x_0,m,t) \underset{x_0\to 0}{\simeq} \frac{x_0}{\sqrt{\pi t}}\left(3-2\gamma_{\mathrm{E}}+\ln\left(\frac{t\tau}{x_0^4}\right)\right)\ .
\end{aligned} \tag{2.90}$$

2.C Computation of the new correction Z_γ^+

Outline of the Calculation

We present here details of the calculation of Z_γ^+, starting from its expression in Laplace variables (2.23), graphically represented in Fig. 2.2. First, we introduce the notation

$$\begin{aligned}\mathcal{S}(m,x_0,s,y) &:= \frac{1}{x_0}\int_0^\infty \mathrm{d}x\, \tilde{P}_0^+(m,x,s)\,\partial_x \tilde{P}_0^+(x,x_0,s+y) \\ &= \frac{1}{x_0}\frac{e^{-(m-x_0)\sqrt{s+y}} - e^{-(m+x_0)\sqrt{s+y}} + 2e^{-x_0\sqrt{s+y}-m\sqrt{s}} - e^{-(m-x_0)\sqrt{s}} - e^{-(m+x_0)\sqrt{s}}}{2y}\,.\end{aligned} \tag{2.91}$$

The expression of $\tilde{P}_0^+$ is given in Eq. (2.24). We see from Eq. (2.23) that one can write $\tilde{Z}_\gamma^+(m_1,s_1;x_0;m_2,s_2)$ as

$$\tilde{Z}_\gamma^+(m_1,s_1;x_0;m_2,s_2) = -2x_0^2\int_{y>0}\mathcal{S}(m_1,x_0,s_1,y)\mathcal{S}(m_2,x_0,s_2,y)\,. \tag{2.92}$$

The minus sign comes from an integration by parts. It is interesting to look at the asymptotics of $\mathcal{S}$ in the limit of $x_0 \to 0$,

$$\mathcal{S}(m,x_0,s,y) \underset{x_0\to 0}{\simeq} \frac{1}{y}\left(e^{-m\sqrt{s+y}}\sqrt{s+y} - e^{-m\sqrt{s}}\sqrt{s+y}\right) \underset{y\to\infty}{\sim} \frac{e^{-m\sqrt{s}}}{\sqrt{y}}\,. \tag{2.93}$$

This implies that the $x_0 \to 0$ limit *can not* be taken before integrating over y, as this induces a new large-y, i.e. short-time divergence. Taking this limit before integration, and regularizing the new divergence with the large-y cutoff Λ would lead to a wrong result. This is expected as the scaling of the result in terms of x_0 depends on H, thus inducing a $\ln(x_0)$ term at order ε.

In the following, we note $\mathcal{S} = \bar{\mathcal{S}} + \delta\mathcal{S}$ with

$$\begin{aligned}\bar{\mathcal{S}}(m,x_0,s,y) &:= \frac{1}{x_0}\frac{e^{-(m-x_0)\sqrt{s+y}} - e^{-(m+x_0)\sqrt{s+y}} + 2e^{-(x_0+m)\sqrt{s}} - e^{-(m-x_0)\sqrt{s}} - e^{-(m+x_0)\sqrt{s}}}{2y}\,, \\ \delta\mathcal{S}(m,x_0,s,y) &:= \frac{1}{x_0}\frac{e^{-x_0\sqrt{s+y}-m\sqrt{s}} - e^{-x_0\sqrt{s}-m\sqrt{s}}}{y}\,.\end{aligned} \tag{2.94}$$

Denoting $\mathcal{S}_i := \mathcal{S}(m_i,x_0,s_i,y)$, the integration over y is a sum of four terms (with the last two related by exchanging points 1 and 2),

$$\int_{y>0}\mathcal{S}_1\mathcal{S}_2 = \int_{y>0}\bar{\mathcal{S}}_1\bar{\mathcal{S}}_2 + \int_{y>0}\delta\mathcal{S}_1\delta\mathcal{S}_2 + \int_{y>0}\bar{\mathcal{S}}_1\delta\mathcal{S}_2 + \int_{y>0}\bar{\mathcal{S}}_2\delta\mathcal{S}_1\,. \tag{2.95}$$

This leads to the following decomposition of $Z_\gamma^+(m_1,t_1;x_0;m_2,t_2)$,

$$Z_\gamma^+ = x_0^2\big[Z_A(m_1,t_1;m_2,t_2) + Z_B(m_1,t_1;x_0;m_2,t_2) + Z_C(m_1,t_1;m_2,t_2) + Z_C(m_2,t_2;m_1,t_1)\big]\,, \tag{2.96}$$

with

$$\begin{aligned}Z_A(m_1,s_1;m_2,s_2) &= -2\mathcal{L}^{-1}_{s_2\to t_2}\circ\mathcal{L}^{-1}_{s_1\to t_1}\Big[\lim_{x_0\to 0}\int_{y>0}\bar{\mathcal{S}}(m_1,x_0,s_1,y)\bar{\mathcal{S}}(m_2,x_0,s_2,y)\Big]\,, \\ Z_B(m_1,s_1;x_0;m_2,s_2) &= -2\mathcal{L}^{-1}_{s_2\to t_2}\circ\mathcal{L}^{-1}_{s_1\to t_1}\Big[\lim_{x_0\to 0}\int_{y>0}\delta\mathcal{S}(m_1,x_0,s_1,y)\delta\mathcal{S}(m_2,x_0,s_2,y)\Big]\,, \\ Z_C(m_1,s_1;m_2,s_2) &= -2\mathcal{L}^{-1}_{s_2\to t_2}\circ\mathcal{L}^{-1}_{s_1\to t_1}\Big[\lim_{x_0\to 0}\int_{y>0}\bar{\mathcal{S}}(m_1,x_0,s_1,y)\delta\mathcal{S}(m_2,x_0,s_2,y)\Big]\,.\end{aligned} \tag{2.97}$$

We anticipate here that Z_A and Z_C have a well-defined $x_0 \to 0$ limit, and only Z_B has a divergence (as shown later). The next step consists in computing these three integrals over y, taking the limit of small x_0, and performing the inverse Laplace transforms *w.r.t.* s_1 and s_2. The order of these manipulations can sometimes be inverted to simplify the calculations.

The term Z_A

In the first term of Eq. (2.97) it is possible to take the $x_0 \to 0$ limit inside the integral, as this integrand converges fast enough for large y, given the asymptotic of $\bar{\mathcal{S}}$,

$$\bar{\mathcal{S}} \underset{x_0\to 0}{\simeq} \frac{e^{-m\sqrt{s+y}}\sqrt{s+y} - e^{-m\sqrt{s}}\sqrt{s}}{y} \ . \tag{2.98}$$

This gives

$$\int_{y>0} \bar{\mathcal{S}}_1\bar{\mathcal{S}}_2 \underset{x_0\to 0}{\simeq} \int_{y>0} \frac{\left(e^{-m_1\sqrt{s_1+y}}\sqrt{s_1+y} - e^{-m_1\sqrt{s_1}}\sqrt{s_1}\right)\left(e^{-m_2\sqrt{s_2+y}}\sqrt{s_2+y} - e^{-m_2\sqrt{s_2}}\sqrt{s_2}\right)}{y^2} \ . \tag{2.99}$$

We can do the inverse Laplace transformations $s_1 \to t_1$ and $s_2 \to t_2$ before integrating over y, using

$$\mathcal{L}^{-1}_{s\to t}\left[-e^{-m\sqrt{s+y}}\sqrt{s+y}\right] = \frac{e^{-\frac{m^2}{4t}}}{2\sqrt{\pi}t^{3/2}}\left(1-\frac{m^2}{2t}\right)e^{-ty} \ . \tag{2.100}$$

One thus finds

$$\mathcal{L}^{-1}_{s_2\to t_2}\circ\mathcal{L}^{-1}_{s_1\to t_1}\int_{y>0}\bar{\mathcal{S}}_1\bar{\mathcal{S}}_2 \underset{x_0\to 0}{\simeq} \frac{e^{-\frac{m_1^2}{4t_1}-\frac{m_2^2}{4t_2}}}{4\pi t_1^{3/2}t_2^{3/2}}\left(1-\frac{m_1^2}{2t_1}\right)\left(1-\frac{m_2^2}{2t_2}\right)\int_{y>0}\frac{(1-e^{-t_1y})(1-e^{-t_2y})}{y^2} \ . \tag{2.101}$$

Integrating over y and using the definition of Z_A, the final result for this term is

$$Z_A(m_1,t_1;m_2,t_2) = \frac{e^{-\frac{m_1^2}{4t_1}-\frac{m_2^2}{4t_2}}}{2\pi(t_1t_2)^{3/2}}\left(1-\frac{m_1^2}{2t_1}\right)\left(1-\frac{m_2^2}{2t_2}\right)\Big[t_1\ln(t_1)+t_2\ln(t_2)-(t_1+t_2)\ln(t_1+t_2)\Big] \ . \tag{2.102}$$

The term Z_B

For the second term of Eq. (2.97), the limit $x_0 \to 0$ cannot be taken inside the integral, as

$$\delta\mathcal{S} = \frac{1}{x_0}\frac{e^{-x_0\sqrt{s+y}-m\sqrt{s}} - e^{-x_0\sqrt{s}-m\sqrt{s}}}{y} \underset{x_0\to 0}{\simeq} \frac{e^{-m\sqrt{s}}}{y}(\sqrt{s}-\sqrt{s+y}) \underset{y\to\infty}{\sim} -\frac{e^{-m\sqrt{s}}}{\sqrt{y}} \ . \tag{2.103}$$

However, we can extract the diverging part by writing

$$\int_{y>0}\delta\mathcal{S}_1\delta\mathcal{S}_2 = e^{-m_1\sqrt{s_1}-m_2\sqrt{s_2}}\ln(x_0^{-2}+1) + \int_{y>0}\left[\delta\mathcal{S}_1\delta\mathcal{S}_2 - \frac{e^{-m_1\sqrt{s_1}-m_2\sqrt{s_2}}}{y+1}\,\Theta(y<x_0^{-2})\right] \ . \tag{2.104}$$

This expression is constructed such that for all $x_0 > 0$ the term added outside the integral and the term subtracted inside the integral cancel. The diverging part when $x_0 \to 0$ is now the

term outside the integral and the integral has a finite limit when $x_0 \to 0$. To proceed, denote $\mathcal{K} := e^{-m_1\sqrt{s_1}-m_2\sqrt{s_2}}$. We then decompose the integral as a sum of three terms,

$$\begin{aligned}\int_{y>0}\left[\delta\mathcal{S}_1\delta\mathcal{S}_2-\frac{\mathcal{K}}{y+1}\Theta(y<x_0^{-2})\right]&=\int_0^{x_0^{-2}}\mathrm{d}y\left[\delta\mathcal{S}_1\delta\mathcal{S}_2-\mathcal{K}\frac{(\sqrt{s_1+y}-\sqrt{s_1})(\sqrt{s_2+y}-\sqrt{s_2})}{y^2}\right]\\&+\mathcal{K}\int_0^{x_0^{-2}}\mathrm{d}y\left[\frac{(\sqrt{s_1+y}-\sqrt{s_1})(\sqrt{s_2+y}-\sqrt{s_2})}{y^2}-\frac{1}{y+1}\right]\\&+\int_{x_0^2}^{\infty}\mathrm{d}y\,\delta\mathcal{S}_1\delta\mathcal{S}_2\ .\end{aligned}\tag{2.105}$$

In the second term we can take the limit of $x_0 \to 0$ to obtain (without the $\mathcal{K}$ factor in front)

$$\begin{aligned}&\int_{y>0}\left[\frac{(\sqrt{s_1+y}-\sqrt{s_1})(\sqrt{s_2+y}-\sqrt{s_2})}{y^2}-\frac{1}{y+1}\right]\\&\quad=-\left(2+\sqrt{\frac{s_1}{s_2}}+\sqrt{\frac{s_2}{s_1}}\right)\ln\left(\sqrt{s_1}+\sqrt{s_1}\right)+\frac{1}{2}\sqrt{\frac{s_1}{s_2}}\ln(s_1)+\frac{1}{2}\sqrt{\frac{s_2}{s_1}}\ln(s_2)-1+\ln(4)\ .\end{aligned}\tag{2.106}$$

For the first and third term, we first perform a rescaling of the integration variable ($y \to x_0^{-2}v$) and then take the limit of $x_0 \to 0$,

$$\int_0^{x_0^{-2}}\mathrm{d}y\left[\delta\mathcal{S}_1\delta\mathcal{S}_2-\mathcal{K}\frac{(\sqrt{s_1+y}-\sqrt{s_1})(\sqrt{s_2+y}-\sqrt{s_2})}{y^2}\right]\underset{x_0\to0}{\simeq}\mathcal{K}\int_0^1\mathrm{d}v\left[\frac{\left(e^{-\sqrt{v}}-1\right)^2}{v^2}-\frac{1}{v}\right]\ ,$$

$$\int_{x_0^2}^{\infty}\mathrm{d}u\,\delta\mathcal{S}_1\delta\mathcal{S}_2\underset{x_0\to0}{\simeq}\mathcal{K}\int_1^{\infty}\mathrm{d}v\frac{\left(e^{-\sqrt{v}}-1\right)^2}{v^2}\ .\tag{2.107}$$

The sum of the last two contributions in the limit of $x_0 \to 0$ is

$$\mathcal{K}\int_1^{\infty}\mathrm{d}v\frac{\left(e^{-\sqrt{v}}-1\right)^2}{v^2}+\mathcal{K}\int_0^1\mathrm{d}v\left[\frac{\left(e^{-\sqrt{v}}-1\right)^2}{v^2}-\frac{1}{v}\right]=\mathcal{K}\left[3-2\gamma_{\mathrm{E}}-2\ln(4)\right]\ .\tag{2.108}$$

Summing all these contribution gives

$$\begin{aligned}\int_{y>0}\delta\mathcal{S}_1\delta\mathcal{S}_2\underset{x_0\to0}{\simeq}e^{-m_1\sqrt{s_1}-m_2\sqrt{s_2}}\Big[&-\left(2+\sqrt{\frac{s_1}{s_2}}+\sqrt{\frac{s_2}{s_1}}\right)\ln\left(\sqrt{s_1}+\sqrt{s_2}\right)\\&+\sqrt{\frac{s_1}{s_2}}\ln\left(\sqrt{s_1}\right)+\sqrt{\frac{s_2}{s_1}}\ln\left(\sqrt{s_2}\right)-2\ln(2x_0)+2-2\gamma_{\mathrm{E}}\Big]\ .\end{aligned}\tag{2.109}$$

We now need a series of Inverse Laplace transforms obtained in appendix 2.G. To deal with the double Laplace inversion, we start with formula (2.172) and use the special function $\mathcal{J}$ defined in Eq. (2.168). Using commutativity of derivation and integration with the Laplace transform, we can use the identity

$$\left(2+\sqrt{\frac{s_1}{s_2}}+\sqrt{\frac{s_2}{s_1}}\right)e^{-m_1\sqrt{s_1}-m_2\sqrt{s_2}}=(\partial_{m_1}+\partial_{m_2})\left(\int_{m_1}+\int_{m_2}\right)e^{-m_1\sqrt{s_1}-m_2\sqrt{s_2}}\tag{2.110}$$

to obtain

$$\begin{aligned}&\mathcal{L}^{-1}_{s_2\to t_2}\circ\mathcal{L}^{-1}_{s_1\to t_1}\left[e^{-m_1\sqrt{s_1}-m_2\sqrt{s_2}}\left(2+\sqrt{\frac{s_1}{s_2}}+\sqrt{\frac{s_2}{s_1}}\right)\ln\left(\sqrt{s_1}+\sqrt{s_2}\right)\right]\\&\quad=(\partial_{m_1}+\partial_{m_2})^2\left\{\frac{e^{-\frac{m_2^2}{4t_2}-\frac{m_1^2}{4t_1}}}{\pi\sqrt{t_1t_2}}\left[\mathcal{J}\left(\frac{(m_2t_1+m_1t_2)^2}{4t_1t_2(t_1+t_2)}\right)+\frac{1}{2}\ln\left(\frac{1}{4t_1}+\frac{1}{4t_2}\right)-\frac{\gamma_{\mathrm{E}}}{2}\right]\right\}\ .\end{aligned}\tag{2.111}$$

For the other terms, the inverse Laplace transforms are decoupled, and can be computed from Eq. (2.173). We get

$$\mathcal{L}^{-1}_{s_2\to t_2}\circ\mathcal{L}^{-1}_{s_1\to t_1}\left[e^{-m_1\sqrt{s_1}-m_2\sqrt{s_2}}\sqrt{\frac{s_1}{s_2}}\ln\left(\sqrt{s_1}\right)\right] \tag{2.112}$$
$$=\partial^2_{m_1}\left\{\frac{e^{-\frac{m_2^2}{4t_2}-\frac{m_1^2}{4t_1}}}{\pi\sqrt{t_1t_2}}\left[\mathcal{J}\left(\frac{m_1^2}{4t_1}\right)+\frac{1}{2}\ln\left(\frac{1}{4t_1}\right)-\frac{\gamma_{\rm E}}{2}\right]\right\}.$$

The sum of all terms, with a prefactor of -2 coming from the definition of Z_B, is

$$Z_B(m_1,t_1;x_0;m_2,t_2)=\frac{m_1m_2e^{-\frac{m_2^2}{4t_2}-\frac{m_1^2}{4t_1}}}{2\pi(t_1t_2)^{3/2}}[2\ln(2x_0)-2+2\gamma_{\rm E}] \tag{2.113}$$
$$+2(\partial_{m_1}+\partial_{m_2})^2\left\{\frac{e^{-\frac{m_2^2}{4t_2}-\frac{m_1^2}{4t_1}}}{\pi\sqrt{t_1t_2}}\left[\mathcal{J}\left(\frac{(m_2t_1+m_1t_2)^2}{4t_1t_2(t_1+t_2)}\right)+\frac{1}{2}\ln\left(\frac{1}{4t_1}+\frac{1}{4t_2}\right)-\frac{\gamma_{\rm E}}{2}\right]\right\}$$
$$-2\,\partial^2_{m_1}\left\{\frac{e^{-\frac{m_2^2}{4t_2}-\frac{m_1^2}{4t_1}}}{\pi\sqrt{t_1t_2}}\left[\mathcal{J}\left(\frac{m_1^2}{4t_1}\right)+\frac{1}{2}\ln\left(\frac{1}{4t_1}\right)-\frac{\gamma_{\rm E}}{2}\right]\right\}+(1\leftrightarrow 2)\,.$$

The derivatives can be computed explicitly, using the relation between $\mathcal{I}$ and $\mathcal{J}$ given in Eq. (2.169),

$$\partial^2_{m_1}\left\{\frac{e^{-\frac{m_2^2}{4t_2}-\frac{m_1^2}{4t_1}}}{\pi\sqrt{t_1t_2}}\left[\mathcal{J}\left(\frac{m_1^2}{4t_1}\right)+\frac{1}{2}\ln\left(\frac{1}{4t_1}\right)-\frac{\gamma_{\rm E}}{2}\right]\right\}= \tag{2.114}$$
$$-\frac{e^{-\frac{m_2^2}{4t_2}-\frac{m_1^2}{4t_1}}}{4\pi(t_1t_2)^{3/2}}t_2\left[\mathcal{I}\left(\frac{m_1}{\sqrt{2t_1}}\right)+\left(\frac{m_1^2}{2t_1}-1\right)\left(\ln(4t_1)+\gamma_{\rm E}\right)\right].$$

The same result holds for the term involving $\partial^2_{m_2}$. For the term involving simultaneously m_1 and m_2, we can use almost the same trick,

$$(\partial_{m_1}+\partial_{m_2})^2\left[e^{-\frac{m_2^2}{4t_2}-\frac{m_1^2}{4t_1}}\mathcal{J}\left(\frac{(m_2t_1+m_1t_2)^2}{4t_1t_2(t_1+t_2)}\right)\right] \tag{2.115}$$
$$=\frac{t_1+t_2}{4t_1t_2}e^{-\frac{m_2^2}{4t_2}-\frac{m_1^2}{4t_1}}\left[2(z^2-1)\mathcal{J}\left(\frac{z^2}{2}\right)-2(2z^2-1)\mathcal{J}'\left(\frac{z^2}{2}\right)+2z^2\mathcal{J}''\left(\frac{z^2}{2}\right)\right]$$
$$=-\frac{t_1+t_2}{4t_1t_2}e^{-\frac{m_2^2}{4t_2}-\frac{m_1^2}{4t_1}}\mathcal{I}\left(\frac{m_1t_2+m_2t_1}{\sqrt{2t_1t_2(t_1+t_2)}}\right).$$

The second line is the explicit derivative of the first line, expressed for simplicity in terms of the variable

$$z=\frac{m_1t_2+m_2t_1}{\sqrt{2t_1t_2(t_1+t_2)}}\,. \tag{2.116}$$

The combination of $\mathcal{J}$ and its derivatives appearing in the second line is exactly the function $\mathcal{I}$, as can be checked from Eq. (2.169). After these simplifications,

$$\begin{aligned} Z_B(m_1,t_1;x_0;m_2,t_2) &\underset{x_0\to 0}{\simeq} \frac{e^{-\frac{m_2^2}{4t_2}-\frac{m_1^2}{4t_1}}}{2\pi(t_1t_2)^{3/2}}\Bigg\{2m_1m_2\big[\ln(2x_0)+\gamma_{\rm E}-1\big] \\ &+ t_2\left[\mathcal{I}\Big(\frac{m_1}{\sqrt{2t_1}}\Big)+\left(\frac{m_1^2}{2t_1}-1\right)\big(\ln(4t_1)+\gamma_{\rm E}\big)\right]+t_1\left[\mathcal{I}\Big(\frac{m_2}{\sqrt{2t_2}}\Big)+\left(\frac{m_2^2}{2t_2}-1\right)\big(\ln(4t_2)+\gamma_{\rm E}\big)\right] \\ &- (t_1+t_2)\left[\mathcal{I}(z)+\Big(z^2-1\Big)\left(\ln\Big(\frac{4t_1t_2}{t_1+t_2}\Big)+\gamma_{\rm E}\Big)\right]\Bigg\}. \end{aligned} \tag{2.117}$$

The term Z_C

For this term, we can take the limit $x_0 \to 0$ inside the integral, as it converges for large y using asymptotics (2.98) and (2.103), giving

$$\int_{y>0}\bar{\mathcal{S}}_1\delta\mathcal{S}_2 \underset{x_0\to 0}{\simeq} e^{-m_2\sqrt{s_2}}\int_{y>0}\frac{e^{-m_1\sqrt{s_1+y}}\sqrt{s_1+y}-e^{-m_1\sqrt{s_1}}\sqrt{s_1}}{y}\,\frac{\sqrt{s_2}-\sqrt{s_2+y}}{y}\,. \tag{2.118}$$

To compute the Laplace inversion $s_1 \to t_1$, we use Eq. (2.100)

$$\begin{aligned} \mathcal{L}^{-1}_{s_1\to t_1}\left[\int_{y>0}\tilde{\mathcal{S}}_1\delta\mathcal{S}_2\right] &= \frac{e^{-\frac{m_1^2}{4t_1}}}{2\sqrt{\pi}t_1^{3/2}}\left(\frac{m_1^2}{2t_1}-1\right)e^{-m_2\sqrt{s_2}}\int_{y>0}\frac{(1-e^{-t_1y})(\sqrt{s_2+y}-\sqrt{s_2})}{y^2} \\ &= \frac{e^{-\frac{m_1^2}{4t_1}}}{2\sqrt{\pi}t_1^{3/2}}\left(\frac{m_1^2}{2t_1}-1\right)\frac{e^{-m_2\sqrt{s_2}}}{\sqrt{s_2}}\int_{v>0}\frac{(1-e^{-t_1s_2v})(\sqrt{v+1}-1)}{v^2}\,. \end{aligned} \tag{2.119}$$

We changed variables $y \to s_2 v$ between the two lines. To perform the inverse Laplace transform with respect to s_2, we need

$$\mathcal{L}^{-1}_{s_2\to t_2}\left[\frac{e^{-m_2\sqrt{s_2}}}{\sqrt{s_2}}e^{-t_1s_2v}\right] = \theta(t_2-vt_1)\frac{e^{-\frac{m_2{}^2}{4(t_2-vt_1)}}}{\sqrt{\pi(t_2-vt_1)}}\,. \tag{2.120}$$

Finally, to compute Z_C, only the integration over v remains to be done,

$$\begin{aligned} Z_C(m_1,t_1;t_2,m_2) &= -\frac{e^{-\frac{m_1^2}{4t_1}}}{\sqrt{\pi}t_1^{3/2}}\left(\frac{m_1^2}{2t_1}-1\right)\int_{v>0}\left(\frac{e^{-\frac{m_2{}^2}{4t_2}}}{\sqrt{\pi t_2}}-\Theta(t_2-vt_1)\frac{e^{-\frac{m_2{}^2}{4(t_2-vt_1)}}}{\sqrt{\pi(t_2-vt_1)}}\right)\frac{\sqrt{v+1}-1}{v^2} \\ &= -\frac{e^{-\frac{m_1^2}{4t_1}}e^{-\frac{m_2^2}{4t_2}}}{2\pi(t_1t_2)^{3/2}}(m_1^2-2t_1)\frac{t_2}{t_1}\int_{v>0}\left(1-\Theta\Big(\frac{t_2}{t_1}-v\Big)\frac{e^{-\frac{m_2^2}{4t_2}\left(\frac{1}{1-vt_1/t_2}-1\right)}}{\sqrt{1-v\frac{t_1}{t_2}}}\right)\frac{\sqrt{v+1}-1}{v^2} \\ &= -\frac{e^{-\frac{m_1^2}{4t_1}}e^{-\frac{m_2^2}{4t_2}}}{2\pi(t_1t_2)^{3/2}}(m_1^2-2t_1)\left[\nu\int_0^\nu \mathrm{d}v\left(1-\frac{e^{-a\left(\frac{1}{1-v/\nu}-1\right)}}{\sqrt{1-v/\nu}}\right)\frac{\sqrt{v+1}-1}{v^2}+\nu\int_\nu^\infty \mathrm{d}v\,\frac{\sqrt{v+1}-1}{v^2}\right]; \end{aligned} \tag{2.121}$$

here we have introduced $\nu = t_2/t_1$ and $a = m_2^2/(4t_2)$. Thus the following integrals needs to be computed,

$$I_1(a,\nu) = \nu\int_0^\nu \mathrm{d}v\left(1-\frac{e^{-a\left(\frac{1}{1-v/\nu}-1\right)}}{\sqrt{1-v/\nu}}\right)\frac{\sqrt{v+1}-1}{v^2} \quad\text{and}\quad I_2(\nu) = \nu\int_\nu^\infty \mathrm{d}v\,\frac{\sqrt{v+1}-1}{v^2}\,. \tag{2.122}$$

The term I_2 is easy,

$$I_2(\nu) = \nu \int_\nu^\infty \mathrm{d}v \, \frac{\sqrt{v+1}-1}{v^2} = \sqrt{\nu+1} - 1 + \nu \, \mathrm{asinh}\left(\frac{1}{\sqrt{\nu}}\right) = \sqrt{\frac{t_1+t_2}{t_1}} - 1 + \frac{t_2}{t_1} \, \mathrm{asinh}\left(\sqrt{\frac{t_1}{t_2}}\right) . \tag{2.123}$$

The other integral is more involved. To evaluate it, we perform a change of variables

$$\begin{aligned} I_1(a,\nu) &= \nu \int_0^\nu \mathrm{d}v \, \left(1 - \frac{e^{-a\left(\frac{1}{1-v/\nu}-1\right)}}{\sqrt{1-\frac{v}{\nu}}}\right) \frac{\sqrt{v+1}-1}{v^2} \\ &= \int_0^\infty \mathrm{d}x \, \left(\frac{1}{\sqrt{x+1}} - e^{-ax}\right) \frac{\sqrt{(\nu+1)x+1} - \sqrt{x+1}}{x^2} . \end{aligned} \tag{2.124}$$

To simplify the integrand, we then take its second derivative with respect to a,

$$\begin{aligned} \partial_a^2 I_1(a,\nu) &= -\int_0^\infty \mathrm{d}x \, e^{-ax} \left(\sqrt{(\nu+1)x+1} - \sqrt{x+1}\right) \\ &= -\frac{\sqrt{\pi}\left(\sqrt{\nu+1}e^{\frac{a}{\nu+1}}\mathrm{erfc}\left(\sqrt{\frac{a}{\nu+1}}\right) - e^a \mathrm{erfc}\left(\sqrt{a}\right)\right)}{2a^{3/2}} . \end{aligned} \tag{2.125}$$

The function

$$f(a) = \frac{1}{2}\mathcal{I}\left(\sqrt{2a}\right) + 3a - 1 + a\ln(a) , \tag{2.126}$$

where $\mathcal{I}$ is defined in (2.167), satisfies

$$f''(a) = -\frac{\sqrt{\pi}}{2}\frac{e^a}{a^{3/2}}\mathrm{erfc}(\sqrt{a}) . \tag{2.127}$$

We can then express the second derivative of I_1 in terms of f,

$$\partial_a^2 I_1(a,\nu) = \frac{1}{1+\nu} f''\left(\frac{a}{1+\nu}\right) - f''(a) . \tag{2.128}$$

After two integrations over a we obtain, with yet unknown functions $A(\nu)$ and $B(\nu)$,

$$I_1(a,\nu) = (\nu+1)\, f\left(\frac{a}{\nu+1}\right) - f(a) + B(\nu)a + A(\nu) . \tag{2.129}$$

The small-a behavior of f can be obtained as

$$f(a) = 2\sqrt{\pi}\sqrt{a} + a\ln(a) - \frac{2\sqrt{\pi}}{3}a^{3/2} + \frac{a^2}{3} + O(a^{5/2}) . \tag{2.130}$$

We can compare this to the limit when a goes to 0 of the initial integral to determinate the integration constants A and B. The limit is computed by taking the limit inside the integral, with result

$$\lim_{a\to 0} I_1(a,\nu) = 1 - \sqrt{\nu+1} + \frac{1}{2}(\nu+1)\ln(\nu+1) - \vartheta \ln\left(\sqrt{\nu+1}+1\right) . \tag{2.131}$$

Finally, we get

$$\begin{aligned} I_1\left(\frac{m_2^2}{4t_2}, \frac{t_2}{t_1}\right) &= \left(1+\frac{t_2}{t_1}\right) f\left(\frac{{m_2}^2}{4t_2}\frac{t_1}{t_2+t_1}\right) - f\left(\frac{{m_2}^2}{4t_2}\right) \\ &\quad + 1 - \sqrt{\frac{t_2+t_1}{t_1}} + \frac{t_2+t_1}{t_1}\ln\left(\sqrt{\frac{t_2+t_1}{t_1}}\right) - \frac{t_2}{t_1}\ln\left(\sqrt{\frac{t_2+t_1}{t_1}}+1\right) . \end{aligned} \tag{2.132}$$

This has been checked numerically with excellent precision.

There are a few terms that cancel between I_1 and I_2, and expressing asinh in terms of ln, and f in terms of $\mathcal{I}$ finally gives

$$Z_C(m_1,t_1;m_2,t_2) = \frac{e^{-\frac{m_1^2}{4t_1}}e^{-\frac{m_2^2}{4t_2}}}{2\pi(t_1t_2)^{3/2}}\left(1-\frac{m_1^2}{2t_1}\right)\Big[(t_1+t_2)\,\mathcal{I}\Big(\frac{m_2}{\sqrt{2t_2}}\sqrt{\frac{t_1}{t_2+t_1}}\Big) \\ -t_1\mathcal{I}\Big(\frac{m_2}{\sqrt{2t_2}}\Big) - 2t_2 + t_1\left(\frac{{m_2}^2}{2t_2}-1\right)\ln\Big(\frac{t_1}{t_2+t_1}\Big) + t_2\ln\Big(\frac{t_1+t_2}{t_2}\Big)\Big]\,. \tag{2.133}$$

We computed numerically the double Laplace transform of (2.133), and checked with high precision agreement with (2.118), where the integral over y is evaluated numerically.

2.D Correction to the third arcsine Law

As stated in the main text, the distribution of $t_{\max}$ can be extracted from our path integral (2.1) as follows:

$$\mathcal{P}_H^T(t) = \lim_{x_0\to 0}\frac{1}{Z^{\mathrm{N}}(T,x_0)}\int_{m_1,m_2>0} Z^+(m_1,t;x_0;m_2,T-t)\,. \tag{2.134}$$

The order-0 contribution (2.13) gives for the normalisation

$$Z^{\mathrm{N}}(x_0,T) = \int_0^T \mathrm{d}t\int_{m_1,m_2>0} Z_0^+(m_1,t;x_0;m_2,T-t) + O(\varepsilon) \underset{x_0\to 0}{\simeq} x_0^2 + O(\varepsilon)\,. \tag{2.135}$$

We recover the well-known *Arcsine Law* distribution for standard Brownian motion,

$$\mathcal{P}_{\frac12}^T(t) = \lim_{x_0\to 0}\frac{\int_{m_1,m_2>0} Z_0^+(m_1,t;x_0;m_2,T-t)}{x_0^2} = \int_{m_1,m_2>0}\frac{m_1m_2e^{-\frac{m_1^2}{4t_1}-\frac{m_2^2}{4t_2}}}{4\pi t_1^{3/2}t_2^{3/2}} = \frac{1}{\pi\sqrt{t(T-t)}}\,. \tag{2.136}$$

Let us now write every term in the ε-expansion: $Z^{\mathrm{N}} = Z^{\mathrm{N}}_{(0)} + \varepsilon Z^{\mathrm{N}}_{(1)} + O(\varepsilon^2)$ and $Z^+ = Z^+_{(0)} + \varepsilon Z^+_{(1)} + O(\varepsilon^2)$. It is important to note that these terms slightly differ from those in Eq. (2.7), where the expansion was done with respect to the non-local perturbation in the action. As computed in Eq. (2.15), the term Z_0^+ contains some order-ε correction, contrary to $Z^+_{(0)}$ which is defined as the constant part of Z^+ in its ε expansion.

Using these new notations, we have

$$\begin{aligned}\mathcal{P}_H^T(t) &= \lim_{x_0\to 0}\frac{\int Z^+_{(0)}}{Z^{\mathrm{N}}_{(0)}}\left[1+\varepsilon\left(\frac{\int Z^+_{(1)}}{\int Z^+_{(0)}} - \frac{Z^{\mathrm{N}}_{(1)}}{Z^{\mathrm{N}}_{(0)}}\right)\right] + O(\varepsilon^2) \\ &= \mathcal{P}^T_{\frac12}(t)\lim_{x_0\to 0}\left[1+\varepsilon\left(\frac{\int Z^+_{(1)}}{\int Z^+_{(0)}} - \frac{Z^{\mathrm{N}}_{(1)}}{Z^{\mathrm{N}}_{(0)}}\right)\right] + O(\varepsilon^2)\,,\end{aligned} \tag{2.137}$$

where $\int$ symbol implicitly denotes integration over m_1 and m_2. The normalisation ensures that the correction to the probability

$$\delta\mathcal{P}^T(t) = \mathcal{P}^T_{\frac12}(t)\lim_{x_0\to 0}\left(\frac{\int Z^+_{(1)}}{\int Z^+_{(0)}} - \frac{Z^{\mathrm{N}}_{(1)}}{Z^{\mathrm{N}}_{(0)}}\right) \tag{2.138}$$

does not change the normalisation, i.e. its integral over t vanishes.

To compute the order-ε correction to the distribution (2.136), we have to compute the integral over m_1 and m_2 of Z_α^+, as well as Z_β^+ and $Z_\gamma^+(m_1,t_1;x_0;m_2,t_2)$. The last term, computed in Appendix 2.C, was decomposed in four terms, see Eq. (2.96). The expressions for these terms are given in Eqs. (2.102), (2.117) and (2.133).Using the identity $\int_{z>0} e^{-\frac{z^2}{2}}(z^2-1)=0$, we find the simplifications

$$\int_{m_1,m_2>0} Z_A = \int_{m_1,m_2>0} Z_C = 0\ . \tag{2.139}$$

Thus, the only contribution of Z_γ^+ comes from Z_B, defined in (2.97),

$$\begin{aligned}\frac{1}{x_0^2}\int_{m_1,m_2>0} Z_\gamma^+(m_1,t_1;x_0;m_2,t_2) &= \int_{m_1,m_2>0} Z_B(m_1,t_1;x_0;m_2,t_2) \\ &= -\frac{2}{\pi\sqrt{t_1t_2}}\left[1+\ln\left(\frac{4t_1t_2}{t_1+t_2}\right)-2\ln(2x_0)+2\gamma_{\mathrm{E}}\right]+\frac{1}{t_1}+\frac{1}{t_2} \\ &\quad -\frac{t_1+t_2}{2\pi(t_1t_2)^{3/2}}\int_{m_1,m_2>0} e^{-\frac{m_1^2}{4t_1}-\frac{m_2^2}{4t_2}}\,\mathcal{I}\left(z=\frac{m_1t_2+m_2t_1}{\sqrt{2t_1t_2(t_1+t_2)}}\right)\end{aligned} \tag{2.140}$$

We have used the identity $\int_0^\infty \mathrm{d}z e^{-z^2/2}\mathcal{I}(z)=\sqrt{2\pi}$. To compute the last integral, we use relation (2.169), which in this case gives

$$\begin{aligned}&\frac{t_1+t_2}{2\pi(t_1t_2)^{3/2}}\int_{m_1,m_2>0} e^{-\frac{m_1^2}{4t_1}-\frac{m_2^2}{4t_2}}\mathcal{I}(z) \\ &\qquad = -\frac{2}{\pi\sqrt{t_1t_2}}\int_{m_1,m_2>0}(\partial_{m_1}+\partial_{m_2})^2\left[e^{-\frac{m_1^2}{4t_1}-\frac{m_2^2}{4t_2}}\mathcal{J}\left(\frac{(m_1t_2+m_2t_1)^2}{4t_1t_2(t_1+t_2)}\right)\right]\ .\end{aligned} \tag{2.141}$$

Only the cross term of the derivatives (i.e. the term with $2\partial_{m_1}\partial_{m_2}$) is not a total derivative and gives a non-zero contribution,

$$\frac{2}{\pi\sqrt{t_1t_2}}\int_{m_2>0} e^{-\frac{m_2^2}{4t_2}}\,\partial_{m_1}\mathcal{J}\left(\frac{(m_2t_1+m_1t_2)^2}{4t_1t_2\,(t_1+t_2)}\right)\bigg|_{m_1=0} = \frac{2}{\pi t_1}\arctan\left(\sqrt{\frac{t_2}{t_1}}\right)\ . \tag{2.142}$$

The final result for this correction is

$$\begin{aligned}\frac{1}{x_0^2}\int_{m_1,m_2>0} Z_\gamma^+(m_1,t_1;x_0;m_2,t_2) &= \frac{-2}{\pi\sqrt{t_1t_2}}\left[\ln\left(\frac{4t_1t_2}{t_1+t_2}\right)-2\ln(2x_0)+1+2\gamma_{\mathrm{E}}\right] \\ &\quad +\frac{1}{t_1}+\frac{1}{t_2}-\frac{2}{\pi t_1}\arctan\left(\sqrt{\frac{t_2}{t_1}}\right)-\frac{2}{\pi t_2}\arctan\left(\sqrt{\frac{t_1}{t_2}}\right)\ .\end{aligned} \tag{2.143}$$

The contributions to the correction from Z_α^+ and Z_β^+ are easily computed from their expressions in terms of propagators given in the main text, cf. Eqs. (2.19) and (2.20), and then using formula (2.90),

$$x_0^{-2}\int\limits_{m_1,m_2>0} P_0^+(x_0,m_1,t_1)P_1^+(x_0,m_2,t_2)+(1\leftrightarrow 2) \underset{x_0\to 0}{\simeq} \frac{1}{\pi\sqrt{t_1t_2}}\left[6-4\gamma_{\mathrm{E}}+\ln(t_1t_2)+\ln\left(\frac{\tau^2}{x_0^8}\right)\right]\ . \tag{2.144}$$

The last term of order ε comes from the rescaling of the diffusive constant, which was made explicit in Eq. (2.15),

$$2[1+\ln(\tau)](t_1\partial_{t_1}+t_2\partial_{t_2})\frac{1}{x_0^2}\int_{m_1,m_2>0} Z_0^+ = -2\frac{[1+\ln(\tau)]}{\pi\sqrt{t_1t_2}}\ . \tag{2.145}$$

Summing all these contributions at order ε, and taking into account the correction from normalisation gives the final result for the order-ε term of the probability,

$$\delta\mathcal{P}^T(t) = \frac{1}{\pi\sqrt{t_1 t_2}}\Bigg\{ -\ln(t_1 t_2) + \sqrt{\frac{t_1}{t_2}}\left[\pi - 2\arctan\left(\sqrt{\frac{t_1}{t_2}}\right)\right] + \sqrt{\frac{t_2}{t_1}}\left[\pi - 2\arctan\left(\sqrt{\frac{t_2}{t_1}}\right)\right] \\ + 2\ln(T) + 4 - 6\gamma_{\mathrm{E}} + \ln\left(\frac{\tau^2}{x_0^4}\right) - \frac{Z^N_{(1)}(T,x_0)}{x_0^2} - 2\big[1+\ln(\tau)\big]\Bigg\} , \tag{2.146}$$

with $t_1 = t$ and $t_2 = T - t$. As expected, the dependence in τ vanishes at the end of the computation, and the order ε of the normalisation factor $Z^N_{(1)}$ is fixed by the condition $\int_0^T \mathrm{d}t\, \delta P^T(t) = 0$, which gives

$$Z^N_{(1)} = x_0^2\big[8\ln(2) + 2 - 6\gamma_{\mathrm{E}} - 4\ln(x_0)\big] . \tag{2.147}$$

Equivalently, the constant term, i.e. the second line of Eq. (2.146), becomes $-8\ln(2)$. The interpretation of this result as well as a comparison to numerical simulations is presented in the main text.

2.E Correction to the maximum-value distribution

Similarly to the distribution of $t_{\max}$, the distribution of m can be computed from the path integral $Z^+(m_1, t_1, x_0, m_2, t_2)$. This is done by taking the limit of small x_0, the integral over m_2 and the integral over t_1 at $t_1 + t_2 = T$ fixed,

$$\mathcal{P}^T_H(m) = \lim_{x_0\to 0} \frac{1}{Z^{\mathrm{N}}(T,x_0)} \int_0^{m_2} \mathrm{d}m_2 \int_0^T \mathrm{d}t\, Z^+(m, t, x_0, m_2, T-t) . \tag{2.148}$$

It is useful to note that the integration over $t = t_1$ at fixed $T = t_1 + t_2$ can be replaced by taking the Laplace transform of Z^+ at equal arguments ($s_1 = s_2 = s$) and then performing the inverse Laplace transform $s \to T$. The normalisation $Z^{\mathrm{N}}(T, x_0)$ is the same as the one for the distribution of $P^T_H(t)$; expanding in ε thus gives the same structure as (2.137), with the $\int$ symbol now being the integrals over $m_2 > 0$ and $t_1 \in [0, T]$.

We start with the contribution of Z_γ. As before, the integral over m_2 of Z_A vanishes, so this term does not contribute. The correction from Z_B can be computed starting with Eq. (2.109), taken at equal Laplace variables (i.e. $s_1 = s_2 = s$),

$$\int_{m_2}\int_t Z_B = 4\frac{e^{-m\sqrt{s}}}{\sqrt{s}}\left[\ln(x_0) - 1 + \gamma_{\mathrm{E}} + 2\ln(2) + \ln(\sqrt{s})\right] . \tag{2.149}$$

To take the inverse Laplace transform, we use Eq. (2.174). This gives

$$\int_{m_2}\int_t Z_B = 4\frac{e^{-\frac{m^2}{4T}}}{\sqrt{\pi T}}\left[\mathcal{J}\left(\frac{m^2}{4T}\right) + \ln\left(\frac{4x_0}{\sqrt{T}}\right) + \frac{\gamma_{\mathrm{E}}}{2} - 1\right] . \tag{2.150}$$

For the contribution of Z_C, it is easier to compute the inverse Laplace transform of Eq. (2.118) ($s_1 = s_2 = s \to T$) before integrating over y. This gives

$$\int_{m_2}\int_t Z_C = -2\frac{e^{-\frac{m^2}{4T}}}{\sqrt{\pi T}}\int_0^\infty \frac{\mathrm{d}y}{y^2}\left[e^{-\frac{m^2}{4T}y}\left(\sqrt{1+y} - 1 - y\right) + \sqrt{1+y} - 1\right] . \tag{2.151}$$

Let us define

$$I_C(a) := \int_0^\infty \frac{\mathrm{d}u}{u^2} \left(e^{-au} \left(\sqrt{1+u} - 1 - u \right) + \sqrt{1+u} - 1 \right) \ . \tag{2.152}$$

After deriving twice *w.r.t.* a, then integrating twice, and fixing the integration constants, we get

$$\begin{aligned} I_C(a) = {} & \gamma_{\mathrm{E}} + 1 + \ln(4) + a[3 - \gamma_{\mathrm{E}} - \ln(4)] \\ & - \frac{a^2}{3}\, {}_2F_2\left(1, 1; \frac{5}{2}, 3; a\right) + \frac{\pi}{2}(2a-1)\mathrm{erfi}(\sqrt{a}) - e^a\sqrt{\pi a} + (1-a)\ln(a) \ . \end{aligned} \tag{2.153}$$

We can express this in terms of the special function $\mathcal{I}$,

$$I_C\left(\frac{z^2}{2}\right) = \gamma_{\mathrm{E}} + 2 + \ln(4) - \frac{z^2}{2}\left[\gamma_{\mathrm{E}} + \ln(4)\right] - \frac{1}{2}\mathcal{I}(z) + \left(1 - \frac{z^2}{2}\right)\ln\left(\frac{z^2}{2}\right) \ , \tag{2.154}$$

This has been checked numerically. The final result for this correction is, with $z := m/\sqrt{2T}$,

$$\int_{m_2}\int_t Z_C = \frac{e^{-\frac{z^2}{2}}}{\sqrt{\pi T}}\left[\mathcal{I}(z) + (z^2-2)\left(\gamma_{\mathrm{E}} + \ln\left(2z^2\right)\right) - 4\right] \ . \tag{2.155}$$

The last corrections are: $x_0^{-2}\int_{m_2}\int_t Z_\alpha^+$ and $x_0^{-2}\int_{m_2}\int_t Z_\beta^+$. The first one is easy to compute using the results for the correction to the propagator recalled in Eq. (2.90), and the inverse Laplace transform (2.174),

$$\begin{aligned} & \frac{1}{x_0^2}\int_0^T \mathrm{d}t \int_0^\infty \mathrm{d}m_2\, P_0^+(x_0, m, t) P_1^+(x_0, m_2, T-t) \\ & \qquad \underset{x_0\to 0}{\simeq} \mathcal{L}^{-1}_{s\to T}\left[\frac{e^{-m\sqrt{s}}}{\sqrt{s}}\left(3 - \ln(4s\tau) - 3\gamma_{\mathrm{E}} + \ln\left(\frac{\tau^2}{x_0^4}\right)\right)\right] \\ & \qquad \underset{x_0\to 0}{\simeq} \frac{e^{-\frac{m^2}{4T}}}{\sqrt{\pi T}}\left[-2\,\mathcal{J}\left(\frac{m^2}{4T}\right) + \ln\left(\frac{T}{\tau}\right) + 2 - 2\gamma_{\mathrm{E}} + \ln\left(\frac{\tau^2}{x_0^4}\right)\right] \ . \end{aligned} \tag{2.156}$$

For the correction from Z_β^+, we start with the Laplace expression of the correction to the propagator (2.86), where the integration over m_2 simplifies the last slice to $\frac{x_0}{\sqrt{s}}$. Then, the needed inverse Laplace transformation is

$$\begin{aligned} & \frac{1}{x_0^2}\int_0^T \mathrm{d}t \int_0^\infty \mathrm{d}m_2\, P_1^+(x_0, m, t) P_0^+(x_0, m_2, T-t) \\ & \qquad \underset{x_0\to 0}{\simeq} \frac{1}{x_0}\mathcal{L}^{-1}_{s\to T}\left[\frac{P_1^+(x_0, m, s)}{\sqrt{s}}\right] = \frac{e^{-\frac{m^2}{4T}}}{\sqrt{\pi T}}\left[-2\mathcal{J}\left(\frac{m^2}{4T}\right) + \frac{m^2}{2T}\ln\left(\frac{T}{\tau}\right) + 2 - 2\gamma_{\mathrm{E}} + \ln\left(\frac{\tau^2}{x_0^4}\right)\right] \ . \end{aligned} \tag{2.157}$$

The final result for this is obtained using Eqs. (2.174)-(2.177).

We now give a summary of all corrections, in the limit of $x_0 \to 0$:

$$x_0^{-2}\int_{t,m_2} P_1^+(x_0,m,t)P_0^+(x_0,m_2,t_2) \simeq \frac{e^{-\frac{m^2}{4T}}}{\sqrt{\pi T}}\left[-2\mathcal{J}\left(\frac{m^2}{4T}\right)+\frac{m^2}{2T}\ln\left(\frac{T}{\tau}\right)+2-2\gamma_{\rm E}+\ln\left(\frac{\tau^2}{x_0^4}\right)\right],$$

$$x_0^{-2}\int_{t,m_2} P_0^+(x_0,m,t)P_1^+(x_0,m_2,t_2) \simeq \frac{e^{-\frac{m^2}{4T}}}{\sqrt{\pi T}}\left[-2\mathcal{J}\left(\frac{m^2}{4T}\right)+\ln\left(\frac{T}{\tau}\right)+2-2\gamma_{\rm E}+\ln\left(\frac{\tau^2}{x_0^4}\right)\right],$$

$$\int_{t,m_2} Z_C(m,t;m_2,t_2) \simeq \frac{e^{-\frac{m^2}{4T}}}{\sqrt{\pi T}}\left[\mathcal{I}\left(\frac{m}{\sqrt{2T}}\right)+\left(\frac{m^2}{2T}-2\right)\left(\gamma_{\rm E}+\ln\left(\frac{m^2}{T}\right)\right)-4\right],$$

$$\int_{t,m_2} Z_B(m,t;m_2,t_2) \simeq \frac{e^{-\frac{m^2}{4T}}}{\sqrt{\pi T}}\left[4\mathcal{J}\left(\frac{m^2}{4T}\right)+4\ln\left(\frac{4x_0}{\sqrt{T}}\right)+2\gamma_{\rm E}-4\right],$$

$$\frac{4(1+\ln(\tau))}{x_0^2}\,T\partial_T\int_t\int_{m_2} Z_0^+ \simeq \frac{e^{-\frac{m^2}{4T}}}{\sqrt{\pi T}}\left[1+\ln(\tau)\left(\frac{m^2}{2T}-1\right)\right].$$

The last line is the correction to the diffusion constant, i.e. the order-ε term appearing in Eq. (2.15). The final result at order ε is

$$\int_{m_2}\int_t Z^+(m,t,m_2,T-t) \tag{2.158}$$
$$= \frac{e^{-\frac{m^2}{4T}}}{\sqrt{\pi T}}\left\{1+\varepsilon\left[\mathcal{I}\left(\frac{m}{\sqrt{2T}}\right)+\left(\frac{m^2}{2T}-2\right)\left(\gamma_{\rm E}+\ln\left(\frac{m^2}{T}\right)\right)+\left(\frac{m^2}{2T}-1\right)\ln(T)+\text{cst}\right]\right\}+O(\varepsilon^2)\,.$$

To better interpret the different terms, we recast the corrections, and especially those as $\frac{m^2}{2T}\ln(T)$ and $\ln(T)$, into an exponential form,

$$\frac{e^{-\frac{m^2}{4T}}}{\sqrt{\pi T}}\left[1+\varepsilon\left(\frac{m^2}{2T}-1\right)\ln(T)\right]+O(\varepsilon^2) = \frac{e^{-\frac{m^2}{4T}}}{\sqrt{\pi T}}e^{\varepsilon\frac{m^2}{2T}\ln(T)}T^{-\varepsilon}+O(\varepsilon^2) = \frac{e^{-\frac{m^2}{4T^{1+2\varepsilon}}}}{\sqrt{\pi}T^{1/2+\varepsilon}}+O(\varepsilon^2)\,. \tag{2.159}$$

This part of the correction gives the correct dimension to the variables in the order-0 result,

$$z=\frac{m}{\sqrt{2t}} \to y=\frac{m}{\sqrt{2}t^H}=\frac{m}{\sqrt{\langle x_t^2\rangle}}\,. \tag{2.160}$$

The other parts of the correction, which are a function of $z=\frac{m}{\sqrt{2t}}$ and which we call $\mathcal{G}(z)$, give a non-trivial change to the scaling function of the distribution,

$$\mathcal{P}_H^T(m) = \frac{e^{-\frac{m^2}{4T^{2H}}}}{\sqrt{\pi}T^H}e^{\varepsilon\left[\mathcal{G}\left(z=\frac{m}{\sqrt{2t}}\right)+\text{cst}\right]}+O(\varepsilon^2) = \frac{e^{-\frac{y^2}{2}}}{\sqrt{\pi}T^H}e^{\varepsilon[\mathcal{G}(y)+\text{cst}]}+O(\varepsilon^2)\,. \tag{2.161}$$

We changed the variable in $\mathcal{G}$ from z to y as it does not change the result at order ε and since it is more consistent in terms of dimensions. The function $\mathcal{G}$ is given by

$$\mathcal{G}(y)=\mathcal{I}(y)+(y^2-2)\left[\ln(2y^2)+\gamma_{\rm E}\right]\,. \tag{2.162}$$

The function $\mathcal{I}$ is regular at $y=0$, and its asymptotic behavior is given in Eq. (2.171); this gives the asymptotics for $\mathcal{G}$ as

$$\mathcal{G}(y)\sim\begin{cases}-2\ln(y) & \text{for } y\to\infty\\ -4\ln(y) & \text{for } y\to 0\,.\end{cases} \tag{2.163}$$

Since these asymptotics are logarithmic new power laws are obtained for the density distribution, both at $m \to 0$ and $m \to \infty$, which multiply the Gaussian term, with

$$\mathcal{P}^T_{\frac{1}{2}+\varepsilon}(m) \times e^{\frac{m^2}{4T^{1+2\varepsilon}}} \sim \begin{cases} m^{-4\varepsilon} \text{ for } m \to 0 \\ m^{-2\varepsilon} \text{ for } m \to \infty \ . \end{cases} \tag{2.164}$$

The constant term in Eq. (2.158) is fixed by normalisation. Instead of computing it at order ε, we can also evaluate it numerically such that (2.161) is exactly normalized, and not only at order ε. This is appropriate for numerical checks and the procedure we adopted for the latter.

2.F Correction to the survival distribution

To compute the survival probability up to time T of a fBm starting in m, we need to take the primitive function w.r.t. m of (2.158). We can deal with the terms involving $\mathcal{I}$ using (2.169); the difficult part comes from

$$\int_0^y \mathrm{d}m\, e^{-\frac{m^2}{2}}(2-m^2)\ln(m) \ . \tag{2.165}$$

To deal with this integration, we consider $e^{-\frac{m^2}{2}}m^a$, compute the primitive function *w.r.t.* m, and then take the derivative *w.r.t.* a, at $a = 0$ and $a = 2$.

The final result can be written as

$$S(y) = \mathrm{erf}\left(\frac{y}{\sqrt{2}}\right) + \varepsilon\mathcal{M}(y) + O(\varepsilon^2) \tag{2.166}$$

This is at leading order in ε equivalent to the exponentiated form given in the main text (2.53), with the function $\mathcal{M}$ given by Eq. (2.54).

2.G Special functions and some inverse Laplace transforms

In our computations there are two combinations of special functions which appear frequently, and which we denote $\mathcal{I}$ and $\mathcal{J}$. Their expressions in terms of hypergeometric functions and error functions are

$$\mathcal{I}(z) = \frac{z^4}{6}\,{}_2F_2\left(1,1;\frac{5}{2},3;\frac{z^2}{2}\right) + \pi(1-z^2)\mathrm{erfi}\left(\frac{z}{\sqrt{2}}\right) - 3z^2 + \sqrt{2\pi}e^{\frac{z^2}{2}}z + 2 \tag{2.167}$$

$$\mathcal{J}(x) = \frac{\pi}{2}\mathrm{erfi}\left(\sqrt{x}\right) - x\,{}_2F_2\left(1,1;\frac{3}{2},2;x\right) \tag{2.168}$$

These functions are linked by

$$\partial_z^2\left[e^{-\frac{z^2}{2}}\mathcal{J}\left(\frac{z^2}{2}\right)\right] = -\frac{1}{2}e^{-\frac{z^2}{2}}\mathcal{I}(z) \ . \tag{2.169}$$

It is useful to give their asymptotics, as their natural definition in terms of a series does not allow for an efficient evaluation at large arguments,

$$\mathcal{J}(x) \underset{x\to\infty}{\simeq} \frac{1}{2}\Big[\ln(4x) + \gamma_{\mathrm{E}}\Big] + \frac{1}{4x} - \frac{3}{16x^2} + \frac{5}{16x^3} - \frac{105}{128x^4} + O\left(\frac{1}{x^5}\right) \tag{2.170}$$

$$\mathcal{I}(z) \underset{z\to\infty}{\simeq} -z^2\left[\ln\left(2z^2\right) + \gamma_{\mathrm{E}}\right] + \ln(2z^2) + \gamma_{\mathrm{E}} + 3 + \frac{1}{2z^2} - \frac{1}{2z^4} + O\left(\frac{1}{z^5}\right) \ . \tag{2.171}$$

These functions appear in the inverse Laplace transforms involving $\ln(x)$ or $\mathrm{Ei}(x)$ functions. We give here the main non-trivial formulas used to deal with Laplace inversions:

$$\begin{aligned}\mathcal{L}^{-1}_{s_2\to t_2}\circ\mathcal{L}^{-1}_{s_1\to t_1}\left[e^{-m_1\sqrt{s_1}-m_2\sqrt{s_2}}\ln\left(\sqrt{s_1}+\sqrt{s_2}\right)\right] \\ = \partial_{m_1}\partial_{m_2}\left\{\frac{e^{-\frac{m_2^2}{4t_2}-\frac{m_1^2}{4t_1}}}{2\pi\sqrt{t_1t_2}}\left[2\mathcal{J}\left(\frac{(m_2t_1+m_1t_2)^2}{4t_1t_2\,(t_1+t_2)}\right)+\ln\left(\frac{1}{4t_1}+\frac{1}{4t_2}\right)-\gamma_{\mathrm{E}}\right]\right\},\end{aligned} \tag{2.172}$$

$$\mathcal{L}^{-1}_{s_2\to t_2}\circ\mathcal{L}^{-1}_{s_1\to t_1}\left[e^{-m_1\sqrt{s_1}-m_2\sqrt{s_2}}\ln\left(\sqrt{s_1}\right)\right] = \partial_{m_1}\partial_{m_2}\left\{\frac{e^{-\frac{m_2^2}{4t_2}-\frac{m_1^2}{4t_1}}}{2\pi\sqrt{t_1t_2}}\left[2\mathcal{J}\left(\frac{m_1^2}{4t_1}\right)-\ln(4t_1)-\gamma_{\mathrm{E}}\right]\right\}, \tag{2.173}$$

$$\mathcal{L}^{-1}_{s\to t}\left[\frac{e^{-m\sqrt{s}}}{m\sqrt{s}}\ln(m^2s)\right] = \frac{e^{-\frac{m^2}{4t}}}{m\sqrt{\pi t}}\left[2\mathcal{J}\left(\frac{m^2}{4t}\right)+\ln\left(\frac{m^2}{4t}\right)-\gamma_{\mathrm{E}}\right], \tag{2.174}$$

$$\mathcal{L}^{-1}_{s\to t}\left[m\sqrt{s}e^{-m\sqrt{s}}\ln(m^2s)\right] = \frac{me^{-\frac{m^2}{4t}}}{2\sqrt{\pi}t^{3/2}}\left\{-\mathcal{I}\left(\frac{m}{\sqrt{2t}}\right)+\left(\frac{m^2}{2t}-1\right)\left[\ln\left(\frac{m^2}{4t}\right)-\gamma_{\mathrm{E}}\right]\right\}, \tag{2.175}$$

$$\mathcal{L}^{-1}_{s\to t}\left[\frac{e^{m\sqrt{s}}}{m\sqrt{s}}\mathrm{Ei}\left(-2m\sqrt{s}\right)\right] = \frac{e^{-\frac{m^2}{4t}}}{2m\sqrt{\pi t}}\left[-2\mathcal{J}\left(\frac{m^2}{4t}\right)+\ln\left(\frac{m^2}{t}\right)+\gamma_{\mathrm{E}}\right], \tag{2.176}$$

$$\mathcal{L}^{-1}_{s\to t}\left[e^{m\sqrt{s}}\mathrm{Ei}\left(-2m\sqrt{s}\right)\right] = \frac{me^{-\frac{m^2}{4t}}}{4\sqrt{\pi}t^{3/2}}\left[2\mathcal{J}\left(\frac{m^2}{4t}\right)-\ln\left(\frac{m^2}{t}\right)-\gamma_{\mathrm{E}}-\frac{2\sqrt{\pi t}}{m}e^{\frac{m^2}{4t}}\mathrm{erfc}\left(\frac{m}{2\sqrt{t}}\right)\right]. \tag{2.177}$$

To derive Eq. (2.172), we start with an integral representation of the logarithm,

$$\ln\left(\sqrt{s_1}+\sqrt{s_2}\right) = \int_0^\infty\frac{\mathrm{d}\alpha}{\alpha}\left(e^{-\alpha}-e^{-\alpha(\sqrt{s_1}+\sqrt{s_2})}\right). \tag{2.178}$$

We compute now the inverse Laplace transform of this integral representation, with the exponential prefactor

$$\begin{aligned}&\mathcal{L}^{-1}_{s_2\to t_2}\circ\mathcal{L}^{-1}_{s_1\to t_1}\left[e^{-m_1\sqrt{s_1}-m_2\sqrt{s_2}}\left(e^{-\alpha}-e^{-\alpha(\sqrt{s_1}+\sqrt{s_2})}\right)\right] \\ &\quad=\frac{m_1m_2e^{-\frac{m_1^2}{4t_1}-\frac{m_2^2}{4t_2}}}{4\pi(t_1t_2)^{3/2}}\left[e^{-\alpha}-\left(1+\frac{\alpha}{m_2}\right)\left(1+\frac{\alpha}{m_2}\right)e^{-\alpha^2\left(\frac{1}{4t_1}+\frac{1}{4t_2}\right)-\alpha\left(\frac{m_1}{2t_1}+\frac{m_2}{2t_2}\right)}\right].\end{aligned} \tag{2.179}$$

To simplify this expression, it is useful to take the primitive with respect to m_1 and m_2,

$$\begin{aligned}\int_{m_1,m_2}\mathcal{L}^{-1}_{s_2\to t_2,s_1\to t_1}\left[e^{-m_1\sqrt{s_1}-m_2\sqrt{s_2}}\left(e^{-\alpha}-e^{-\alpha(\sqrt{s_1}+\sqrt{s_2})}\right)\right] \\ =\frac{e^{-\frac{m_2^2}{4t_2}-\frac{m_1^2}{4t_1}}}{\pi\sqrt{t_1t_2}}\frac{e^{-\alpha}-e^{-\alpha^2\left(\frac{1}{4t_1}+\frac{1}{4t_2}\right)-\alpha\left(\frac{m_1}{2t_1}+\frac{m_2}{2t_2}\right)}}{\alpha}.\end{aligned} \tag{2.180}$$

We still have to deal with the integration over α which is now an integral of the form

$$\int_{\alpha>0}\frac{e^{-\alpha}-e^{-\alpha^2A-\alpha B}}{\alpha}. \tag{2.181}$$

We can compute this integral by deriving w.r.t A, integrating over α, and then integrating over A; alternatively, we can use the same strategy with B. The two results are

$$\int_{\alpha>0} \frac{e^{-\alpha} - e^{-\alpha^2 A - \alpha B}}{\alpha} = \frac{1}{2}\Big[\pi\,\mathrm{erfi}\Big(\frac{B}{2\sqrt{A}}\Big) + \ln(A) - 2\ln(B) - \gamma_{\mathrm{E}}\Big] - \frac{B^2\,{}_2F_2\Big(1,1;\frac{3}{2},2;\frac{B^2}{4A}\Big)}{4A} + C_B\ , \tag{2.182}$$

$$\int_{\alpha>0} \frac{e^{-\alpha} - e^{-\alpha^2 A - \alpha B}}{\alpha} = \frac{\pi}{2}\mathrm{erfi}\Big(\frac{B}{2\sqrt{A}}\Big) - \frac{B^2\,{}_2F_2\Big(1,1;\frac{3}{2},2;\frac{B^2}{4A}\Big)}{4A} + C_A\ . \tag{2.183}$$

Thus

$$C_A - C_B = \frac{1}{2}\Big[\ln(A) - 2\ln(B) - \gamma_{\mathrm{E}}\Big]\ , \tag{2.184}$$

and the case $A = 0$, $B = 1$, allows us to conclude on $C_A = \frac{1}{2}\ln(A) - \frac{\gamma_{\mathrm{E}}}{2}$ and $C_B = \ln(B)$. The final result for the integral is

$$\begin{aligned}\int_{\alpha>0} \frac{e^{-\alpha} - e^{-\alpha^2 A - \alpha B}}{\alpha} &= \frac{\pi}{2}\mathrm{erfi}\Big(\frac{B}{2\sqrt{A}}\Big) - \frac{B^2\,{}_2F_2\Big(1,1;\frac{3}{2},2;\frac{B^2}{4A}\Big)}{4A} + \frac{1}{2}\ln(A) - \frac{\gamma_{\mathrm{E}}}{2} \\ &= \mathcal{J}\left(\frac{B^2}{4A}\right) + \frac{1}{2}\ln(A) - \frac{\gamma_{\mathrm{E}}}{2}\ .\end{aligned} \tag{2.185}$$

We checked this result numerically with very good precision.

Applying this formula to the integral over α and specifying $A = \frac{1}{4t_1} + \frac{1}{4t_2}$ and $B = \frac{m_1}{2t_1} + \frac{m_2}{2t_2}$, we obtain Eq. (2.172). The same computation, with $A = \frac{1}{4t_1}$, and $B = \frac{m_1}{2t_1}$ gives Eq. (2.173).

To derive Eq. (2.176) (with $m = 1$ for simplicity), we start with the integral representation of the exponential integral function,

$$e^{\sqrt{s}}\mathrm{Ei}\left(-2\sqrt{s}\right) = -\int_0^\infty \frac{e^{-\sqrt{s}-x}}{\sqrt{s}\,(2\sqrt{s}+x)}\,\mathrm{d}x = -\int_0^\infty \frac{e^{-\sqrt{s}(2y+1)}}{y+1}\mathrm{d}y\ . \tag{2.186}$$

Doing the inverse Laplace transform inside the integral leads to

$$\begin{aligned}\mathcal{L}^{-1}_{s\to t}\left[e^{\sqrt{s}}\mathrm{Ei}\left(-2\sqrt{s}\right)\right] &= -\int_0^\infty \frac{(2y+1)e^{-\frac{(2y+1)^2}{4t}}}{2\sqrt{\pi}t^{3/2}(y+1)}\mathrm{d}y = -\frac{e^{-\frac{1}{4t}}}{\sqrt{\pi}t^{3/2}}\int_0^\infty \frac{te^{-u}}{\sqrt{4tu+1}+1}\mathrm{d}u\ . \\ &= \frac{e^{-\frac{1}{4t}}\left[6t\left(\pi\mathrm{erfi}\left(\frac{1}{2\sqrt{t}}\right) + \ln(t) - \gamma + 2\right) - {}_2F_2\left(1,1;2,\frac{5}{2};\frac{1}{4t}\right)\right]}{24\sqrt{\pi}t^{5/2}} - \frac{1}{2t}\ .\end{aligned} \tag{2.187}$$

To express this result in terms of our special function $\mathcal{J}$, we can use the following relation between Hypergeometric functions,

$${}_2F_2\left(1,1;2,\frac{5}{2};a\right) = 3\,{}_2F_2\left(1,1;\frac{3}{2},2;a\right) - \frac{3\left[e^a\sqrt{\frac{\pi}{4a}}\mathrm{erf}(\sqrt{a}) - 1\right]}{a}\ . \tag{2.188}$$

This can be checked by Taylor expansion. With that, and the definition of $\mathcal{J}$ in Eq. (2.168), we obtain the announced result (2.177). Equation (2.176) is obtained from there by taking one derivative.

2.H Check of the covariance function

As a check of the action, we computed the two-point correlation function (i.e. the covariance function). The needed path integral is

$$\langle X_{t_1} X_{t_2} \rangle = \int_x \int_{X_0=0}^{X_T=x} \mathcal{D}[X] X_{t_1} X_{t_2} e^{-S[X]} \ . \tag{2.189}$$

At first order in ε, we can expand this path integral using Eq. (5.7) ,

$$\langle X_{t_1} X_{t_2} \rangle = \langle X_{t_1} X_{t_2} \rangle_0 + \frac{\varepsilon}{2} \int_0^{t-\tau} \mathrm{d}\tau_1 \int_{\tau_1+\tau}^{t} \mathrm{d}\tau_2 \frac{\left\langle X_{t_1} X_{t_2} \dot{X}_{\tau_1} \dot{X}_{\tau_2} \right\rangle_0}{\tau_2 - \tau_1} + O(\varepsilon^2) \ . \tag{2.190}$$

Here, averages $\langle \bullet \rangle_0$ are performed with the action $S_0[X]$ given in Eq. (2.9), i.e. the action of standard Brownian motion with diffusive constant $D_{\varepsilon,\tau} = 1 + 2\varepsilon[1 + \ln(\tau)] + O(\varepsilon^2)$. This action is quadratic, and using Wick contractions allows us to write

$$\langle X_{t_1} X_{t_2} \dot{X}_{\tau_1} \dot{X}_{\tau_2} \rangle_0 = 4\big(\min(t_1, t_2) \delta(\tau_1 - \tau_2) + \Theta(t_1 - \tau_1)\Theta(t_2 - \tau_2) + \Theta(t_1 - \tau_2)\Theta(t_2 - \tau_1) \big) + O(\varepsilon) \ . \tag{2.191}$$

In this equation, we used only the zeroth order for the diffusive constant ($D_{\varepsilon,\tau} = 1 + O(\varepsilon)$); the first term does not contribute since τ_1 and τ_2 do not coincide due to the time regularization.

The last two terms require to compute the integrals

$$\begin{aligned} \int_0^{\min(t_1, t_2-\tau)} \mathrm{d}\tau_1 \int_{\tau_1+\tau}^{t_2} \mathrm{d}\tau_2 \, \frac{1}{\tau_2 - \tau_1} + \int_0^{\min(t_2, t_1-\tau)} \mathrm{d}\tau_1 \int_{\tau_1+\tau}^{t_1} \mathrm{d}\tau_2 \frac{1}{\tau_2 - \tau_1} \\ = t_1 \ln(t_1) + t_2 \ln(t_2) - |t_1 - t_2| \ln|t_1 - t_2| - 2\min(t_1, t_2)(\ln(\tau) + 1) \ . \end{aligned} \tag{2.192}$$

We now sum all contributions to order ε, the Brownian result with the rescaled diffusive constant being $\langle X_{t_1} X_{t_2} \rangle_0 = 2D_{\varepsilon,\tau} \min(t_1, t_2)$. This gives

$$\begin{aligned} \langle X_{t_1} X_{t_2} \rangle &= 2D_{\varepsilon,\tau} \min(t_1, t_2) + 2\varepsilon \left(t_1 \ln(t_1) + t_2 \ln(t_2) - |t_1 - t_2| \ln|t_1 - t_2| \right) \\ &\quad - 4\varepsilon \min(t_1, t_2)(\ln(\tau) + 1) + O(\varepsilon^2) \\ &= 2\min(t_1, t_2) + 2\varepsilon \left(t_1 \ln(t_1) + t_2 \ln(t_2) - |t_1 - t_2| \ln|t_1 - t_2| \right) + O(\varepsilon^2) \\ &= t_1^{1+2\varepsilon} + t_2^{1+2\varepsilon} - |t_1 - t_2|^{1+2\varepsilon} + O(\varepsilon^2) \ . \end{aligned} \tag{2.193}$$

The τ dependence in the diffusive constant and in the first correction to the action cancel, and we recover the fBm correlation function at first order in ε. We also see that the correction to the diffusive constant is equivalent to setting $\ln(\tau) = -1$.

2.I The Davis and Harte algorithm

The numerical results presented in this thesis are obtained via the Davis and Harte algorithm which allows us to generate sample of fractional Brownian of size N with a computation time of order $N \ln(N)$. To present how it works, let's define $\gamma(k)$ the autocorrelation function of the fractional Brownian noise (i.e. the increments of the fractional Brownian motion):

$$\gamma(k) = \langle (X_{n+k+1} - X_{n+k})(X_{n+1} - X_n) \rangle = |k+1|^{2H} + |k-1|^{2H} - 2|k|^{2H} \tag{2.194}$$

where n is arbitrary as the fractional Brownian noise is a stationary process. To generate a Gaussian process, it is standard to compute the square root of it's auto-correlation matrix. Let's define

$$\begin{cases} r_k = \gamma(k) \text{ for } 0 \le k < N \\ r_N = 0 \\ r_k = \gamma(2N - k) \text{ for } N < k < 2N \end{cases} \ . \tag{2.195}$$

From fast Fourier transform, we can compute

$$\lambda_k = \sum_{j=0}^{2N-1} r_j \exp\left(2\pi i \frac{jk}{2N}\right) \ . \tag{2.196}$$

Then, we generate W_0, W_N, $V_k^{(1)}$ and $V_k^{(1)}$ (for $1 \leq k < N$) as independent, standard, normal random variables and define for $1 \leq k < N$

$$\left\{ \begin{array}{rl} W_k & = \frac{1}{\sqrt{2}} \left(V_k^{(1)} + i V_k^{(2)}\right) \\ W_{2N-k} & = \frac{1}{\sqrt{2}} \left(V_k^{(1)} - i V_k^{(2)}\right) \end{array} \right. \ . \tag{2.197}$$

Finally, we obtain a fractional Brownian noise sample as

$$Z_k = \frac{1}{\sqrt{2N}} \sum_{j=0}^{2N-1} \sqrt{\lambda_j} W_j \exp\left(2\pi i \frac{jk}{2N}\right) \ . \tag{2.198}$$

Z_k is defined for $0 \leq k < 2N$ but only the N first terms ($0 \leq k < N$) have the distribution of a fractional Brownian noise. Z_k for $N \leq k < 2N-1$ has also the distribution of a fractional Brownian noise but is not independent of the first sample, and so have no use in a numerical simulation.

To check that we have indeed generated a fractional Brownian noise, we need to verify that the sample as the right covariance function

$$\langle Z_n Z_{n+k} \rangle = \frac{1}{2N} \sum_{j_1, j_2 = 0}^{2N-1} \sqrt{\lambda_{j_1} \lambda_{j_2}} \, \langle W_{j_1} W_{j_2} \rangle \exp\left(2\pi i \frac{n j_1 + (n+k) j_2}{2N}\right) \ . \tag{2.199}$$

From the definition of W, we have

$$\begin{aligned} \langle W_k W_{2N-k} \rangle &= 1 \text{ for } 1 \leq k < N \\ \langle W_0 W_0 \rangle &= 1 \\ \langle W_N W_N \rangle &= 1 \ , \end{aligned} \tag{2.200}$$

all other correlations being zero. Using the symmetry of (r_k), we write the result of the fast Fourier transform as :

$$\lambda_j = \gamma(0) + 2 \sum_{l=1}^{N-1} \gamma(l) \cos\left(\pi \frac{lj}{N}\right) \tag{2.201}$$

and we note that $\lambda_k = \lambda_{2N-k}$ pour $1 \leq k < N$.

$$
\begin{aligned}
\langle Z_n Z_{n+k} \rangle &= \frac{1}{2N}\left[\lambda_0 + \lambda_N e^{-i\pi k} + \sum_{j=1}^{N-1}\sqrt{\lambda_j \lambda_{2N-j}}e^{2\pi i \frac{kj}{2N}} + \sum_{j=1}^{N-1}\sqrt{\lambda_{2N-j}\lambda_j}e^{-2\pi i \frac{kj}{2N}}\right] \\
&= \frac{1}{2N}\left[\lambda_0 + \lambda_N(-1)^k + 2\sum_{j=1}^{N-1}\lambda_j \cos\left(\pi\frac{kj}{N}\right)\right] \\
&= \frac{1}{2N}\Bigg[\gamma(0) + 2\sum_{l=1}^{N-1}\gamma(l) + (-1)^k\left(\gamma(0) + 2\sum_{l=1}^{N-1}\gamma(l)\cos(\pi l)\right) \\
&\qquad + 2\sum_{j=1}^{N-1}\left(\gamma(0) + 2\sum_{l=1}^{N-1}\gamma(l)\cos\left(\pi\frac{lj}{N}\right)\right)\cos\left(\pi\frac{kj}{N}\right)\Bigg] \\
&= \frac{1}{2N}\Bigg[\gamma(0)\left(1 + (-1)^k + 2\sum_{j=1}^{N-1}\cos\left(\pi\frac{kj}{N}\right)\right) \\
&\qquad + 2\sum_{l=1}^{N-1}\gamma(l)\left(1 + (-1)^{k+l} + 2\sum_{j=1}^{N-1}\cos\left(\pi\frac{lj}{N}\right)\cos\left(\pi\frac{kj}{N}\right)\right)\Bigg] \\
&= \gamma(k)
\end{aligned}
\tag{2.202}
$$

This proves that (Z_k) has the right distribution (i.e. it is Gaussian with right auto-correlation function) and we can obtain a fractional Brownian motion sample by simply taking the cumulative of (Z_k).

Chapter 3

The first and second arcsine laws

3.1 Presentation of the chapter

This chapter contains partially unpublished results from joint work with K. Wiese, T. Sadhu and myself, as well as results from [124]. We extend the perturbative expansion of the fBm, which allowed us to derive the new result for the distribution of $t_{\max}$ in chapter 2, to treat also the first two arcsine laws, i.e. the distributions of the observables t_+ and t_{last} as defined in the introduction, section 1.2.3. To this aim, we first derive in section 3.2 a generalized propagator containing information both on the position and the positive time for a standard Brownian motion. This is used as a starting point for the perturbative expansion of the distribution of t_+, similarly to chapter 2. Surprisingly we obtain the same result, at first order, as for the distribution of $t_{\max}$. Numerical simulations are in excellent agreement with this analytical result, and allow us to conjecture that a second order calculation should distinguish between the two distributions (the ones of t_+ and $t_{\max}$).

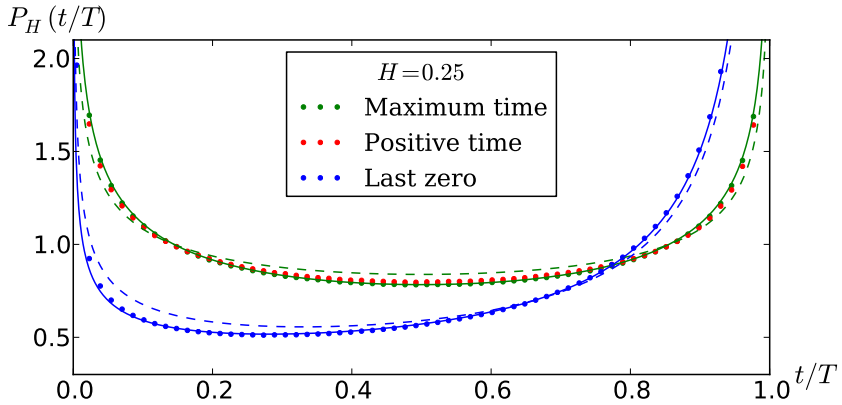

Figure 3.1: The three *Arcsin laws* for the fractional Brownian motion with $H = 1/4$. The dots represent results from numerical simulations, the dotted line the expected results from scaling (identical for the positive time and the maximum time) wherever the plain lines include the non-trivial corrections computed in this thesis, chapters 2 and 3.

The distribution of the time of the last zero requires a different approach, as there is no non-trivial correction at first-order. In section 3.4, using symmetry arguments, we compute the correction at second-order in ε, and compare it to numerics.

Even if it is not necessary to derive these results, we give in appendix 3.A the expression of the action at second order which should allow us to compute any observable defined for the fBm

at second order in ε.

3.2 Positive time of a Brownian motion

In this section, we investigate the distribution of the time spend up to time T by a Brownian motion X_t in the positive half space. This time, denoted t_+, is a random variable defined by

$$t_+ := \int_0^T \mathrm{d}t\, \Theta(X_t) \ , \tag{3.1}$$

where Θ is the Heaviside function: $\Theta(x) = 1$ if $x > 0$, and $\Theta(x) = 0$ otherwise.

Below, we first consider a discrete random walk and derive the Laplace transform (i.e. generating function) of the distribution of t_+ using combinatorial methods. Taking the continuous-time limit allows us to obtain the distribution of t_+ for Brownian motion, and recover the second arcsine law. This also gives us an explicit construction for the propagator with constraint on the value of t_+ for a standard Brownian motion, which we will use in our perturbative framework to obtain new results on the fractional Brownian motion.

3.2.1 Positive time of a discrete random walk

Consider a discrete random walk X_n with discrete steps ± 1 (without bias), starting at $X_0 = 0$. We denote $N_{n,x}$ the number of paths which go from 0 to x in n steps. This number is non-zero only if x and n have the same parity and x is smaller than n. It can be obtained by retaining the term of order q^x from the generating function for all paths, $(q + q^{-1})^n$, i.e.

$$\left(q + \frac{1}{q}\right)^n = \sum_{i=0}^{n} q^i \left(\frac{1}{q}\right)^{n-i} \binom{n}{i} \ . \tag{3.2}$$

Identifying $x = 2i - n$ yields

$$N_{n,x} = \binom{n}{\frac{n+x}{2}} \ . \tag{3.3}$$

It can also be deduced as follows: Paths ending in x have $n_+ = \frac{n+x}{2}$ up segments, and $n_- = \frac{n-x}{2}$ down segments. The number of paths with n_+ up segments is $\binom{n}{n_+}$, which again yields Eq. (3.3).

Denote by $N^+_{n,x}$ the number of *strictly positive paths*, i.e. $X_i > 0$ for all $i > 0$, which go from 0 to $x > 0$ in n steps. By the reflexion principle, illustrated on figure 3.2, this is the same as the number of paths that go from 1 to x in $n - 1$ steps, minus the number of paths which start at -1 and go to x in $n - 1$ steps,

$$N^+_{n,x} = N_{n-1,x-1} - N_{n-1,x+1} = \frac{x}{n} N_{n,x} \ . \tag{3.4}$$

The ratio

$$\frac{N^+_{n,x}}{N_{n,x}} = \frac{x}{n} \tag{3.5}$$

is the probability that a path from 0 to x in n steps is *strictly positive*, also known as the Ballot theorem[1].

[1] The ballot theorem states that if in an election candidate A receives p votes and candidate B receives q votes with $p > q$, the probability that A stays ahead of B throughout the count is $(p - q)/(p + q)$, see Refs. [129, 2].

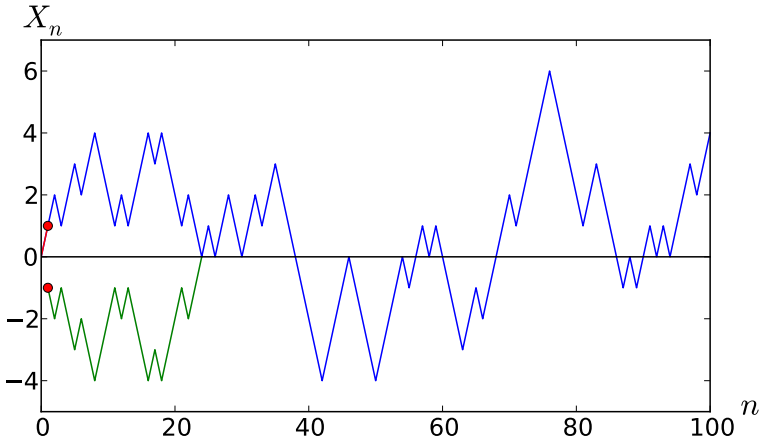

Figure 3.2: Illustration of the reflection principle: Every path emanating from 1 and attaining zero again (blue) is compensated by a *reflected* path emanating from -1 (green).

Another quantity of interest is the number of *excursions*, i.e. paths that go from $X_0 = 0$ to $X_{2n} = 0$ with all intermediate positions positive, and which we denote $N_{2n}^{+,\text{first}}$, because the end point is the first zero of the path. Such a path necessarily has $X_{2n-1} = 1$, which gives

$$N_{2n}^{+,\text{first}} = N_{2n-1,1}^{+} = \frac{1}{2n-1}\binom{2n-1}{n} = \frac{(2n-2)!}{n!(n-1)!} \,. \tag{3.6}$$

We now study the time when a random process is positive: A segment S_i from $i-1$ to i is considered *positive* if $X_{i-1} + X_i > 0$, and *negative* otherwise. Note that contrary to the positions X_i, a segment S_i is either positive or negative. The time t_+ a random walk is positive is defined as the number of positive segments.

Denote $N_{2n,2k}^{\text{pos}}$ the number of bridge paths of length $2n$ with $2k$ positive intervals; by convention we set $N_{0,0}^{\text{pos}} := 1$. We can use Eq. (3.6) to get a recursion relation for $N_{2n,2k}^{\text{pos}}$, with $n \geq 1$,

$$N_{2n,2k}^{\text{pos}} = \sum_{i=1}^{n} \Big[N_{2i}^{+,\text{first}} N_{2(n-i),2(k-i)}^{\text{pos}} + N_{2i}^{+,\text{first}} N_{2(n-i),2k}^{\text{pos}} \Big]. \tag{3.7}$$

This is illustrated in figure 3.2. In this sum, $2i$ is the position of the first zero (after the origin) of the path of lenght $2n$. Since the path does not change sign these $2i$ first segments are either all positive (first term inside the sum) or negative (second term).

To solve this equation, we introduce two generating functions:

$$\tilde{p}^{\text{pos}}(\nu,\rho) := \sum_{n\geq 0}\sum_{k\geq 0} \nu^{2k}\rho^{2n} \frac{N_{2n,2k}^{\text{pos}}}{2^{2n}} \,, \tag{3.8}$$

$$\tilde{p}^{+,\text{first}}(\rho) := \sum_{n>0} \rho^{2n} \frac{N_{2n}^{+,\text{first}}}{2^{2n}} = \frac{1-\sqrt{1-\rho^2}}{2} \,. \tag{3.9}$$

Inserting these definitions into Eq. (3.7) transforms the recursion relation into an algebraic equation

$$\tilde{p}^{\text{pos}}(\nu,\rho) = \Big[\tilde{p}^{+,\text{first}}(\nu\rho) + \tilde{p}^{+,\text{first}}(\rho) \Big] \tilde{p}^{\text{pos}}(\nu,\rho) + 1 \,. \tag{3.10}$$

Eq. (3.10) can be solved as

$$\tilde{p}^{\text{pos}}(\nu,\rho) = \frac{1}{1 - \tilde{p}^{+,\text{first}}(\nu\rho) - \tilde{p}^{+,\text{first}}(\rho)} \,. \tag{3.11}$$

This is a geometric sum of the form

$$\tilde{p}^{\rm pos}(\nu,\rho) = \sum_{n\geq 0} \left[\tilde{p}^{+,\rm first}(\nu\rho) + \tilde{p}^{+,\rm first}(\rho)\right]^n \ . \tag{3.12}$$

Its interpretation is simple: All bridges can be constructed as a sequence of first-return bridges. In a first-return bridge each factor of ρ comes with a factor of ν for the positive paths, and alone for negative paths.

Using the explicit expression of Eq. (3.9), we obtain

$$\tilde{p}^{\rm pos}(\nu,\rho) = \frac{2}{\sqrt{1-(\nu\rho)^2}+\sqrt{1-\rho^2}} \ . \tag{3.13}$$

Other generating functions can be obtained as well: First, for the probability to return to zero (including the term with zero steps) the latter is

$$\tilde{p}_0(\rho) := \sum_{n\geq 0} \rho^n \frac{N_{n,x}}{2^n} = \frac{1}{\sqrt{1-\rho^2}} \ . \tag{3.14}$$

For the probability to return to 0 without having become negative, this is (including the term with zero steps)

$$\tilde{p}_0^{\geq 0}(\rho) = \frac{1}{1-\tilde{p}^+_{\rm first}(\rho)} \equiv \tilde{p}^{\rm pos}(0,\rho) = \frac{2}{1+\sqrt{1-\rho^2}} \ . \tag{3.15}$$

The generating function for paths starting at zero and ending in x without ever returning to zero can be obtained as well

$$\tilde{p}^+_x(\rho) := \sum_{n\geq 0} \rho^n \frac{N^+_{n,x}}{2^n} = \frac{\rho^x}{\left(1+\sqrt{1-\rho^2}\right)^x} = \frac{\left(1-\sqrt{1-\rho^2}\right)^x}{\rho^x} \ . \tag{3.16}$$

This can be understood by considering the path from the end: One can first go up and down to the starting value x for a number $n \geq 0$ steps, before going down by one step, leading to $\tilde{p}_0^{\geq 0}(\rho) \times \frac{\rho}{2}$ for the generating function to (backwards!) reach $x-1$. Repeating this x times, and using Eq. (3.15), we arrive at Eq. (3.16).

3.2.2 Propagators in continuous time

We now wish to take the continuum limit. To this aim, we note that in the limit of a time-discretisation step $\delta t \to 0$, the process

$$X_t \simeq \sqrt{2\delta t} X_n \ , \quad \text{with} \quad n = \text{floor}\left(\frac{t}{\delta t}\right) \equiv \left\lfloor \frac{t}{\delta t} \right\rfloor \tag{3.17}$$

converges to a Brownian motion, as already mentioned in the introduction (1.5). The normalisation ensure that we recover the covariance function (1.19) with $H = 1/2$.

Denote by $\mathcal{P}(t_+, X_0 = x_1, X_T = x_2)$ the probability distribution of the positive time t_+ within the interval $[0,T]$ and the end point $X_T = x_2$ for a standard Brownian motion X_t starting at $X_0 = x_1$. This is formally defined as

$$\mathcal{P}(t_+, X_0 = x_1, X_T = x_2) = \partial_{t_+}\partial_{x_2} \text{Prob}\left(\int_t \Theta(X_t) > t_+, X_T > x_2 | X_0 = x_1\right) \ . \tag{3.18}$$

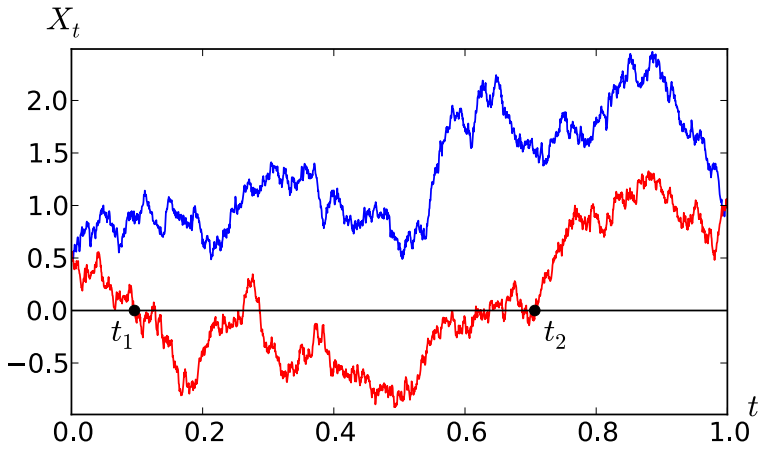

Figure 3.3: In red (bottom curve) a contribution to $\tilde{W}_1^+(\lambda, s, x_1, x_2)$, where the path reaches 0 at least once (here for $x_1 = 0.5$ and $x_2 = 1$). In blue (top curve) the additional contribution to $\tilde{W}_2^+(\lambda, s, x_1, x_2)$, where the path never reaches 0, possible when x_1 and x_2 have the same sign (here for $x_1 = 0.5$ and $x_2 = 1$).

For our perturbative expansion it is useful to have this in Laplace variables, namely

$$\tilde{W}^+(\lambda, s, x_1, x_2) = \int_0^\infty \mathrm{d}T \int_0^T \mathrm{d}t_+ e^{-sT-\lambda t_+} \mathcal{P}(t_+, X_0 = x_1, X_T = x_2) \ . \tag{3.19}$$

We now use the result from the previous section, starting with the special case $x_1 = x_2 = 0$. The probability distribution for a Brownian that its positive time, up to time T, is t_+ and that $X_0 = X_T = 0$, i.e. the process is a bridge, can be obtained from the discrete case via

$$\mathcal{P}(t_+, X_T)\mathrm{d}t_+\mathrm{d}X_T\Big|_{X_T=0} \underset{\delta t\to 0}{\simeq} \frac{1}{2^n} N_{n,k}^{\mathrm{pos}} \ . \tag{3.20}$$

Here $n = \lfloor T/\delta t \rfloor$, $k = \lfloor t_+/\delta t \rfloor$, and δt is the time discretisation step. This allows us to relate the generating function (3.13) to the Laplace transform of the continuous-time distribution $\tilde{W}^+$ with $x_1 = x_2 = 0$, which we denote $\tilde{W}^+(\lambda, s)$, setting $\nu \to e^{-\delta t\lambda}$, $\rho \to e^{-\delta t s}$ and then taking the limit of $\delta t \to 0$. The measure $\mathrm{d}t_+\mathrm{d}B_T$ gives a factor of $\sqrt{2}\delta t^{3/2}$, cf. Eq. (3.17). This yields

$$\begin{aligned} \tilde{W}^+(\lambda, s)\sqrt{2}\delta t^{3/2} \simeq \tilde{p}^{\mathrm{pos}}(e^{-\delta t\lambda}, e^{-\delta t s})\delta t^2 &\simeq \frac{2\delta t^2}{\sqrt{1-e^{-2\delta t(s+\lambda)}} + \sqrt{1-e^{-2\delta t s}}} \\ &\simeq \frac{\sqrt{2}\delta t^{3/2}}{\sqrt{\lambda+s}+\sqrt{s}} + O(\delta t^2) \ . \end{aligned} \tag{3.21}$$

Both sides of the equation have the same scaling with δt and thus we obtain

$$\tilde{W}^+(\lambda, s) = \frac{1}{\sqrt{\lambda+s}+\sqrt{s}} \ . \tag{3.22}$$

From this result for the bridge we obtain the expression for $\tilde{W}(\lambda, s, x_1, x_2)$ by distinguishing two cases, see Fig. 3.3: The first case is when the process changes sign at least once. It can be decomposed into a constant-sign part (contributing to t_+ or not, depending on the signe of x_1), a bridge part, and another constant sign part ending in x_2. The other case is when the process never changes sign, which corresponds to the survival probability and can be expressed using the method of images.

We recall the Laplace transform of this propagator from x_1 to x_2, conditioned that the path has never touched zero,

$$\tilde{P}_0^+(x_1,x_2;s) = \frac{e^{-\sqrt{s}|x_1-x_2|} - e^{-\sqrt{s}|x_1+x_2|}}{2\sqrt{s}}\,\Theta(x_1x_2)\ . \tag{3.23}$$

The *normalized* limit $x_1 \to 0$ is

$$\tilde{P}_0^+(x_2;s) = \lim_{x_1\to 0}\frac{1}{x_1}\tilde{P}_0^+(x_1,x_2;s) = e^{-\sqrt{s}x_2}\,\Theta(x_2)\ . \tag{3.24}$$

The final result is the sum of two terms,

$$\tilde{W}^+(\lambda,s,x_1,x_2) = \tilde{W}_1^+(\lambda,s,x_1,x_2) + \tilde{W}_2^+(\lambda,s,x_1,x_2)\ . \tag{3.25}$$

The first contribution involves a crossing, and is a product of two factors (3.24) and one factor (3.22),

$$\tilde{W}_1^+(\lambda,s,x_1,x_2) = e^{-\sqrt{s+\lambda\Theta(x_1)}|x_1|}\frac{1}{\sqrt{s+\lambda}+\sqrt{s}}e^{-\sqrt{s+\lambda\Theta(x_2)}|x_2|}\ , \tag{3.26}$$

The Θ functions in the exponential are understood as follows: If $x_1 > 0$, then s is changed to $s+\lambda$, since this segment contributes both to T and t_+. In the opposite case $x_1 < 0$, this segment contributes only to T but not to t_+, thus s remains unchanged. The same argument applies to the last factor as a function of the sign of x_2.

The contribution when the walk never changes sign is

$$\tilde{W}_2^+(\lambda,s,x_1,x_2) = \frac{e^{-\sqrt{s+\lambda\Theta(x_1)}|x_1-x_2|} - e^{-\sqrt{s+\lambda\Theta(x_1)}|x_1+x_2|}}{2\sqrt{s+\lambda\Theta(x_1)}}\Theta(x_1x_2)\ . \tag{3.27}$$

This is the propagator (3.23), with again s shifted to $s+\lambda$ if x_1, and as a consequence also x_2, are positive.

The result for $\tilde{W}^+(\lambda,s,x_1,x_2)$ can also be obtained by solving the Fokker-Planck equation

$$\partial_{x_2}^2\tilde{W}^+(\lambda,s,x_1,x_2) = [s+\lambda\Theta(x_2)]\,\tilde{W}^+(\lambda,s,x_1,x_2) + \delta(x_1-x_2)\ . \tag{3.28}$$

One verifies that $\tilde{W}_1^+ + \tilde{W}_2^+$ is indeed a solution.

As a check, we consider Brownian motion starting at 0 and without any constraint at the end point. Integrating $\tilde{W}_+$ over the last variable gives

$$\int_{-\infty}^{\infty}\mathrm{d}x\,\tilde{W}^+(\lambda,s,0,x) = \frac{1}{\sqrt{s(s+\lambda)}}\ . \tag{3.29}$$

The corresponding probability distribution for t_+ is known as one of the Arcsine laws. Indeed, computing the double Laplace transform from this known result (1.10) yields Eq. (3.29):

$$\int_0^\infty \mathrm{d}T\int_0^T \mathrm{d}t_+\,e^{-sT-\lambda t_+}\frac{1}{\pi\sqrt{t_+(T-t_+)}} = \frac{1}{\sqrt{s(s+\lambda)}}\ . \tag{3.30}$$

3.3 Time of a fBm remains positive

As derived in the previous section, the Laplace transform ($t_+ \to \lambda$ and $T \to s$) of the probability density that a Brownian motion X_t goes from $X_0 = x_1$ to $X_T = x_2$ while being positive during a time t_+ in between is

$$\begin{aligned}\tilde{W}^+(\lambda, s, x_1, x_2) =& \frac{\exp\left(-|x_1|\sqrt{\lambda\Theta(x_1)+s} - |x_2|\sqrt{\lambda\Theta(x_2)+s}\right)}{\sqrt{\lambda+s}+\sqrt{s}} \\ &+ \frac{\Theta(x_1x_2)\left(e^{-|x_1-x_2|\sqrt{\lambda\Theta(x_1)+s}} - e^{-|x_1+x_2|\sqrt{\lambda\Theta(x_1)+s}}\right)}{2\sqrt{\lambda\Theta(x_1)+s}} .\end{aligned} \tag{3.31}$$

To compute the correction at order ε to the first arcsine law, we follow the same procedure as for the time of the maximum $t_{\max}$ (third arcsine law), cf. section 2.2.3. The path integral to study is now

$$Z(t_+, T) = \int_{-\infty}^{\infty} \mathrm{d}x \int_{X_0=0}^{X_T=x} \mathcal{D}[X]\delta\left(\int_0^T \mathrm{d}t\, \Theta(X_t) - t_+\right) e^{-S[X]} , \tag{3.32}$$

or in Laplace variables ($t_+ \to \lambda$ and $T \to s$)

$$\tilde{Z}(\lambda, s) = \int_0^{\infty} \mathrm{d}T e^{-sT} \int_{-\infty}^{\infty} \mathrm{d}x \int_{X_0=0}^{X_T=x} \mathcal{D}[X] e^{-\lambda\int_0^T \mathrm{d}t\,\Theta(X_t)} e^{-S[X]} . \tag{3.33}$$

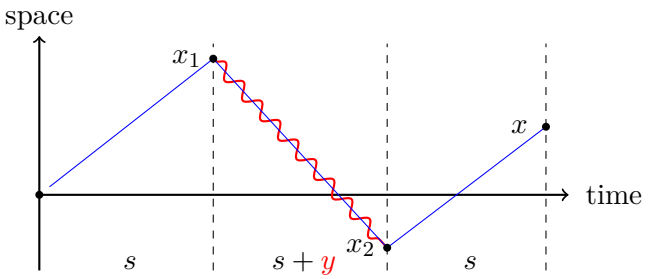

Figure 3.4: This diagram represents the order ε correction to the distribution of the positive time, for a fBm of Hurst exponent $H = 1/2 + \varepsilon$. The blue lines are propagators $\tilde{W}_+$ (3.31) and the red curvy line is the interaction, non-local in time, which shifts the Laplace variable s of the propagator by y in the middle slice. The contribution of this diagram is given by integrating over x_1, x_2 and x for the space variables (without positivity constraint, contrary to the diagrams of Fig. 2.2), and over $y > 0$ for the interaction variable, cf. Eq. (3.34).

In this case there is no point whose value is specified, and there is only one diagram to take into account, represented in Fig. 3.4.

The integrations are easy to do, as there is no non-trivial limit $x_0 \to 0$ to take in this case. The analytical expression of the diagram 3.4, which is the order ε term of (3.33), is

$$\begin{aligned}\tilde{Z}_1(s,\lambda) &= 2\int_{x,x_1,x_2} \int_0^{\infty} \mathrm{d}y\, \tilde{W}_+(s,\lambda,0,x_1)\,\partial_{x_1}\tilde{W}_+(s+y,\lambda,x_1,x_2)\,\partial_{x_2}\tilde{W}_+(s,\lambda,x_2,x) \\ &= \frac{2}{s}\left[\frac{\log(16)}{\sqrt{\kappa+1}} + \frac{1}{2}\left(\frac{1}{\sqrt{\kappa+1}}+1\right)\log(\kappa+1) - \left(\frac{1}{\kappa+1}+\frac{2}{\sqrt{\kappa+1}}+1\right)\log\left(\sqrt{\kappa+1}+1\right)\right] .\end{aligned} \tag{3.34}$$

with $\kappa = \lambda/s$. The interaction shifts the Laplace variable s of the second propagator by y and acts as $2\partial_{x_1}$ on the second propagator and as $2\partial_{x_2}$ on the last one, with an overall prefactor $\varepsilon/2$.

As fBm is a self-similar process, the probability distribution of t_+ can be written in the form

$$\mathcal{P}^T_{H=\frac{1}{2}+\varepsilon}(t_+) = \frac{1}{T}\left(\frac{1}{\pi\sqrt{\vartheta(1-\vartheta)}} + \varepsilon g_1^+(\vartheta)\right) + O(\varepsilon^2), \quad \text{with} \quad \vartheta = t_+/T \ . \tag{3.35}$$

The correction we want to compute, $g_1^+(\vartheta)$, is related to $\overline{g}_1^+(\kappa) := \tilde{Z}_1(1,\kappa)$ via

$$\overline{g}_1^+(\kappa) := \int_0^1 \mathrm{d}\vartheta \frac{g_1^+(\vartheta)}{1+\kappa\vartheta} \ . \tag{3.36}$$

The scaling form of Eq. (3.35) and the integral transform appearing here (3.36) are discussed in detail in section 4.3.1. The inverse of the transformation (3.36) can be computed using an analytical continuation of $\overline{g}_1^+(\kappa)$:

$$g_1^+(\vartheta) = \frac{1}{2\pi i\vartheta} \lim_{\alpha\to\pi^-}\left[\overline{g}_1^+\left(\frac{e^{-i\alpha}}{\vartheta}\right) - \overline{g}_1^+\left(\frac{e^{i\alpha}}{\vartheta}\right)\right] \ , \tag{3.37}$$

which, together with the expression of $\overline{g}_1^+(\kappa)$ from (3.34)

$$\overline{g}_1^+(\kappa) = \frac{8\log(2)}{\sqrt{\kappa+1}} + \left(\frac{1}{\sqrt{\kappa+1}}+1\right)\log(\kappa+1) - 2\left(\frac{1}{\kappa+1}+\frac{2}{\sqrt{\kappa+1}}+1\right)\log\left(\sqrt{\kappa+1}+1\right) \ , \tag{3.38}$$

allows us to obtain the analytical expression of $g_1^+(\vartheta)$,

$$g_1^+(\vartheta) = \frac{2(1-2\vartheta)\arccos(\sqrt{\vartheta})}{\pi\vartheta(\vartheta-1)} + \frac{1}{\vartheta} - \frac{\ln(\vartheta(1-\vartheta))}{\pi\sqrt{\vartheta(1-\vartheta)}} - \frac{8\ln(2)}{\pi\sqrt{\vartheta(1-\vartheta)}} \ . \tag{3.39}$$

Surprisingly, this is the same result as for the correction to the distribution of $t_{\max}$ (2.40). This means that we have, up to second order corrections, the same distributions for $t_{\max}$ and t_+:

$$\boxed{\mathcal{P}^T_{H=\frac{1}{2}+\varepsilon}(t_{\max}) + O(\varepsilon^2) = \mathcal{P}^T_{H=\frac{1}{2}+\varepsilon}(t_+) + O(\varepsilon^2) = \frac{e^{\varepsilon\mathcal{F}(\vartheta)}}{\pi[t(T-t)]^H} \ ,} \tag{3.40}$$

with the expression of $\mathcal{F}$ given in Eq. (2.42).

We test this with numerical simulations, extracting $\mathcal{F}$ from an estimated distribution of t_+ for various values of H. This is represented on Fig. 3.5 Left. The agreement is very good, but we can see that the deviations due to order ε^2 terms are larger than for the distribution of $t_{\max}$, as shown on Fig. 3.5 Right.

3.4 Last zero of a fBm

3.4.1 The Brownian case

To derive the second arcsine law (i.e. distribution of the time of the last zero) for Brownian motion, we consider paths going from $X_0 = 0$ to $X_t = x_0 > 0$ without constraint, and then from $X_t = x_0 > 0$ to $X_T = x > 0$ with positivity constraint. Taking the limit $x_0 \to 0$ forces the path to have its last zero at time t. The weight of these paths as a function of t, integrated over the end point x, is then proportional to the distribution of t_{last}. This is obtained via the simple computation

$$\int_0^\infty \mathrm{d}x\, P_0(0,x_0,t)P_0^+(x_0,x,T-t) \underset{x_0\to 0}{\simeq} \frac{x_0}{2}\frac{1}{\pi\sqrt{t(T-t)}} \ , \tag{3.41}$$

and we recover, with a normalisation $x_0/2$, the arcsine distribution (1.10).

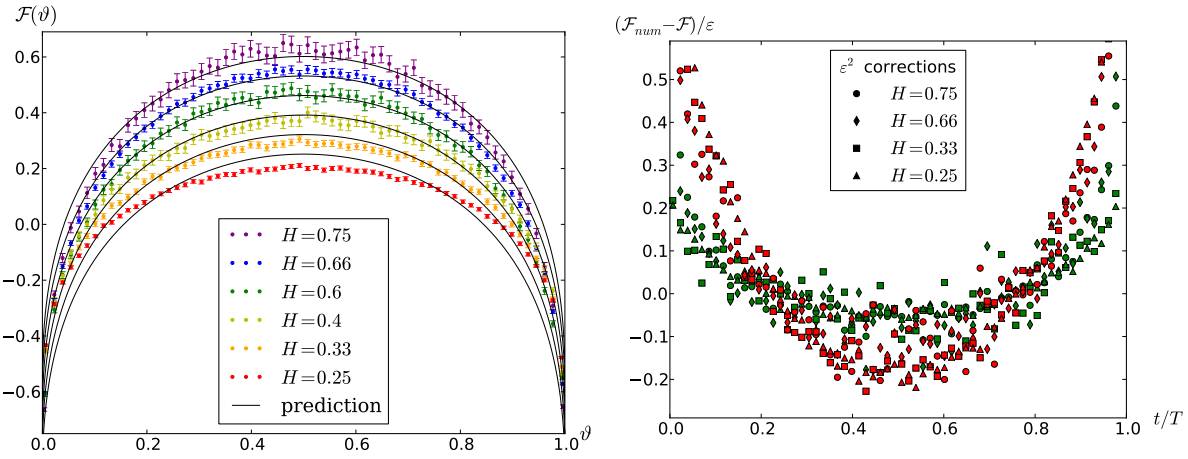

Figure 3.5: Left: comparison of a numerical estimation of $\mathcal{F}$ to the prediction (2.42) in the case of the distribution of t_+ for various values of H (vertically translated for a better visualisation), see section 2.4.1 for details on the numerical procedure. Right: Comparison between the estimated order ε^2 corrections (2.68) for the distribution of t_+ (red) and $t_{\max}$ (green), indicating that are different.

3.4.2 Scaling and perturbative expansion for the distribution of the last zero

For a fBm with generic Hurst exponent, we can look at the scaling of $\mathcal{P}(t_{\text{last}} = t)$ close to the boundaries. A path with its last zero at time t, is composed of a bridge of length t, whose probability scale with t^{-H}, and a survival process of length $T-t$ whose probability scale with $(T-t)^{-\theta}$, with the survival exponent $\theta = 1-H$. When the process is non-Markovian ($H \neq 1/2$), the two parts are not independent and the probability of such paths is hard to evaluate, but we can still gives its asymptotics:

$$\mathcal{P}_H^T(t_{\text{last}} = t) \sim \begin{cases} t^{-H} & \text{for } t \to 0 \\ (T-t)^{H-1} & \text{for } t \to T \end{cases} . \tag{3.42}$$

We see that contrary to the case of t_+ and $t_{\max}$, the distribution of t_{last} is not symmetric under time reversion $t \to T-t$.

To go beyond scaling results, we again write a path integral which encodes the distribution in the limit of $x_0 \to 0$,

$$Z^{\text{last}}(x_0, t, T) = \int_0^\infty \mathrm{d}x \int_{X_0=0}^{X_T=x} \mathcal{D}[X]\delta(X_t = x_0) \prod_{t'=t}^{T} \Theta(X_{t'}) e^{-S[X]} \tag{3.43}$$

and expand in ε using the expansion of the action (2.3). As there is a point whose value is imposed, $X_t = x_0$, there is three different contributions, represented on figure 3.6.

Interestingly, these contributions are quite easy to compute due to symmetry. Diagrams (b) and (c) only correct the free propagator from 0 to x_0 and the constrained propagator from x_0 to x respectively. The diagram (a), which should be the most difficult to compute, is in fact irrelevant in the $x_0 \to 0$ limit. To understand that, we can express the order ε correction to Z^{last} as

$$Z_1^{\text{last}}(x_0, t, T) = -\frac{\varepsilon}{2} \int_0^{T-\tau} \mathrm{d}\tau_1 \int_{\tau_1+\tau}^{T} \mathrm{d}\tau_2 \, \frac{\langle \dot{X}_{\tau_1} \dot{X}_{\tau_2} \rangle}{|\tau_2 - \tau_1|} , \tag{3.44}$$

where $\langle \dots \rangle$ indicates average over a Brownian motion $X_{t'}$ constrained by $X_0 = 0$, $X_t = x_0$ and $X_{t'} > 0 \ \forall t' \in [t, T]$, and τ is the time cut-off. This is similar to (2.17), but we replace the path integral notation by the average, which are formally identical.

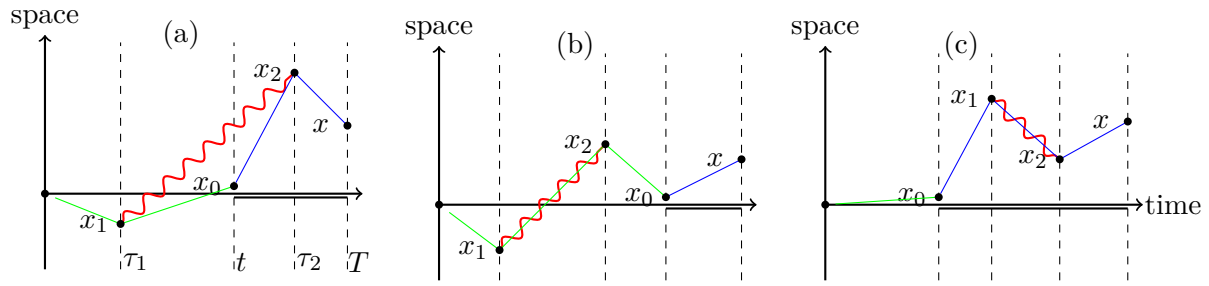

Figure 3.6: The three contributions at order ε to the distribution of the last zero t_{last}. Green lines represent propagators without constraint, while blue lines represent propagators with positivity constraint. The double line on the time axis indicates the absorbing boundary.

The three diagrams of Fig. 3.6 correspond to the different time ordering of τ_1, τ_2 and t. For the diagram (a), we have $\tau_1 < t < \tau_2 < T$ and then $\dot{X}_{\tau_1}$ is independent of $\dot{X}_{\tau_2}$ (because of the constraint $X_t = x_0$ and the Markov property). As $\langle \dot{X}_{\tau_1} \rangle = x_0/t$, diagram (a) is subleading in the limit of $x_0 \to 0$ (it is of order x_0^2) compared to diagrams (b) and (c) (which are of order x_0) and thus does not correct the distribution of t_{last}.

We then have the following ε-expansion

$$\mathcal{P}^T_{H=\frac{1}{2}+\varepsilon}(t_{\text{last}} = \vartheta T) = \frac{\sin(H\pi)}{\pi T} \frac{1}{\vartheta^H (1-\vartheta)^{1-H}} + O(\varepsilon^2) \ , \tag{3.45}$$

where we have resummed the contributions of diagrams (b) and (c) in the power law prefactor, giving respectively $\vartheta^{\frac{1}{2}} \to \vartheta^H$ and $(1-\vartheta)^{\frac{1}{2}} \to (1-\vartheta)^{1-H}$.

3.4.3 The two non-trivial diagrams at second order

We now present briefly the computations allowing us to obtain the distribution of t_{last} at second order in ε. For that, we need to write the action up to second order in ε,

$$S[X] = S_0[X] - \frac{\varepsilon}{2} \int_{T>\tau_2>\tau_1>0} \frac{\dot{X}_{\tau_1} \dot{X}_{\tau_2}}{|\tau_2 - \tau_1|} - \varepsilon^2 \int \dot{X}_{\tau_1} \dot{X}_{\tau_2} \mathcal{C}_2^{-1}(\tau_2, \tau_1) + O(\varepsilon^3) \ , \tag{3.46}$$

with $\mathcal{C}_2^{-1}(\tau_1, \tau_2)$ a function computed in appendix 3.A, but whose expression is not needed here. Expanding the exponential of the action in (3.43), the correction of order ε^2 of Z^{last} can be written as

$$Z_2^{\text{last}}(x_0, t, T) = \frac{1}{8} \int_{T>\tau_2>\tau_1>0} \int_{T>\tau_4>\tau_3>0} \frac{\langle \dot{X}_{\tau_1} \dot{X}_{\tau_2} \dot{X}_{\tau_3} \dot{X}_{\tau_4} \rangle}{|\tau_2 - \tau_1||\tau_4 - \tau_3|} + \int_{T>\tau_2>\tau_1>0} \langle \dot{X}_{\tau_1} \dot{X}_{\tau_2} \rangle \mathcal{C}_2^{-1}(\tau_1, \tau_2) \ . \tag{3.47}$$

The first term of (3.47) gives diagrams with two interactions, i.e. two loops diagrams. The different time orderings give a total of 15 diagrams. Luckily, the simplification used in the previous section is still helpful: all diagrams with an odd number of interaction vertices in the interval $[0, t]$ vanish in the limit $x_0 \to 0$, and all diagrams with all vertices in either $[0, t]$ or in $[t, T]$ contribute only to the (known) correction of the scaling behavior.

The second term of (3.47) gives one-loop diagrams with a new interaction given by $\mathcal{C}_2^{-1}$. The diagrams are the same as in Fig. 3.6, and, as the nature of the interaction does not matter in the arguments of the previous section, they also correct only the scaling behavior, with terms of order ε^2.

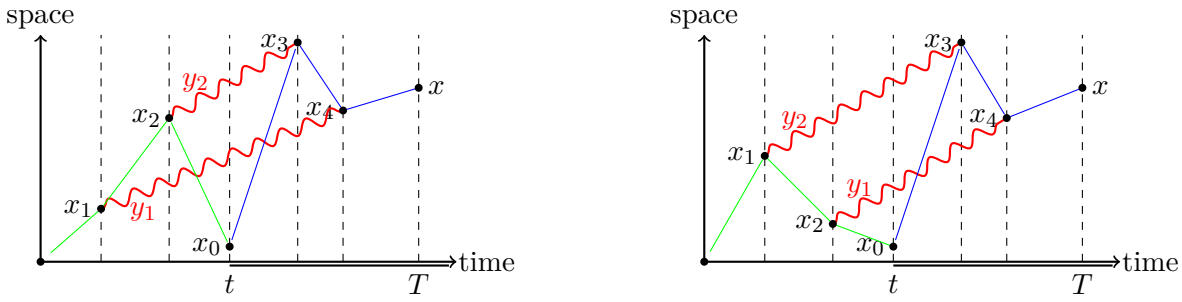

Figure 3.7: The diagrams $\mathcal{D}_1$ (left) and $\mathcal{D}_2$ (right). The double line in the time axe indicates when there is an absorbing boundary, and the propagator are either free ones (in green), or constrained ones (in blue). Each interaction carries a variable y_i which shifts the Laplace variable of the propagator between its two vertexes, and each vertexe (x_1, x_2, x_3 and x_4) acts as $2\partial_{x_i}$ on the propagator starting at x_i.

All this leaves only 2 diagrams $\mathcal{D}_1$ and $\mathcal{D}_2$ with a non-trivial contribution to the distribution of t_{last}, represented on Fig. 3.7. The expansion of the distribution of t_{last} is then

$$\mathcal{P}^T_{H=\frac{1}{2}+\varepsilon}(t_{\text{last}} = \vartheta T) = \frac{\sin(H\pi)}{\pi T}\frac{1}{\vartheta^H(1-\vartheta)^{1-H}} + 4\varepsilon^2 \lim_{x_0\to 0}\frac{2}{x_0}(\mathcal{D}_1+\mathcal{D}_2) + O(\varepsilon^3)\ . \tag{3.48}$$

As we said, all diagrams other than $\mathcal{D}_1$ and $\mathcal{D}_2$ are either vanishing or already taken into account in the power law prefactor. The combinatorial factor of 4 written above is

$$\left(\frac{1}{2}\right)^2 \frac{1}{2!} \times 2 \times 2^4 = 4\ , \tag{3.49}$$

where each interaction contributes a $\frac{\varepsilon}{2}$, the $\frac{1}{2!}$ is from the expansion of the exponential, compensated because in each diagram the two interactions can be interchanged; finally each of the four derivatives contributes a factor of 2. The normalisation $2/x_0$ comes from the 0-order computations (3.41).

The contributions of these diagrams, presented on figure 3.7, are easily expressed in term of Laplace variables, $T \to s$ and $t \to \lambda$:

$$\begin{aligned}\mathcal{D}_1 = \int_{y_1,y_2>0}\int_{x_1,x_2} &\tilde{P}_0(x_0,x_1,s+\lambda)\partial_{x_1}\tilde{P}_0(x_1,x_2,s+\lambda+y_1)\partial_{x_2}P_0(x_2,x_0,s+\lambda+y_1+y_2)\\ &\times\int_{x_3,x_4,x>0}\tilde{P}_0^+(x_0,x_3,s+y_1+y_2)\partial_{x_3}\tilde{P}_0^+(x_3,x_4,s+y_1)\partial_{x_4}\tilde{P}_0^+(x_4,x,s)\end{aligned} \tag{3.50}$$

$$\begin{aligned}\mathcal{D}_2 = \int_{y_1,y_2>0}\int_{x_1,x_2} &P_0(x_0,x_1,s+\lambda)\partial_{x_1}P_0(x_1,x_2,s+\lambda+y_2)\partial_{x_2}P_0(x_2,x_0,s+\lambda+y_1+y_2)\\ &\times\int_{x_3,x_4,x>0}P_+(x_0,x_3,s+y_1+y_2)\partial_{x_3}P_+(x_3,x_4,s+y_1)\partial_{x_4}P_+(x_4,x,s)\ .\end{aligned} \tag{3.51}$$

Note the only change between the two diagrams in red. The usual scaling property makes the dependence on s of these diagrams trivial: $\mathcal{D}_i(s,\lambda) = \frac{1}{s}\mathcal{D}_i(1,\kappa)$ with $\kappa = \frac{\lambda}{s}$.

The integrations over space variables are similar in the two cases, and we can combine the

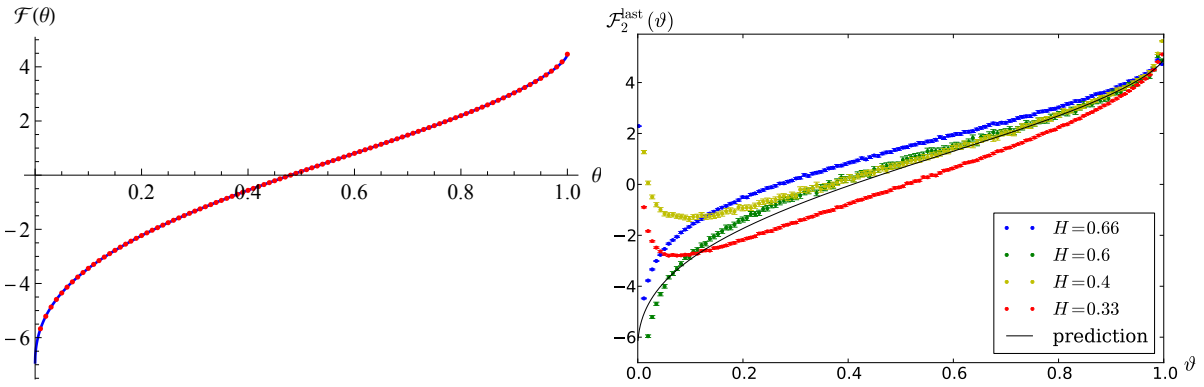

Figure 3.8: Left: the results of numerical integrations, red dots, and the fit (3.56) in plain line blue. Right: Numerical simulations for various values of H (cf. legend) compared to the prediction (3.56) from our perturbative expansion. For ϑ close to 0, higher order corrections are dominate even for H close to 1/2 but for ϑ close to one, the agreement with our prediction is very good.

two to obtain

$$\begin{aligned}\overline{g}_2(\kappa) =& 4 \lim_{x_0\to 0} \frac{2}{x_0}\big(\mathcal{D}_1(1,\kappa)+\mathcal{D}_2(1,\kappa)\big)\\ =& -4\int_{y_1,y_2>0} \frac{\sqrt{y_1+y_2+1}\,(\sqrt{y_1+1}+\sqrt{y_2+1}-\sqrt{y_1+y_2+1}-1)}{y_1^2y_2^2\,(y_1+y_2)}\\ &\times\Big(y_2\left(\sqrt{\kappa+1}-\sqrt{\kappa+y_1+1}\right)+y_1\left(\sqrt{\kappa+y_1+y_2+1}-\sqrt{\kappa+y_1+1}\right)\Big)\ .\end{aligned} \tag{3.52}$$

We were not able to deal with the integrations over y_1 and y_2 analytically. However, numerical integration and the inversion formula already used in Eq. (3.37), which writes here as

$$g_2(\vartheta) = \lim_{\alpha\to\pi^-}\left[\overline{g}_2\left(\frac{e^{-i\alpha}}{\vartheta}\right)-\overline{g}_2\left(\frac{e^{i\alpha}}{\vartheta}\right)\right], \tag{3.53}$$

allows us to obtain a good estimation for the ε^2-correction. It is useful to define

$$\mathcal{F}_2^{\text{last}}(\vartheta) := \pi\sqrt{\vartheta(1-\vartheta)}g_2(\vartheta) \tag{3.54}$$

such that we can write the expansion of the distribution of t_{last} in our usual way:

$$\boxed{\mathcal{P}^T_{H=\frac12+\varepsilon}(t_{\text{last}}=\vartheta T)=\frac{1}{T}\frac{\sin(H\pi)}{\pi\vartheta^H(1-\vartheta)^{1-H}}\exp\Big(\varepsilon^2\mathcal{F}_2^{\text{last}}(\vartheta)\Big)+O(\varepsilon^3)\ .} \tag{3.55}$$

The results from numerical integration for $\mathcal{F}_2^{\text{last}}$ are plotted on figure 3.8, red dots, and a good fit is given by:

$$\begin{aligned}\mathcal{F}_2^{\text{last}}(\vartheta) \simeq& 11.595\,\vartheta^{3/2}-10.743\,\vartheta^2+8.301\,\vartheta\\ &+13.302\,\sqrt{\vartheta}+13.231\,(1-\vartheta)^{3/2}-2.166\,\sqrt{1-\vartheta}-17.979\end{aligned} \tag{3.56}$$

3.A Action at second order

We recall here the computation, and extend it at second order, of the expansion in ε of the action of a fBm path with Hurst exponent $H = \frac{1}{2} + \varepsilon$ which was done in [125]. As a Gaussian process, the action has the form

$$S[X] = \frac{1}{2} \int X_{t_1} X_{t_2} G(t_1, t_2) \tag{3.57}$$

where $G(t_1, t_2)$ is the inverse of the correlation function of a fBm (1.19). But we can also start from the correlations of $\dot{X}$ and write the action as

$$S[X] = \frac{1}{2} \int \dot{X}_{t_1} \dot{X}_{t_2} \mathcal{C}^{-1}(t_1, t_2) \ . \tag{3.58}$$

This correlation function is

$$\begin{aligned} \langle \dot{X}_{t_1} \dot{X}_{t_2} \rangle =& \mathcal{C}(t_1, t_2) = 2\delta(t_1 - t_2) 2H |t_2 - t_1|^{2H-1} + 2H(2H-1)|t_1 - t_2|^{2(H-1)} \\ =& 2\delta(t_1 - t_2)(1 + 2\varepsilon)\tau^{2\varepsilon} + \frac{2\varepsilon}{|t_1 - t_2|} + \frac{4\varepsilon^2 \big(\log |t_1 - t_2| + 1 \big)}{|t_1 - t_2|} + O(\varepsilon^3) \\ =& 2D_{\varepsilon,\tau} \left[\delta(t_1 - t_2) + \frac{\varepsilon}{|t_1 - t_2|} + \frac{2\varepsilon^2 \ln \left| \frac{t_1 - t_2}{\tau} \right|}{|t_1 - t_2|} + O(\varepsilon^3) \right] \ . \end{aligned} \tag{3.59}$$

In the first line, the first term is not well defined and needs to be regularized using the time cutoff τ. In the second line we expand the second term in ε and reorganize the expansion in the last line. The rescaled diffusion constant appearing here is

$$D_{\varepsilon,\tau} = (1 + 2\varepsilon)\tau^{2\varepsilon} \ . \tag{3.60}$$

We compute the inverse of $\mathcal{C}$ order by order in ε, which gives

$$\mathcal{C}^{-1}(t_1, t_2) = \frac{1}{2D_\varepsilon} \left[\delta(t_1 - t_2) - \frac{\varepsilon}{|t_1 - t_2|} - \frac{2\varepsilon^2 \log \left| \frac{t_1 - t_2}{\tau} \right|}{|t_1 - t_2|} + \int_s \frac{\varepsilon^2}{|s - t_1||s - t_2|} + O(\varepsilon^3) \right] \ . \tag{3.61}$$

The order-ε term is already known and used in [125], as well as in the previous chapters of this thesis. The next term is new and gives the correction to the action at order ε^2: $S_2[X] = \int \dot{X}_{t_1} \dot{X}_{t_2} \mathcal{C}_2^{-1}(t_1, t_2)$ with

$$\mathcal{C}_2^{-1}(t_1, t_2) = -\frac{2 \log \left| \frac{t_1 - t_2}{\tau} \right|}{|t_1 - t_2|} + \int_s \frac{1}{|s - t_1||s - t_2|} \ . \tag{3.62}$$

Chapter 4

Fractional Brownian bridges and positive time

4.1 Presentation of the chapter

This chapter is based on joint work by K. Wiese and my self published in [130]. We extend the results of the previous chapters to the case of fBm bridges, focusing on the three observables:

(i) the time $t_{\max}$ the random process achieves its maximum,

(ii) the value m of this maximum,

(iii) the time t_+ the process is positive, aka its *positive time*.

We will show that at leading order in $\varepsilon = H - \frac{1}{2}$, the probability distributions for $t_{\max}$ and t_+ are different for the bridge case, contrary to standard Brownian bridge where the tow distributions are simply uniform. The first order computations in ε are enough to distinguish them, contrary to the case of a fBm with a free end point, cf. section 3.3. And as we will see in chapter 5, the distribution of the maximum of a fBm bridge have intersting links to the Pickands constants.

Finally we test our analytical results against numerical simulations for $H = 0.4$, $H = 0.6$, and $H = 0.66$. This is achieved by constructing a *subtracted* process out of each realization of a fBm with free endpoints. This procedure yields the same statistics as a fractional Brownian bridge, and is much more efficiently simulated than an unconstrained fBm, for which one retains only realizations which are bridges.

This chapter is organised as follows: Section 4.2 introduces some general results about Gaussian bridges, as well as their application to fractional Brownian motion.

Section 4.3 studies t_+, the time spent by the process in the positive half space. General considerations using the self-similarity of the process are presented and used to simplified the perturbative expansion described in the previous chapters, with technical steps left to appendix 4.B. The analytical results obtained are then compared to numerical simulations.

Section 4.4 presents results on the extreme-value statistics for a fBm bridge: the maximum value m as well as the time $t_{\max}$ to reach it. Some of these results are derived from the general result (2.34) of chapter 2; but we also present a new and simpler way to obtain the maximum-value distribution.

Several appendices complete this chapter: Appendix 4.B contains details about the inverse of an integral transform appearing in our calculation, and its relation to the Abel transform. Appendix 4.C summarises the necessary inverse Laplace transforms needed in the main text.

4.2 Preliminaries: Gaussian Bridges

Consider a real-valued process X_t, starting at $X_0 = 0$. We define a *bridge*, denoted X_t^{B}, to be the same process *conditioned* to be at a at time T. Its one- and two-point correlation functions are

$$\langle X_{t_1}^{\mathrm{B}} \rangle = \frac{\langle X_{t_1} \delta(X_T - a) \rangle}{\langle \delta(X_T - a) \rangle} \ , \tag{4.1}$$

$$\langle X_{t_1}^{\mathrm{B}} X_{t_2}^{\mathrm{B}} \rangle = \frac{\langle X_{t_1} X_{t_2} \delta(X_T - a) \rangle}{\langle \delta(X_T - a) \rangle} \ . \tag{4.2}$$

We now assume that X_t is a centered Gaussian process, i.e. $\langle X_t \rangle = 0$ for all t, and that cumulants of order higher than 2 vanish. To express the correlation function of the bridge process in terms of the unconditioned process, we insert the identity $\delta(x) = \int_{-\infty}^{\infty} e^{ikx} \frac{\mathrm{d}k}{2\pi}$ into the above equations. After some lines of algebra presented in appendix 4.A, we arrive at

$$\langle X_{t_1}^{\mathrm{B}} \rangle = a \frac{\langle X_{t_1} X_T \rangle}{\langle X_T^2 \rangle} \tag{4.3}$$

$$\langle X_{t_1}^{\mathrm{B}} X_{t_2}^{\mathrm{B}} \rangle = \langle X_{t_1} X_{t_2} \rangle - \Big[\langle X_T^2 \rangle - a^2 \Big] \frac{\langle X_{t_1} X_T \rangle \langle X_{t_2} X_T \rangle}{\langle X_T^2 \rangle^2} \ . \tag{4.4}$$

Consider now the *subtracted* process X_t^{S} defined from the original process X_t as

$$X_t^{\mathrm{S}} := X_t - (X_T - a) \frac{\langle X_t X_T \rangle}{\langle X_T^2 \rangle} \ . \tag{4.5}$$

One easily checks that its one and two-point correlation functions coincide with those of X_t^{B} given in Eqs. (4.3)–(4.4). This is sufficient to conclude that X_t^{B} and X_t^{S} are the same processes,

$$X_t^{\mathrm{S}} \overset{\text{law}}{=} X_t^{\mathrm{B}} \ . \tag{4.6}$$

While this result was derived in Ref. [131] by other methods, the prescription (4.5) does not seem to be generally known, apart for Brownian motion $X_t := B_t$ where the subtracted process (4.5) reduces to

$$B_t^{\mathrm{S}} = B_t - \frac{t}{T} \Big(B_T - a \Big) \ . \tag{4.7}$$

But this simple linear subtraction does not lead to the correct correlation function for other processes than the standard Brownian motion.

For fractional Brownian motion with Hurst exponent H, the subtracted term is non-linear in t, containing the expression

$$f\left(\vartheta := \frac{t}{T} \right) := \frac{\langle X_t X_T \rangle}{\langle X_T^2 \rangle} = \frac{1}{2} \Big[1 + \vartheta^{2H} - (1 - \vartheta)^{2H} \Big] \ . \tag{4.8}$$

The equivalence (4.6) is crucial for the numerical simulations presented in this work. Simulating bridge process using its definition requires to discard almost all generated paths, while the subtracted process can be constructed from every generated path without loss of statistics.

4.3 Time a fBm birdge remains positive

As in section 3.2, we denote $\tilde{W}^+(\lambda, s, x_1, x_2)$ the propagator in Laplace variable wich contains information on the positive time of the process. Its expression is given in Eq. (3.31). To recover the distribution of t_+ for a Brownian Bridge, i.e. $x_1 = x_2 = 0$, we have

$$\tilde{W}^+(\lambda, s, 0, 0) = \tilde{W}^+(\lambda, s) = \frac{1}{\sqrt{\lambda + s} + \sqrt{s}} \ . \tag{4.9}$$

Let us note some subtleties. Eq. (4.9) is the double Laplace transform of the probability distribution that the Brownian process spends a time t_+ in the positive half space *and* ends in 0 at time T. If we want to have the conditional probability distribution for t_+, knowing that the process is a bridge, we need to divide the result by the probability density to return to $x = 0$ at time T, which is $(2\sqrt{\pi T})^{-1}$. The double Laplace transform to compute is then

$$\int_0^\infty \mathrm{d}T \int_0^T \mathrm{d}t_+ e^{-sT-\lambda t_+} \frac{1}{T} \frac{1}{2\sqrt{\pi T}} = \frac{1}{\sqrt{\lambda + s} + \sqrt{s}} \ . \tag{4.10}$$

Here $1/T$ is the uniform probability distribution (1.27) of t_+ for a Brownian Bridge,

$$\mathcal{P}_{1/2}^{\text{bridge}}(t_+) = \frac{1}{T} \ , \tag{4.11}$$

and $(2\sqrt{\pi T})^{-1}$ is the probability density to return to 0 at time T. This indeed reproduces Eq. (4.9).

4.3.1 Scale invariance and a useful transformation

The fact that fBm is a scale invariant (i.e. self affine) process implies interesting properties for various distributions. For t_+, and similarly for other temporal observables, the distribution $\mathcal{P}_H^T(t_+)$ for a fBm process defined on $[0, T]$ (with either a free end-point or a constrained one) takes the scaling form

$$\mathcal{P}_H^T(t_+) = \frac{1}{T} g\left(\vartheta = \frac{t_+}{T}\right) \ . \tag{4.12}$$

Using this, the double Laplace transform of the distribution can be reformulated using a one-variable transformation:

$$\begin{aligned} \tilde{\mathcal{P}}_H(\lambda, s) = \int_0^\infty \mathrm{d}T \int_0^T \mathrm{d}t_+ e^{-sT-\lambda t_+} \mathcal{P}_H^T(t_+) &= \int_0^\infty \mathrm{d}T \int_0^1 \mathrm{d}\vartheta \, e^{-T(s+\lambda\vartheta)} g(\vartheta) \\ &= \frac{1}{s} \int_0^1 \mathrm{d}\vartheta \frac{g(\vartheta)}{1 + \frac{\lambda}{s}\vartheta} = \frac{1}{s} \bar{g}\left(\kappa = \frac{\lambda}{s}\right) . \end{aligned} \tag{4.13}$$

The scaling function $g(\vartheta)$ encoding the distribution $\mathcal{P}_H^T(t_+)$, and the scaling function $\bar{g}(\kappa)$ encoding its double Laplace transform $\tilde{P}(\lambda, s)$, are related by a simple integral transform which we denote $\mathcal{K}_1$,

$$\mathcal{K}_1[g](\kappa) := \int_0^1 \mathrm{d}\vartheta \, \frac{g(\vartheta)}{1 + \kappa\vartheta} = \bar{g}(\kappa) \ . \tag{4.14}$$

For the case of interest, a fBm bridge of lenght T, this relation is more complicated since we can not compute directly the double Laplace transform of $\mathcal{P}_H^{\text{bridge}}(t_+)$, but only the transform of an unnormalised distribution, which we write $Z^{\text{N}}(T)\mathcal{P}_H^{\text{bridge}}(t_+)$. As we will see, the normalisation factor $Z^{\text{N}}(T)$, which is the probability density to return to 0 at time T, is a power law,

$$Z^{\text{N}}(T) = C \, T^{\alpha - 1} \ , \tag{4.15}$$

with some constant C. In this case, the double Laplace transform of the unnormalised distribution is computed as

$$\begin{aligned}\int_0^\infty \mathrm{d}T \int_0^T \mathrm{d}t_+ e^{-sT-\lambda t_+} C T^{\alpha-1} \mathcal{P}_H^{\text{bridge}}(t_+) &= \int_0^1 \mathrm{d}\vartheta \int_0^\infty \mathrm{d}T\, C T^{\alpha-1} e^{-T(s+\lambda\vartheta)} g(\vartheta) \\ &= \frac{C\,\Gamma(\alpha)}{s^\alpha} \int_0^1 \mathrm{d}\vartheta \frac{g(\vartheta)}{\left(1+\frac{\lambda}{s}\vartheta\right)^\alpha} \\ &\stackrel{!}{=} \frac{C\,\Gamma(\alpha)}{s^\alpha} \mathcal{K}_\alpha[g]\left(\kappa = \frac{\lambda}{s}\right) \ . \end{aligned} \tag{4.16}$$

Here we generalised the $\mathcal{K}$ transform to another exponent,

$$\mathcal{K}_\alpha[g](\kappa) := \int_0^1 \mathrm{d}\vartheta\, \frac{g(\vartheta)}{(1+\kappa\vartheta)^\alpha} \ . \tag{4.17}$$

If $\bar{g}(\kappa) = \mathcal{K}_\alpha[g](\kappa)$ is the $\mathcal{K}_\alpha$ transform of a function $g(\vartheta)$ normalised to unity, then $\bar{g}(\kappa) \to 1$ for $\kappa \to 0$. If further $g(\vartheta)$ is time-reversal symmetric, $g(\vartheta) = g(1-\vartheta)$ for $\vartheta \in [0,1]$, then the function $\bar{g}(\kappa)$ has the symmetry

$$\bar{g}(\kappa) = \frac{1}{(1+\kappa)^\alpha} \bar{g}\left(-\frac{\kappa}{1+\kappa}\right) \ . \tag{4.18}$$

4.3.2 FBm bridge with $H = \frac{1}{2} + \varepsilon$

The path-integral approach presented in Section 2.2 yields an expression for the (unnormalised) density distribution of t_+ for a bridge,

$$Z^{\text{pos}}(t_+, T) = \int_{X_0=0}^{X_T=0} \mathcal{D}[X]\, \delta\left(\int_0^T \mathrm{d}t\, \Theta(X_t) - t_+\right) e^{-S[X]} \ . \tag{4.19}$$

It is useful to consider its double Laplace transform ($T \to s$ and $t_+ \to \lambda$), which we denote with a tilde

$$\tilde{Z}^{\text{pos}}(\lambda, s) = \int_0^\infty \mathrm{d}T\, e^{-sT} \int_{X_0=0}^{X_T=0} \mathcal{D}[X]\, e^{-S[X] - \lambda \int_0^T \mathrm{d}t\, \Theta(X_t)} \ . \tag{4.20}$$

Using the ε-expansion (5.7) for the action, we compute this perturbatively, expanding around Brownian motion. The resulting series in ε has the form

$$\tilde{Z}^{\text{pos}}(\lambda, s) = \tilde{Z}_0^{\text{pos}}(\lambda, s) + \varepsilon \tilde{Z}_1^{\text{pos}}(\lambda, s) + O(\varepsilon^2) \ . \tag{4.21}$$

The first term of this expansion, the result for Brownian motion, is as in Eq. (4.9) obtained from the propagator $\tilde{W}^+$,

$$\tilde{Z}_0^{\text{pos}}(\lambda, s) = \tilde{W}^+(\lambda, s) = \frac{1}{\sqrt{s}} \frac{1}{\sqrt{1+\kappa}+1} = \frac{\bar{g}_0(\kappa)}{2\sqrt{s}} \ . \tag{4.22}$$

Here we denoted

$$\bar{g}_0(\kappa) = \int_0^1 \mathrm{d}\vartheta \frac{g_0(\vartheta)}{\sqrt{1+\kappa\vartheta}} = \frac{2}{\sqrt{1+\kappa}+1} \ . \tag{4.23}$$

This can be inverted to

$$g_0(\vartheta) = 1 \ . \tag{4.24}$$

This reproduces the known result that the probability distribution (1.27) for a Brownian bridge is uniform [10, 11].

To compute the order-ε term $\tilde{Z}_1^{\rm pos}(\lambda, s)$, we use the same diagrammatic rules as in Chapter 2, Section 2.2.4. As seen there, these rules are easily expressed in Laplace variables, which is why we compute the expansion of $\tilde{Z}^{\rm pos}(\lambda, s)$. The first order-$\varepsilon$ correction comes from the non-local interaction in the action, given in the second line of Eq. (5.7), and can be written as

$$\tilde{Z}_{1\rm A}^{\rm pos}(\lambda, s) = 2\int_0^\Lambda \mathrm{d}y \int_{-\infty}^{\infty}\mathrm{d}x_1 \int_{-\infty}^{\infty}\mathrm{d}x_2\; \tilde{W}^+(\lambda, s, 0, x_1)\, \partial_{x_1}\tilde{W}^+(\lambda, s+y, x_1, x_2)\, \partial_{x_2}\tilde{W}^+(\lambda, s, x_2, 0)\ . \tag{4.25}$$

As explained in chapter 2, Eq. 2.75, the large-y cutoff Λ, which is necessary as the integral is logarithmically divergent, is linked to the short-time (UV) regularisation τ introduced in Eq. (5.7) by $\Lambda = e^{-\gamma_{\rm E}}/\tau$. Performing the integrations over space variables and over y, and after some simplifications, we obtain

$$\tilde{Z}_{1\rm A}^{\rm pos}(\lambda, s) = \frac{1}{\sqrt{s}}\Bigg[\left(\frac{4}{\sqrt{\kappa+1}}+4\right)\ln\left(\sqrt{\kappa+1}+1\right) - \frac{2\kappa+2+\sqrt{\kappa+1}}{\kappa}\ln(\kappa+1) + \frac{\ln(s\tau)+7-7\ln(4)+\gamma_{\rm E}}{\sqrt{\kappa+1}+1}\Bigg]\ . \tag{4.26}$$

We have expressed the result in terms of the dimensionless variable $\kappa = \lambda/s$. The second order-ε correction comes from the rescaling of the diffusive constant, cf. Eq. (2.4). It is computed by rescaling T in the result for the Brownian, setting $T \to D_{\varepsilon,\tau}T$. In Laplace variables, this is equivalent to writing

$$\tilde{Z}_0^{\rm pos}(\lambda, s) \to \frac{1}{D_{\varepsilon,\tau}}\tilde{Z}_0^{\rm pos}\left(\frac{\lambda}{D_{\varepsilon,\tau}}, \frac{s}{D_{\varepsilon,\tau}}\right)\ . \tag{4.27}$$

Extracting the order-ε term gives

$$\tilde{Z}_{1B}^{\rm pos}(\lambda, s) = -\frac{1+\ln(\tau)}{2\sqrt{s}}\frac{2}{\sqrt{1+\kappa}+1}\ . \tag{4.28}$$

Resumming all order-ε corrections,

$$\tilde{Z}_1^{\rm pos}(\lambda, s) = \tilde{Z}_{1A}^{\rm pos}(\lambda, s) + \tilde{Z}_{1B}^{\rm pos}(\lambda, s)\ , \tag{4.29}$$

the τ dependence vanishes. The $\ln(s)$ term in Eq. (4.26) is proportional to $\bar{g}_0(\kappa)$, such that we can recast it as an order-ε correction to the exponent of the prefactor: $s^{-1/2} \to s^{H-1} + O(\varepsilon^2)$. This allows us to write the path integral (4.20) in the form

$$\tilde{Z}^{\rm pos}(\lambda, s) = \frac{\Gamma(1-H)}{2\sqrt{\pi}s^{1-H}}\left[\bar{g}_0(\kappa) + \varepsilon\bar{g}_1^{\rm pos}(\kappa)\right] + O(\varepsilon^2)\ . \tag{4.30}$$

With this choice of prefactor, the constant C in Eq. (4.16) is $C = (2\sqrt{\pi})^{-1}$, and $\bar{g}_1^{\rm pos}(\kappa)$ is

$$\bar{g}_1^{\rm pos}(\kappa) = 8\left(\frac{1}{\sqrt{\kappa+1}}+1\right)\ln\left(\sqrt{\kappa+1}+1\right) - 2\frac{2\kappa+2+\sqrt{\kappa+1}}{\kappa}\ln(\kappa+1) + 4\frac{3-4\ln(4)}{\sqrt{\kappa+1}+1}\ . \tag{4.31}$$

We recall that this function contains contributions from $\tilde{Z}_{1\rm A}^{\rm pos}$, $\tilde{Z}_{1\rm B}^{\rm pos}$ and the expansion of

$$\frac{1}{\sqrt{\pi}}\Gamma\left(\frac{1}{2}-\varepsilon\right) = 1 + \varepsilon\left[\gamma_{\rm E} + \ln(4)\right] + O(\varepsilon^2)\ , \tag{4.32}$$

due to the choice of normalisation in Eq. (4.30).

We know that the distribution of the positive time has the form given in Eq. (4.12). After expanding it in ε it gives

$$\mathcal{P}^{\text{bridge}}_{H=\frac{1}{2}+\varepsilon}(t_+) = \frac{1}{T}\Big[g_0(\vartheta) + \varepsilon g_1^{\text{pos}}(\vartheta)\Big] + O(\varepsilon^2) \ , \tag{4.33}$$

where, as before, $\vartheta = t_+/T$.

We have seen in Section 4.3.1 that the scaling functions $g(\vartheta)$ and $\bar{g}(\kappa)$ are related via the $\mathcal{K}_{1-H}$ transform, where the index of the transformation is fixed by the prefactor s^{H-1} in Eq. (4.30).

Expanding with respect to ε in the definition of the $\mathcal{K}$ transform gives

$$\begin{aligned}\bar{g}(\kappa) = \int_0^1 \mathrm{d}\vartheta \frac{1}{(1+\kappa\vartheta)^{\frac{1}{2}-\varepsilon}} g(\vartheta) &= \int_0^1 \mathrm{d}\vartheta \frac{1+\varepsilon\ln(1+\kappa\vartheta)}{\sqrt{1+\kappa\vartheta}}\left[g_0(\vartheta)+\varepsilon g_1(\vartheta)\right] + O(\varepsilon^2) \\ &= \bar{g}_0(\kappa) + \varepsilon\int_0^1 \mathrm{d}\vartheta \frac{\left[g_1(\vartheta) + g_0(\vartheta)\ln(1+\kappa\vartheta)\right]}{\sqrt{1+\kappa\vartheta}} + O(\varepsilon^2)\end{aligned} \tag{4.34}$$

The order-ε correction $g_1(\vartheta)$ that we are looking for is then given by

$$g_1(\vartheta) = \mathcal{K}^{-1}_{\frac{1}{2}}\left[\bar{g}_1(\kappa) - \bar{g}_{0,1}(\kappa)\right] \ , \tag{4.35}$$

where we have defined

$$\bar{g}_{0,1}(\kappa) = \int_0^1 \mathrm{d}\vartheta \, \frac{\ln(1+\kappa\vartheta)}{\sqrt{1+\kappa\vartheta}} g_0(\vartheta) = \frac{2}{\kappa}\left\{2 + \sqrt{1+\kappa}\big[\ln(\kappa+1) - 2\big]\right\} \ . \tag{4.36}$$

This contribution is valid both for t_+ and $t_{\max}$, since both observables have the same distribution at order zero, and both have the same power law from scaling.

We now have to deal with the inverse $\mathcal{K}_{\frac{1}{2}}$ transform in Eq. (4.35). This is linked to the Abel transform, on which details are given in Appendix 4.B. The final result for the order-ε correction is

$$g_1^{\text{pos}}(\vartheta) = 4\left[2 - \frac{1}{\sqrt{\vartheta}+1} + \ln\left(\frac{\sqrt{\vartheta}+1}{4\sqrt{\vartheta}}\right) - \frac{1}{\sqrt{1-\vartheta}+1} + \ln\left(\frac{\sqrt{1-\vartheta}+1}{4\sqrt{1-\vartheta}}\right)\right] . \tag{4.37}$$

We can check that the integral of $g_1^{\text{pos}}(\vartheta)$ over $[0,1]$ vanishes, such that Eq. (4.33) is correctly normalised at order ε. We also checked that by computing numerically the $\mathcal{K}_{1/2}$ transform of this result reproduces $\bar{g}_1^{\text{pos}}(\kappa) - \bar{g}_{0,1}(\kappa)$ with excellent precision.

Close to the boundary, the asymptotics is

$$g_1^{\text{pos}}(\vartheta) \underset{\vartheta\to 0,1}{\simeq} -2\ln(\vartheta) - 2\ln(1-\vartheta) \ . \tag{4.38}$$

This asymptotics can be recast into a power law consistent with scaling. The distribution of t_+ for a fBm bridge with $H = \frac{1}{2} + \varepsilon$ can then be written as

$$\boxed{\mathcal{P}^{\text{bridge}}_{H=\frac{1}{2}+\varepsilon}(t_+) = \frac{\exp\Big(\varepsilon\left[\mathcal{F}^{\text{pos}}(\vartheta) - 4\right]\Big)}{T[\vartheta(1-\vartheta)]^{2H-1}} + O(\varepsilon^2) \ .} \tag{4.39}$$

The scaling function $\mathcal{F}^{\text{pos}}(\vartheta)$ has by definition vanishing integral, and is given by

$$\boxed{\mathcal{F}^{\text{pos}}(\vartheta) = 4\left[3 - \frac{1}{\sqrt{\vartheta}+1} + \ln\left(\frac{\sqrt{\vartheta}+1}{4}\right) - \frac{1}{\sqrt{1-\vartheta}+1} + \ln\left(\frac{\sqrt{\vartheta}+1}{4}\right)\right] .} \tag{4.40}$$

4.3.3 Numerical results

To test our analytical predictions, we compare them to results from numerical simulations, using the same methods as in chapter 2 with details given in its appendix 2.I. As presented in section 4.2, we were able to transform each generated fBm path in a fBm bridge path with the correct weight. Then, from a large number of generated paths (typically 10^6), we construct a numerical estimation $\mathcal{P}_H^{\text{bridge}}(t_+)$ of the distribution of t_+ for various values of H, choosing $T = 1$. This is shown on Fig. 4.1, where results for the distributions of both t_+ and $t_{\max}$ are given. To compare to the analytical result (4.40), we extract $\mathcal{F}^{\text{pos}}_{\text{num}}$ from these distributions, using

$$\mathcal{F}^{\text{pos}}_{\text{num}}(\vartheta) = \frac{1}{\varepsilon} \ln\Big(T[\vartheta(1-\vartheta)]^{2H-1} \mathcal{P}^{\text{bridge}}_{H=\frac{1}{2}+\varepsilon}(\vartheta) \Big) \ . \tag{4.41}$$

As is shown in Fig. 4.2 (left), when $\varepsilon \to 0$, $\mathcal{F}^{\text{pos}}_{\text{num}}(\vartheta)$ converges to $\mathcal{F}^{\text{pos}}(\vartheta)$. The deviation being antisymmetric in ε strongly suggests that there is an order-ε^2 correction to the distribution of t_+, which we did not calculate here.

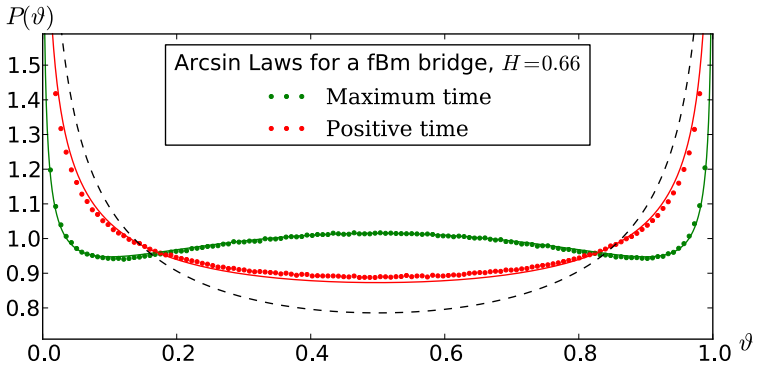

Figure 4.1: Comparison of the two "Arcsine laws" for a fBm bridge with Hurst exponent $H = 0.66$. Dots represent the distribution extracted from numerical simulations, the plain lines represent the analytical result at order ε given in Eqs. (4.39) and (4.46), and the dashed line is the scaling form (identical for both observables).

4.4 Extremum of fBm Bridges

In chapter 2 , a general formula was derived for the path integral over fBm paths X_t starting at m_1, going to $x_0 \approx 0$ at time t_1 and ending in m_2 at time $t_1 + t_2 = T$, while staying positive, $X_t > 0$ for all $t \in [0, T]$. This quantity, denoted $Z^+(m_1, t_1; x_0; m_2, t_2)$, is the result, up to first-order term, of an ε expansion and its expression is given in (2.34).

Here we apply this result to fBm bridges. The general result for $Z^+(m_1, t_1; x_0; m_2, t_2)$, restricted to $m_1 = m_2 = m$, and choosing $t_1 + t_2 = T$, immediately gives the joint distribution of the maximum m, and the time $t_{\max} = t_1$ when this maximum is attained. In a second step, we can then integrate over t_1 at T fixed, or over m at t_1 and t_2 fixed, to obtain the distributions of m and $t_{\max}$.

We will finally rederive these results in a simpler way, taking advantage of the scaling transformations introduced in section 4.3.1.

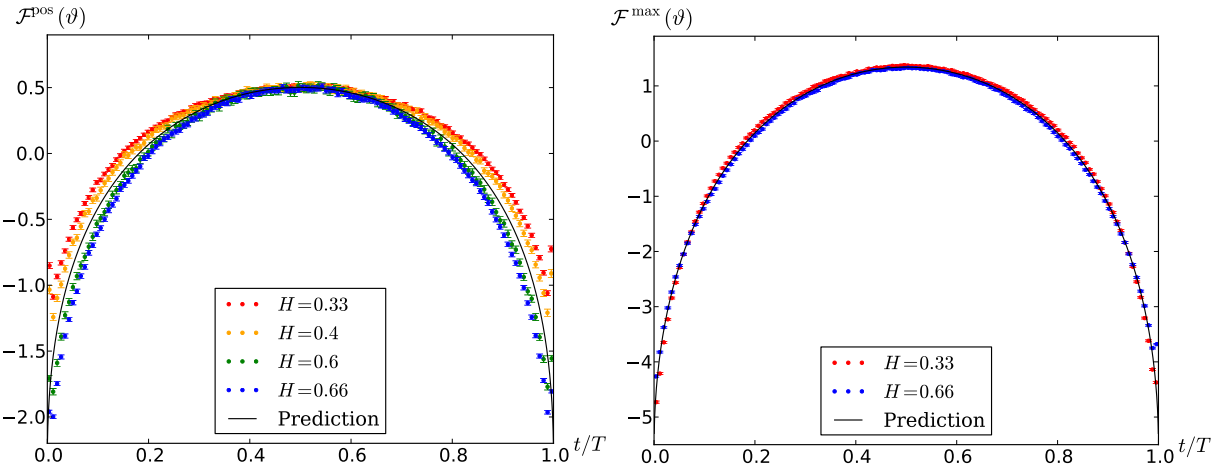

Figure 4.2: Left: Numerical estimation of the scaling function $\mathcal{F}^{\rm pos}(\vartheta)$, from top to bottom for $H = 0.33$ (red dots), $H = 0.4$ (orange dots), $H = 0.6$ (green dots), and $H = 0.66$ (blue dots), compared to the analytical result given in Eq. (4.40) (plane line). Right: *ibid* for $\mathcal{F}^{\rm max}(\vartheta)$ for $H = 0.33$ (blue dots, bottom) and $H = 0.66$ (red dots, top), the analytical result (plane line) is given in Eq. (4.47). For both plots, and for each value of H, the statistics is done with 5×10^6 sampled paths, discretized with $N = 2^{12}$ points.

4.4.1 Distribution of the time to reach the maximum

Starting with Eq. (2.34) and following the procedure section 2.3.3, we express the probability for $t_{\rm max}$, denoted $\mathcal{P}_H^{\rm bridge}(t_{\rm max})$, as

$$\mathcal{P}_H^{\rm bridge}(t_{\rm max}) = \frac{1}{Z^{\rm N}(T)} \int_0^\infty {\rm d}m \, Z^+(m,t;x_0;m,T-t) \; . \tag{4.42}$$

The integral over m accounts for all possible values of the maximum. $Z^{\rm N}(T)$ is a normalisation factor such that the integral over $t_{\rm max}$ of $\mathcal{P}_H^{\rm bridge}(t_{\rm max})$ is normalised to unity,

$$Z^{\rm N}(T) = \int_0^T {\rm d}t \int_0^\infty {\rm d}m \, Z^+(m,t;x_0;m,T-t) = \frac{x_0^{2-4\varepsilon}}{\sqrt{4\pi}}(1+\varepsilon C_1) + O(\varepsilon^2) \; . \tag{4.43}$$

The constant C_1 can be computed from Z^+, but it is equivalent to require that the order-ε term in Eq. (4.42) does not change the normalisation, such that the distribution $\mathcal{P}_H^{\rm bridge}(t_{\rm max})$ remains normalised to one.

Expanding the distribution of $t_{\rm max}$ in the same way as for Eq. (4.33), the order-ε term becomes, setting again $\vartheta = t_{\rm max}/T$, and $T = 1$

$$\begin{aligned} g_1^{\rm max}(\vartheta) &= 2\sqrt{\pi} \int_0^\infty {\rm d}m \left[Z_1^+(m,\vartheta;x_0;m,1-\vartheta) - C_1 Z_0^+(m,\vartheta;x_0;m,1-\vartheta) \right] \\ &= 2\Big[6(\sqrt{1-\vartheta}+\sqrt{\vartheta}) - 3\vartheta\ln(1-\vartheta) - 3(1-\vartheta)\ln(\vartheta) + (4-3\vartheta)\ln(2-\vartheta) \\ &\quad + (3\vartheta+1)\ln(\vartheta+1) + (6\vartheta-4){\rm arcth}(\sqrt{1-\vartheta}) + (2-6\vartheta){\rm arcth}(\sqrt{\vartheta}) - 8 - 4\ln(2) \Big] \; . \end{aligned} \tag{4.44}$$

This result will be checked from Eq. (4.71) given below. Demanding that $g_1^{\rm max}(\vartheta)$ has integral zero fixed the constant C_1 to $C_1 = 4\ln(2) - \gamma_{\rm E}$.

Close to the boundary, the correction has the same asymptotics as in the calculation for t_+, namely

$$g_1^{\rm max}(\vartheta) \underset{\vartheta\to 0,1}{\simeq} -2\ln(\vartheta) - 2\ln(1-\vartheta) \; , \tag{4.45}$$

which indicates the same change in the power-law behaviour of $\mathcal{P}_H^{\text{bridge}}(t_{\max})$. Again taking an exponential resummation of the order-ε correction, we obtain a formula similar to Eq. (4.39), but with a different scaling function $\mathcal{F}^{\max}(\vartheta)$,

$$\boxed{\mathcal{P}^{\text{bridge}}_{H=\frac{1}{2}+\varepsilon}(t_{\max}) = \frac{\exp\Big(\varepsilon\big[\mathcal{F}^{\max}(\vartheta)-4\big]\Big)}{T[\vartheta(1-\vartheta)]^{2H-1}} + O(\varepsilon^2)\ .} \tag{4.46}$$

$\mathcal{F}^{\max}(\vartheta)$ is a bounded function of $\vartheta \in [0,1]$ and can be expressed from Eq. (4.44) as

$$\boxed{\mathcal{F}^{\max}(\vartheta) = g_1^{\max}(\vartheta) + 2\ln\big(\vartheta(1-\vartheta)\big) + 4\ .} \tag{4.47}$$

The constant 4 was added in Eq. (4.47) and subtracted in Eq. (4.46) to have $\int_0^1 \mathrm{d}\vartheta\, g_1^{\max}(\vartheta) = \int_0^1 \mathrm{d}\vartheta\, \mathcal{F}^{\max}(\vartheta) = 0$.

The two distributions, for t_+ and $t_{\max}$, at order ε are plotted in Fig. 4.1. While both functions have the same power-law behavior for ϑ close to 0 or 1, their difference is clearly visible. The result (4.47) for $\mathcal{F}^{\max}(\vartheta)$ is compared with great precision to numerical simulations on figure 4.2 (right).

4.4.2 The maximum-value distribution

Similarly to the distribution of $t_{\max}$, the distribution of the maximum value $m = \max_{t\in[0,T]} X_t$ can be expressed from the result Eq. 2.34 :

$$\mathcal{P}_H^{\text{bridge}}(m) = \frac{1}{Z^{\text{N}}(T)} \int_0^T \mathrm{d}t\, Z^+(m,t;x_0;m,T-t)\ . \tag{4.48}$$

This calculation is rather cumbersome, but it is possible to give a simpler derivation, where we do not constrain paths to go close to the boundary, but construct $\mathcal{P}_H^{\text{bridge}}(m)$ by taking a derivative of its cumulative distribution, the survival probability, conditioned such that the end point of the process is the same as the starting point. In this framework, the order-ε correction to $\mathcal{P}_H^{\text{bridge}}(m)$ can, due to the non-local term in the action (5.7), be expressed in Laplace variables ($T \to s$) using the diagrammatic rules presented in 2.2.4. The integrals to be computed are

$$\begin{aligned}\tilde{Z}^{\max}_{1A}(m,s) &= 2\partial_m \int_0^\Lambda \mathrm{d}y \int_{x_1,x_2>0} \tilde{P}_0^+(m,x_1;s)\,\partial_{x_1}\tilde{P}_0^+(x_1,x_2;s+y)\,\partial_{x_2}\tilde{P}_0^+(x_2,m;s) \qquad (4.49)\\ &= 2(a+1)e^{2a}\,\mathrm{Ei}(-4a) - 2\,\mathrm{Ei}(-2a) + 2e^{-2a}\left\{a\left[\ln\left(\frac{m^2}{4\tau}\right) - \ln(a) - 1\right] + \ln\left(\frac{2\tau}{m^2}\right) - \gamma_{\text{E}}\right\}\ ,\end{aligned}$$

where $a := \sqrt{s}m$ is a dimensionless variable, $\Lambda = e^{-\gamma_{\text{E}}}/\tau$, and the propagator $\tilde{P}_0^+(x_1,x_2;s)$ is defined in Eq. (3.23). To deal with the inverse Laplace transform, we use formulas already derived in 2.G , plus similar formulas collected in appendix 4.C. The final result for the correction after the inverse Laplace transformation is

$$\begin{aligned}Z^{\max}_{1A}(m,T) = \frac{ze^{-z^2}}{\sqrt{\pi}T}\Big\{&2z\sqrt{\pi}e^{z^2}\mathrm{erfc}(z) + 4(1-z^2)\mathcal{J}\Big(z^2\Big) + 2z^2\left[\ln\left(\frac{Tz^2}{\tau}\right) + \gamma_{\text{E}} - 1\right] \qquad (4.50)\\ &+ \ln\left(\frac{\tau^3}{T^3z^8}\right) - 4\gamma_{\text{E}} + 1\Big\}\ .\end{aligned}$$

We introduced the scaling variable $z := m/\sqrt{T}$. The special function $\mathcal{J}$ defined in Eq. 2.168 is

$$\mathcal{J}(x) = \frac{1}{2}\pi\,\mathrm{erfi}\left(\sqrt{x}\right) - x\,{}_2F_2\left(1,1;\frac{3}{2},2;x\right)\ . \tag{4.51}$$

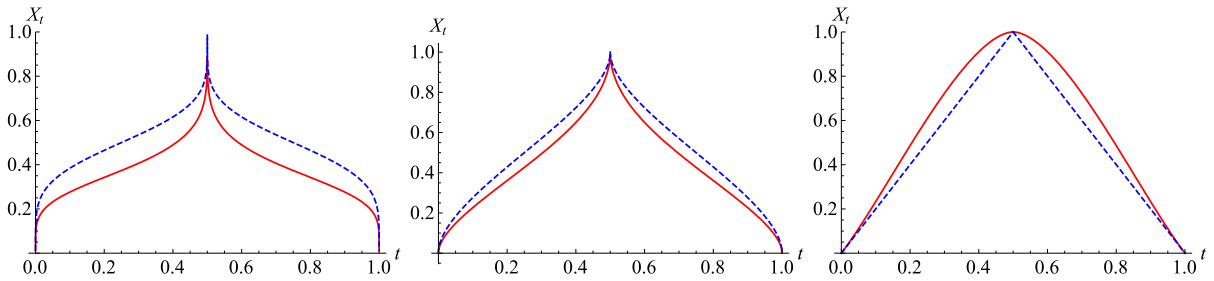

Figure 4.3: Plain red line: optimal paths for fBm conditioned to $X_0 = 0$, $X_{1/2} = 1$ and $X_1 = 0$, for, from left to right, $H = 0.1$, $H = 0.25$ and $H = 1$. The blue dashed-line represents the optimal paths when neglecting the correlation between $[0, 1/2]$ and $[1/2, 1]$.

For a Brownian bridge we have

$$Z_0^{\max}(m,T) = \frac{m}{\sqrt{\pi}T^{\frac{3}{2}}} e^{-\frac{m^2}{T}} \ , \tag{4.52}$$

which, after normalisation, allows to recover the distribution (1.29).

The second order-ε correction, which comes from the rescaling of the diffusive constant, is obtained by replacing $T \to D_{\varepsilon,\tau} T$ in Eq. (4.52); for the order-ε term this gives

$$Z_{1B}^{\max}(m,T) = \frac{z e^{-z^2}}{\sqrt{\pi}T}(2z^2 - 3)(1 + \ln \tau) \ . \tag{4.53}$$

Resumming these corrections up to order ε cancels all τ dependencies; recasting the relevant corrections into the power-law prefactor and the Gaussian tail and expressing the result in terms of the dimensionless variable $y := m/T^H$ finally yields

$$\boxed{\mathcal{P}_H^{\text{bridge}}(m) = 2\sqrt{\pi}T^H \left[Z_0^{\max} + \varepsilon(Z_{1A}^{\max} + Z_{1B}^{\max})\right] + O(\varepsilon^2) = \frac{2y^{1-8\varepsilon}}{T^H} e^{-y^2 A_\varepsilon + \varepsilon \mathcal{G}(y) + \text{cst}} + O(\varepsilon^2) \ .} \tag{4.54}$$

The special function $\mathcal{G}$ appearing here is as defined in Refs. [125],

$$\mathcal{G}(y) = -4\left(y^2 - 1\right)\mathcal{J}\left(y^2\right) + 2\sqrt{\pi}e^{y^2} y \operatorname{erfc}(y) + 2y^2\left[\ln\left(4y^2\right) + \gamma_{\text{E}}\right] - 4\gamma_{\text{E}} - 2 \ . \tag{4.55}$$

This result contains several non-trivial predictions: First, at small m, the distribution $\mathcal{P}_H^{\text{bridge}}(m)$ has a power law given by $m^{1-8\varepsilon+O(\varepsilon^2)}$. This can be obtained by considering the probability starting at m to remain positive (survive) up to time T,

$$\mathcal{S}(T,m) := \int_0^m \mathrm{d}m_1 \, \mathcal{P}_H(m_1) \ . \tag{4.56}$$

In this relation the dependence of $\mathcal{P}_H(m)$ on T is implicit. It is valid both for the case of a bridge and of a free endpoint. A surviving bridge process (starting and ending in $m \to 0$) needs to survive both at its beginning and at its end, thus we expect that for small m

$$\mathcal{S}^{\text{bridge}}(T,m) \sim \left[\mathcal{S}^{\text{free}}(T,m)\right]^2 \ . \tag{4.57}$$

Using the fact that $\mathcal{P}_H^{\text{free}}(m) \sim m^{\frac{1}{H}-2}$, cf. Eq. 2.28, implies that

$$\mathcal{P}_H^{\text{bridge}}(m) \sim m^{\frac{2}{H}-3} \ . \tag{4.58}$$

This is in agreement with our order-ε result.

Second, at large m, $\mathcal{P}_H^{\text{bridge}}(m)$ has a Gaussian tail with the dimensionless variable $y^2 = z^2/T^{2\varepsilon} = m^2/T^{2H}$ and a non-trivial number $A_\varepsilon = 1 + 4\varepsilon \ln(2) + O(\varepsilon^2)$. We will see in the next section why this number appears, and how we can compute it exactly (i.e. for all H).

Third, there is a crossover in the power-law behavior at large y, given by the asymptotic behaviour of the function $\mathcal{G}(y)$,

$$\mathcal{G}(y) \underset{y\to\infty}{\simeq} 4\ln(y) \ . \tag{4.59}$$

This yields a subleading power-law behaviour at large m

$$\mathcal{P}_H^{\text{bridge}}(m)\, e^{A_\varepsilon \frac{m^2}{T^{2H}}} \sim m^{1-4\varepsilon+O(\varepsilon^2)} \ . \tag{4.60}$$

4.4.3 Optimal path for fBm, and the tail of the maximum distribution

In this section, we study the tail of the maximum distribution for fBm. Contrary to a process with a free endpoint, the maximum is not taken at the end, and as a consequence the tail is not simply given by the known propagator evaluated at time T at position m.

We start with some general considerations: If we choose $t_1, ..., t_n \in \mathbb{R}$, then the density distribution for a fBm path X_t to take values $X_{t_1} = x_1, ..., X_{t_n} = x_n$ can be expressed, using the Gaussian nature of the process X_t, as

$$\mathcal{P}_n(x_1, x_2, ..., x_n) = \exp\left(-\frac{1}{2}\sum_{ij} x_i \mathcal{M}_{ij} x_j\right) \ . \tag{4.61}$$

The matrix $\mathcal{M}_{ij}$ is given by

$$\mathcal{M}_{ij}^{-1} = \langle X_{t_i} X_{t_j}\rangle = t_i^{2H} + t_j^{2H} - |t_i - t_j|^{2H} \ . \tag{4.62}$$

To study bridges, consider now two points, $x_1 = x$ at time $t_1 = t$ with $0 < t < T$ and $x_2 = 0$ at time $t_2 = T$. The probability distribution of x given $x_T = 0$ is then given by

$$\mathcal{P}(x_t = x | x_T = 0) = \mathcal{P}_2(x, 0) = \exp\left(-\frac{\mathcal{M}_{11}\, x^2}{2}\right) \ . \tag{4.63}$$

The matrix element in question is (with $\vartheta = t/T$)

$$\frac{\mathcal{M}_{11}}{2} = \frac{1}{T^{2H}} \frac{1}{4\vartheta^{2H} - \left[\vartheta^{2H} - (1-\vartheta)^{2H} + 1\right]^2} \ . \tag{4.64}$$

It takes its minimum for $\vartheta = \frac{1}{2}$. The tail for the maximum of a bridge is thus given by Eq. (4.63) with the matrix element $\mathcal{M}_{11}$ in Eq. (4.64) evaluated at $\vartheta = \frac{1}{2}$: If we take a realisation of X_t with a large value of the maximum value m, the path typically reaches m close to the center of the interval, as it is the point where the process has maximum variance. This means that when $m = \max_{s\in[0,t]} X_s \gg t^H$, we have $t_{\max} \approx t/2$, which also means that $m \approx X_{t/2}$. The Gaussian tail of the maximum value distribution should then be the same as the tail of $X_{t/2}$ distribution (with power law corrections due to the fluctuation of $t_{\max}$ around $t/2$, cf. chapter 5). This gives for large m

$$\mathcal{P}_H^T(m) \sim \mathcal{P}(x_{T/2} = m | x_T = 0) = e^{-\frac{m^2}{T^{2H}} \frac{4^H}{4-4^H} + O(\ln(m))} \ . \tag{4.65}$$

This heuristic argument is consistent with the result from our ε expansion, and allows us to predict the *exact* value of the constant A_ε,

$$A_\varepsilon = \frac{4^H}{4-4^H} = 1 + 4\ln(2)\varepsilon + O(\varepsilon^2) \ . \tag{4.66}$$

We can go further and study the shape of the optimal path with conditions $X_0 = X_1 = 0$ and $X_{1/2} = 1$. This is done by considering $\mathcal{P}_n(x, 1, 0)$, taken at time $t_1 = t$, $t_2 = 1/2$ and $t_3 = T = 1$. We then find $X_t^{\rm SP} = x$ which minimises the "energy" $-\ln \mathcal{P}_3(x, m, 0)$. This is for $0 \le \vartheta \le \frac{1}{2}$ achieved for

$$X_t^{\rm SP} = \frac{m}{4-4^H}\Big[2 - 2(1-2\vartheta)^{2H} + 4^H(1-\vartheta)^{2H} + 4^H\vartheta^{2H} - 4^H\Big]. \tag{4.67}$$

For $\frac{T}{2} < t \le T$ one has $X_t^{\rm SP} = X_{T-t}^{\rm SP}$. This is represented for $m = 1$ and $T = 1$ in red in Fig. 4.3 for various values of H. It is interesting to observe that this *optimal path* is not a straight line going from $X_0 = 0$ to $X_{1/2} = 1$ and back to $X_1 = 1$, but at $t = 1/2$ peaked for $H < 1/2$, and smoothened for $H > 1/2$. It is equivalently interesting to compare this to the optimal path which goes from $X_0 = 0$ to $X_{1/2} = 1$, without imposing any constraint at $t = 1$, plus a similar segment from $X_{1/2} = 1$ to $X_1 = 0$ without constraint on X_0 (blue dashed lines). This would indeed be the optimal path if there were no correlations between times $t < 1/2$ and $t > 1/2$.

We finally note that the limit of $H \to 1$ is non-trivial, and given by (see right of Fig. 4.3)

$$X_t^{\rm SP} = \frac{m}{\ln(4)}\Big\{(1-2\vartheta)^2\ln(1-2\vartheta) - 2(1-\vartheta)^2\ln(1-\vartheta) + \vartheta[\ln(16) - 2\vartheta\ln(4\vartheta)]\Big\} \ , \quad 0 \le t \le \frac{T}{2} \tag{4.68}$$

and $X_t^{\rm SP} = X_{T-t}^{\rm SP}$ for $\frac{T}{2} < t < T$. We expect this also to be the lowest-energy fluctuation for the fBm bridge.

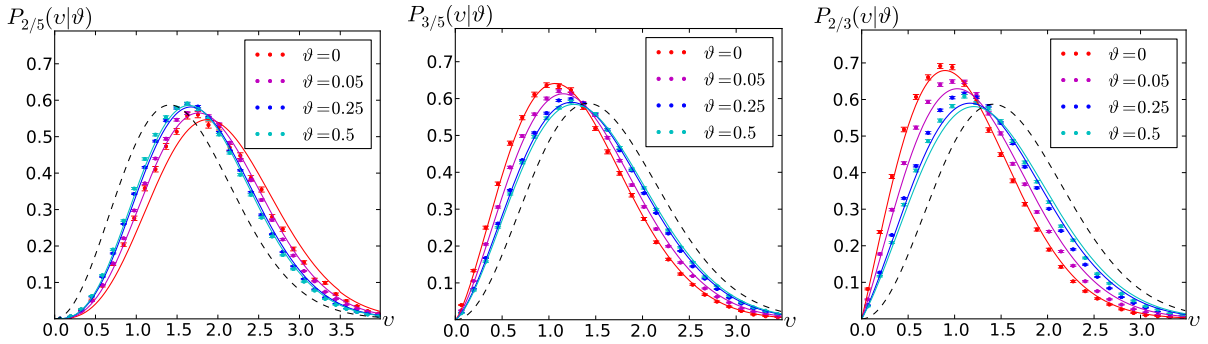

Figure 4.4: Numerical results for $\mathcal{P}_H(v|\vartheta)$ for $H = \frac{2}{5}$ (left), $H = \frac{3}{5}$ (middle) and $H = \frac{2}{3}$ (right). The values of ϑ are chosen as $\vartheta = 0$, $\vartheta = 0.05$, $\vartheta = 0.25$ to $\vartheta = 0.5$, the maximum useful value due to the symmetry $\vartheta \to 1 - \vartheta$. We used $N = 2^{18}$ points, and 5×10^6 samples.

4.4.4 Joint Distribution of m and $t_{\rm max}$

To obtain the joint distribution of m and $t_{\rm max}$, we start with Eq. (2.34), and specify $m_1 = m_2 = m$. This is equivalent, in the notations of section 2.3.2, to setting

$$y_1 = \frac{m}{\sqrt{2}\vartheta^H} \ , \ y_2 = \frac{m}{\sqrt{2}(1-\vartheta)^H} \ \text{ where } \vartheta = \frac{t_{\rm max}}{T} \ . \tag{4.69}$$

The resulting expression can more compactly be written in terms of

$$v := \frac{m}{\sqrt{2}[\vartheta(1-\vartheta)]^H} \ . \tag{4.70}$$

Recasting terms proportional to $\ln(\vartheta)$, $\ln(1-\vartheta)$ and $\ln(\upsilon)$ into the prefactor, we get

$$Z^+(m,\vartheta;x_0;m,1-\vartheta)=\frac{x_0^{2-4\varepsilon}\upsilon^{2-8\varepsilon}e^{-\frac{\upsilon^2}{2}}}{2\pi[\vartheta(1-\vartheta)]^{3H-1}}\Big\{1+\varepsilon\Big[\mathcal{F}(\upsilon,\vartheta)+C_2\Big]\Big\}+O(\varepsilon^2)\ , \tag{4.71}$$

with

$$\begin{aligned}\mathcal{F}(\upsilon,\vartheta)=&\frac{\mathcal{I}(\upsilon(1-\vartheta))+\mathcal{I}(\upsilon\vartheta)-\mathcal{I}(\upsilon)+2(\upsilon^2-1)}{\upsilon^2\vartheta(1-\vartheta)}-\frac{\mathcal{I}(\upsilon(1-\vartheta))}{1-\vartheta}-\frac{\mathcal{I}(\upsilon\vartheta)}{\vartheta}+2\,\mathcal{I}\Big(\upsilon\sqrt{1-\vartheta}\Big)\\&+2\,\mathcal{I}\Big(\upsilon\sqrt{\vartheta}\Big)+\upsilon^2\big(\ln(2\upsilon^2)+\gamma_{\rm E}\big)-12-8\ln(2)\ ,\end{aligned} \tag{4.72}$$

$$C_2=4\Big[2-\gamma_{\rm E}+\ln(2)\Big]\ . \tag{4.73}$$

First, this result allows us to recover Eqs. (4.44) and (4.47), noting that

$$\mathcal{F}^{\max}(\vartheta)=\sqrt{\frac{2}{\pi}}\int_0^\infty {\rm d}\upsilon\,\upsilon^2e^{-\frac{\upsilon^2}{2}}\mathcal{F}(\upsilon,\vartheta)\ . \tag{4.74}$$

As we defined $\int_0^1{\rm d}\vartheta\,\mathcal{F}^{\max}(\vartheta)=0$, there is an additional constant C_2, related to the prefactor $\upsilon^{-8\varepsilon}$ in Eq. (4.71).

Second, we can extract the conditional probability of υ, given ϑ. This is interesting since for a Brownian the latter depends only on the variable υ introduced in Eq. (4.70),

$$\mathcal{P}^{\rm bridge}_{H=\frac12}(\upsilon|\vartheta)=\sqrt{\frac{2}{\pi}}\upsilon^2e^{-\frac{\upsilon^2}{2}}\ . \tag{4.75}$$

For a generic value of $H=\frac12+\varepsilon$, our ε expansion, recast in an exponential form, gives

$$\boxed{\mathcal{P}^{\rm bridge}_{H}(\upsilon|\vartheta)=\sqrt{\frac{2}{\pi}}\upsilon^{\frac{2}{H}-2}e^{-\frac{\upsilon^2}{2}+\varepsilon[\mathcal{F}(\upsilon,\vartheta)+C_2-\mathcal{F}^{\max}(\vartheta)]}+O(\varepsilon^2)\ .} \tag{4.76}$$

The functions $\mathcal{F}(\upsilon,\vartheta)$ and $\mathcal{F}^{\max}(\vartheta)$ are defined in Eqs. (4.72) and (4.47). The exponent in Eq. (4.76) can be derived from scaling. To this aim, note that the probability to have a maximum of m up to time T is

$$\mathcal{P}_H(m)=\partial_m\mathcal{S}(T,m)\ . \tag{4.77}$$

On the other hand, the probability that the maximum m is taken at time T is

$$\mathcal{P}_H(m|T)=\partial_T\mathcal{S}(T,m)\ . \tag{4.78}$$

We conclude that for small m

$$\mathcal{P}^{\rm bridge}_H(m|T)\sim\frac{m}{T}\mathcal{P}^{\rm bridge}_H(m)\sim m^{\frac{2}{H}-2}\sim\upsilon^{\frac{2}{H}-2}\ . \tag{4.79}$$

This exponent, written in Eq. (4.76), agrees with the perturbative expansion

$$\frac{2}{H}-2=2-8\varepsilon+O(\varepsilon^2)\ . \tag{4.80}$$

Finally, using the result (4.64), and expressing it in terms of υ predicts a tail $e^{-A'_\varepsilon\upsilon^2}$, with

$$\begin{aligned}A'_\varepsilon&=\frac{2[\vartheta(1-\vartheta)]^{2H}}{4\vartheta^{2H}-\left[\vartheta^{2H}-(1-\vartheta)^{2H}+1\right]^2}\\&=\frac12\left[1+\varepsilon^2\frac{[(1-\vartheta)\ln(1-\vartheta)+\vartheta\ln(\vartheta)]^2}{2(1-\vartheta)\vartheta}+O(\varepsilon^3)\right]\ .\end{aligned} \tag{4.81}$$

Thus our resummation (4.76) is correct to order ε; whether at higher order it is preferential to use v introduced in Eq. (4.70) with A'_ε given in Eq. (4.81), or whether one should keep $e^{-v^2/2}$ for the tail and redefine v can only be answered after a second-order calculation.

We verified the prediction (4.76) for $\mathcal{P}_H^{\text{bridge}}(v|\vartheta)$ numerically, see Fig. 4.4. The agreement is good for H close to $\frac{1}{2}$, both for $\varepsilon = -\frac{1}{10}$ and $\varepsilon = \frac{1}{10}$ (left two figures). Corrections of order ε^2 can be anticipated, since our numerical results for both $\varepsilon = -\frac{1}{10}$ and $\varepsilon = \frac{1}{10}$ show approximately the same (small) deviation from the analytics, independent of the sign of ε.

These putative $O(\varepsilon^2)$ corrections also explain the larger systematic deviations for $H = \frac{2}{3}$, i.e. $\varepsilon = \frac{1}{6}$ (right plot).

4.5 Conclusions

In this chapter we developed a systematic analytical framework to treat bridge processes for fractional Brownian motion, in an expansion around Brownian motion. We considered the probability of the time t_+ that a bridge process is positive, and of the time $t_{\max}$ it achieves its maximum. For a Brownian bridge, both t_+ and $t_{\max}$ have the same uniform probability distribution. For a fractional Brownian bridge, both observables have the same power-law behavior for times close to the beginning and end, but the subleading scaling functions are rather different. We calculate them to first order in ε, and verified them to high precision with numerical simulations. We also obtained and checked the joint distribution of the maximum m, and the time $t_{\max}$ when this maximum is taken. These tests were possible due to the development of an efficient algorithm to generate samples of fBm bridges.

4.A Details on correlation functions for Gaussian bridges

Starting from Eqs. (4.1) and (4.2), and inserting the identity $\delta(x) = \int_{-\infty}^{\infty} e^{ikx} \frac{\mathrm{d}k}{2\pi}$, we obtain

$$\langle \delta(X_T - a) \rangle = \int_{-\infty}^{\infty} \frac{\mathrm{d}k}{2\pi} \langle e^{ik(X_T - a)} \rangle = \int_{-\infty}^{\infty} \frac{\mathrm{d}k}{2\pi} e^{-ika}\ e^{-\frac{k^2}{2}\langle X_T^2 \rangle} = \frac{e^{-\frac{a^2}{2\langle X_T^2 \rangle}}}{\sqrt{2\pi}\sqrt{\langle X_T^2 \rangle}} , \tag{4.82}$$

$$\begin{aligned} \langle X_{t_1} \delta(X_T - a) \rangle = \int_{-\infty}^{\infty} \frac{\mathrm{d}k}{2\pi} \langle X_{t_1} e^{ik(X_T - a)} \rangle &= \int_{-\infty}^{\infty} \frac{\mathrm{d}k}{2\pi} e^{-ika}\, ik\, \langle X_{t_1} X_T \rangle e^{-\frac{k^2}{2}\langle X_T^2 \rangle} \\ &= \frac{e^{-\frac{a^2}{2\langle X_T^2 \rangle}}}{\sqrt{2\pi}\sqrt{\langle X_T^2 \rangle}} \frac{a \langle X_{t_1} X_T \rangle}{\langle X_T^2 \rangle} , \end{aligned} \tag{4.83}$$

and

$$\begin{aligned} \langle X_{t_1} X_{t_2} \delta(X_T - a) \rangle &= \int_{-\infty}^{\infty} \frac{\mathrm{d}k}{2\pi} \left\langle X_{t_1} X_{t_2} e^{ik(X_T - a)} \right\rangle \\ &= \int_{-\infty}^{\infty} \frac{\mathrm{d}k}{2\pi} e^{-ika} e^{-\frac{k^2}{2}\langle X_T^2 \rangle} \Big[\langle X_{t_1} X_{t_2} \rangle - k^2 \langle X_{t_1} X_T \rangle \langle X_{t_2} X_T \rangle \Big] \\ &= \frac{e^{-\frac{a^2}{2\langle X_T^2 \rangle}}}{\sqrt{2\pi}\sqrt{\langle X_T^2 \rangle}} \times \left[\langle X_{t_1} X_{t_2} \rangle + \Big(a^2 - \langle X_T^2 \rangle \Big) \frac{\langle X_{t_1} X_T \rangle \langle X_{t_2} X_T \rangle}{\langle X_T^2 \rangle^2} \right] . \end{aligned} \tag{4.84}$$

From the first to the second line of the last two equations we used Wick's theorem and its consequence,

$$\langle X_1 f(X_2) \rangle = \langle X_1 X_2 \rangle \langle f'(X_2) \rangle \tag{4.85}$$

and the fact that X_t has mean zero. Putting everything together, we arrive at Eqs. (4.3) and (4.4).

4.B Abel transform and inversion of $\mathcal{K}_{\frac{1}{2}}$ transform

For a real function $g(\vartheta)$ non-vanishing on the interval $[0,1]$, we consider the transformation $\mathcal{K}_{\frac{1}{2}}$ defined as

$$\bar{g}(\kappa) \equiv \mathcal{K}_{\frac{1}{2}}[g](\kappa) := \int_0^1 \frac{g(\vartheta)}{\sqrt{1+\kappa\vartheta}}\,\mathrm{d}\vartheta \ . \tag{4.86}$$

The question is how to reconstruct g, knowing $\bar{g}$.

The Abel transform F of a function f is defined as [132, 133]

$$F(y) = \int_y^\infty \frac{2rf(r)}{\sqrt{r^2-y^2}}\,\mathrm{d}r \ . \tag{4.87}$$

The inverse formula, allowing to recover f from F, is

$$f(r) = -\frac{1}{\pi}\int_r^\infty \frac{F'(y)}{\sqrt{y^2-r^2}}\,\mathrm{d}y \ . \tag{4.88}$$

To make the link with $\mathcal{K}_{\frac{1}{2}}$, we change variables from ϑ to $r := \sqrt{\vartheta}$ in Eq. (4.86), and introduce $f(r) := g(\vartheta = r^2)$. Then, for $\kappa > 0$,

$$\bar{g}(\kappa) = \int_0^1 \frac{f(r)}{\sqrt{1+\kappa r^2}}\,2r\,\mathrm{d}r = \frac{2}{\sqrt{\kappa}}\int_0^\infty \frac{f(r)r}{\sqrt{\frac{1}{\kappa}+r^2}}\,\mathrm{d}r \ . \tag{4.89}$$

In the last equality, we changed the upper integration limit, using $f(r) = 0$ for $r > 1$. We now continue $\bar{g}(\kappa)\sqrt{\kappa}$ in the complex plane from real positive to real negative κ, by setting $\kappa = e^{i\varphi}/y^2|_{\varphi=\pm\pi}$ with $y > 0$. This gives

$$\bar{g}(\kappa)\sqrt{\kappa} = \int_y^\infty \frac{2rf(r)}{\sqrt{r^2-y^2}}\,\mathrm{d}r + \int_0^y \frac{2rf(r)}{\sqrt{r^2-y^2}}\,\mathrm{d}r = F(y) + e^{-i\varphi/2}G(y) \ . \tag{4.90}$$

We have split the integral over r into two parts: the first part is a real function $F(y) \in \mathbb{R}$, which is the Abel transform of $f(r)$. The second term is purely imaginary because of the denominator; which of the two possible branches is taken depends on how we continued $\bar{g}(\kappa)\sqrt{\kappa}$, choosing either of the branches $\varphi = \pm\pi$. This means that we can express the Abel transform $F(y)$ of $f(r)$ from $\bar{g}(\kappa)$ as

$$F(y) = \Re\Big[\,\bar{g}(\kappa)\sqrt{\kappa}\big|_{\kappa=-1/y^2}\Big] \ , \tag{4.91}$$

where $\Re$ denotes the real part. We can now use formula (4.88) to invert the Abel transform.

Since $f(r)$ vanishes for $r > 1$, according to the definition (4.87) also $F(y)$ vanishes for $y > 1$. One can thus reduce the upper bound in Eq. (4.88) to 1. Finally reintroducing the function $g(\vartheta)$ instead of $f(r)$, we get

$$g(\vartheta) = -\frac{1}{\pi}\int_{\sqrt{\vartheta}}^1 \frac{F'(y)}{\sqrt{y^2-\vartheta}}\,\mathrm{d}y \ , \tag{4.92}$$

where $F(y)$ is defined from $\bar{g}(\kappa)$ in Eq. (4.91). We now want to apply this to compute $g_1(\vartheta)$ from Eq. (4.35). We need to compute the inverse $\mathcal{K}_{1/2}$ transform of

$$\begin{aligned}\bar{g}_1^{\mathrm{pos}}(\kappa) - \bar{g}_{0,1}(\kappa) = 8\left(\frac{1}{\sqrt{\kappa+1}}+1\right)\ln\left(\sqrt{\kappa+1}+1\right) \\ - 16\frac{\ln(4)-1}{\sqrt{\kappa+1}+1} - \frac{4\left(\kappa+\sqrt{\kappa+1}+1\right)\ln(\kappa+1)}{\kappa} \ .\end{aligned} \tag{4.93}$$

From scaling, we expect that close to the boundary

$$g_1(\vartheta) \simeq -2\ln\Big(\vartheta(1-\vartheta)\Big)\ . \tag{4.94}$$

To simplify the calculation, we subtract this divergent part. Define

$$\begin{aligned}\bar{g}^{\ln}(\kappa) &:= \int_0^1 \mathrm{d}\vartheta\, \frac{\ln\big(\vartheta(1-\vartheta)\big)+2}{\sqrt{1+\kappa\vartheta}} \\ &= \frac{4[\ln(2)-1]}{1+\sqrt{\kappa+1}} + \frac{2\sqrt{\kappa+1}\ln(\kappa+1)}{\kappa} + \frac{4\left(1-\sqrt{\kappa+1}\right)\ln\left(\sqrt{\kappa+1}+1\right)}{\kappa}\ .\end{aligned} \tag{4.95}$$

Setting $\bar{g}(\kappa) := \bar{g}_1^{\mathrm{pos}}(\kappa) - \bar{g}_{0,1}(\kappa) + 2\bar{g}^{\ln}(\kappa)$ in Eq. (4.91) yields

$$F(y) = -\frac{8y^2\ln(y)}{\sqrt{1-y^2}} - 24\sqrt{1-y^2}\ln(2) - \frac{8\left(y^2-1\right)\arcsin(y)}{y}\ . \tag{4.96}$$

Computing the integral (4.92) finally gives

$$\begin{aligned}g(\vartheta) &= \mathcal{K}^{-1}_{\frac{1}{2}}\Big[\bar{g}_1(\kappa) - \bar{g}_{0,1}(\kappa) + 2\bar{g}^{\ln}(\kappa)\Big] \\ &= 4\left[3 - \frac{1}{\sqrt{1-\vartheta}+1} - \frac{1}{\sqrt{\vartheta}+1} + \ln\left(\frac{(\sqrt{\vartheta}+1)(\sqrt{1-\vartheta}+1)}{16}\right)\right]\ .\end{aligned} \tag{4.97}$$

Adding the logarithmic terms, we recover the result (4.37) given in the main text.

4.C Inverse Laplace transforms, and other useful relations

In this appendix we give a table of useful relations for the inverse Laplace transforms encountered in this article.

All appearing hypergeometric functions can be eliminated by using the two special functions already used in chapter 2 and named $\mathcal{I}(x)$ and $\mathcal{J}(x)$,

$$\mathcal{I}(x) = \frac{1}{6}x^4\,{}_2F_2\left(1,1;\frac{5}{2},3;\frac{x^2}{2}\right) + \pi\left(1-x^2\right)\mathrm{erfi}\left(\frac{x}{\sqrt{2}}\right) + \sqrt{2\pi}e^{\frac{x^2}{2}}x + 2 - 3x^2\ , \tag{4.98}$$

$$\mathcal{J}(x) = \frac{1}{2}\pi\,\mathrm{erfi}\left(\sqrt{x}\right) - x\,{}_2F_2\left(1,1;\frac{3}{2},2;x\right) \tag{4.99}$$

These functions are related to each other by the relations

$$\mathcal{I}(x) = 2 + 2(1-x^2)\,\mathcal{J}\left(\frac{x^2}{2}\right) + \sqrt{2\pi}e^{\frac{x^2}{2}}x\ \mathrm{erfc}\left(\frac{x}{\sqrt{2}}\right)\ , \tag{4.100}$$

$$\mathcal{I}(x) = -2\,e^{\frac{x^2}{2}}\partial_x^2\left[e^{-\frac{x^2}{2}}\mathcal{J}\left(\frac{x^2}{2}\right)\right]\ . \tag{4.101}$$

To arrive at these identities, and to express everything in terms of one of these two functions, two non-trivial relations between hypergeometric functions were used (they can be checked by Taylor-expansion to high order)

$$-3\,{}_2F_2\left(1,1;\frac{3}{2},2;\frac{x^2}{2}\right) + {}_2F_2\left(1,1;2,\frac{5}{2};\frac{x^2}{2}\right) + \frac{6}{x^2}\left[\sqrt{\frac{\pi}{2}}\frac{e^{\frac{x^2}{2}}}{x}\,\mathrm{erf}\left(\frac{x}{\sqrt{2}}\right) - 1\right] = 0 \tag{4.102}$$

$$-x^3\Big[3\,{}_2F_2\left(1,1;\frac{3}{2},2;-\frac{x^2}{2}\right)+{}_2F_2\left(1,1;2,\frac{5}{2};\frac{x^2}{2}\right)\Big] \tag{4.103}$$
$$+\operatorname{erf}\left(\frac{x}{\sqrt{2}}\right)\left[3\pi x\operatorname{erfi}\left(\frac{x}{\sqrt{2}}\right)-3\sqrt{2\pi}e^{\frac{x^2}{2}}\right]+6x=0\ .$$

We now express the needed inverse Laplace transforms either in terms of $\mathcal{I}$ or $\mathcal{J}$, depending on which form is more compact.

Transforms involving only $e^{-\sqrt{s}}$, and powers of $\sqrt{s}$ are elementary,

$$\mathcal{L}^{-1}_{s\to t}\Big[e^{-\sqrt{s}}\Big]=\frac{e^{-\frac{1}{4t}}}{2\sqrt{\pi}t^{3/2}} \tag{4.104}$$

$$\mathcal{L}^{-1}_{s\to t}\Big[e^{-\sqrt{s}}\sqrt{s}\Big]=-\frac{e^{-\frac{1}{4t}}(2t-1)}{4\sqrt{\pi}t^{5/2}} \tag{4.105}$$

$$\mathcal{L}^{-1}_{s\to t}\Big[\frac{e^{-\sqrt{s}}}{\sqrt{s}}\Big]=\frac{e^{-\frac{1}{4t}}}{\sqrt{\pi t}}\ . \tag{4.106}$$

Transforms with an additional factor of $\ln(s)$ are

$$\mathcal{L}^{-1}_{s\to t}\Big[e^{-\sqrt{s}}\sqrt{s}\ln(s)\Big]=-\frac{e^{-\frac{1}{4t}}}{4\sqrt{\pi}t^{5/2}}\left\{-2t\,\mathcal{I}\Big(\frac{1}{\sqrt{2t}}\Big)+(2t-1)\Big[\ln(4t)+\gamma_{\rm E}\Big]\right\} \tag{4.107}$$

$$\mathcal{L}^{-1}_{s\to t}\Big[\frac{e^{-\sqrt{s}}\ln(s)}{\sqrt{s}}\Big]=\frac{e^{-\frac{1}{4t}}}{\sqrt{\pi t}}\left[2\,\mathcal{J}\Big(\frac{1}{4t}\Big)-\ln(4t)-\gamma_{\rm E}\right] \tag{4.108}$$

$$\mathcal{L}^{-1}_{s\to t}\Big[e^{-\sqrt{s}}\ln(s)\Big]=\frac{e^{-\frac{1}{4t}}}{4\sqrt{\pi}t^{5/2}}\left[2\,\mathcal{J}\Big(\frac{1}{4t}\Big)-\ln(4t)-\gamma_{\rm E}\right]-\frac{\operatorname{erfc}\left(\frac{1}{2\sqrt{t}}\right)}{t}\ . \tag{4.109}$$

Transforms involving the exponential integral function are

$$\mathcal{L}^{-1}_{s\to t}\Big[\operatorname{Ei}\left(-\sqrt{s}\right)\Big]=-\frac{\operatorname{erfc}\left(\frac{1}{2\sqrt{t}}\right)}{2t} \tag{4.110}$$

$$\mathcal{L}^{-1}_{s\to t}\Big[e^{\sqrt{s}}\operatorname{Ei}\left(-2\sqrt{s}\right)\Big]=\frac{e^{-\frac{1}{4t}}}{4\sqrt{\pi}t^{3/2}}\left[2\,\mathcal{J}(\frac{1}{4t})+\ln(t)-\gamma_{\rm E}\right]-\frac{\operatorname{erfc}\left(\frac{1}{2\sqrt{t}}\right)}{2t} \tag{4.111}$$

$$\mathcal{L}^{-1}_{s\to t}\Big[\sqrt{s}e^{\sqrt{s}}\operatorname{Ei}\left(-2\sqrt{s}\right)\Big]=\frac{e^{-\frac{1}{4t}}}{8\sqrt{\pi}t^{5/2}}\left\{2t\,\mathcal{I}\Big(\frac{1}{\sqrt{2t}}\Big)+(2t-1)\Big[\ln(t)-\gamma_{\rm E}\Big]-8t\right\} \tag{4.112}$$

$$\mathcal{L}^{-1}_{s\to t}\Big[\frac{e^{\sqrt{s}}\operatorname{Ei}\left(-2\sqrt{s}\right)}{\sqrt{s}}\Big]=\frac{e^{-\frac{1}{4t}}}{2\sqrt{\pi t}}\left[\gamma_{\rm E}-2\,\mathcal{J}\Big(\frac{1}{4t}\Big)-\ln(t)\right]\ . \tag{4.113}$$

Chapter 5

FBm with drift and Pickands constants

5.1 Presentation of the chapter

This chapter is based on yet unpublished work with A. Rosso and K. J. Wiese. We extend here the perturbative approach to fBm to include drift. Applying this to a specific drift allows us to investigate observables related to Pickands' constants, an object defined and motivated the introduction, in section 1.3.5. For $0 < \alpha \leq 2$, the Pickands constant $\mathcal{H}_\alpha$ is defined from a fBm with drift and Hurst exponent $H = \alpha/2$, cf. Eq. (1.33). In section 5.3, the perturbative expansion around Brownian motion with linear drift allows us to obtain a new result for the value of the Pickands constants near $\alpha = 1$, which goes beyond the two known values $\mathcal{H}_1 = 1$ and $\mathcal{H}_2 = 1/\sqrt{\pi}$. In section 5.4 we present interesting links between fBm bridges and Pickands' constant, which gives an independent test, using our results of chapter 4, of our result on Pickands' constant.

To simplify the discussion in the next sections, we define a process z_t with an arbitrary drift strength μ

$$z_t = X_t + \mu |t|^\alpha \ , \tag{5.1}$$

where X_t is a fBm with Hurst exponant $H = \alpha/2$. Setting $\mu = -1$ allows to recover $z_t = \chi_t$, as appearing in (1.33). But Pickands constants can also be computed with $\mu = 1$, using

$$\mathcal{H}_\alpha = \lim_{T\to\infty} \frac{1}{T} \mathbb{E}(e^{-\min_{t\in[0,T]} z_t}) \ , \tag{5.2}$$

which simply uses the fact that the distribution of the maximum with a negative drift is the same as the distribution of the minimum (in absolute value) with a positive drift.

5.2 Brownian motion with drift, $\alpha = 1$

Here we recall some results about Brownian motion with drift which will be useful in order to study Pickands constant around $\alpha = 1$.

For $\alpha = 1$ the process X_t is a standard Brownian B_t, with covariance $\langle B_t B_s \rangle = 2D \min(t, s)$. The propagator of the process $z_t = B_t + \mu t$ with positivity constraint, that we denote P^+_μ, is

given by

$$\begin{aligned} P_\mu^+(x_0,x,T) &:= \partial_x \mathbb{P}(z_T < x,\, \forall t \in [0,T]\, z_t > 0 | z_0 = x_0) \\ &= \frac{e^{\frac{\mu}{2D}(x-x_0)-\frac{\mu^2}{4D}T}}{\sqrt{4\pi DT}}\left(e^{-\frac{(x-x_0)^2}{4DT}} - e^{-\frac{(x+x_0)^2}{4DT}}\right) \\ &= e^{\frac{\mu}{2D}(x-x_0)-\frac{\mu^2}{4D}T} P_0^+(x_0,x,T)\ . \end{aligned} \tag{5.3}$$

Here P_0^+ is the same propagator for the process with no drift. For our purpose of computing Pickands' constant, we choose $\mu = D = 1$. We can recover a generic diffusive constante D (with $\mu = D$) with a global rescaling of time $T \to DT$, as can be checked on Eq. (5.3). The survival probability Q of this process, which is defined as the probability to stay positive up to time T while starting at $x_0 > 0$, can be computed from P_μ^+:

$$Q_{\alpha=1}(x_0,T) = \int_0^\infty \mathrm{d}x\, P_{\mu=1}^+(x_0,x,T) = \frac{1}{2}\left[\mathrm{erf}\left(\frac{x_0+T}{2\sqrt{T}}\right) - e^{-x_0}\mathrm{erfc}\left(\frac{x_0-T}{2\sqrt{T}}\right) + 1\right]. \tag{5.4}$$

From that, we can extract the distribution of m, defined as $m = -\min_{t\in[0,T]} z_t$,

$$\mathcal{P}_{\alpha=1}^T(m) = \partial_m Q_{\alpha=1}(m,T) = \frac{1}{2}e^{-m}\mathrm{erfc}\left(\frac{m-T}{2\sqrt{T}}\right) + \frac{e^{-\frac{(m+T)^2}{4T}}}{\sqrt{\pi T}}\ . \tag{5.5}$$

The result (5.5) allows to extract Pickands' constant, via its main definition given in the introduction (1.33):

$$\int_0^\infty \mathrm{d}m\, e^m \mathcal{P}_{\alpha=1}^T(m) = \left(\frac{T}{2}+1\right)\left[\mathrm{erf}\left(\frac{\sqrt{T}}{2}\right)+1\right] + \sqrt{\frac{T}{\pi}}e^{-\frac{T}{4}} \underset{T\to\infty}{\simeq} T + 2 + \mathcal{O}(e^{-\frac{T}{4}}). \tag{5.6}$$

The Pickands constant is the coefficient of the linear term in the large-T asymptotics, and we recover the exact result for the Brownian case:

$$\mathcal{H}_1 = 1$$

.

5.3 Pertubative expansion around Brownian motion: $\alpha = 1 + \epsilon$

5.3.1 Action with drift

For $\alpha = 1+\epsilon$, with ϵ a small parameter[1], we construct in appendix 5.A the action for the process z_t, defined in Eq. (5.1) with $\mu = 1$. This follows the ideas of [125] and [123]. It writes

$$\mathcal{S}[z_t] = \mathcal{S}_0[z_t] + \epsilon \mathcal{S}_1[z_t] + O(\epsilon^2)\ , \tag{5.7}$$

with

$$\begin{aligned} \mathcal{S}_0[z_t] &= \int_0^T \mathrm{d}t\, \frac{\dot{z}_t^2}{4D_{\epsilon,\tau}} - \frac{(z_T - z_0)}{2} + \frac{D_{\epsilon,\tau}T}{4}\ , \\ \mathcal{S}_1[z_t] &= -\frac{1}{4}\int_0^T \mathrm{d}t\, \dot{z}_t \log\left(\frac{t}{T-t}\right) - \frac{1}{4}\int_0^{T-\tau}\mathrm{d}t_1 \int_{t_1+\tau}^T \mathrm{d}t_2\, \frac{\dot{z}_{t_1}\dot{z}_{t_2}}{t_2-t_1}\ . \end{aligned} \tag{5.8}$$

[1] Note the difference with the expansion parameter used in the previous chapters, $\varepsilon = H - \frac{1}{2}$, which gives a factor 2 of difference $\epsilon = \varepsilon/2$.

We recognise $\mathcal{S}_0$ as the standard Brownian action with a renormalised diffusion constant

$$D_{\epsilon,\tau} = 1 + \epsilon[1 + \ln(\tau)] + \mathcal{O}(\epsilon^2) \ , \tag{5.9}$$

and a linear drift $\mu = D_{\epsilon,\tau}$. The time τ is a regularization cutoff for coinciding times (a UV cutoff). We will see that it has no impact on the distribution of observables which can be extracted from the path integral.

The order-ϵ term contains a new term as compared to the previous chapters, due to the non linearity in the drift of the process z_t when $\alpha \neq 1$. This means that on top of the diagrams with the interaction, non-local in time, that we computed for our other observables, we need to take into account a new type of correction.

5.3.2 Survival probability and Pickands constants

To investigate the Pickands constants, we start with a path integral representation for the survival probability of the process z_t,

$$Q_\alpha(m,T) = \frac{1}{Z^{\mathrm{N}}(T)} \int_0^\infty \mathrm{d}x \int_{z_0=m}^{z_T=x} \mathcal{D}[z_t]\, \Theta[z_t] e^{-\mathcal{S}[z_t]} \ , \tag{5.10}$$

where $\Theta[z_t]$ constrains the path z_t to remain positive, and the normalisation constant $Z^{\mathrm{N}}(T)$ is the sum over all paths without the constraint (and thus independent of m because of the translational symmetry). Computing the path integral in (5.10), using the ϵ-expansion of the action (5.7), allows us to write

$$\begin{aligned} Z^{\mathrm{N}}(T) Q_\alpha(m,T) &= Z_0^+(m,T) + \epsilon Z_1^+(m,T) + O(\epsilon^2) \\ &= \langle \Theta[z_t] \rangle_0 + \epsilon \Big[\langle \Theta[z_t] \mathcal{S}_1[z_t] \rangle_0 + (1 + \ln \tau) T \partial_T Z_0^+(m,T) \Big] + O(\epsilon^2) \ . \end{aligned} \tag{5.11}$$

The averages $\langle ... \rangle_0$ denote averages over paths z_t with respect to the standard Brownian action with drift ($\mu = D = 1$), initial conditon $z_0 = m$ and a free end-point z_T. The term $Z_0^+ \equiv \langle \Theta[z] \rangle_0$ identifies with $Q_{\alpha=1}(m,T)$, the survival distribution for the Brownian given in (5.4). For the order-ϵ term Z_1^+, there is a contribution due to the non local correction to the action $\mathcal{S}_1$, cf. Eq. (5.8), and a contribution due to the rescaling of the diffusive constant (and the drift) in $\mathcal{S}_0$, $D = 1 \to D_{\epsilon,\tau}$.

Before expliciting these terms, we show how this leads to the Pickands constant. Using $Z_N(T) = \lim_{m\to\infty} Z_N(T) Q_\alpha(m,T)$, because Q_α is a cumulative, we arrive at

$$Q_\alpha(m,T) = Z_0^+(m,T)[1 - \epsilon \lim_{m\to\infty} Z_1^+(m,T)] + \epsilon Z_1^+(m,T) + O(\epsilon^2) \ . \tag{5.12}$$

Then, the Pickands constant is obtain from the large-T asymptotic of

$$\begin{aligned} &\int_0^\infty \mathrm{d}m\, e^m \partial_m Q_\alpha(m,T) = \int_0^\infty \mathrm{d}m\, e^m \partial_m Z_0^+(m,T) \\ &+ \epsilon \left[\int_0^\infty \mathrm{d}m\, e^m \partial_m Z_1^+(m,T) - \lim_{m\to\infty} Z_1^+(m,T) \int_0^\infty \mathrm{d}m\, e^m \partial_m Z_0^+(m,T) \right] + O(\epsilon^2) \ . \end{aligned} \tag{5.13}$$

The first term was already computed in Eq. (5.6). For the ϵ-order term, the function $Z_1^+(m,T)$ can be expressed from the bare propagator $P^+_{\mu=1}$, given in (5.3), and its cumbersome Laplace transform $\tilde{Z}_1^+(m,s)$ as derived in appendix. The asymptotics

$$\int_0^\infty \mathrm{d}m\, e^m \partial_m Z_1^+(m,T) \underset{T\to\infty}{=} \frac{T^2}{4} \left[\ln\left(\frac{T}{\tau}\right) - 1 \right] + \frac{T}{2} \left[\ln\left(\frac{T}{\tau}\right) - 1 - 2\gamma_{\mathrm{E}} \right] + O(\ln(T)) \tag{5.14}$$

and

$$\lim_{m\to\infty} Z_1^+(m,T) = \frac{T}{4}\left[\ln\left(\frac{T}{\tau}\right) - 1\right] \ , \tag{5.15}$$

allow us to compute Pickands constant at order-ϵ. Combining these contributions according to (5.13) cancels all τ dependency, and finally gives

$$\boxed{\mathcal{H}_{1+\epsilon} = 1 - \epsilon\gamma_{\rm E} + O(\epsilon^2) \ ,} \tag{5.16}$$

where $\gamma_{\rm E}$ is the Euler-Mascheroni constant, whose numerical value is $\gamma_{\rm E} \approx 0.577$. This result, which gives the derivative of the Pickands constant at $\alpha = 1$, can be compared to the extensive numerical simulation of [94], see figure 5.1.

5.3.3 Maximum-value distribution in the large time limit

For standard Brownian motion, $\alpha = 1$, the distribution $\mathcal{P}^T_{\alpha=1}(m)$ given in (5.5) has the interesting property to converge to a non trivial limit when $T \to \infty$, namely,

$$\mathcal{P}^\infty_{\alpha=1}(m) = \lim_{T\to\infty} \partial_m Q_{\alpha=1}(m,T) = e^{-m} \ . \tag{5.17}$$

Using the same expansion as in (5.13), we can express this distribution for $\alpha = 1+\epsilon$,

$$\mathcal{P}^T_\alpha(m) = \partial_m Z_0^+(m,T) + \epsilon\left[\partial_m Z_1^+(m,T) - \lim_{m\to\infty} Z_1^+(m,T)\partial_m Z_0^+(m,T)\right] + \mathcal{O}(\epsilon^2) \ .$$

The expression of $\tilde{Z}_1^+(m,s)$, which is given in appendix 5.B, allows us in principle to compute $\mathcal{P}^T_\alpha(m)$ for a generic T, but we restrict ourselves to the large T limit for simplicity. Using the asymptotic

$$\partial_m Z_1^+(m,T) \underset{T\to\infty}{=} -e^{-m}\left\{1 + \gamma_{\rm E} + \ln(m) + \frac{T}{4}\left[1 + \log\left(\frac{\tau}{T}\right)\right]\right\} - \mathrm{Ei}(-m) + \mathcal{O}(T^{-1}) \ , \tag{5.18}$$

and the one given in (5.15), we see that $\mathcal{P}^T_\alpha(m)$ converges at large T to a non-trivial distribution which reads

$$\mathcal{P}^\infty_{\alpha=1+\epsilon}(m) = e^{-m}\Big\{1 - \epsilon\big[1 + \gamma_{\rm E} + e^m \mathrm{Ei}(-m) + \log(m)\big]\Big\} + \mathcal{O}(\varepsilon^2) \ . \tag{5.19}$$

This is in agreement with our following conjecture: for all $\alpha \in (0,2)$, the distribution $\mathcal{P}^T_\alpha(m)$ converges to a distribution $\mathcal{P}^\infty_\alpha(\mathrm{m})$ which has the following large-m asymptotics:

$$\mathcal{P}^\infty_\alpha(m) \underset{m\to\infty}{\simeq} \frac{\mathcal{H}_\alpha}{\alpha} m^{\frac{1}{\alpha}-1} e^{-m} \ . \tag{5.20}$$

5.4 Maximum-value of a fBm Bridge and Pickands constants

We recall here one of the theorems [84] involving Pickands' constant which gives interesting links to the results of chapter 4. It assumes that a centered process X_t, defined on some interval $[0,T]$, has a unique time t_0 of maximum variance, normalized to one for simplicity. Close to t_0, we assume that the variance verifies

$$\langle X_t^2\rangle = 1 - a|t-t_0|^\beta + o\left(|t-t_0|^\beta\right) \quad \text{when} \ \ t \to t_0, \tag{5.21}$$

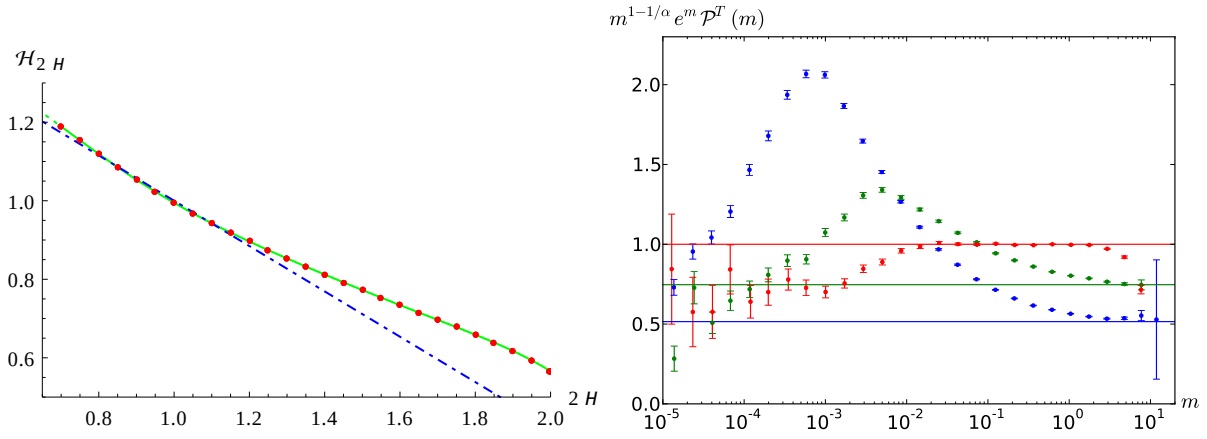

Figure 5.1: Left: Comparison between the numerical values of Pickands constants from [94] (red dots, interpolated with the green line) and the slope at $\alpha = 2H = 1$ predicted by our perturbative expansion (blue dotted line). Right: Test on the asymptotic behavior of $\mathcal{P}_\alpha^\infty(m)$, for $\alpha = 1.$ (red), $\alpha = 1.2$ (green) and $\alpha = 1.5$ (blue). Plain lines represent the conjectured limits for large m, using numerical value of $\mathcal{H}_\alpha$ from [94]. Numerical parameters are $T = 8$ and $dt = 2^{-14}$.

and the covariance

$$\langle X_t X_s \rangle = 1 - c|t-s|^\alpha + o\left(|t-s|^\alpha\right) \quad \text{when} \quad s,t \to t_0 \ . \tag{5.22}$$

This defines two constants $a, c > 0$ and two exponents α and β. Interestingly, a rescaled fBm bridge verifies all these hypothesis. The maximum variance is obviously located at the middle of the time interval, and the s are deduced from the covariance function of a fBm Bridge, cf. 4.2. For a fBm bridge, which we denote B_t here, of length 1, i.e. $B_0 = B_1 = 0$, and Hurst exponent H, we have

$$\langle B_{t_1} B_{t_2} \rangle = t_1^{2H} + t_2^{2H} - |t_1 - t_2|^{2H} - \frac{1}{2}\left(t_1^{2H} + 1 - |1-t_1|^{2H}\right)\left(t_2^{2H} + 1 - |1-t_2|^{2H}\right) \ . \tag{5.23}$$

The maximum variance is $\langle B_{1/2}^2 \rangle = (4^{1-H} - 1)/2$, and then after proper rescaling, the hypothesis (5.21) and (5.22) are verfied with

$$\alpha = 2H \ , \quad \beta = 2 \ , \quad a = \frac{4\alpha(2^{1-\alpha}\alpha - \alpha + 1)}{4 - 2^\alpha} \ , \quad c = \frac{2^{\alpha+1}}{4 - 2^\alpha} \ . \tag{5.24}$$

We are in the case $\beta > \alpha$, for which the theorem predicts the asymptotics (1.38), written here for the specific values of α and β,

$$\text{Prob}\left(\max_{t\in[0,T]} \frac{B_t}{\sqrt{\langle B_{1/2}^2 \rangle}} > u \right) \simeq \sqrt{\frac{\pi}{a}} \mathcal{H}_\alpha c^{\frac{1}{\alpha}} u^{\frac{1}{H}-1} \frac{e^{-\frac{u^2}{2}}}{\sqrt{2\pi} u} \quad \text{when} \quad u \to \infty \ . \tag{5.25}$$

This can be compared to the results obtained within our perturbative expansion in chapter 4, with the final result given in Eq. (4.54). The large-u (or m in the notation of chapter 4) power-law confirms our prediction (4.60), as $\frac{1}{H} - 1 = 1 - 4\varepsilon + O(\varepsilon^2)$. But the result (5.25) also gives the prefactor, which can be compared successfully with our full result at order-ε given in Eq. (4.54). This is an independent check for our prediction (5.16), but can also be used as a way to extract numerically the value of the Pickands constants. Figure 5.4 gives two examples of such estimations.

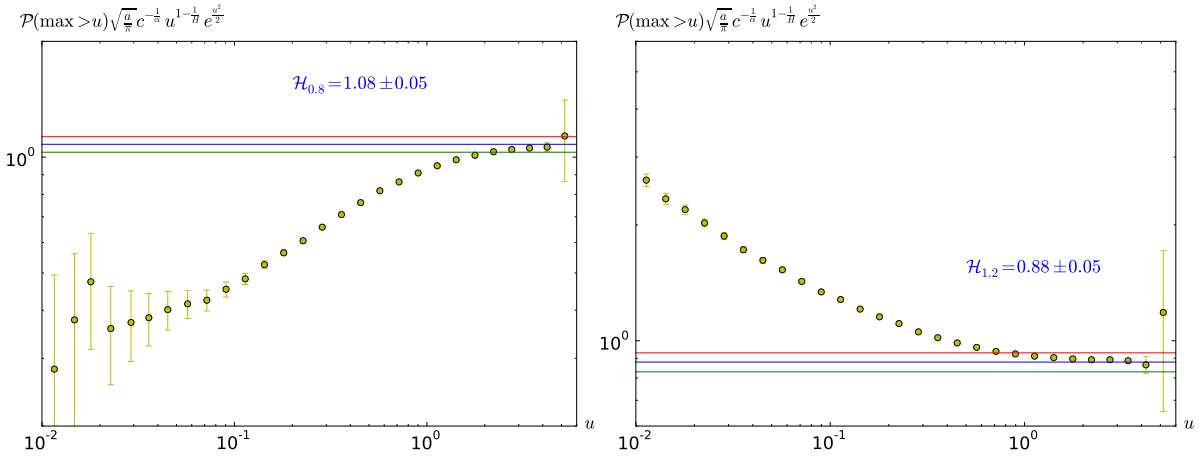

Figure 5.2: The distribution of the maximum-value of a rescaled fBm Bridge, divided by the all terms of the asymptotics given in Eq. (5.25) apart the Pickands constant. This should converge at large u to a plateau whose value is exactly the Pickands constant corresponding to the Hurst exponent of the fBm. Left: numerical simulations with $H = 0.4$, right: numerical simulations with $H = 0.6$. In both cases, the value of the Pickands constant extracted is in agreement with the prediction (5.16) and with the numerical results of Dieker and Yakier [94].

5.A Derivation of the action

Here we derive the action for the process $z_t = X_t + \mu\, t^\alpha$, where X_t is a fractional Brownain motion with Hurst exponent $H = \alpha/2 = (1+\epsilon)/2$ and diffusive constant $D = 1$, i.e. close to a standard Brownian motion. The action for X_t is already known, and recalled here in Eq. 2.3. From this, it is possible to obtain the action for z_t by simply making the change of variables $\dot{X}_t \to \dot{z}_t - \mu\,[1 + \epsilon(1 + \ln t)] + O(\varepsilon^2)$. Expanding each term of the action, we get

$$\begin{aligned}\int_0^T \mathrm{d}t\, \frac{\dot{X}_t^2}{4D_{\epsilon,\tau}} \to \int_0^T \mathrm{d}t\, \frac{\dot{z}_t^2}{4D_{\epsilon,\tau}} - \mu\frac{z_T - z_0}{2D_{\epsilon,\tau}} + \frac{\mu^2 T}{4D_{\epsilon,\tau}} \\ - \epsilon\frac{\mu}{2}\int_0^T \mathrm{d}t\, \dot{z}_t(1 + \ln t) + \epsilon\frac{\mu^2 T\ln(T)}{2} + O(\varepsilon^2)\ ,\end{aligned} \tag{5.26}$$

and

$$\begin{aligned}\int_0^{T-\tau}\mathrm{d}t_1 \int_{t_1+\tau}^T \mathrm{d}t_2\, \frac{\dot{X}_{t_1}\dot{X}_{t_2}}{t_2 - t_1} \to \int_0^{T-\tau}\mathrm{d}t_1 \int_{t_1+\tau}^T \mathrm{d}t_2\, \frac{\dot{z}_{t_1}\dot{z}_{t_2}}{t_2 - t_1} - \mu^2 T\left[\ln\left(\frac{\tau}{T}\right) + 1\right] \\ - \mu\int_0^T \mathrm{d}t\, \dot{z}_t\left[\log\left(\frac{t}{\tau}\right) + \log\left(\frac{T-t}{\tau}\right)\right] + O(\epsilon)\ .\end{aligned} \tag{5.27}$$

There are some simplifications:

$$\mu^2\frac{T}{4D_{\varepsilon,\tau}} + \epsilon\frac{\mu^2 T\log(T)}{2} + \epsilon\frac{\mu^2 T}{4}\left[\ln\left(\frac{\tau}{T}\right) + 1\right] = \mu^2\frac{T^{1+\epsilon}}{4} + O(\epsilon^2)\ , \tag{5.28}$$

$$\int_0^T \mathrm{d}t\, \dot{z}_t \log\left(\frac{t(T-t)}{\tau^2}\right) - 2\int_0^T \mathrm{d}t\, \dot{z}_t(1 + \ln t) = \int_0^T \mathrm{d}t\, \dot{z}_t \log\left(\frac{T-t}{t}\right) - 2(z_T - z_0)(1 + \log\tau)\ . \tag{5.29}$$

After recombining all these terms, we finally get

$$\begin{aligned}\mathcal{S}[z_t] = \int_0^T \mathrm{d}t\, \frac{\dot{z}_t^2}{4D_{\epsilon,\tau}} - \mu\frac{(z_T - z_0)}{2} + \mu^2\frac{T^{1+\epsilon}}{4} \\ - \mu\frac{\epsilon}{4}\int_0^T \mathrm{d}t\, \dot{z}_t \log\left(\frac{t}{T-t}\right) - \frac{\epsilon}{4}\int_0^{T-\tau}\mathrm{d}t_1 \int_{t_1+\tau}^T \mathrm{d}t_2\, \frac{\dot{z}_{t_1}\dot{z}_{t_2}}{t_2 - t_1} + O(\epsilon^2)\ .\end{aligned} \tag{5.30}$$

The last term of the first line does not depend on z_t and acts only as a global normalisation which has no impact on the observables we compute from this action. We choose to change it to $\mu^2 T D_{\epsilon,\tau}/4$ for simplicity and fix $\mu = 1$, which finally gives the expressions (5.7) and (5.8) given in the main text.

5.B Details of calculations

In this appendix, we give the details of the computation for the order-ϵ correction in the path integral (5.10). The difficult contribution was written $\langle \mathcal{S}_1[z_t]\Theta[z_t]\rangle_0$ in (5.11), which we now decompose in two terms using the expression of $\mathcal{S}_1$ given in (5.8):

$$Z^+_{1A}(m,T) = \frac{1}{4}\int_0^{T-\tau} \mathrm{d}t_1 \int_{t_1+\tau}^{T} \mathrm{d}t_2 \frac{\left\langle \dot{z}_{t_1}\dot{z}_{t_2}\Theta[z] e^{\frac{Z_T - Z_0}{2} - \frac{T}{4}} \right\rangle_0}{t_2 - t_1} \ , \tag{5.31}$$

and

$$Z^+_{1B}(m,T) = \frac{1}{4}\int_0^{t} \mathrm{d}t \left\langle \dot{z}_t\, \Theta[z] e^{\frac{Z_T - Z_0}{2} - \frac{T}{4}} \right\rangle_0 \log\left(\frac{t}{T-t}\right) \ . \tag{5.32}$$

Here, the averages $\langle ... \rangle_0$ denote averages with respect to the standard Brownian action, with no drift, as the drift is now enforced explicitely by the exponential factors. We can express these in term of the bare propagator with positivity constrain P_0^+. Following the diagrammatic rules defined in chapter 2, the first correction can be written in the Laplace variable ($T \to s$) as

$$\tilde{Z}^+_{1A}(m,s) = \int_{x_i, y>0} e^{\frac{x_3 - m}{2}} \tilde{P}_0^+(m, x_1, \bar{s})\, \partial_{x_1}\tilde{P}_0^+(x_1, x_2, \bar{s}+y)\, \partial_{x_2}\tilde{P}_0^+(x_2, x_3, \bar{s}) \ . \tag{5.33}$$

We have introduce $\bar{s} = s + 1/4$, a shifted variable due to the term $e^{-T/4}$. As explained in [125], and recalled in chapter 2, each $\dot{z}_{t_i}$ in (5.31) corresponds to a $-2\partial_{x_i}$ in (5.33). And to account for the factor $(t_2 - t_1)^{-1}$, we use the identity $(t_2 - t_1)^{-1} = \int_{y>0} e^{-y(t_2 - t_1)}$ which produces another shift in the second propagator, with a new variable y which we need to integrate over. As a recall, the expression of the propagator in Laplace variable appearing here is:

$$\tilde{P}_0^+(x_1, x_2, s) = \frac{e^{-\sqrt{s}|x_1 - x_2|} - e^{-\sqrt{s}(x_1 + x_2)}}{2\sqrt{s}} \ . \tag{5.34}$$

The second correction, due to the non linearity in the drift, is given by

$$Z^+_{1B}(m,T) = \frac{1}{2}\int\limits_{x_i>0}\int_0^T \mathrm{d}t\, e^{\frac{x_2 - m}{2}} P_0^+(m, x_1, t)\partial_{x_1} P_0^+(x_1, x_2, T-t) \log\left(\frac{T-t}{t}\right) e^{-\frac{T}{4}} \ . \tag{5.35}$$

In order to compute the Laplace transformation of this, we use the following integral representation of the logarithm:

$$\ln\left(\frac{T-t}{t}\right) = \int_0^\infty \frac{\mathrm{d}y}{y}\left(e^{-yt} - e^{-y(T-t)}\right) \ . \tag{5.36}$$

Inserting this in (5.35) and taking the Laplace transfomr gives

$$\begin{aligned}\tilde{Z}^+_{1B}(m,s) = \int_0^\infty \frac{\mathrm{d}y}{y} \int_{x_i>0} e^{\frac{x_2 - m}{2}} \Big[&\tilde{P}_0^+(m, x_1, \bar{s}+y)\, \partial_{x_1}\tilde{P}_0^+(x_1, x_2, \bar{s}) \\ &- \tilde{P}_0^+(m, x_1, \bar{s})\, \partial_{x_1}\tilde{P}_0^+(x_1, x_2, \bar{s}+y)\Big] \ .\end{aligned} \tag{5.37}$$

In the two terms $\tilde{Z}^+_{1A}$ and $\tilde{Z}^+_{1B}$, the integrals over the space variables x_i can be computed quite easly, as the Laplace transformed propagator $\tilde{P}^+_0$ is exponential in these variable (contrary to the case before Laplace transformation, where the dependence is Gaussian). For the integral over y, $\tilde{Z}^+_{1A}$ has a logarithmic divergence at large y wich corresponds to the UV divergence when $t_2 \to t_1$ in (5.31). The necessary large y cutoff Λ (such that the integration over y is performed in the interval $[0, \Lambda]$) equivalent to the UV cutoff τ is given by $\Lambda = e^{-\gamma_{\rm E}}/\tau$, as explained in chapter 2[2]. Combining these two terms finally gives

$$\begin{aligned} & s^2\Big(\tilde{Z}_{1A}(m,s) + \tilde{Z}_{1B}(m,s)\Big) \qquad (5.38)\\ &= -\frac{e^{(\sqrt{\bar{s}}-\frac{1}{2})m}}{8\sqrt{\bar{s}}}\Big[8\bar{s}^{3/2}(m+1) + 8s\bar{s}m + 4\bar{s} - 2\sqrt{\bar{s}}(m-1) - 1\Big]\mathrm{Ei}\Big(-2\sqrt{\bar{s}}m\Big)\\ &\quad + \frac{e^{-(\sqrt{\bar{s}}+\frac{1}{2})m}}{16\sqrt{\bar{s}}}\Big[\Big(8\bar{s}^{3/2} + 8s\bar{s}m + 4\bar{s} + 2\sqrt{\bar{s}} - 1\Big)\big(\log(4\bar{s}\tau) + 1 + \gamma_{\rm E}\big) - 8\sqrt{\bar{s}}\\ &\qquad\qquad + \Big(8\bar{s}^{3/2} - 8s\bar{s}m + 4\bar{s} - 6\sqrt{\bar{s}} - 1\Big)\left(\log\left(\frac{m^2}{\tau}\right) - 1 + \gamma_{\rm E}\right)\Big]\\ &\qquad + \frac{1}{2}\Big[\mathrm{Ei}\Big(-\frac{m}{2} - m\sqrt{\bar{s}}\Big) + e^{-m}\mathrm{Ei}\Big(\frac{m}{2} - m\sqrt{\bar{s}}\Big) - \log(s\tau) - \gamma_{\rm E}\Big] \end{aligned}$$

with, as before, $\bar{s} = s + \frac{1}{4}$.

From this expression, and denoting $\tilde{Z}^+_{1AB} = \tilde{Z}^+_{1A} + \tilde{Z}^+_{1B}$, it is possible to compute the asymptotics used in the main text, first in the Laplace variable:

$$\begin{aligned} \tilde{Z}_{1AB}(m,s) &\underset{s\to 0}{\simeq} \frac{(e^{-m}-1)(\log(s\tau)+\gamma_{\rm E})}{4s^2} \qquad (5.39)\\ &\quad + \frac{e^{-m}(\log(m)+\gamma_{\rm E}) - (m+1)\mathrm{Ei}(-m)}{s} + \mathcal{O}(\ln(s)) \ ,\\ \tilde{Z}_{1AB}(m,s) &\underset{m\to\infty}{\simeq} -\frac{\log(s\tau)+\gamma_{\rm E}}{4s^2} + O(e^{-m}) \ , \qquad (5.40) \end{aligned}$$

and

$$\int_0^\infty \mathrm{d}m\, e^m \partial_m \tilde{Z}^+_{1AB}(m,s) \underset{s\to 0}{\simeq} -\frac{\log(s\tau)+\gamma_{\rm E}-\frac{1}{2}}{2s^3} - \frac{\log(s\tau^3)+3\gamma_{\rm E}+2}{2s^2} + O\Big(\frac{1}{s}\Big) \ . \qquad (5.41)$$

For the last one, it is important to note that the integral over m has to be computed before the $s \to 0$ limit is taken.

The other ε-order correction in (5.10) comes from the change of the diffusive constant in the Brownian action, from $D = 1$ to $D_{\epsilon,\tau} = 1 + \epsilon(1 + \ln\tau) + \mathcal{O}(\epsilon)$, with the corresponding change in the drift such that the term linear in z_t in $\mathcal{S}_0$, cf. (5.8), stays unchanged. This change is equivalent to do $T \to D_{\epsilon,\tau}T$ in the result for the Brownian, which, as stated in the main text, gives an ε-order correction of the form $(1 + \ln\tau)T\partial_T Z^+_0(m,T)$ in (5.11). Then, combining

$$(1+\ln\tau)T\partial_T \int_0^\infty \mathrm{d}m\, e^m \partial_m \tilde{Z}^+_0(m,T) \underset{T\to\infty}{\simeq} (1+\ln\tau)T + O(e^{-T/4}) \qquad (5.42)$$

and the inverse Laplace transformation of (5.41) gives the result (5.14) of the main text. For the tow other asymptotics, the rescaling of the diffusive constant has no impact as

$$\lim_{T\to\infty} T\partial_T Z^+_0(m,T) = \lim_{m\to\infty} T\partial_T Z^+_0(m,T) = 0 \ . \qquad (5.43)$$

and then formula (5.18) and (5.15) are computed directly from (5.39) and (5.40) respectively, via an inverse Laplace transformation.

[2]This comes from the requirement: $\int_0^T \mathrm{d}t \int_0^\Lambda e^{-yt} = \log(\Lambda T) + \gamma_{\rm E} + \mathcal{O}(e^{-T\Lambda}) \overset{!}{=} \ln(T/\tau) = \int_\tau^T \frac{\mathrm{d}t}{t}$.

5.C Derivation from scaling of (5.20)

The heuristic derivation of (5.20) is : for $m \ll T^\alpha$ and $T \gg 1$ we have $\mathcal{P}_\alpha^T(m) \simeq \mathcal{P}_\alpha^\infty(m)$, and for $m \gg T^\alpha$, we have $\mathcal{P}_\alpha^T(m) \simeq e^{-\frac{(m-T^\alpha)^2}{4T^\alpha}}$ because very large values of the minimum are reached almost surely at the end of the interval. Then using the relation of $\mathcal{P}_\alpha^T(m)$ with the Pickands constant, we get

$$\int_0^\infty \mathrm{d}m\, e^{-m}\mathcal{P}_\alpha^T(m) \simeq \int_0^{T^\alpha} \mathrm{d}m\, e^{-m}\mathcal{P}_\alpha^\infty(m) \simeq \mathcal{H}_\alpha T \text{ when } T \to \infty\ . \tag{5.44}$$

From this, assuming that the large m behaviour of $\mathcal{P}_\alpha^\infty(m)$ is exponential times a power law, the unique possibility is the one given in (5.20).

Chapter 6

Mean-field theory for avalanches, the Brownian force model

6.1 Presentation of the chapter

This chapter presents results from joint work with P. Le Doussal and K. Wiese [134], with essentially the same presentation as the article. It is structured as follows: In section 6.2 we precise the definition of the BFM, introduced in section 1.4, and of the main avalanche observables, together with the general method to obtain their distributions from the instanton equation. Section 6.3 starts by recalling the calculation of the distributions of the global size (total swept area) S and of the local jump size S_r of an avalanche, for an arbitrary kick amplitude. In Section 6.3.3 we extend thes calculations to the joint density $\rho(S_r, S)$ of local and global size for single avalanches, i.e. in the limit of an infinitesimal kick. In Section 6.4 we study the case of an interface driven at a single point. When the *force* at this point is imposed, we find a new exponent $\tau_0 = 5/3$ for the probability distribution function (PDF) of the local jump S_0 at that point. When the local *displacement* is imposed, we find a new exponent $\tau = 7/4$ for the PDF of the global size S. In Section 6.5 we show that the extension ℓ of a *single avalanche* along one internal direction (i.e. the total length in $d = 1$) is finite; we calculate its distribution, following either a local or a global kick. In all cases it exhibits a divergence $P(\ell) \sim \ell^{-3}$ at small ℓ, with the same prefactor. All these exponents can be found in Table 6.1. Finally, in Section 6.6 we study the *position* of the interface, which is a non-stationary process. We explain how the Larkin and BFM roughness exponents emerge from the dynamics. Most of our results are tested in a numerical simulation of the equation of motion in $d = 1$.

Driving protocol	Observable	Exponent
any force kick	global size S	$\tau = 3/2$
uniform force kick	local size S_0	$\tau_0 = 4/3$
uniform force kick	S_0 at fixed S	$\tau_0 = 2/3$
localized force kick	local size S_0	$\tau_0 = 5/3$
local displacement imposed	global size S	$\tau = 7/4$
any force kick	extension ℓ	$\kappa = 3$

Table 6.1: Summary of small-scale exponents for different distributions in the Brownian-Force Model, depending on the observable and the driving protocol.

The technical parts of the calculations are presented in Appendices 6.A to 6.J, together with general material about Airy, Weierstrass and Elliptic functions. A short presentation of the numerical methods is also included.

6.2 Avalanche observables in the BFM

6.2.1 The Brownian Force Model

We have introduced and motivated the Brownian Force Model (BFM) in the introduction, section 1.4. In this chapter, it is defined as a random process $\dot{u}_{xt}$, which represents a velocity field and is solution of the stochastic differential equation (in the Ito sense):

$$\eta\partial_t\dot{u}_{xt} = \nabla_x^2\dot{u}_{xt} + \sqrt{2\sigma\dot{u}_{xt}}\,\xi_{xt} + m^2(\dot{w}_{xt} - \dot{u}_{xt}) \ . \tag{6.1}$$

This equation models the overdamped time evolution, with friction η, of the velocity field $\dot{u}_{xt} \geq 0$ of an interface with internal coordinate $x \in \mathbb{R}^d$; the space-time dependence is denoted by indexes $\dot{u}(x,t) \equiv \dot{u}_{xt}$. It is the sum of three contributions:

- short-ranged elastic interactions expressed as the Laplacian of $\dot{u}_{xt}$,
- stochastic contributions from a disordered medium, where ξ is a unit Gaussian white noise (both in x and t) :
$$\overline{\xi_{xt}\xi_{x't'}} = \delta^d(x-x')\,\delta(t-t'), \tag{6.2}$$
- a confining quadratic potential of curvature m^2, centered at w_{xt}, acting as a driving. By analogy with field theory, we refer to m as a mass.

The driving velocity is chosen positive, $\dot{w}_{xt} \geq 0$, as well as the initial velocitiy $\dot{u}_{xt=0} \geq 0$. Using the Middleton theorem [121], it implies that $\dot{u}_{xt} \geq 0$ for all $t > 0$, which ensures that (6.1), and especially the terms in $\sqrt{\dot{u}_{xt}}$, is well defined.

Equation (6.1), taken here as a definition, can also be derived from the equation of motion of an elastic interface, parametrized by a displacement field u_{xt} in a quenched random force field $F(u,x)$,

$$\eta\partial_t u_{xt} = \nabla_x^2 u_{xt} + F(u_{xt},x) + m^2(w_{xt} - u_{xt}) \ . \tag{6.3}$$

The random force field is a collection of independent one-sided Brownian motions in the u direction with correlator

$$\overline{F(u,x)F(u',x')} = 2\sigma\delta^d(x-x')\min(u,u') \ . \tag{6.4}$$

Taking the temporal derivative ∂_t of Eq. (6.3), and assuming forward motion of the interface, one obtains Eq. (6.1) for the velocity variable $\partial_t u_{xt} \equiv \dot{u}_{xt}$ (we use indifferently ∂_t or a dot to denote time derivatives). The fact that the equation for the velocity is Markovian even for a quenched disorder is remarkable and results from the properties of the Brownian motion.

Details of the correspondence are given in [116, 117] where subtle aspects of the position theory, and its links to the mean-field theory of realistic models of interfaces in short-ranged disorder via the Functional Renormalisation Group (FRG) are discussed. In the last section of this paper we will mention some properties of the position theory of the Brownian force model.

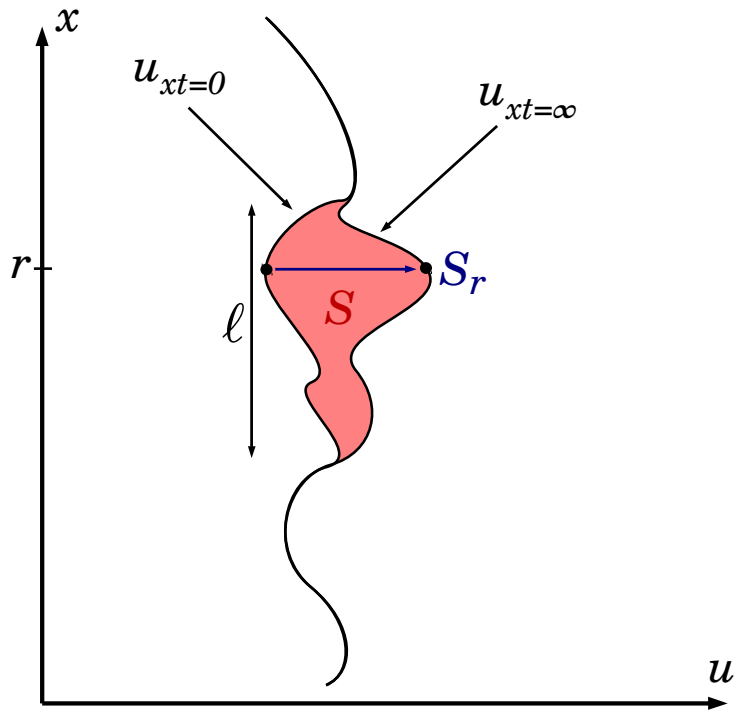

Figure 6.1: An avalanche in $d = 1$.

6.2.2 Avalanche observables and scaling

The BFM (6.1) allows to study the statistics of avalanches as the dynamical response of the interface to a change in the driving. We consider solutions of (6.1), responses to a driving of the form

$$\dot{w}_{xt} = \delta w_x \; \delta(t) \; , \; \delta w_x \geq 0 \; , \; \delta w = L^{-d} \int_x \delta w_x > 0 \; . \tag{6.5}$$

The initial condition is

$$\dot{u}_{xt=0} = 0 \; . \tag{6.6}$$

This solution describes an avalanche which starts at time $t = 0$ and ends when $\dot{u}_{xt} = 0$ for all x. The time at which the avalanche ends, also called avalanche duration, was studied in [95] and its distribution given in various situations, as well as its joint distribution with the avalanche size, defined in (6.7)

Within the description (6.3), i.e. in the displacement theory, it corresponds to an interface pinned, i.e. at rest, in a metastable state at $t < 0$. It is submitted at $t = 0$ to a jump in the total applied force $m^2\delta w$. More precisely, the center of the confining potential jumps at $t = 0$ from w_x (where it was for $t < 0$) to $w_{xt=0^+} = w_x + \delta w_x$ (where it stays for all $t > 0$). As a consequence, the interface moves forward (since $\delta w_x \geq 0$) up to a new metastable state. This is represented in figure 6.1, where $u_{xt=0}$ is the initial metastable state and $u_{xt=\infty}$ is the new metastable state at the end of the avalanche. In fact, as we can see from the distribution of avalanche durations, the new metastable state is reached almost surely in a finite time. For details on these metastable states and the system's preparation see [116, 117, 95].

The discussion of the avalanche observables will be the central question of this chapter. They

can be computed from the solution of (6.1) given (6.5) and (6.6); they are represented in figure 6.1 for a more visual definition in the case $d = 1$.

- Global size of the avalanche:

$$S = \int_{x\in\mathbb{R}^d} \int_0^\infty \dot{u}_{tx} \, \mathrm{d}t \ . \tag{6.7}$$

  This is the total area swept by the interface during the avalanche.

- Local size of the avalanche:

$$S_r = m^{-1} \int_{x\in\{r\}\times\mathbb{R}^{d-1}} \int_0^\infty \dot{u}_{tx} \, \mathrm{d}t \ . \tag{6.8}$$

  This is the size of the avalanche localized on a hyperplane, where one of the internal coordinates is r; the factor m^{-1} allows to express S and S_r using the same units (see below). In $d = 1$ this yields $S_r = m^{-1} \int_0^\infty \dot{u}_{tr} \, dt$, i.e. the transversal jump at the point r of the interface. For $d > 1$ the variable r is still one-dimensional, and S_r the total displacement in a hyperplane of the interface.

- Avalanche extension:

  For $d = 1$, the extension (denoted ℓ) of an avalanche is the lenght of the part of the interface which (strictly) moves during the avalanche. The generalisation to avalanches of a d-dimensional interface is done with the definition

$$\ell = \int_{-\infty}^{\infty} \mathrm{d}r \ \Theta(S_r > 0) \ , \tag{6.9}$$

  where Θ is the Heaviside function. Note that even for a d-dimensional interface, the extension ℓ is a unidimensional observable (cf. figure 6.2).

Note that

$$S_r > 0 \ \Leftrightarrow \ \mathrm{Supp} \bigcap \{r\} \times \mathbb{R}^{d-1} \neq \emptyset \tag{6.10}$$

where Supp denotes all the points of the interface moving during an avalanche (i.e. its support).

We use natural scales (or units) to switch to dimensionless expressions, both for the (local and global) avalanche size S_m, as for the time τ_m expressed as

$$S_m = \frac{\sigma}{m^4} \ , \qquad \tau_m = \frac{\eta}{m^2} \ . \tag{6.11}$$

The extension, a length in the internal direction of the interface, is expressed in units of m^{-1}. This is equivalent to setting $m = \sigma = \eta = 1$. All expressions below, except explicit mention, are expressed in these units.

While S_m is the large-size cutoff for avalanches, there is generically also a small-scale cutoff. As in the BFM the disorder is scale-invariant (by contrast with more realistic models with short-ranged smooth disorder), it is the increment in the driving δw which sets the small-scale cutoff for the local and global size of avalanches. They scale as $\min(S) \sim \delta w^2$ (global size) and $\min(S_r) \sim \delta w^3$ (local size).

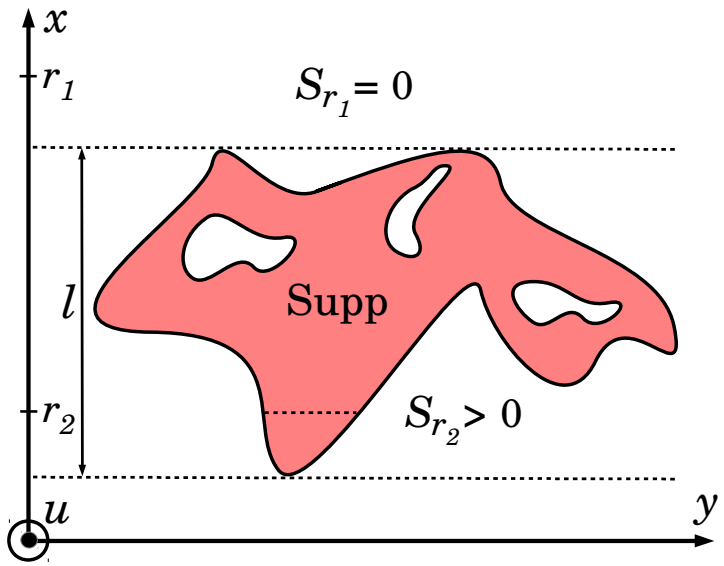

Figure 6.2: An avalanche in $d = 2$; the transverse direction is orthogonal to the plane of the figure and the colored zone corresponds to the support of the avalanche.

Masseless case

There are cases of interest where the limit $m \to 0$ is taken. Reminding that the driving force is $f_{xt} = m^2 w_{xt}$, in this limit w_{xt} disappears from the equation of motion. We can however drive with a fixed increase in the applied force (kick), by replacing in the equations of motion (6.1) and (6.3)

$$\begin{aligned} m^2(w_{xt} - u_{xt}) &\to f_{xt} \\ m^2(\dot{w}_{xt} - \dot{u}_{xt}) &\to \dot{f}_{xt} \ . \end{aligned} \tag{6.12}$$

Note that the small-scale properties of avalanches are unchanged as they are independent of m. The definition of the observables is the same except that the factor of m^{-1} is not added in the definition (6.8). To bring σ and η to unity, we then define time in units of η and displacements u in units of σ. The results will still have an unfixed dimension of length. In some of them, the system size L leads to dimensionless quantities (it also acts as a cutoff for large sizes, although we will not use this explicitly).

6.2.3 Generating functions and instanton equation

To compute the distribution of the observables presented above, we use a result from [116, 117] which allows us to express the average over the disorder of generating functions (Laplace transforms) of $\dot{u}_{xt}$, solution of (6.1). In dimensionless units, this result reads

$$G[\lambda_{xt}] = \left\langle \exp\left(\int_{xt} \lambda_{xt} \dot{u}_{xt} \right) \right\rangle = e^{\int_{xt} \dot{w}_{xt} \tilde{u}_{xt}} \ . \tag{6.13}$$

Here $\langle \cdots \rangle$ denotes the average over disorder and $\int_{xt}$ denotes integration over $x \in \mathbb{R}^d$ (or $[0, L]^d$ when a finite volume is needed for regularization) and $t \in [0, \infty[$. $\tilde{u}$ is a solution of the differential equation (called instanton equation)

$$\partial_x^2 \tilde{u} + \partial_t \tilde{u} - \tilde{u} + \tilde{u}^2 = -\lambda_{xt} \ . \tag{6.14}$$

Since avalanche observables that we consider are integrals of the velocity field over all times (cf. observable definitions above), the sources λ_{xt} we need in (6.13) are time independent. Thus we only need to solve the space dependent, but time independent, instanton equation

$$\tilde{u}_x'' - \tilde{u}_x + \tilde{u}_x^2 = -\lambda_x \ . \tag{6.15}$$

The prime denotes derivative w.r.t x. In the massless case discussed above, the term $-\tilde{u}_x$ is absent, all other terms are identical.

The global avalanche size implies a uniform source in the instanton equation: $\lambda_x = \lambda$, while the local size implies a localized source $\lambda_x = \lambda\delta^1(x)$. To obtain information on the extension of avalanches, we need to consider a source localized at two different points in space, $\lambda_x = \lambda_1\delta(x - r_1) + \lambda_2\delta(x - r_2)$.

This instanton approach, which derives from the Martin-Siggia-Rose formulation of (6.1), allows us to compute exactly disorder averaged observables for any form of driving, by solving a "simple" ordinary differential equation, which depends on the observable we want to compute, i.e. on λ_{xt}, but not on the form of the driving $\dot{w}_{xt}$. For a derivation of (6.13) and (6.14) we refer to [116].

6.3 Distribution of avalanche size

6.3.1 Global size

As defined in (6.7) the global size of an avalanche is the total area swept by the interface. Its PDF was calculated in [116, 115, 117] and reads, in dimensionless units,

$$P_{\delta w}(S) = \frac{\delta\hat{w}}{2\sqrt{\pi}S^{\frac{3}{2}}} e^{-\frac{(S-\delta\hat{w})^2}{4S}} \ . \tag{6.16}$$

Here $\delta\hat{w} = L^d\delta w$. This result does not depend on the spatial form of the driving (it can be localized, uniform, or anything in between), as long as it is applied as a force on the interface. Driving by imposing a specific displacement at one point of the interface is another interesting case that leads to a different behavior, see Section 6.4.2.

We can test this against a direct numerical simulation of the equation of motion (6.1). There is excellent agreement over 5 decades, with no fitting parameter, see Fig. 6.3.

Avalanches have the property of infinite divisiblity, i.e. they are Lévy processes with singular measure. Details on this can be found in Section V of [112] (and references therein) and section 4 of [122] (and references therein). This can be written as an equality in distribution, i.e. for probabilities,

$$P_{\delta w_1} * P_{\delta w_2} \overset{d}{=} P_{\delta w_1 + \delta w_2} \ . \tag{6.17}$$

It implies that we can extract from the probability distribution (6.16) the *single avalanche* density per unit δw that we denote $\rho(S)$ and which is defined as

$$P_{\delta w}(S) \underset{\delta\hat{w}\ll 1}{\simeq} \delta w\, \rho(S) \ . \tag{6.18}$$

This avalanche density contains the same information as the full distribution (6.16); its expression is

$$\rho(S) = \frac{L^d}{2\sqrt{\pi}S^{\frac{3}{2}}} e^{-\frac{S}{4}} \sim S^{-\tau} \ . \tag{6.19}$$

It is proportional to the system volume since avalanches occur anywhere along the interface. It defines the avalanche exponent $\tau = \frac{3}{2}$ for the BFM. Due to the divergence when $S \to 0$ it is not

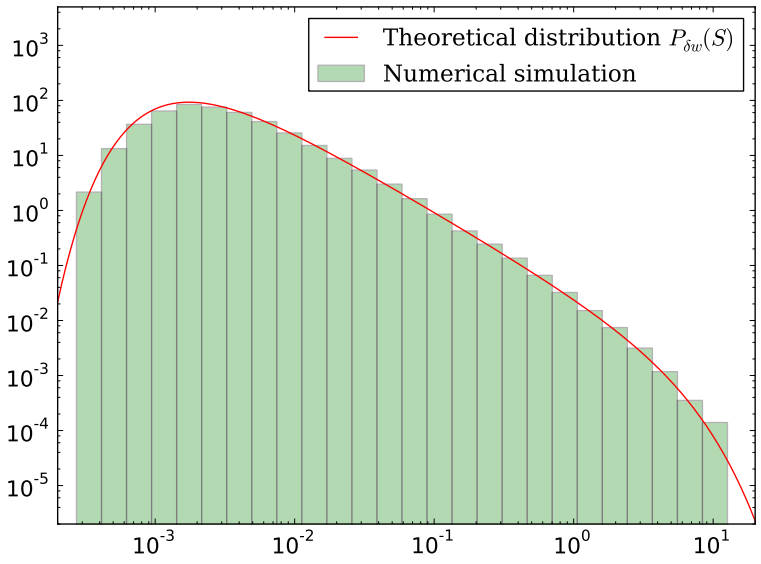

Figure 6.3: Green histogram : global avalanche-size distribution from a direct numerical simulation of a discretized version of Eq. (6.1) with parameters : $N = 1024, m = 0.01, df = m^2\delta w = 1$ and $dt = 0.05$. Red line : theoretical result given in Eq. (6.16). For details about the simulation see appendix 6.H.

normalizable (it is not a PDF), but as the interface follows on average the confining parabola, it has the following property

$$\int_0^\infty dS\, S\rho(S) = L^d \ . \tag{6.20}$$

In this picture, typical, i.e. almost all avalanches are of vanishing size, $S \approx 0$, or more precisely $S \leq \delta\hat{w}^2$, but moments of avalanches are dominated by non-typical large avalanches (of order S_m).

6.3.2 Local size

We now investigate the distribution of local size S_r as defined in Eq. (6.8). We have to specify the form of the kick; we start with one uniform (in x): $\delta w_x = \delta w$ for all $x \in \mathbb{R}$. In this case the system is translationnaly invariant, and we can choose $r = 0$, as any local size will have the same distribution.

The distribution of S_0 is obtained by solving Eq. (6.15) with the source $\lambda_x = \lambda\delta(x)$, and then computing the inverse Laplace transform with respect to λ of $G(\lambda) = \exp(\delta w \int_x \tilde{u}^\lambda)$, where $\tilde{u}^\lambda$ is the instanton solution (depending on λ). This has been done in [117]; the final result is

$$P_{\delta w}(S_0) = \frac{2\times 3^{\frac{1}{3}}}{S_0^{\frac{4}{3}}} e^{6\delta\hat{w}}\delta\hat{w}\,\mathrm{Ai}\left(\left(\frac{3}{S_0}\right)^{\frac{1}{3}}(S_0+2\delta\hat{w})\right) \underset{\delta\hat{w}\ll 1}{\simeq} \delta w \frac{2L^{d-1}}{\pi S_0}\mathrm{K}_{\frac{1}{3}}\left(\frac{2S_0}{\sqrt{3}}\right) \ . \tag{6.21}$$

Here $\delta\hat{w} = L^{d-1}\delta w$, Ai is the Airy function, and K_ν the Bessel function. We use that $\mathrm{Ai}(x) = \frac{1}{\pi}\sqrt{\frac{x}{3}}\mathrm{K}_{\frac{1}{3}}\left(\frac{2}{3}x^{3/2}\right)$ for $x > 0$. This distribution has again the property of infinite divisibility, which is far from obvious on the final results but, can be checked numerically.

The small-δw limit defines the density per unit δw of the local sizes of a "single avalanche",

which is given by

$$\rho(S_0) = \frac{2L^{d-1}}{\pi S_0} \mathrm{K}_{\frac{1}{3}}\left(\frac{2S_0}{\sqrt{3}}\right) \underset{S_0 \ll 1}{\simeq} L^{d-1} \frac{\sqrt[6]{3}\,\Gamma(1/3)}{\pi {S_0}^{4/3}} \sim S_0^{-\tau_\phi} \ . \tag{6.22}$$

Its small-size behavior defines the local size exponent $\tau_\phi = \frac{4}{3}$ for the BFM.

The distribution (6.21), or the density (6.22), can be compared to the results of direct numerical simulations of the BFM, and the agreement is very good over 7 decades, *without any fitting parameter*, cf. Fig. 6.4.

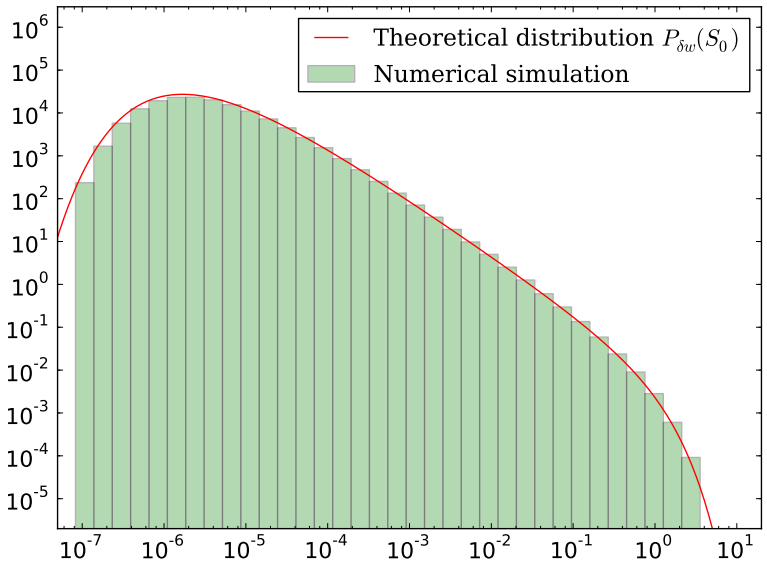

Figure 6.4: Green histogramm: Local avalanche-size distribution from a direct numerical simulation of a discretized version of (6.1)with parameters $N = 1024, m = 0.01, df = m^2\delta w = 1$, and $dt = 0.05$. Red line: the theoretical result given in Eq. (6.21). For details about the simulation see appendix 6.H.

Another interesting property is that the tail of large local sizes behaves as $\rho(S_0) \simeq_{S_0 \gg 1} S_0^{-3/2} e^{-2S_0/\sqrt{3}}$, i.e. with the same power-law exponent in the pre-exponential factor as the global size.

6.3.3 Joint global and local size

We now extend these results with a new calculation of the joint density of local and global sizes. This observable is readily accessible in experiments where the spatial structure can be recorded (cf. fracture experiments [101]); this gives a good test of the mean-field nature of the avalanches, or deviations thereof. Consider $P_{\delta w}(S_0, S)$, the joint PDF of local size S_0 and global size S, following a uniform kick δw. For arbitrary δw it does not admit a simple explicit form (see Appendix 6.D). We thus again consider the "single avalanche" limit $\delta w \to 0$. It defines the joint density $\rho(S, S_0)$, via $P_{\delta w}(S_0, S) \simeq \delta w\, \rho(S_0, S)$, which we now calculate. Equivalently one can consider the conditional probability $P_{\delta w}(S_0|S)$ of the local size, given that the global size is S. In the limit $\delta w \to 0$ these two objects are related by

$$P_{0^+}(S_0|S) = \frac{\rho(S_0, S)}{\rho(S)} \ , \tag{6.23}$$

where $\rho(S)$ is given in Eq. (6.19); the two factors of δw cancel. For simplicity we discuss the result for $P_{0^+}(S_0|S)$, which is easily possible for experimental data, as one usually bins the avalanches by their size. While both $\rho(S)$ and $\rho(S_0, S)$ are not probabilities, i.e. they cannot be normalized to one, we will show that the conditional probability $P_{0^+}(S_0|S)$ is well-defined, and normalized to unity.

A natural decomposition of this conditional PDF is

$$P_{0^+}(S_0|S) = \hat{P}_{0^+}(S_0|S) + \delta(S_0)\left(1 - \int_{u>0} \hat{P}_{0^+}(u|S)\right) . \tag{6.24}$$

The first term is the smooth part defined for $S_0 > 0$ which comes from the avalanches containing the point $r = 0$. The second term arises from all avalanches which do not contain the point $r = 0$. This term contains a substraction so that the total probability is normalized to unity, $\int_{S_0} P_{0^+}(S_0|S) = 1$, as it should be.

The smooth part is calculated using the instanton-equation approach. The details are given Appendix 6.D. The final result takes the scaling form

$$\hat{P}_{0^+}(S_0|S) = \frac{1}{L}\frac{4 \times 3^{\frac{2}{3}}}{S_0^{\frac{2}{3}}} e^{-\frac{2}{3}\alpha^3}\left[\alpha\,\mathrm{Ai}(\alpha^2) - \mathrm{Ai}'(\alpha^2)\right] \tag{6.25}$$

with

$$\alpha := \frac{3^{\frac{2}{3}} S_0^{\frac{2}{3}}}{S} . \tag{6.26}$$

The factor $1/L$ is natural since only a fraction of order $1/L$ of avalanches contains the point $r = 0$. As written, this smooth part is not normalized. Its integral is equal to the probability p that the point S_0 has moved (i.e. $S_0 > 0$) during an avalanche, for which we find

$$p := \int_0^\infty dS_0\, \hat{P}_{0^+}(S_0|S) = \frac{S^{\frac{1}{4}}}{L}\frac{3\Gamma\left(\frac{1}{4}\right)}{\sqrt{\pi}} . \tag{6.27}$$

The scaling of this probability with size shows that in a single avalanche only a finite portion of the interface is moving. If we assume statistical translational invariance we deduce that

$$p = \langle \ell \rangle_S / L , \tag{6.28}$$

where ℓ is the extension defined in (6.9), and $\langle \ell \rangle_S$ its mean value conditioned to the global size S. Hence we deduce that

$$\langle \ell \rangle_S = \frac{3\Gamma\left(\frac{1}{4}\right)}{\sqrt{\pi}} S^{\frac{1}{4}} . \tag{6.29}$$

In the following sections we will in fact calculate the PDF of the extension ℓ.

By dividing by p, we can now define a genuine normalized PDF for S_0, $\tilde{P}_{0^+}(S_0|S)$, conditioned to both S and $S_0 > 0$, so that the decomposition (6.24) becomes

$$P_{0^+}(S_0|S) = p\,\tilde{P}_{0^+}(S_0|S) + \delta(S_0)(1-p) . \tag{6.30}$$

Explicitly

$$\tilde{P}_{0^+}(S_0|S) = \frac{4\sqrt{\pi} e^{-\frac{2}{3}\alpha^3}}{3^{\frac{1}{3}}\Gamma\left(\frac{1}{4}\right) S_0^{\frac{2}{3}} S^{\frac{1}{4}}}\left[\alpha\,\mathrm{Ai}(\alpha^2) - \mathrm{Ai}'(\alpha^2)\right] , \tag{6.31}$$

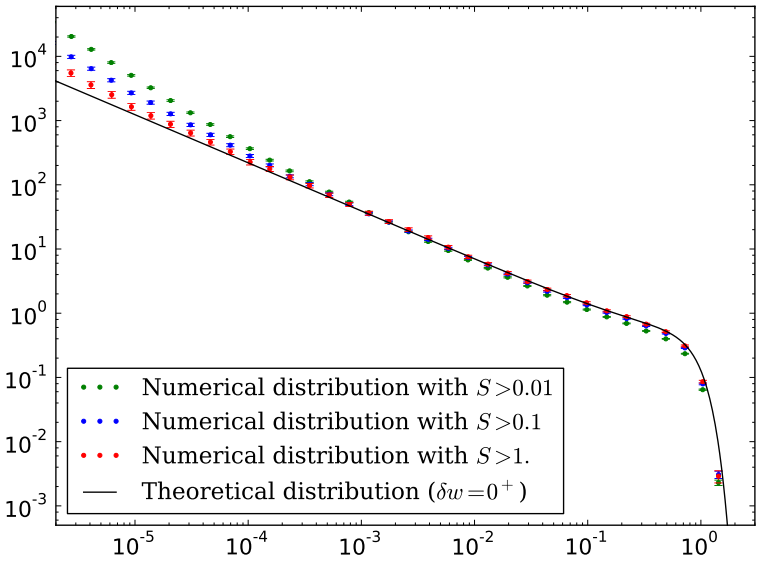

Figure 6.5: Distribution of α, defined in Eq. (6.26), from numerical simulations. This is compared to the theoretical prediction (6.33). Keeping only large-size avalanches, this converges (without any adjustable parameter) to the $\delta w = 0^+$ result. Numerical parameters used here are $N = 1024, m = 0.02, \delta w = 10, dt = 0.01$, different from the one used in Fig. 6.3 and 6.4 as we want to be close to the $\delta w = 0^+$ limit.

with α defined in Eq. (6.26). It is now normalized to unity, $\int_{S_0>0} \tilde{P}_{0^+}(S_0|S) = 1$. One sees that the typical local size scales as $S_0 \sim S^{3/4}$. Computing the first moment we find its conditional average to be $\langle S_0 \rangle_{S,S_0>0} = \frac{\sqrt{\pi}}{3\Gamma(1/4)} S^{3/4}$. Its PDF has two limiting behaviors,

$$\tilde{P}_{0^+}(S_0|S) \simeq \begin{cases} \dfrac{e^{-\frac{12 S_0^4}{S^3}}}{\Gamma(\frac{5}{4}) S^{\frac{3}{4}}} & \text{for } S_0 \gg S^{\frac{3}{4}} \\ \dfrac{\sqrt{\pi}}{3^{\frac{2}{3}} \Gamma(\frac{1}{3}) \Gamma(\frac{5}{4}) S_0^{\frac{2}{3}} S^{\frac{1}{4}}} & \text{for } S_0 \ll S^{\frac{3}{4}} \ . \end{cases} \tag{6.32}$$

The first one shows that the probability of avalanches which are "peaked" at $r = 0$ decays very fast. The second shows an integrable divergence at small S_0 with an exponent $2/3$. Comparing, for instance, with the behavior of the local size density (6.22), we see that conditioning on S yields a rather different behavior and exponent.

It is interesting to note that changing variables in Eq. (6.31) from S_0 to α, defined in (6.26), gives

$$\tilde{P}_{0^+}(\alpha|S) = \frac{\sqrt{3\pi} e^{-\frac{2}{3}\alpha^3}}{\Gamma\left(\frac{1}{4}\right) \alpha^{\frac{3}{4}}} \left[\alpha \, \mathrm{Ai}(\alpha^2) - \mathrm{Ai}'(\alpha^2) \right] , \tag{6.33}$$

which is now independent of S, and thus easier to test numerically as it does not require any conditionning. Figure 6.5 shows the agreement of these predictions with numerical simulations, in the limit of large S which is equivalent to $\delta w = 0^+$ as used in the theoretical derivation.

6.3.4 Scaling exponents

Let us now discuss the various exponents obtained until now. They are consistent with the usual scaling arguments for interfaces. If an avalanche has an extension of order ℓ (in the codirection

of the hyperplane over which the local size is calculated), the transverse displacement scales as $u \sim \ell^\zeta$. Here the roughness exponent ζ for the BFM with short-range elasticity is

$$\zeta_{\rm BFM} = 4 - d \ . \tag{6.34}$$

The avalanche exponent for the global size follows the Narayan-Fisher (NF) prediction [107]

$$\tau = 2 - \frac{2}{d+\zeta} \ \stackrel{\rm BFM}{\longrightarrow} \ \frac{3}{2} \ . \tag{6.35}$$

The global size then scales as $S \sim \ell^{d+\zeta}$, since all d internal directions are equivalent, and the transverse response scales with the roughness exponent ζ. In turn this gives $\ell \sim S^{\frac{1}{d+\zeta}}$. In the BFM with short-range elasticity this leads to $\ell \sim S^{1/4}$ as found above.

Similarly, the local size, defined here as the avalanche size inside a d_ϕ-dimensionel subspace, is $S_0 \sim \ell^{d_\phi+\zeta}$, leading to a generalized NF value $\tau_\phi = 2 - \frac{2}{d_\phi+\zeta}$. In the BFM we have focused on the case $d_\phi = d-1$ (i.e. the subspace is an hyperplane), hence $d_\phi + \zeta = 3$ and the local size exponent becomes $\tau_\phi = 4/3$. It also implies $S_0 \sim \ell^3$, hence $S_0 \sim S^{3/4}$ as found above.

6.4 Driving at a point: avalanche sizes

Here we briefly study avalanche sizes for an interface driven only in a small region of space, e.g. at a point. There are two main cases:

- the local force on the point is imposed, which in our framework means to consider a local kick $\delta w_x = \delta w\, \delta(x)$. In the massless setting it amounts to use $f_x = \delta f\, \delta(x)$,
- the displacement $u_{x=0,t}$ of one point of the interface is imposed.

As we now see this leads to different universality classes and exponents.

6.4.1 Imposed local force

Consider an avalanche following a local kick at $x = 0$, i.e. $\delta w_x = \delta w_0 \delta(x)$. In the BFM the distribution of the global size of an avalanche does not depend on whether the kick is local in space or not. One still obtains [117] the global-size distribution as given in Eq. (6.16) with $\delta\hat{w} = \int_x \delta w_x = \delta w_0$.

The distribution of the *local size at the point of the kick* is more interesting. The calculation is performed in Appendix 6.C. For simplicity we restrict to $d = 1$, the general case can be obtained as above by inserting factors of L^{d-1}. The full result for the PDF, $P_{\delta w_0}(S_0)$, is given in (6.107) and is bulky. In the limit $\delta w_0 \to 0$ it simplifies. Noting $P_{\delta w_0}(S_0) \simeq \delta w_0 \rho(S_0)$, the corresponding local-size density becomes

$$\rho(S_0) = -\frac{1}{3^{1/3} S_0^{5/3}} {\rm Ai}'\left(3^{1/3} S_0^{2/3}\right) \ . \tag{6.36}$$

At small S_0, or equivalently in the massless limit at fixed $\delta f_0 = m^2 \delta w_0$, it diverges as

$$\rho(S_0) \underset{S_0 \ll 1}{\simeq} \frac{S_0^{-5/3}}{3^{2/3}\Gamma(1/3)} \sim S_0^{-\tau_{0,\rm loc.driv.}} \ . \tag{6.37}$$

This leads to a new avalanche exponent

$$\tau_{0,\rm loc.driv.} = \frac{5}{3} \ . \tag{6.38}$$

The cutoff at small size is given by the driving, $S_0 \sim \delta w_0^{3/2}$. At large S_0 the PDF is cut by the scale $S_m \equiv 1$ and decays as

$$\rho(S_0) \underset{S_0 \gg 1}{\simeq} \frac{S_0^{-3/2}}{2\sqrt{\pi} 3^{1/4}} e^{-2S_0/\sqrt{3}} \ . \tag{6.39}$$

6.4.2 Imposed displacement at a point

We analyze the problem in the massless case. To impose the displacement at point $x = 0$ we replace in the equation of motion (6.1) and (6.3), $m^2 \to m^2 \delta(x)$. Hence there is no global mass, but a local one to drive the interface at a point. To impose the displacement, we consider the limit $m^2 \to \infty$. In that limit $u_{x=0,t} = w_{0,t}$, and the local size of the avalanche S_0 is equal to δw_0.

While the local size S_0 is fixed by the driving, we can calculate the distribution of global sizes. It is obtained in Appendix 6.E using an instanton equation with a Dirac mass term. It can be mapped onto the same instanton equation as studied for the joint PDF of local and global sizes. The Laplace-transform of the result for the PDF is given in Eq. (6.133). Its small-driving limit, i.e. the density, is

$$\rho(S) = \frac{\sqrt{3}}{\Gamma(1/4) S^{7/4}} \sim S^{-\tau_{\text{loc.driv.}}} \tag{6.40}$$

with a distinct exponent

$$\tau_{\text{loc.driv.}} = \frac{7}{4} \ . \tag{6.41}$$

6.5 Distribution of avalanche extension

In this section we study the distribution of avalanche extension. In the BFM they can be calculated analytically. We start by recalling standard scaling arguments.

6.5.1 Scaling arguments for the distribution of extension

As mentioned in the last section, we expect that the global size S and the extension ℓ of avalanches are related by the scaling relation

$$S \sim \ell^{d+\zeta} \tag{6.42}$$

in the region of small avalanches $S \ll S_m$ (in dimensionfull units). From the definition of the avalanche-size exponent

$$P(S) \sim S^{-\tau} \tag{6.43}$$

and using the change of variables $P(S)dS = P(\ell)d\ell$ we find

$$P(\ell) \sim \ell^{-\kappa} \ \text{ with } \ \kappa = 1 + (\tau - 1)(d + \zeta) \ . \tag{6.44}$$

Using the value for τ from the NF relation (6.35) we obtain

$$\tau = 2 - \frac{2}{d + \zeta} \ . \tag{6.45}$$

For short-range elasticity, this yields

$$\kappa = d + \zeta - 1 \ . \tag{6.46}$$

The prediction for the BFM is that $\zeta_{\rm BFM} = 4 - d$ and $\tau_{\rm BFM} = 3/2$, which leads to

$$\kappa_{\rm BFM} = 3 \tag{6.47}$$

in all dimensions. We will now check this prediction from the scaling relations with exact calculations on the BFM model in $d = 1$.

6.5.2 Instanton equation for two local sizes

If we want to investigate the joint distribution of two local sizes at points r_1 and r_2, we need to solve the instanton equation with two local sources,

$$\tilde{u}_x'' - \tilde{u}_x + \tilde{u}_x^2 = -\lambda_1 \delta(x - r_1) - \lambda_2 \delta(x - r_2) \ . \tag{6.48}$$

This solution is difficult to obtain for general values of λ_1 and λ_2. Nevertheless $\lambda_{1,2} \to -\infty$ is an interesting solvable limit, and sufficient to compute the extension distribution. Let us denote by $\tilde{u}_{r_1,r_2}(x)$ a solution of Eq. (6.48) with $r_1 < r_2$ in this limit $\lambda_{1,2} \to -\infty$. It allows to express the probability that two local sizes in an avalanche following an arbitrary kick δw_x equal 0,

$$\begin{aligned} &\mathbb{P}_{\delta w_x}(S_{r_1} = 0, S_{r_2} = 0) \\ &\qquad = \exp\left(\int_{x \in \mathbb{R}^d} \delta w_x \, \tilde{u}_{r_1,r_2}(x) \right) \ . \end{aligned} \tag{6.49}$$

We further restrict for simplicity to the massless case, i.e. without the linear term $\tilde{u}_x$ in Eq. (6.48). One easily sees from the latter equation that $\tilde{u}_{r_1,r_2}$ takes the scaling form

$$\tilde{u}_{r_1,r_2}(x) = \frac{1}{(r_1 - r_2)^2} f\left(\frac{2x - r_1 - r_2}{2(r_2 - r_1)} \right) \ . \tag{6.50}$$

The function $f(x)$ is solution of

$$f''(x) + f(x)^2 = 0 \ . \tag{6.51}$$

It diverges at $x = \pm\frac{1}{2}$, vanishes at $x \to \pm\infty$ and is negative everywhere: $f(x) \leq 0$. As $\delta w_x \geq 0$, the latter is a necessary condition s.t. the probability (6.49) is bounded by one.

In the interval $x \in]-\frac{1}{2}, \frac{1}{2}[$, the scaling function $f(x)$ can be expressed in terms of the Weierstrass $\mathcal{P}$-function, see (6.174),

$$f(x) = -6\,\mathcal{P}\left(x + \frac{1}{2}; g_2 = 0; g_3 = \frac{\Gamma(1/3)^{18}}{(2\pi)^6} \right) \ . \tag{6.52}$$

The value of $g_3 > 0$ is consistent with the required period $2\Omega = 1$, see (6.171). Note from Appendix 6.I that there is another solution of the form (6.52) with $g_3 = -\left(2\sqrt{\pi} \frac{\Gamma(1/3)}{4^{\frac{1}{3}}\Gamma(5/6)} \right)^6 < 0$ which violates the condition $f(x) \leq 0$, hence is discarded. For $|x| \geq 1/2$, the function $f(x)$ reads

$$f(x) = -\frac{6}{(|x| - 1/2)^2} \ . \tag{6.53}$$

One property of the solution $\tilde{u}_{r_1,r_2}(x)$ is that it diverges as $\sim (x - r_{1,2})^{-2}$ when $x \approx r_{1,2}$. There are thus two cases:

(i) - the driving δw_x is non-zero at one of these points, or vanishes too slowly near this point (e.g. only linearly or slower). Then the integral in (6.49) is not convergent, equal to $-\infty$, which implies

$$\mathbb{P}_{\delta w_x}(S_{r_1} = 0, S_{r_2} = 0) = 0 \ .$$

This means that the avalanche contains surely at least one of the points r_1 or r_2.

(ii) - If δw_x vanishes fast enough, for example if δw_x is localised away from $x = \pm r_{1,2}$ (e.g $\delta w_x = \delta w \delta(x - y)$ for some $y \in \mathbb{R} \backslash \{r_1, r_2\}$), the probablity (6.49) becomes non trivial.

6.5.3 Avalanche extension with a local kick

We now consider a local kick centered at $x = 0$, i.e. $w_x = \delta w_0\, \delta(x)$. If further $0 < r_1 < r_2$, then

$$\mathbb{P}_{\delta w_0}(S_{r_1} = 0, S_{r_2} = 0) = \mathbb{P}_{\delta w_0}(S_{r_1} = 0) \ . \tag{6.54}$$

This comes from the fact that in the interval $x \in [-\infty, r_1]$, the solution $\tilde{u}_{r_1,r_2}(x)$ is identical to the instanton solution with only one infinite source at r_1 (in other word, it does not "feel" the source in r_2). This shows for instance that the support of the avalanche is larger or equal than the set of points where the driving is non-zero.

This property also shows that avalanches are connected, i.e. it is impossible to draw a plane where the interface did not move between two moving parts of the interface. As a function of r (which is one-dimensional), the support (i.e. the set of points where $S_r > 0$) of an avalanche following a local kick at $x = 0$ must be an interval. Since this interval contains $x = 0$ we will write it as $[-\ell_1, \ell_2]$ with $\ell_1 > 0$ and $\ell_2 > 0$. This allows to define the extension of an avalanche as $\ell = \ell_1 + \ell_2$.

To calculate the joint PDF of ℓ_1 and ℓ_2 for a kick at $x = 0$ we consider (6.49) with $r_1 = -x_1 < 0 < r_2 = x_2$. Using the previous results about the instanton equation with two sources, and the fact that the interface model is translationaly invariant, we obtain the joint cumulative distribution for $\ell_1 > 0$ and $\ell_2 > 0$:

$$F_{\delta w_0}(x_1, x_2) := \mathbb{P}_{\delta w_0}\left(\ell_1 < x_1, \ell_2 < x_2\right) \ . \tag{6.55}$$

It can, for any $x_1, x_2 > 0$, be expressed in terms of the function f obtained in the preceding section,

$$\begin{aligned} F_{\delta w_0}(x_1, x_2) = \mathbb{P}_{\delta w_0}(S_{r_1} = 0, S_{r_2} = 0) &= \exp\left(\int_x \delta w_0 \delta(x)\, \tilde{u}_{-x_1,x_2}(x)\right) \\ &= e^{\delta w_0 \frac{1}{(x_1+x_2)^2} f\left(-\frac{x_2-x_1}{2(x_1+x_2)}\right)} \ . \end{aligned} \tag{6.56}$$

Since the argument of f is within the interval $]-\frac{1}{2}, \frac{1}{2}[$ we must use the expression (6.52).

From this one can obtain several results. First taking $x_2 \to \infty$ one obtains the PDF of ℓ_1 alone,

$$\mathbb{P}_{\delta w}\left(\ell_1\right) = \frac{12\delta w}{\ell_1^3} e^{-\delta w \frac{6}{\ell_1^2}} \ . \tag{6.57}$$

A similar result holds for ℓ_2.

In principle, one can now obtain the distribution of avalanches extension

$$\mathbb{P}_{\delta w_0}(\ell) = \int_0^\infty d\ell_1 \int_0^\infty d\ell_2\, \delta(\ell - \ell_1 - \ell_2) \partial_{\ell_1} \partial_{\ell_2} F_{\delta w_0}(\ell_1, \ell_2) \tag{6.58}$$

It has a rather complicated expression. Let us define in addition to the total length, the aspect ratio

$$k = \frac{\ell_1 - \ell_2}{2(\ell_1 + \ell_2)} \quad , \quad -\frac{1}{2} < k < \frac{1}{2} \ . \tag{6.59}$$

Using a change of variables, we obtain the joint density of total extension and aspect ratio in the limit $\delta w_0 \to 0$,

$$\rho\left(\ell, k\right) := \lim_{\delta w_0 \to 0} \frac{1}{\delta w_0} \mathbb{P}_{\delta w_0}\left(\ell, k\right) = \frac{R(k)}{\ell^3} \ , \tag{6.60}$$

$$R(k) := 6f(k) + 6kf'(k) + \left(k^2 - \frac{1}{4}\right) f''(k) \ . \tag{6.61}$$

The function $f(x)$ was defined in Eq. (6.52). While the probability as a function of ℓ decays as ℓ^{-3}, the dependence on the aspect ratio is more complicated and plotted in figure 6.6. Note that in this expression $f(k)$ can be replaced by $f_{\rm reg}(k) := f(k) + \frac{6}{(k+\frac{1}{2})^2} + \frac{6}{(k-\frac{1}{2})^2}$, which is a regular function of k, vanishing at $k = \pm\frac{1}{2}$. Integration over k gives

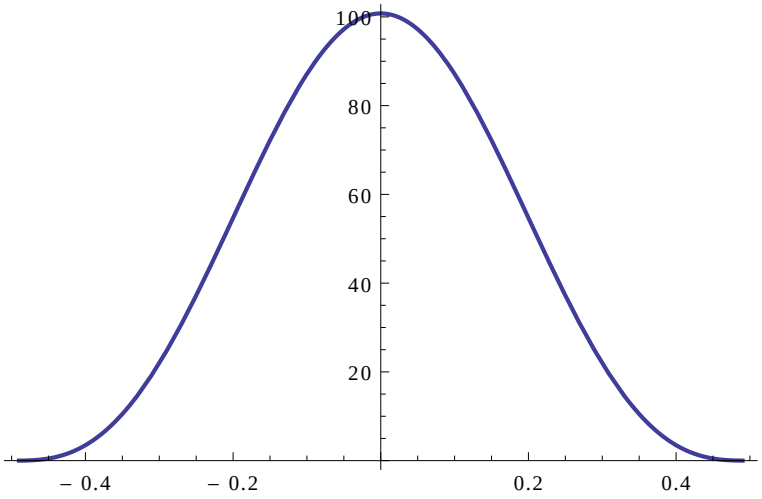

Figure 6.6: Decay amplitude $R(k)$ as a function of the aspect ratio k involved in the joint density of ℓ and k, and defined in Eqs. (6.60) and (6.61).

$$\rho\,(\ell) = \frac{B}{\ell^3} \qquad \text{with} \qquad B = 24 + 2\int_{-1/2}^{1/2} f_{\rm reg}(k) = 8\sqrt{3}\pi\ . \tag{6.62}$$

6.5.4 Avalanche extension with a uniform kick

If a kick extends over the whole system, as e.g. a uniform kick $\delta w_x = \delta w$, the avalanche will have almost surely an infinite extension as the local size is non-zero everywhere,

$$\mathbb{P}_{\delta w}\,(S_r = 0) = 0 \quad \text{for any } \ r \in \mathbb{R}\ . \tag{6.63}$$

However, in the limit of a small δw which is also the limit of a "single avalanche", we can recover the result for the distribution of extension. This is consistent with the idea that "single avalanches" do not depend on the way they are triggered. These calculations allow to obtain the extension distribution without solving explicitly the instanton equation. (The use of elliptic integrals is in fact equivalent to the use of Weierstrass functions as solutions of the instanton equation, cf. Appendix 6.I).

We now focus on the following ratio of generating functions

$$\frac{\langle e^{\lambda_1 s_0 + \lambda_2 s_r}\rangle}{\langle e^{\lambda_1 s_0}\rangle\langle e^{\lambda_2 s_r}\rangle} \tag{6.64}$$

in the limit $\lambda_1, \lambda_2 \to -\infty$. It compares the probability that both local sizes $s_0 := S_0$ and $s_r := S_r$ are simultaneously 0 to the product of the two probabilties that each one is 0.

We can express this ratio, using the instanton-equation approach, as

$$\begin{aligned} &\lim_{\lambda_1,\lambda_2\to-\infty} \frac{\langle e^{\lambda_1 s_0 + \lambda_2 s_r}\rangle}{\langle e^{\lambda_1 s_0}\rangle\langle e^{\lambda_2 s_r}\rangle} \\ &\quad = \exp\Big(\int_x \delta w_x \big[\tilde u_r(x) - \tilde u_\infty(x) - \tilde u_\infty(x-r)\big]\Big) \end{aligned} \tag{6.65}$$

where $\tilde{u}_r := \tilde{u}_{r_1=0,r_2=r}$. We denote by $\tilde{u}_\infty := \tilde{u}_{r_1=0,r_2=\infty}$, the solution of the instanton equation with one source at $r = 0$ and the other one at infinity. It is the same as the solution for only one source in $r = 0$. The above expression is valid for any form of driving δw_x.

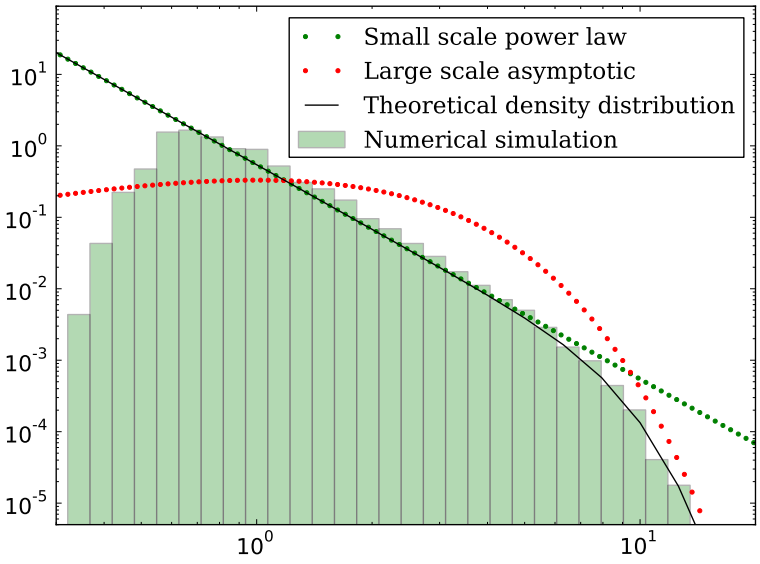

Figure 6.7: The distribution of extension $\rho(\ell)$, as obtained from the elliptic integrals (6.141) and (6.137) (black line). The (straight) green dotted line is the small-ℓ asymptotics (6.68), whereas the (curved) red dotted line is the large-ℓ asymptotics (6.70). The numerical simulation (green histogram) is cut at small scale due to discretization effects. Numerical parameters are $N = 2^{10}$, $m = 0.05$, $dw = 100$ and $dt = 0.01$.

We can now specify to the case of small and uniform driving $\delta w_x = \delta w$; the quantity of interest is then

$$Z(r) = \int_x \tilde{u}_r(x) - \tilde{u}_\infty(x) - \tilde{u}_\infty(x - r) \ . \tag{6.66}$$

While $\tilde{u}_r(x)$ is not integrable, $Z(r)$ is well defined as the two $\tilde{u}_\infty$ terms cancel precisely the two non-integrable poles located at $x = 0$ and $x = r$.

Using that $\tilde{u}_r$ is a solution of Eq. (6.48), we can obtain an expression of $Z(r)$ as an elliptic integral, see Appendix 6.F for details of the calculation. The formulas written there are for the massive case, but only allow to get an implicit expression for $Z(r)$. They however allow us to extract the small-scale behavior of the avalanche-extension distribution (equivalently the massless limit). For small r, the behavior of $Z(r)$ is

$$Z(r) \simeq \frac{4\sqrt{3}\pi}{r} \ . \tag{6.67}$$

To understand the connection with the avalanche extension, we need to get back to the interpretation of (6.64). Now that we have specified the kick to be uniform, the two averages of the denominator are independent of r, and act only as a normalization constants. The numerator, in the limit of $\lambda_{1,2} \to -\infty$, is the probability that both s_0 and s_r are simultaneously equal to 0. Deriving this two times w.r.t. r (which lets the denominator invariant) gives the probability that the avalanche start in $x = 0$ and end in $x = r$. Dividing by δw and taking the limit[1] $\delta w \to 0$,

[1]Note that the denominators can then be set to unity. There is no ambiguity since the calculation could be performed first at finite but large λ_i, and setting δw to zero after taking the derivative and dividing by δw, and only at the end taking the limit of infinite λ_i.

we obtain the extension density in the limit of a single avalanche as

$$\begin{aligned}\rho(\ell) =& \frac{1}{\delta w}\partial_r^2 e^{\delta w Z(r)}|_{\delta w=0^+, r=\ell} \\ =& \partial_r^2 \left.\tilde{Z}(r)\right|_{r=\ell} \simeq \tilde{B}\ell^{-3} \text{ when } \ell \to 0\end{aligned} \tag{6.68}$$

with

$$\tilde{B} = 8\sqrt{3}\pi \ . \tag{6.69}$$

We recover here the ℓ^{-3} divergence for small ℓ of the extension of avalanches. Note that this calculation gives exactly the same prefactor as in Eq. (6.62), which confirms that we are studying the same object, namely a "single avalanche".

Finally, in the massive case, one can also compute the tail of the extension distribution, resulting into (see Appendix 6.F)

$$\rho(\ell) \simeq 72\,\ell e^{-\ell} \text{ when } \ell \to \infty \ . \tag{6.70}$$

6.6 Non-stationnary dynamics in the BFM

The easiest way to construct a position theory equivalent to the BFM model defined in Eq. (6.1) is to consider the non-stationnary evolution of an elastic line in some specific quenched disorder, given in Eq. (6.3). We refer to Ref. [112] for a more general introduction to the position, or displacement theory of elastic interfaces. The disorder considered here has the correlations of independent one-sided Brownian motions, as given in Eq. (6.4).

Consider the initial condition $u_{xt=0} = 0$. We can then compute the correlation function of the position

$$u_{xt} = \int_0^t \dot{u}_{xs}\, ds$$

for a uniform driving $w_t = vt\,\theta(t)$, starting at $t = 0$. The calculation is sketched in Appendix 6.J. In dimensionless units and in Fourier space, the result reads

$$\begin{aligned}\langle u_{qt}u_{-qt}\rangle^c = v\Bigg[&\frac{2q^2(t-1)+2t-5}{\left(q^2+1\right)^3} - \frac{4e^{-\left(q^2+1\right)t}}{q^2\left(q^2+1\right)^3} \\ &+ \frac{4e^{-t}}{q^2\left(2q^2+1\right)} + \frac{e^{-2\left(q^2+1\right)t}}{\left(q^2+1\right)^3\left(2q^2+1\right)}\Bigg] \ .\end{aligned} \tag{6.71}$$

At large times, the displacement correlations behave as (restoring units)

$$\langle u_{qt}u_{-qt}\rangle^c \underset{t\to\infty}{\simeq} \frac{2\sigma v t}{(q^2+m^2)^2} \ . \tag{6.72}$$

The q dependence is similar to the so-called Larkin random-force model [135], but with a time-dependent amplitude, i.e. the effective disorder is growing with time, which is natural given the correlations of the disorder (6.4). The correlation of the position thus remains non-stationary at all times[2].

[2]Note that there are stationary versions of the BFM, which we will not discuss here, see discussions in e.g. [115, 116, 117].

From Eq. (6.72) one obtains the correlations of the displacement in real space, still in the large-t limit

$$\begin{aligned}\overline{(u_{xt}-u_{0t})^2} &\simeq 2vt\int\frac{d^dq}{(2\pi)^d}\frac{1}{(q^2+m^2)^2}(1-\cos qx)\\ &\sim vt\times x^{2\zeta_L}\end{aligned} \tag{6.73}$$

with $\zeta_L = (4-d)/2$ the Larkin roughness exponent. Note that the average displacement is $\overline{u_{xt}} = vt - \frac{1-e^{-m^2t}}{m^2}$ (see Appendix 6.J). Hence we see that the BFM roughness scaling $u \sim x^{4-d}$ is dimensionally consistent with the correlation at large times,

$$\overline{(u_{xt}-u_{0t})^2} \simeq 2\ \overline{u_{xt}}\ x^{4-d}\ . \tag{6.74}$$

This result, $\zeta = 4-d = \varepsilon$, is in agreement with the FRG approch: the position theory of the BFM model is an exact fixed point for the flow equation of the FRG with a roughness exponent $\zeta = \varepsilon$, as discussed in [112, 116].

6.7 Conclusion

We presented a general investigation of the Brownian Force Model, using its exact solvability via the instanton equation in various settings. After reviewing the results and the calculations of [110, 115, 116, 117], we extended the study in several directions.

First, we computed observables containing information about the spatial structure of avalanches in the BFM: the joint density of S and S_0 (or equivalently, the distribution of the local size S_0 at fixed total global size S), and the distribution of the extension ℓ of an avalanche. These distributions display power laws in their small-scale regime, which we recovered using scaling arguments, together with universal amplitudes.

We also extended the method to study new driving protocols relevant to distinct experimental setups. The derived results show new exponents for the small-scale behavior of the global avalanche-size distribution following a locally imposed displacement, and for the small-scale behavior of the local-size distribution following a localized kick.

Finally, we presented results for the non-stationary dynamics of the BFM, focusing on observables which exist only in the position theory, such as the roughness exponent. This explains why both the Larkin roughness and the BFM roughness (emerging from the FRG approach), play a role in this model, depending on whether the driving is stationary or not.

6.A Airy functions

We recall the definition of the Airy function:

$$\mathrm{Ai}(z) := \int_{-\infty}^{\infty}\frac{dt}{2\pi}e^{i\frac{t^3}{3}+izt}\ . \tag{6.75}$$

The following formula is useful for $a\in\mathbb{R}^*$,

$$\begin{aligned}\Phi(a,b,c) =& \int_C\frac{dz}{2i\pi}e^{a\frac{z^3}{3}+bz^2+cz}\\ =&|a|^{-1/3}e^{\frac{2b^3}{3a^2}-\frac{bc}{a}}\mathrm{Ai}\left(\frac{b^2}{|a|^{4/3}}-\frac{c\ \mathrm{sgn}(a)}{|a|^{1/3}}\right)\ .\end{aligned} \tag{6.76}$$

It can be obtained from (6.75), deforming the contour C, e.g. to $z = -\frac{b}{a}+i\mathbb{R}$.

6.B General considerations on the instanton equation

Sourceless equation

Massive case

It is useful to start with the simpler sourceless instanton equation

$$y'' = y - y^2 \ . \tag{6.77}$$

Here we denote by a prime the derivative with respect to x. It can be interpreted as the classical equation of motion of a particule (of mass 2) in a potential $V(y) = -y^2 + \frac{2y^3}{3}$, represented in Fig. 6.8. Multiplying by y' and integrating once, we obtain $y' = \pm\sqrt{E - V(y)}$, where E is a real integration constant equivalent to the total "energy" of the particle. Its phase-space diagram (y, y') is represented in Fig. 6.9.

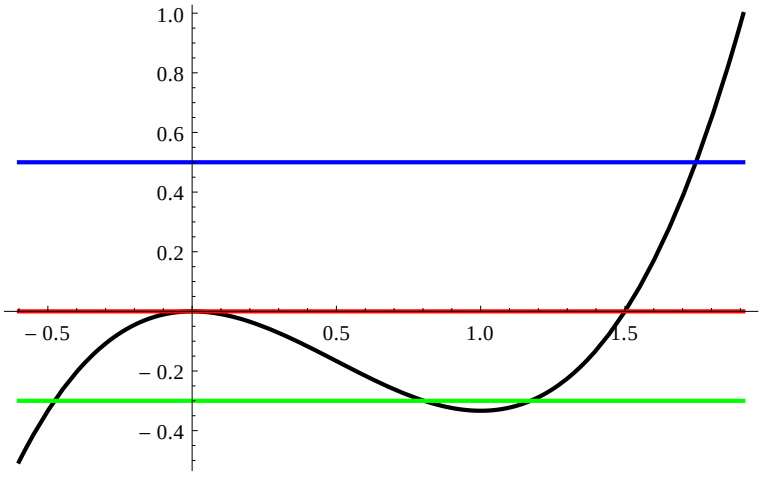

Figure 6.8: Representation of the potential energy $V(y)$ as a function of y, and lines of constant total energy, with $E = 0$ in red, $E > 0$ in blue and, $E < 0$ in green.

From figures 6.8 and 6.9, we see that:

(i) - there is exactly one positive $E = 0$ solution $y^+(x)$ defined for all $x \in \mathbb{R}$, up to a shift $x \to x + x_0$. It reads

$$\begin{aligned} &\int_{y^+(x)}^{3/2} \frac{dy}{\sqrt{y^2 - \frac{2}{3}y^3}} = |x| \\ &\Leftrightarrow \ y^+(x) = \frac{3}{1 + \cosh x} = \frac{3}{2}\left[1 - \tanh^2\left(\frac{x}{2}\right)\right] \ . \end{aligned} \tag{6.78}$$

(ii) - There is exactly one negative $E = 0$ (zero energy) solution $y^-(x)$ defined for all $x \in \mathbb{R}^*$, namely

$$\begin{aligned} &\int_{-\infty}^{y^-(x)} \frac{dy}{\sqrt{y^2 - \frac{2}{3}y^3}} = |x| \\ &\Leftrightarrow \ y^-(x) = \frac{3}{1 - \cosh x} = \frac{3}{2}\left[1 - \coth^2\left(\frac{x}{2}\right)\right] \ . \end{aligned} \tag{6.79}$$

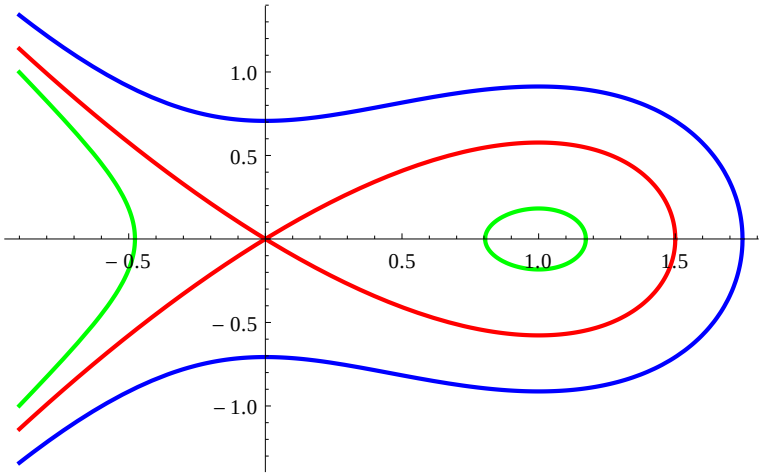

Figure 6.9: Phase-space diagram, i.e. trajectories represented with y' as a function of y. The case $E = 0$ is in red, $E > 0$ in blue and and $E < 0$ in green. We can see that properties of the solution (periodicity, divergences, etc.) strongly depend on the value of E.

(iii) - There are two classes of solutions with $E \neq 0$. The first class is defined on an interval of finite length $r(E)$ with

$$r(E) = 2\int_{-\infty}^{t} \frac{dy}{\sqrt{E + y^2 - \frac{2}{3}y^3}} \tag{6.80}$$

where $t \neq 0$ denotes the smallest real root of $E = -t^2 + \frac{2}{3}t^3$. This integral is convergent at large negative y due to the cubic term, and also convergent near the root $y = t$ (for $E \to 0$ it diverges logarithmically). If one chooses $x = 0$ as center of the interval, the solution $y(x)$ satisfies

$$\int_{y(x)}^{t} \frac{dy}{\sqrt{E + y^2 - \frac{2}{3}y^3}} = |x| \ . \tag{6.81}$$

It diverges at both ends $x = \pm r(E)/2$. It is sometimes more convenient to choose $x = 0$ as the endpoint of the interval $]0, r(E)[$. Then, for $x \in]0, r(E)[$ one has

$$\int_{-\infty}^{y(x)} \frac{dy}{\sqrt{E + y^2 - \frac{2}{3}y^3}} = x \ . \tag{6.82}$$

Setting $y = \frac{1}{2} - z$, this can be rewritten as

$$\sqrt{6}\int_{\frac{1}{2}-y(x)}^{\infty} \frac{dz}{\sqrt{4z^3 - 3z + (1 + 6E)}} = x \ . \tag{6.83}$$

This gives, in terms of the Weirstrass elliptic function $\mathcal{P}$,

$$y(x) = \frac{1}{2} - \mathcal{P}\left(\frac{x}{\sqrt{6}}; g_2 = 3, g_3 = -1 - 6E\right) \ . \tag{6.84}$$

It diverges at $x = 0$ and $x = r(E)$, and is the proper solution on the interval $]0, r(E)[$, see Appendix 6.I.

The second class of solutions with $E \neq 0$ exists only for $-\frac{1}{3} < E < 0$; these solutions are periodic on the whole real line. As can be seen from Figs. 6.8 and 6.9, $y(x)$ varies in a bounded and strictly positive interval. We will not discuss these solutions as they will not be needed below.

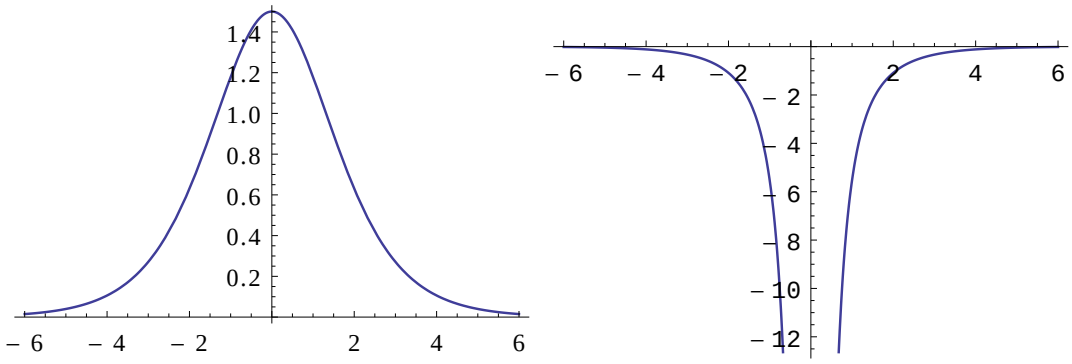

Figure 6.10: Solutions with energy 0 of equation (6.77); left : $y^+(x)$, right : $y^-(x)$.

Massless case

Consider now the massless sourceless equation,

$$y'' = -y^2 \ . \tag{6.85}$$

The analysis is similar to the massive case discussed above with $V(y) = -\frac{2}{3}y^3$. Its solutions have the following properties:

(i) - there is no positive $E = 0$ solution.

(ii) - There is only one negative $E = 0$ solution $y^-(x)$ defined for all $x \in \mathbb{R}^*$,

$$\int_{-\infty}^{y^-(x)} \frac{dy}{\sqrt{-\frac{2}{3}y^3}} = |x| \Leftrightarrow y^-(x) = -\frac{6}{x^2} \ . \tag{6.86}$$

It can be obtained by considering the limit $x \ll 1$ in the solution (6.79).

(iii) - There is now only one class of solutions with $E \neq 0$ (the periodic ones have disappeared). They are defined on an interval of length $r(E)$. They have $E = \frac{2}{3}t^3$, hence $t = (3E/2)^{1/3}$ and

$$\begin{aligned} r(E) &= 2\int_{-\infty}^{t} \frac{\mathrm{d}y}{\sqrt{\frac{2}{3}t^3 - \frac{2}{3}y^3}} \\ &= \begin{cases} \sqrt{6\pi}\left(\frac{2}{3|E|}\right)^{1/6} \frac{\Gamma(1/3)}{\Gamma(5/6)} \ , & E > 0 \\ \sqrt{6\pi}\left(\frac{2}{3|E|}\right)^{1/6} \frac{2\Gamma(7/6)}{\Gamma(2/3)} \ , & E < 0 \ . \end{cases} \end{aligned} \tag{6.87}$$

The solution $y(x)$ satisfies for $x \in]0, r(E)[$

$$\int_{-\infty}^{y(x)} \frac{dy}{\sqrt{E - \frac{2}{3}y^3}} = x \ . \tag{6.88}$$

It can be expressed in terms of the Weirstrass function,

$$y(x) = -\mathcal{P}\left(\frac{x}{\sqrt{6}}; g_2 = 0, g_3 = -6E\right) \ . \tag{6.89}$$

It diverges at $x = 0$ and $x = r(E)$. The periods are consistent with $\sqrt{6} \times 2\Omega$ (see Appendix 6.I) using the relation $\frac{\Gamma(7/6)}{\Gamma(2/3)} = \frac{\Gamma(1/3)^3}{4\times 2^{1/3}\pi^{3/2}}$. Note also the relation $\frac{\Gamma(1/3)}{\Gamma(5/6)} = \frac{2\times 2^{2/3}\pi^{3/2}}{3\Gamma(2/3)^3}$.

Instanton solution with a single delta source

We now use these results to construct the solutions in presence of sources. For a single delta source this was done in [110] and [117]. We first recall and then extend this analysis, as a more general approach is needed here.

Massive case

Consider the instanton equation

$$\tilde{u}''(x) - \tilde{u}(x) + \tilde{u}(x)^2 = -\lambda\delta(x) \ . \tag{6.90}$$

We are looking for a solution defined for all $x \in \mathbb{R}$. Other physical requirements[3] (e.g. from the derivation of the dynamical action) is that $\tilde{u}(x)$ vanishes as $x \to \pm\infty$, and that the solution is analytic around $\lambda = 0$ (obtainable in a power series in λ). We need a function which is piecewise solution of Eq. (6.77) for $x \in]-\infty, 0[$ and for $x \in]0, \infty[$, with a discontinuity in its derivative,

$$\tilde{u}'(0^+) - \tilde{u}'(0^-) = -\lambda \ . \tag{6.91}$$

As we have seen in the previous section, in order to be defined on an infinite interval, it must be constructed from the zero-energy $E = 0$ solutions $y^{\pm}(x)$ of (6.77) up to a shift $x \to x + x_0$. By symmetry it reads $\tilde{u}(x) = y^{\pm}(|x| + x_0)$ where $x_0 \equiv x_0(\lambda)$ is chosen to satisfy the condition (6.91). The procedure is illustrated in Fig. 6.11. Note that the sign of λ dictates which of the branches $\pm$ must be chosen. To summarize,

$$\tilde{u}^{\lambda}(x) = \frac{3}{1 + s_\lambda \cosh(|x| + x_0)} = \frac{3}{2}\big[1 - h_\lambda(|x| + x_0)^2\big] \ . \tag{6.92}$$

The function $x_0(\lambda)$ is determined from

$$\lambda = \frac{6 s_\lambda \sinh(x_0)}{\big[1 + s_\lambda \cosh(x_0)\big]^2} = \frac{3}{2} h_\lambda(x_0)\big[1 - h_\lambda(x_0)^2\big] \tag{6.93}$$

with $s_\lambda = \mathrm{sgn}(\lambda)$, $h_\lambda(x) = \tanh(\frac{x}{2})$ for $\lambda > 0$ and $h_\lambda(x) = \coth(\frac{x}{2})$ for $\lambda < 0$. [4]

This form does not make explicit that $\tilde{u}^{\lambda}(x)$ is analytic in λ near $\lambda = 0$. We will thus use the following equivalent form. Introduce $z = h_\lambda(x_0)$. Equation (6.93) can then be rewritten as a cubic equation for $z \equiv z(\lambda)$,

$$\lambda = 3z(1 - z^2) \ . \tag{6.94}$$

The trigonometric addition rules allow to rewrite

$$\begin{aligned} \tilde{u}^{\lambda}(x) &= \frac{3(1 - z^2)}{2\Big[\cosh\big(\frac{x}{2}\big) + z \sinh\Big(\frac{|x|}{2}\Big)\Big]^2} \\ &= \frac{6(1 - z^2) e^{-|x|}}{\big[1 + z + (1 - z) e^{-|x|}\big]^2} \ . \end{aligned} \tag{6.95}$$

The appropriate branch for (6.94) is the one for which $z \to 1$ as $\lambda \to 0$ (corresponding to $x_0 \to \infty$). As can be seen in Fig. 6.12, this branch is defined for $\lambda \in]-\infty, \lambda_c = \frac{2}{\sqrt{3}}[$, while $z(\lambda)$

[3] Because of finite range elasticity, the the effect at $x = 0$ of a kick at x must decay at large x. Because of the cutoff S_m, the positive integer moments of avalanche sizes must exist

[4] Note that formally $x_0 \to x_0 + i\pi$ is equivalent to $\lambda \to -\lambda$.

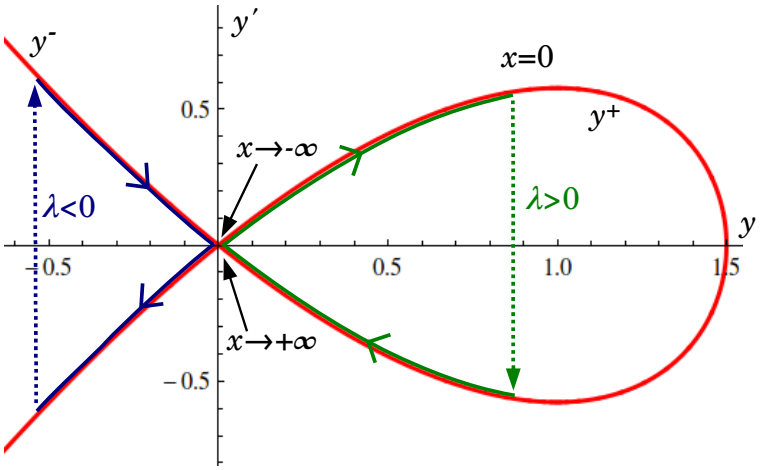

Figure 6.11: Graphical representation of the construction of solutions of the instanton equation for $\lambda > 0$ (blue) and $\lambda < 0$ (green). The dotted part of the curve represents the discontinuity in the derivative. The red line represents the $E = 0$ solution of (6.77), the only one needed to solve the instanton equation with one local source.

decreases from $z(-\infty) = \infty$ to $z_c = z(\lambda_c) = 1/\sqrt{3}$. The other branches are solutions of (6.90) but do not satisfy the physical requirements mentioned above.

Equations (6.94) and (6.95) thus define the solution to the instanton equation for $\lambda \in]-\infty, \lambda_c[$, in a way which is explicitly analytic around $\lambda = 0$. For instance one can check that the small-λ expansion

$$\tilde{u}^\lambda(x) = \frac{\lambda}{2} e^{-|x|} + \frac{\lambda^2}{6}\left(e^{-|x|} - \frac{1}{2}e^{-2|x|}\right) + \mathcal{O}(\lambda^3) \tag{6.96}$$

obtained by iteratively solving Eq. (6.90) at small λ, is reproduced by Eqs. (6.94) and (6.95).

Finally the partition sum corresponding to an homogeneous kick is expressed as

$$Z(\lambda) = \int_{-\infty}^{\infty} dx\ \tilde{u}^\lambda(x) = 6(1-z)\ . \tag{6.97}$$

Hence, from Eq. (6.94), it satisfies

$$\lambda = \frac{1}{72} Z(Z-6)(Z-12)\ , \tag{6.98}$$

recovering the result obtained in [110].

Massless case

The massless instanton equation

$$\tilde{u}''(x) + \tilde{u}(x)^2 = -\lambda\delta(x) \tag{6.99}$$

is solved similarly. For $\lambda < 0$ there is a solution defined for all $x \in \mathbb{R}$,

$$\tilde{u}^\lambda(x) = -\frac{6}{(|x| + x_0)^2} \quad , \quad x_0^3 = -\frac{24}{\lambda}\ . \tag{6.100}$$

Note that for the massless case the physical solution is not required to be analytic in λ at $\lambda = 0$ (i.e. integer moments of avalanche sizes diverge). This solution can be obtained from (6.95) in the (formal) double limit of small x and large z, with $x_0 = 2/z$. The equation determining z now is $\lambda = -3z^3$. The generating function for a uniform kick becomes $Z = -6z = (72\lambda)^{1/3}$.

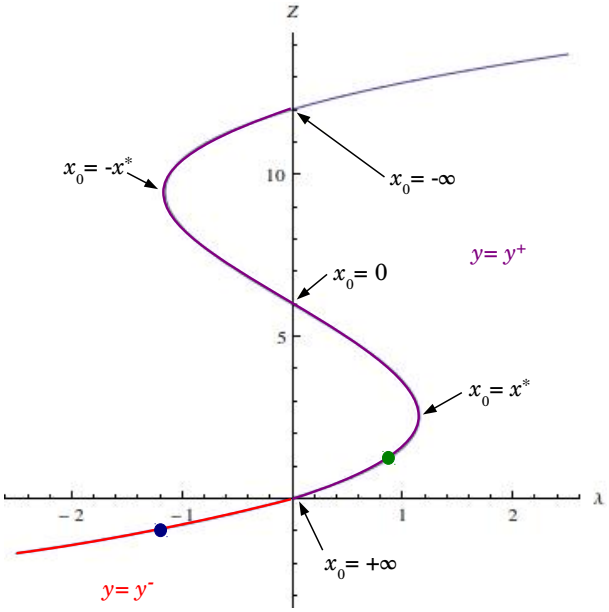

Figure 6.12: The generating function $Z(\lambda) = 6(1-z)$ is represented here with some indications of the link with the construction of the instanton solution; the green and blue dot correspond to the solutions represented in figure 6.11.

6.C Calculation of probabilities and densities of S_0

For an arbitrary kick δw_x, in the massive case, the Laplace transform of the distribution of local size is

$$\int dS_0\, e^{\lambda S_0} P_{\delta w_x}(S_0) = \exp\left(L^{d-1} \int dx\, \delta w_x \tilde{u}^\lambda(x) \right) . \tag{6.101}$$

Here $\tilde{u}^\lambda(x)$ is given in Eq. (6.95). Performing the Laplace inversion in general is difficult, but there are some tractable cases.

Uniform kick

Let us start with a uniform kick $\delta w_x = \delta w$, and $\delta \hat{w} = L^d \delta w$. It is more efficient to take a a derivative of Eq. (6.101) w.r.t. λ and write the Laplace inversion for $S_0 P_w(S_0)$,

$$S_0 P_{\delta w}(S_0) = \int_C \frac{d\lambda}{2i\pi} e^{-\lambda S_0} \partial_\lambda e^{6\delta\hat{w}(1-z(\lambda))} . \tag{6.102}$$

Here C is an appropriate contour parallel to the imaginary axis and we used that $\int dx\, \tilde{u}(x) = 6(1-z)$. The function $z(\lambda)$ is solution of $\lambda = 3z(1-z^2)$. One can now use z as integration variable and rewrite

$$S_0 P_{\delta w}(S_0) = 6\delta\hat{w} e^{6\delta\hat{w}} \int_C \frac{dz}{2i\pi} e^{-3z(1-z^2)S_0} e^{-6\delta\hat{w}z} , \tag{6.103}$$

using $d\lambda\partial_\lambda = dz\partial_z$. We will be sloppy here about the integration contour, as this procedure is heuristic to guess the result, which will then be tested (see below). As the exponential contains a cubic term, we use the Airy integral formula of Appendix 6.A leading to

$$S_0 P_w(S_0) = 6\delta\hat{w} e^{6\delta\hat{w}} \Phi(a,b,c) . \tag{6.104}$$

Here Φ is defined in Eq. (6.76), with $a = 9S_0$, $b = 0$ and $c = -(3S_0 + 6\delta\hat{w})$. This immediately leads to formula (6.21) in the main text. We have checked numerically that it reproduces the correct Laplace transform (6.101) for $\lambda < \lambda_c$.

Local kick

For a local kick it is possible to calculate the PDF of the local jump at the position of the kick.

Consider a local kick at $x = 0$, i.e. $\delta w_x = \delta w_0 \delta(x)$. For simplicity in this subsection we set $d = 1$. Inserting this value in (6.101) we find that the LT of the PDF of the local size at the same point S_0 reads

$$\int dS_0\, e^{\lambda S_0} P_{\delta w_0}(S_0) = e^{\frac{3}{2}(1-z^2)\delta w_0} \tag{6.105}$$

using $\tilde{u}^\lambda(0) = \frac{3}{2}(1-z^2)$. The same manipulations as above lead to

$$\begin{aligned} S_0 P(S_0) &= -\int_C \frac{dz}{2i\pi} e^{-3z(1-z^2)S_0} \partial_z e^{\frac{3}{2}(1-z^2)\delta w_0} \\ &= 3\delta w_0 e^{\frac{3\delta w_0}{2}} \int_C \frac{dz}{2i\pi} z\; e^{-3z(1-z^2)S_0 - \frac{3}{2}z^2\delta w_0} \\ &= 3\delta w_0 e^{\frac{3\delta w_0}{2}} \partial_c \Phi(a,b,c)|_{a=9S_0, b=-\frac{3\delta w_0}{2}, c=-3S_0} \ . \end{aligned} \tag{6.106}$$

Using Eq. (6.76) leads to

$$\begin{aligned} P_{\delta w_0}(S_0) &= \frac{\delta w_0 e^{\delta w_0 - \frac{\delta w_0^3}{36 S_0^2}}}{3^{1/3} S_0^{5/3}} \left[\frac{\delta w_0}{2 \times 3^{1/3} S_0^{2/3}} \mathrm{Ai}(u) - \mathrm{Ai}'(u) \right] \\ u &= 3^{1/3} S_0^{2/3} + \frac{\delta w_0^2}{4 \times 3^{2/3} S_0^{4/3}} \ . \end{aligned} \tag{6.107}$$

We can check normalization, and that $\langle S_0 \rangle = \frac{1}{2}\delta w_0$, consistent with the small-λ expansion of (6.105). The asymptotics are

$$P_{\delta w_0}(S_0) \simeq \begin{cases} \dfrac{\delta w_0^{3/2} e^{\frac{\delta w_0}{2} - \frac{\delta w_0^3}{18 S_0^2}}}{\sqrt{6\pi} S_0^2} & \text{for } \ S_0 \ll 1 \\ \dfrac{\delta w_0 e^{\delta w_0 - \frac{2}{\sqrt{3}} S_0}}{2\sqrt[4]{3}\sqrt{\pi} S_0^{3/2}} & \text{for } \ S_0 \gg 1 \ . \end{cases} \tag{6.108}$$

This result, and the new exponent $\tau = 5/3$ of the divergence at small S_0, which appear when $\delta w_0 \to 0$, is discussed in the main text.

6.D Calculation of the joint density of S and S_0

We will obtain the joint density from the generating function of S_0 and S,

$$\langle e^{\lambda S_0 + \mu S} \rangle = e^{\int_x \delta w_x \tilde{u}_x} \tag{6.109}$$

in terms of the solution of the instanton equation. Let us consider a uniform kick $\delta w_x = \delta w$.

Instanton equation and its solution

Massive case

Here $\tilde{u}$ (that we will also denote $\tilde{u}^{\lambda,\mu}$ to make the dependence on the sources explicit) is the solution, in the variable x, of the instanton equation

$$\tilde{u}'' - \tilde{u} + \tilde{u}^2 = -\lambda\delta(x) - \mu \ . \tag{6.110}$$

We must solve this equation with similar requirements as discussed below for Eq. (6.90), except that now the instanton goes to a constant at infinity (since the source acts everywhere). Clearly, the new uniform source can be removed by a shift $\tilde{u} \to \tilde{u} + c$, where the constant c verifies $\mu = c - c^2$. This results in the mass term $-\tilde{u} \to -(1-2c)\tilde{u}$, which can be brought back to Eq. (6.110) with $\mu = 0$, i.e. Eq. (6.90), by a simple scale transformation. At the end one can check that given $\tilde{u}^{\lambda}(x)$ the solution of Eq. (6.90), the solution of Eq. (6.110), noted $\tilde{u}^{\lambda,\mu}(x)$, is given by

$$\tilde{u}^{\lambda,\mu}(x) = \frac{1-\beta^2}{2} + \beta^2 \tilde{u}^{\lambda/\beta^3}(\beta x) \ . \tag{6.111}$$

The constant $\beta > 0$ such that

$$\beta^2 = \beta_\mu^2 := \sqrt{1-4\mu} \ . \tag{6.112}$$

In summary, the instanton solution is

$$\tilde{u}^{\lambda,\mu}(x) = \frac{1-\beta^2}{2} + \frac{6\beta^2(1-z^2)e^{-\beta|x|}}{\left[1+z+(1-z)e^{-\beta|x|}\right]^2} \ , \tag{6.113}$$

where z is the solution of

$$\frac{\lambda}{\beta^3} = 3z(1-z^2) \ . \tag{6.114}$$

It is connected to $z = 1$ at $\lambda = 0$.

Massless case

It is useful to also give the solution in the massless case, for which one needs to solve

$$\tilde{u}'' + \tilde{u}^2 = -\lambda\delta(x) - \mu \tag{6.115}$$

for $\mu \leq 0$. Using a shift and a rescaling we can check that the solution now is

$$\tilde{u}^{\lambda,\mu}(x) = \frac{-\beta^2}{2} + \beta^2 \tilde{u}^{\lambda/\beta^3}(\beta x) \ . \tag{6.116}$$

The parameter $\beta > 0$ such that $\beta^2 = \sqrt{-4\mu}$, and $\tilde{u}^{\lambda}(x)$ is the *massive* instanton solution. In summary, this gives

$$\tilde{u}^{\lambda,\mu}(x) = \frac{-\beta^2}{2} + \frac{6\beta^2(1-z^2)e^{-\beta|x|}}{\left[1+z+(1-z)e^{-\beta|x|}\right]^2} \tag{6.117}$$

where z is again the solution (6.114). If $\mu \to 0$, hence $\beta \to 0$ we recover the massless instanton (6.100).

Joint distribution

Let us again consider the massive case. To obtain the joint probability distribution $P_{\delta w}(S, S_0)$, we need to calculate the generating function $Z(\lambda, \mu)$,

$$\begin{aligned}\langle e^{\lambda S_0 + \mu S}\rangle = &\int_0^\infty \int_0^\infty P_{\delta w}(S_0, S) e^{\lambda S_0 + \mu S} dS\, dS_0 \\ =&e^{\delta w Z(\lambda,\mu)}\end{aligned} \tag{6.118}$$

Integrating (6.113), we obtain

$$\begin{aligned}Z(\lambda,\mu) = \int_x \tilde{u}^{\lambda,\mu}(x) &= L^d \frac{1-\beta^2}{2} + L^{d-1} 6\beta z(1-z) \\ &=: L^d Z_1(\mu) + L^{d-1} Z_2(\lambda,\mu)\ .\end{aligned} \tag{6.119}$$

$Z_1(\mu)$ is the generating function for the distribution of the total size of avalanches and $Z_2(\lambda,\mu)$ a new term defined by (6.119). The volume factors come from the coordinates along which the instanton solution is constant.

From equations (6.114) and (6.119), we can express λ as a function of Z_2 and β,

$$\lambda = 3\beta^3 \left(1 - \frac{Z_2}{6\beta}\right)\left[1 - \left(1 - \frac{Z_2}{6\beta}\right)^2\right]\ . \tag{6.120}$$

This is equivalent to $Z_2(\lambda,\mu) = \beta Z\left(\frac{\lambda}{\beta^3}\right)$ where $Z \equiv Z(\lambda)$ is the generating function of the local size, which was implicitly defined as a solution of Eq. (6.98).

Considering the limit of small δw, we obtain $P_{\delta w}(S, S_0) \approx \delta w\, \rho(S, S_0)$, which defines the joint density $\rho(S, S_0)$ of total and local sizes in the limit of a single avalanche. To simplify the computation, we decompose the distribution $\rho(S, S_0)$ as

$$\begin{aligned}\rho(S,S_0) &= \overline{\rho}(S,S_0) + \delta(S_0)\left(\rho(S) - \bar{\rho}(S)\right) \\ \bar{\rho}(S) &= \int_{S_0>0} \overline{\rho}(S,S_0)\ .\end{aligned} \tag{6.121}$$

Here $\overline{\rho}(S, S_0)$ is the smooth part of the joint density for S and S_0, and is also the joint density of single avalanches containing 0 (i.e. $S_0 > 0$). The second term takes into account all avalanches that occur away from 0: the $\delta(S_0)$ ensures that the avalanche does not contain 0 and the subtraction ensure that $\int_{S_0} \rho(S, S_0) = \rho(S)$ where $\rho(S)$ is the global size density. As we will check at the end of the calculation, the correct generating function for $\overline{\rho}$ is $Z_2(\lambda,\mu)L^{d-1} + 6\left(1-\beta_\mu\right)L^{d-1}$.

As $\rho(S)$ is already known, we only want to compute $\overline{\rho}(S, S_0)$. To eliminate the term $\delta(S_0)$ we multiply (6.121) by S_0 and use that $S_0\rho(S, S_0) = S_0\overline{\rho}(S, S_0)$. Multiplication by S_0 is equivalent to taking a derivative with respect to λ in the generating function,

$$\begin{aligned}S_0\, \overline{\rho}(S_0,S) =&\ L^{d-1} \int_{-i\infty}^{i\infty} \frac{\mathrm{d}\mu}{2\pi i} e^{-\mu S} \int_{-i\infty}^{i\infty} \frac{\mathrm{d}\lambda}{2\pi i} e^{-\lambda S_0} \partial_\lambda Z_2(\lambda,\mu) \\ =&\ L^{d-1} \int_{-i\infty}^{i\infty} \frac{\mathrm{d}\mu}{2\pi i} e^{-\mu S} \int_{-i\infty}^{i\infty} \frac{\mathrm{d}Z}{2\pi i} e^{-\frac{\beta^3}{72}\frac{Z}{\beta}\left(6-\frac{Z}{\beta}\right)\left(12-\frac{Z}{\beta}\right)S_0}\ .\end{aligned} \tag{6.122}$$

Here we changed variables from λ to Z_2 (and dropped the index) using (6.120). To simplify the calculations, we introduce a new variable x, such that $Z = 2\times 3^{\frac{1}{3}}x + 6\beta$, with β defined in

Eq. (6.112),

$$\begin{aligned}
\overline{\rho}(S_0,S) &= L^{d-1}\frac{2\times 3^{\frac{1}{3}}}{S_0}\int_{-i\infty}^{i\infty}\frac{\mathrm{d}\mu}{2\pi i}\,e^{-\mu S}\int_{-i\infty}^{i\infty}\frac{\mathrm{d}x}{2\pi i}\,e^{-\frac{x^3}{3}S_0+3^{1/3}\beta^2 xS_0}\\
&= L^{d-1}\times 2\times 3^{\frac{1}{3}}\frac{e^{-S/4}}{S_0}\int_{-i\infty}^{i\infty}\frac{\mathrm{d}x}{2\pi i}\,e^{-\frac{x^3}{3}S_0}\,\frac{1}{4}\int_{-i\infty}^{i\infty}\frac{\mathrm{d}y}{2\pi i}\,e^{-\frac{yS}{4}+(-y)^{1/2}3^{1/3}xS_0}\\
&= L^{d-1}\times 2\times 3^{\frac{1}{3}}\frac{e^{-S/4}}{S_0}\int_{-i\infty}^{i\infty}\frac{\mathrm{d}x}{2\pi i}\,e^{-\frac{x^3}{3}S_0}\int_0^{\infty}\frac{\mathrm{d}y}{4\pi}e^{-\frac{yS}{4}}\sin\left(\sqrt{y}3^{\frac{1}{3}}xS_0\right)\\
&= L^{d-1}\times 2\times 3^{\frac{2}{3}}\frac{e^{-S/4}}{\sqrt{\pi}S^{\frac{2}{3}}S_0}\int_{-i\infty}^{i\infty}\frac{\mathrm{d}x}{2\pi i}\,e^{-\frac{x^3}{3}S_0}xS_0e^{-\frac{(3^{1/3}xS_0)^2}{S}}\ . \qquad (6.123)
\end{aligned}$$

The steps of this calculations are: first a linear change of variable $4\mu-1\to y$, such that $\beta=(-y)^{\frac{1}{2}}$, then a deformation of the contour of integration to integrate on both sides of the branch cut $\mathbb{R}^+$. Finally, the last integration can be performed in terms of Airy functions (e.g. using Appendix 6.A),

$$\begin{aligned}
\overline{\rho}(S,S_0) &= \frac{6L^{d-1}}{\sqrt{\pi}S^2}e^{-\frac{S}{4}}F\left(\sqrt{3}S_0/S^{\frac{3}{4}}\right) \qquad (6.124)\\
F(u) &= \frac{1}{u^{\frac{2}{3}}}e^{-\frac{2}{3}u^4}\left(u^{\frac{4}{3}}\mathrm{Ai}\left(u^{\frac{8}{3}}\right)-\mathrm{Ai}'\left(u^{\frac{8}{3}}\right)\right)\ .
\end{aligned}$$

The density of avalanches with global size S and which contain 0, i.e. with $S_0>0$ is

$$\begin{aligned}
\overline{\rho}(S) &= \int_0^{\infty}\mathrm{d}S_0\,\overline{\rho}(S,S_0) = L^{d-1}\times 2\sqrt{\frac{3}{\pi}}\left[\int_0^{\infty}\mathrm{d}u\,F(u)\right]\frac{e^{-\frac{S}{4}}}{S^{\frac{5}{4}}}\\
&= L^{d-1}\frac{3\,\Gamma\left(\frac{1}{4}\right)}{2\pi}\frac{e^{-\frac{S}{4}}}{S^{\frac{5}{4}}}\ , \qquad (6.125)
\end{aligned}$$

where

$$\frac{3\,\Gamma\left(\frac{1}{4}\right)}{2\pi}=2\sqrt{\frac{3}{\pi}}\int_0^{\infty}\mathrm{d}u\,F(u)\approx 1.7311012158\ . \qquad (6.126)$$

To test our solution one can check that

$$\int_0^{\infty}\mathrm{d}s\,\frac{3\,\Gamma\left(\frac{1}{4}\right)}{2\pi}\frac{e^{-\frac{S}{4}}}{S^{\frac{5}{4}}}(e^{\mu S}-1)=6\left[1-(1-4\mu)^{\frac{1}{4}}\right]\ . \qquad (6.127)$$

We have checked numerically several other requirements, originating from the definitions, namely

$$\begin{aligned}
&\int_0^{\infty}\mathrm{d}S\,\bar{\rho}(S,S_0)=\rho_0(S_0)=\frac{2L^{d-1}}{\pi S_0}K_{1/3}\left(2S_0/\sqrt{3}\right)\\
&\int_0^{\infty}\mathrm{d}S\int_0^{\infty}\mathrm{d}S_0\,S_0\bar{\rho}(S,S_0)=L^{d-1}\\
&\int_0^{\infty}\mathrm{d}S\int_0^{\infty}\mathrm{d}S_0\,S\bar{\rho}(S,S_0)=6L^{d-1}\\
&\int_0^{\infty}\mathrm{d}S\int_0^{\infty}\mathrm{d}S_0\,\bar{\rho}(S,S_0)e^{\mu S}(e^{\lambda S_0}-1)=Z_2(\lambda,\mu)L^{d-1}\ .
\end{aligned}$$

6.E Imposed local displacement

We set for simplicity $d = 1$ in this section. The PDF of the global size in presence of imposed position driving is obtained from

$$\overline{e^{\mu S}} = e^{m^2 \tilde{u}_{x=0} \delta w} \ , \tag{6.128}$$

where $\tilde{u}_x$ is the solution of a slightly modified instanton equation:

$$\tilde{u}_x'' - m^2 \delta(x) \tilde{u}_x + \tilde{u}_x^2 = -\mu \tag{6.129}$$

and we have kept explicit the local mass. This equation is the same as the *massless* Eq. (6.115), with $\lambda = -m^2 \tilde{u}_{x=0}$, a self-consistency condition. Using its solution given in Eqs. (6.117) and (6.114) we eliminate λ and z in the system

$$\begin{cases} \lambda & = -m^2 \tilde{u}_{x=0} = -m^2 \beta^2 \left(1 - \frac{3}{2} z^2\right) \\ \dfrac{\lambda}{\beta^3} & = 3z(1 - z^2) \end{cases} \tag{6.130}$$

with $\beta = (-4\mu)^{1/4}$. It is then easy to see that there is a solution such that $m^2 \tilde{u}_{x=0}$ remains finite when $m^2 \to \infty$, in which case $z \to \sqrt{\frac{2}{3}}$ and

$$\lim_{m^2 \to \infty} m^2 \tilde{u}_{x=0} = -\sqrt{\frac{2}{3}} \beta^3 \ . \tag{6.131}$$

Hence we find

$$P_{\delta w_0}(S) = \mathrm{LT}^{-1}_{-\mu \to S} \, e^{-\delta w \sqrt{\frac{2}{3}} (-4\mu)^{3/4}} \ . \tag{6.132}$$

The result for the density is simpler,

$$S\rho(S) = -\mathrm{LT}^{-1}_{-\mu \to S} \, \partial_\mu \sqrt{\frac{2}{3}} (-4\mu)^{3/4} \ , \tag{6.133}$$

leading to

$$\rho(S) = \frac{\sqrt{3}}{\Gamma(1/4) S^{7/4}} \tag{6.134}$$

and a new exponent $7/4$ discussed in the main text.

6.F Some elliptic integrals for the distribution of avalanche extension

Here we make explicit the calculation for the density of extensions sketched in the main text. The relevant generating function, defined in the main text in Eq. (6.66), is

$$Z(r) = \int_x \tilde{u}_r(x) - \tilde{u}_\infty(x) - \tilde{u}_\infty(x - r) \ . \tag{6.135}$$

The integrand is represented on Fig. 6.13.Here $\tilde{u}_r(x)$ is the solution of the instanton equation with two local sources, one at $x = 0$ and one at $x = r$. The solution $\tilde{u}_\infty$ with one source at $x = 0$ and one at infinity is equivalent to the solution with only one source at $x = 0$.

The first simplification in the calculation of this integral is the symmetry arround $r/2$. Another is that, for $x \in]-\infty, 0[$, $\tilde{u}_r(x) - \tilde{u}_\infty(x)$ cancels exactly. Then, the idea is to express the integral for $Z(r)$ without explicitly solving the instanton equation, using the change of variables

$$\int \tilde{u} \, \mathrm{d}x = \int \tilde{u} \frac{\mathrm{d}u}{\tilde{u}'} \ . \tag{6.136}$$

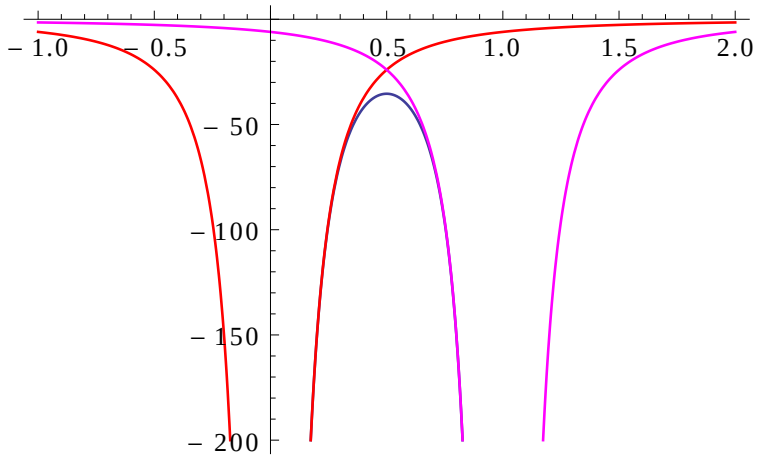

Figure 6.13: Instanton solutions involved in the computation of $Z(r)$ for $r = 1$: in blue, $\tilde{u}_1(x)$, in red $\tilde{u}_\infty(x)$ and in purple, $\tilde{u}_\infty(x-1)$.

This requires to express the derivative of $\tilde{u}$ w.r.t. x as a function of $\tilde{u}$, which is easy because $\tilde{u}$ is solution of a differential equation, and to decompose the integral into two parts such that the change of variables is well defined: from $x = -\infty$ to $x = 0$ and from $x = 0$ to $x = r/2$. The rest is deduced by symmetry.

In these two intervals, $\tilde{u}_\infty(x-r)$ does not contain a pole, and can safely be computed separately. Moreover, as we said, $\tilde{u}_r(x) - \tilde{u}_\infty(x)$ vanishes in the first interval, i.e. for $x \in]-\infty, 0]$. This leaves only the integral of $\tilde{u}_r(x) - \tilde{u}_\infty(x)$ over x running from $x = 0$ to $x = r/2$. To simplify notations we introduce the variable $t < 0$,

$$t := \tilde{u}_r(r/2) \ , \tag{6.137}$$

which is in one-to-one correspondance with r, and is a nice parameter to express Z. Indeed, after the change of variables (6.136), the integral now runs from $u = -\infty$ to $u = t$, and for $0 < x < r/2$, with $\tilde{u} \equiv \tilde{u}_r$, we have

$$\tilde{u}_r' = \sqrt{-t^2 + \frac{2}{3}t^3 + \tilde{u}^2 - \frac{2}{3}\tilde{u}^3} \ . \tag{6.138}$$

Further, with $\tilde{u} \equiv \tilde{u}_\infty$,

$$\tilde{u}_\infty' = \sqrt{\tilde{u}^2 - \frac{2}{3}\tilde{u}^3} \ . \tag{6.139}$$

This comes from the results of Appendix 6.B, and the relation $E = -t^2 + \frac{2}{3}t^3$. To express r in terms of t, we use the same idea as in the derivation of Eq. (6.136),

$$r = 2\int_0^{r/2} \mathrm{d}x = 2\int_{-\infty}^{t} \frac{\mathrm{d}\tilde{u}_r}{\tilde{u}_r'} \ . \tag{6.140}$$

Putting these ingredients together, we obtain $Z(r)$ as a function of t, which we call $\tilde{Z}(t)$, in term of an elliptic integral, as well as the expression of r as a function of t,

$$\begin{aligned} \tilde{Z}(t) &= 2\int_{-\infty}^{t} \left(\frac{u}{\sqrt{-t^2 + \frac{2}{3}t^3 + u^2 - \frac{2}{3}u^3}} - \frac{u}{\sqrt{u^2 - \frac{2}{3}u^3}} \right) \mathrm{d}u - 2\int_t^0 \frac{u}{\sqrt{u^2 - \frac{2}{3}u^3}} \mathrm{d}u \\ &= 2t\int_1^\infty \left(\frac{y}{\sqrt{y^2 - 1 - \frac{2}{3}t(y^3-1)}} - \frac{1}{\sqrt{1 - \frac{2}{3}ty}} \right) \mathrm{d}y - 6 + 2\sqrt{9 - 6t} \ , \end{aligned} \tag{6.141}$$

$$\begin{aligned} r(t) &= 2\int_{-\infty}^{t} \frac{\mathrm{d}u}{\sqrt{-t^2+\frac{2}{3}t^3+u^2-\frac{2}{3}u^3}} \\ &= 2\int_{1}^{\infty} \frac{\mathrm{d}y}{\sqrt{y^2-1-\frac{2}{3}t(y^3-1)}} \ . \end{aligned} \tag{6.142}$$

We now use this to characterise the small-size divergence of the extension distribution. This is encoded in the small r behavior of $Z(r)$, which corresponds to the large-t behavior of $\tilde{Z}(t)$. For the latter, we have

$$\begin{aligned} Z(t) &\simeq -2\sqrt{\frac{3}{2}}\left[\int_1^\infty du\left(\frac{u}{\sqrt{u^3-1}}-\frac{1}{\sqrt{u}}\right)-2\right]|t|^{\frac{1}{2}} \\ &\simeq 2\sqrt{6\pi}\frac{\Gamma(5/6)}{\Gamma(1/3)}|t|^{\frac{1}{2}} \ , \end{aligned} \tag{6.143}$$

which is also the exact result in the massless limit. We next need to invert Eq. (6.142) in the large-t limit,

$$|t| \simeq A^2 r^{-2} \ , \quad A = 2\sqrt{6\pi}\frac{\Gamma(7/6)}{\Gamma(2/3)} = \sqrt{6}\frac{\Gamma(1/3)^3}{4^{2/3}\pi} \ . \tag{6.144}$$

The small-r behavior of $Z(r)$ is then given by

$$Z(r) \simeq 4\sqrt{3}\pi\, r^{-1} \ . \tag{6.145}$$

For small $|t|$ we find

$$r(t) \simeq 2\ln(12/|t|) \tag{6.146}$$

and

$$\tilde{Z}(t) \simeq t^2 \ln(1/|t|) \tag{6.147}$$

which leads to

$$\tilde{Z}(r) = 72\ re^{-r} + O(e^{-r}) \tag{6.148}$$

This leads to the tail of the extension density,

$$\rho(\ell) = \partial_r^2 \tilde{Z}(r)\Big|_{r=\ell} \simeq 72\,\ell\, e^{-\ell} \text{ when } \ell \to \infty \ . \tag{6.149}$$

6.G Joint distribution for extension and total size

For simplicity, we consider only $m = 0$ (massless limit). To obtain the joint distribution of extension and total size we have to add a global source μ to the instanton equation, in addition to the two local sources, whose parameters are sent to infinity. With the same tricks as previously, cf. Appendix 6.D and notably Eq. (6.116), we change this problem to a new one with a mass $\beta = (-4\mu)^{\frac{1}{4}}$, but no global source. The generating function is now a function of r, the distance between the two local sources and β, the new mass. As in Appendix 6.F, we can change the variable r to the new parameter t defined in Eq. (6.142) and express everything in terms of elliptic integrals:

$$\begin{aligned} r(t,\beta) &= 2\int_t^\infty \frac{\mathrm{d}y}{\sqrt{-\beta^2t^2-\frac{2}{3}t^3+\beta^2y^2+\frac{2}{3}y^3}} = \beta^{-1} f\left(\frac{t}{\beta^2}\right) \ , \\ Z(t,\beta) &= -2\int_t^\infty \left(\frac{y}{\sqrt{-\beta^2t^2-\frac{2}{3}t^3+\beta^2y^2+\frac{2}{3}y^3}}-\frac{1}{\sqrt{\frac{2}{3}y}}\right)\mathrm{d}y + 2\sqrt{6t} = \beta\, g\left(\frac{t}{\beta^2}\right) \ . \end{aligned} \tag{6.150}$$

The functions f and g are

$$\begin{aligned} f(x) &= 2\int_x^\infty \frac{\mathrm{d}u}{\sqrt{-x^2-\frac{2}{3}x^3+u^2+\frac{2}{3}u^3}} = 2\int_1^\infty \frac{\mathrm{d}u}{\sqrt{u^2-1+\frac{2}{3}x(u^3-1)}} \ , \\ g(x) &= -2x\int_1^\infty \left(\frac{u}{\sqrt{u^2-1+\frac{2}{3}x(u^3-1)}} - \frac{1}{\sqrt{\frac{2}{3}xu}}\right)\mathrm{d}u + 2\sqrt{6x} \ . \end{aligned} \tag{6.151}$$

From that, we have $Z(r,\beta) = \beta\,(g\circ f^{-1})\,(\beta r)$ and then $\partial_r^2 Z(r,\beta) = \beta^3\,(g\circ f^{-1})''\,(\beta r)$ which gives

$$\rho(l,s) = \frac{1}{4l^7} F\left(\frac{sl^{-4}}{4}\right) \ , \tag{6.152}$$

where F is the inverse LT of $x \mapsto (-x)^{\frac{3}{4}}(g\circ f^{-1})''\left((-x)^{\frac{1}{4}}\right)$ with g and f the functions previously defined. Giving an analytic expression for this scaling function F seems out of reach for now.

6.H Numerics

We test most of our results with a direct numerical simulation of the equation of motion (6.1). This is done by discretizing both time and space. To avoid the $\sqrt{\delta t}$ term (where δt is the time discretization) from a naive Euler time discretisation, we use the method of [136]. It allows to express the exact propagator of the $d = 0$ version of (6.1) in terms of random distributions (Poisson and Gamma distribution). We review this result here.

Let us start with the $d = 0$ stochastic equation,

$$\partial_t \dot{u}_t = \alpha - \beta \dot{u}_t + \sqrt{2\sigma \dot{u}_t}\,\eta(t) \tag{6.153}$$

where η is a Gaussian white noise and α is positive (so that $\dot{u}$ remains non-negative at all times). It can be integrated exactly using Bessel functions (cf. [116] for a derivation of this using the instanton equation for the ABBM model):

$$P(\dot{u}_t|\dot{u}_0) = \frac{\beta}{\sigma}\frac{\sqrt{\frac{\dot{u}_t}{\dot{u}_0}}^{-1+\alpha}}{2\sinh\left(\frac{\beta t}{2}\right)} I_{-1+\alpha}\left(\frac{\beta}{\sigma}\frac{\sqrt{\dot{u}_t\dot{u}_0}}{\sinh\left(\frac{\beta t}{2}\right)}\right)\left(e^{\frac{\beta t}{2}}\right)^\alpha e^{-\frac{\beta}{\sigma}\frac{\dot{u}_0 e^{-\beta t}+\dot{u}_t}{1-e^{-\beta t}}} \ . \tag{6.154}$$

To use this representation efficiently in a numerical algorithm, the trick is to expand it in a series, and then express it as a combination of two distributions,

$$\begin{aligned} P(\dot{u}_t|\dot{u}_0) &= \sum_{n=0}^\infty \frac{\dot{u}_t^{n-1+\alpha}\dot{u}_0^n}{n!\Gamma(n+\alpha)}\left(\frac{\beta}{2\sigma\sinh\left(\frac{\beta t}{2}\right)}\right)^{2n+\alpha}\left(e^{\frac{\beta t}{2}}\right)^\alpha e^{-\frac{\beta}{\sigma}\frac{\dot{u}_0}{e^{\beta t}-1}} e^{-\frac{\beta}{\sigma}\frac{\dot{u}_t}{1-e^{-\beta t}}} \\ &= \sum_{n=0}^\infty \mathrm{Poisson}\left[\frac{\beta}{\sigma}\frac{\dot{u}_0}{e^{\beta t}-1}\right](n)\,\mathrm{Gamma}\left[n+\alpha, \frac{1-e^{-\beta t}}{\beta}\sigma\right](\dot{u}_t) \ . \end{aligned} \tag{6.155}$$

The Poisson and Gamma distributions used above are

$$\mathrm{Poisson}\,[\lambda]\,(n) = e^{-\lambda}\frac{\lambda^n}{n!} \text{ for } n \in \mathbb{N} \tag{6.156}$$

$$\mathrm{Gamma}\,[k,\theta]\,(x) = \frac{1}{\theta(k-1)!}\left(\frac{x}{\theta}\right)^{k-1} e^{-\frac{x}{\theta}} \text{ for } x \in \mathbb{R} \tag{6.157}$$

This means that we can generate $\dot{u}_t$ at time t from $\dot{u}_0$ by choosing first n according to the Poisson distribution and then choosing $\dot{u}_t$ from a Gamma distribution with a shape depending on n. This can be summed up as a nice equality between random variables,

$$\dot{u}_t = \text{Gamma}\left[\text{Poisson}\left[\frac{\beta}{\sigma}\frac{\dot{u}_0}{e^{\beta t}-1}\right] + \alpha, \frac{1-e^{-\beta t}}{\beta}\sigma\right] \tag{6.158}$$

To use this in a numerical simulation of Eq. (6.1), we first write a discretized (in space) version of the latter,

$$\partial_t \dot{u}_{i,t} = (\dot{u}_{i+1,t} + \dot{u}_{i-1,t}) - (m^2+2)\dot{u}_{i,t} + \sqrt{2\sigma \dot{u}_{i,t}}\xi_{i,t} + m^2 \delta w_{i,t} \ . \tag{6.159}$$

Choosing $\alpha = \dot{u}_{i+1,t} + \dot{u}_{i-1,t}$, which is assumed to be constant on the time interval $[t, t+\delta t]$, and $\beta = m^2 + 2$ in Eq. (6.157) allows us to generate $\dot{u}_{i,t+\delta t}$, knowing all $\dot{u}_{i,t}$, with a correct probability distribution at order δt.

6.I Weierstrass and Elliptic functions

Here we recall some properties of Weierstrass's elliptic function $\mathcal{P}$ (source [137] chapter 18, and Wolfram Mathworld). It appears in complex analysis as the only doubly periodic function on the complex plane with a double pole $1/z^2$ at zero[5]. Denoting ω_1, ω_2 the two (a priori complex) primitive half-periods, every point of the lattice $\Lambda = \{2m\omega_1 + 2n\omega_2 | (n,m) \in \mathbb{Z}^2\}$ is a pole of order 2 for $\mathcal{P}$. It can be constructed for $z \in \mathbb{C} - \Lambda$ as

$$\mathcal{P}(z|\omega_1,\omega_2) := \frac{1}{z^2} + \sum_{(m,n)\neq(0,0)} \frac{1}{(z-2m\omega_1-2n\omega_2)^2} - \frac{1}{(2m\omega_1+2n\omega_2)^2} \ . \tag{6.160}$$

It is an even function of the complex variable z, with $\mathcal{P}(z) = \mathcal{P}(-z)$. Note that the choice of primitive vectors $(2\omega_1, 2\omega_2)$ is not unique, since one can alternatively choose any linear combination. The conventional choice of roots g_2 and g_3 is defined from its expansion around $z = 0$,

$$\mathcal{P}(z|\omega_1,\omega_2) = \frac{1}{z^2} + \frac{g_2}{20}z^2 + \frac{g_3}{28}z^4 + \mathcal{O}(z^6) \ . \tag{6.161}$$

The function $\mathcal{P}$ is alternatively denoted

$$\mathcal{P}(z|\omega_1,\omega_2) = \mathcal{P}(z; g_2, g_3) \tag{6.162}$$

the latter being defined in Mathematica as WeierstrassP$[z, \{g_2, g_3\}]$. More explicitly, the parameters g_2, g_3 are expressed from the half-periods as

$$g_2 = 60 \sum_{(m,n)\neq(0,0)} \frac{1}{(2m\omega_1+2n\omega_2)^4} \qquad \text{and} \qquad g_3 = 140 \sum_{(m,n)\neq(0,0)} \frac{1}{(2m\omega_1+2n\omega_2)^6} \ . \tag{6.163}$$

The Weierstrass elliptic function verifies an interesting homogeneity property,

$$\mathcal{P}(\lambda z; \lambda^{-4} g_2, \lambda^{-6} g_3) = \lambda^{-2} \mathcal{P}(z; g_2, g_3) \ , \tag{6.164}$$

and the non-linear differential equation

$$\mathcal{P}'(z)^2 = 4\mathcal{P}(z)^3 - g_2 \mathcal{P}(z) - g_3 \ . \tag{6.165}$$

[5]It also appears as the second derivative of the Green function of the free field on a torus.

It is thus linked to elliptic integrals. Restricting now to $g_2, g_3 \in \mathbb{R}$ and focusing on $z \in \mathbb{R}$ one can choose one half-period to be real, which we denote Ω [6]. The function $\mathcal{P}(z)$ is then periodic in $\mathbb{R}$ of period 2Ω and diverges at all points $2m\Omega$, $m \in \mathbb{Z}$. It is defined in the fundamental interval $]0, 2\Omega[$, repeated by periodicity. In this interval it satisfies the symmetry $\mathcal{P}(2\Omega - z; g_2, g_3) = \mathcal{P}(z; g_2, g_3)$. Its values in the first half-interval, i.e. for $z \in [0, \Omega]$ are such that (with $y \in [e_1, \infty]$)

$$z = \int_y^\infty \frac{\mathrm{d}t}{\sqrt{4t^3 - g_2 t - g_3}} \Leftrightarrow y = \mathcal{P}(z; g_2, g_3) \tag{6.166}$$

where e_1 is the largest real root of the polynomial in t

$$4t^3 - g_2 t - g_3 = 4(t - e_1)(t - e_2)(t - e_3) \ . \tag{6.167}$$

The roots e_i are all real if $\Delta = g_2^3 - 27 g_3^2 > 0$ and only one, namely e_1, is real if $\Delta < 0$. Hence the period is given by

$$\Omega = \int_{e_1}^\infty \frac{\mathrm{d}t}{\sqrt{4t^3 - g_2 t - g_3}} \ , \ \mathcal{P}(\Omega) = e_1 \ , \ \mathcal{P}'(\Omega) = 0 \ . \tag{6.168}$$

It is always finite, except when e_1 is a double root, in which case $\Delta = 0$ and the period is infinite $\Omega = \infty$.

For $g_2 = 0$ the integral (6.168) can be calculated explicitly using

$$\int_1^\infty \frac{\mathrm{d}u}{\sqrt{u^3 - 1}} = \frac{\Gamma(1/3)^3}{4^{\frac{2}{3}}\pi} = \frac{-\sqrt{\pi}\,\Gamma(1/6)}{\Gamma(-1/3)} \ , \tag{6.169}$$

$$\int_{-1}^\infty \frac{\mathrm{d}u}{\sqrt{u^3 + 1}} = \sqrt{\pi}\frac{\Gamma(1/3)}{\Gamma(5/6)} \ . \tag{6.170}$$

The half-periods are

$$\Omega = \begin{cases} \dfrac{1}{4\pi}\Gamma(1/3)^3 g_3^{-1/6} & \text{when } \ g_3 > 0 \\ \sqrt{\pi}\dfrac{\Gamma(1/3)}{4^{\frac{1}{3}}\Gamma(5/6)}|g_3|^{-1/6} & \text{when } \ g_3 < 0 \end{cases} \ , \tag{6.171}$$

and the other period can be chosen as $\frac{1}{2}\Omega(1 + i\sqrt{3})$.

Finally, taking another derivative of (6.165) we see that the Weierstrass function also satisfies

$$\mathcal{P}''(z) = 6\mathcal{P}(z)^2 - \frac{g_2}{2} \ , \tag{6.172}$$

and $\mathcal{P}(z; g_2, g_3)$ is the only solution of this differential equation which satisfies (6.161).

From this we can find solutions of the instanton equation

$$\tilde{u}_x'' - A\tilde{u}_x + \tilde{u}_x^2 = 0 \ , \tag{6.173}$$

where $A = 1$ is the massive case and $A = 0$ the massless case. Comparing with Eq. (6.172) we see that a family of solutions are

$$\tilde{u}_x = \frac{A}{2} - 6b^2\mathcal{P}\left(c + bx; \frac{A^2}{12b^4}, g_3\right) \ . \tag{6.174}$$

Because of the homogeneity relation (6.164), this is a two-parameter family. These solutions are periodic. In the massless case $A = 0$, the period of (6.174) is Ω/b where Ω is given by (6.171).

[6] The conventions are such that if $\Delta < 0$, $\Omega = \omega_1$ is real and ω_2 imaginary (for $g_3 > 0$ and the reverse for $g_3 < 0$), and if $\Delta < 0$, $\Omega = \omega_1 \pm \omega_2$.

6.J Non-stationary dynamics

In the velocity theory the observables of the BFM are calculated from the dynamical action

$$\mathcal{S}[\dot{u},\tilde{u}] = \int_{t,q} \tilde{u}_{-q,t}(\partial_t + q^2 + m^2)\tilde{u}_{q,t} - \sigma \int_{t,x} \tilde{u}_{xt}^2 \dot{u}_{xt}$$

where $\tilde{u}$ is the response field. The quadratic part of the action, $\mathcal{S}_0$, defines the free response function,

$$\langle \dot{u}_{q,t}\tilde{u}_{q,t'}\rangle_{\mathcal{S}_0} := R_{q,t-t'} = \theta(t-t')e^{-(q^2+m^2)(t-t')} \ . \tag{6.175}$$

Standard perturbation theory in the disorder σ is then performed, and has the peculiarity to contain only tree diagrams. It is easy to see that the average velocity is not corrected by the disorder, hence its value is the same as in the free theory. In presence of a uniform driving $w = vt$, and taking into account the initial condition $\dot{u}_{xt=0} = 0$, one has

$$\overline{\dot{u}_{x,t}} = \langle \dot{u}_{xt}\rangle_{\mathcal{S}} = v\left(1 - e^{-m^2 t}\right) \ . \tag{6.176}$$

This implies

$$\overline{u_{xt}} = vt - \frac{1 - e^{-m^2 t}}{m^2} \ . \tag{6.177}$$

Next we compute the connected correlations, where q means Fourier space and x real space,

$$\begin{aligned} \overline{\dot{u}_{q,t_1}\dot{u}_{-q,t_2}}^c &= \langle \dot{u}_{q,t_1}\dot{u}_{-q,t_2}\rangle_{\mathcal{S}} \\ &= \sigma \int_{s,x} \langle \dot{u}_{q,t_1}\dot{u}_{-q,t_2}\tilde{u}_{x,s}^2 \dot{u}_{x,s}\rangle_{\mathcal{S}_0} \\ &= 2\sigma \int_s \langle \dot{u}_{xs}\rangle_{\mathcal{S}_0} R_{q,t_1-s}R_{q,t_2-s} \ . \end{aligned} \tag{6.178}$$

Calculating this integral, and further integrating over t_1 and t_2 we obtain

$$\overline{u_{q,t}u_{-q,t}}^c = \int_0^t \mathrm{d}t_1 \int_0^t \mathrm{d}t_2 \ \overline{\dot{u}_{q,t_1}\dot{u}_{-q,t_2}}^c \ . \tag{6.179}$$

This is the final result given in the main text, see Eq. (6.71). Alternatively we can obtain the correlations of u_{xt} using

$$\begin{aligned} e^{\mu_x u_{xt_1}} &= \int_x \mu_x \overline{U_{xt_1}} + \frac{1}{2}\int_{x_1x_2} \mu_{x_1}\mu_{x_2}\overline{U_{x_1t_1}U_{x_2t_2}}^c + ... \\ &= \exp\left(vm^2 \int_{x,t>0} \tilde{u}_{xt}^\lambda\right) \ , \end{aligned} \tag{6.180}$$

where $\tilde{u}_{xt}^\lambda$ is the solution of the space-time dependent instanton equation with a source $\lambda_{xt} = \mu_x\theta(t)\theta(t_1-t)$. Using the perturbation method in the source of Section III.H of [117], specializing to that source in (261), we obtain at the end the same result as above.

Chapter 7

General conclusion

In this thesis, I have presented analytical calculations for the distribution of several observables. Table 7.1 summarize the main new results, from chapters 2 and 3, concerning fractional Brownian process (starting at $X_0 = 0$ and ending at a free end-point at final time chosen here to be $T = 1$ for simplicity), in comparison with the corresponding results for the Brownian motion. In each of these results, the scaling behavior is expressed in terms of the Hurst exponent H of the fBm process, while the other terms are computed in an ε-expansion and involve scaling functions (denoted with calligraphic letters) whose expressions are given in the main text. All of these results are obtained, discussed and compared to numerical simulations in the main text.

Observable	Brownian motion	ε expansion for fBM with $H = 1/2 + \varepsilon$
Maximum value m	$\mathcal{P}(m) = \frac{e^{-m^2/4}}{\sqrt{\pi}}$	$= \frac{m^{\frac{1}{H}-2} e^{-m^2/4}}{\sqrt{\pi}} e^{\varepsilon\left[\mathcal{G}(m/\sqrt{2})+4\ln(m)+\text{cst}\right]} + O(\varepsilon^2)$ with $\mathcal{G}(y)$ given in Eq. (2.46)
time of the max $t_{\max}$	$\mathcal{P}(t) = \frac{1}{\pi\sqrt{t(1-t)}}$	$= \frac{1}{\pi[t(1-t)]^H} \exp(\varepsilon\, \mathcal{F}(t)) + O(\varepsilon^2)$ with $\mathcal{F}(t)$ given in Eq. (2.42)
last zero t_{last}	$\mathcal{P}(t) = \frac{1}{\pi\sqrt{t(1-t)}}$	$= \frac{\sin(\pi H)}{\pi t^H (1-t)^{1-H}} \exp\Big(\varepsilon^2 \mathcal{F}_2^{\text{last}}(t)\Big) + O(\varepsilon^3)$ with $\mathcal{F}_2^{\text{last}}(t)$ given in Eq. (3.56)
positive time t_+	$\mathcal{P}(t) = \frac{1}{\pi\sqrt{t(1-t)}}$	$= \frac{1}{\pi[t(1-t)]^H} \exp(\varepsilon \mathcal{F}(t)) + O(\varepsilon^2)$ with $\mathcal{F}(t)$ given in Eq. (2.42)
$\upsilon = \frac{m}{\sqrt{2} t_{\max}^H}$ at given $t_{\max}$	$\mathcal{P}(\upsilon\|t) = \upsilon e^{-\frac{\upsilon^2}{2}}$	$= \upsilon^{\frac{1}{H}-1} e^{-\frac{\upsilon^2}{2}} e^{\varepsilon[\mathcal{G}(\upsilon\|t)+4\ln(\upsilon)]} + O(\varepsilon^2)$ with $\mathcal{G}(\upsilon\|t)$ given in Eq. (2.61)

Table 7.1: Summary of distributions for fractional Brownian motion with a free end-point.

Table 7.2 references in the same way the similar results obtained for a fBm process constrained to start and end at the origin, also called bridge process: $X_{t=0} = X_{t=1} = 0$. the observable t_{last} does not appear here as it is trivial in this case. The results for Brownian bridge are also recalled.

Observable	Brownian bridge	fBM bridge with $H = 1/2 + \varepsilon$
Maximum value m	$\mathcal{P}(m) = 2me^{-m^2}$	$= m^{\frac{2}{H}-3} e^{-m^2 \frac{4^H}{4-4^H} + \varepsilon \mathcal{G}(m) + \text{cst}} + O(\varepsilon^2)$ with $\mathcal{G}(m)$ given in Eq. (4.55)
time of the max $t_{\max}$	$\mathcal{P}(t) = 1$	$= \frac{1}{[t(1-t)]^{2H-1}} \exp(\varepsilon\,[\mathcal{F}^{\max}(t) - 4]) + O(\varepsilon^2)$ with $\mathcal{F}^{\max}(t)$ given in Eq. (4.47)
positive time t_+	$\mathcal{P}(t) = 1$	$= \frac{1}{[t(1-t)]^{2H-1}} \exp(\varepsilon\,[\mathcal{F}^{\text{pos}}(t) - 4]) + O(\varepsilon^2)$ with $\mathcal{F}^{\text{pos}}(t)$ given in Eq. (4.40)
$\upsilon = \frac{m}{\sqrt{2}[t_{\max}(1-t_{\max})]^H}$ at given $t_{\max}$	$\mathcal{P}(\upsilon\|t) = \sqrt{\frac{2}{\pi}} \upsilon^2 e^{-\frac{\upsilon^2}{2}}$	$= \sqrt{\frac{2}{\pi}} \upsilon^{\frac{2}{H}-2} e^{-\frac{\upsilon^2}{2} + \varepsilon[\mathcal{F}(\upsilon,t) - \mathcal{F}^{\max}(t) + \text{cst}]} + O(\varepsilon^2)$ with $\mathcal{F}(\upsilon, t)$ given in Eq. (4.72)

Table 7.2: Summary of distributions for fractional Brownian motion with an end-point constrained to the origin (i.e. bridge process, $X_{t=0} = X_{t=1} = 0$).

For future research, it would be interesting to extend these results to second-order in ε, notably to prove analytically the difference between the distributions of $t_{\max}$ and t_+ in the case of a free end-point. As mentioned in chapter 5, the links between these distributions and the Pickands constant should be investigated in more details, which could give an non-perturbative check for some of these results.

The pertubative methods developed in this thesis should also allow to obtain distribution for other observables (records statistics, ...) or for other process (fBm with linear drift or other constraints). It could also be interesting to study the effect of non-Gaussian perturbations, on top of the non-Markovian one treated here, to obtain results for a larger class of stochastic processes.

Bibliography

[1] B. Derrida, "Random-energy model: An exactly solvable model of disordered systems," Phys. Rev. B **24**, 2613 (1981). URL http://dx.doi.org/10.1103/physrevb.24.2613. 1.1

[2] W. Feller, *Introduction to Probability Theory and Its Applications* (John Wiley & Sons, 1950). 1.2, 1

[3] N. G. Van Kampen, *Stochastic processes in physics and chemistry* (North-Holland, 2007). 1.2, 1.2.2

[4] A. Einstein, "Über die von der molekularkinetischen Theorie der Wärme geforderte Bewegung von in ruhenden Flüssigkeiten suspendierten Teilchen," Annalen der Physik **322**, 549–560 (1905). 1.2.1

[5] H. S. Wio, R. R. Deza, and J. M. López, *An Introduction to Stochastic Processes and Nonequilibrium Statistical Physics*, Series on adv. in stat. mech. (World Scientific, 2012). 1.2.2

[6] G. Uhlenbeck and L. Ornstein, "On the Theory of the Brownian Motion," Phys. Rev. **36**, 823–841 (1930). URL http://journals.aps.org/pr/pdf/10.1103/PhysRev.36.823. 1.2.2, 1.2.5, 1.3.2

[7] I. Eliazar and J. Klafter, "Markov-breaking and the emergence of long memory in Ornstein–Uhlenbeck systems," J. Phys. A: Mathematical and Theoretical **41**(12), 122,001 (2008). URL http://stacks.iop.org/1751-8121/41/i=12/a=122001. 1.2.2

[8] R. García-García, A. Rosso, and G. Schehr, "Longest excursion of fractional Brownian motion: Numerical evidence of non-Markovian effects," Phys. Rev. E **81**(1), 010,102 (2010). URL http://journals.aps.org/pre/pdf/10.1103/PhysRevE.81.010102. 1.2.2

[9] I. Eliazar and M. F. Shlesinger, "Langevin unification of fractional motions," J. Phys. A: Mathematical and Theoretical **45**(16), 162,002 (2012). URL http://stacks.iop.org/1751-8121/45/i=16/a=162002. 1.2.2

[10] P. Lévy, "Sur certains processus stochastiques homogènes," Compositio Mathematica **7**, 283–339 (1940). URL http://eudml.org/doc/88744. 1.2.3, 1.3.4, 4.3.2

[11] Y. Nikitin and E. Orsingher, "The intermediate arc-sine law," Stat. & Proba. Letters **49**(2), 119 – 125 (2000). URL http://www.sciencedirect.com/science/article/pii/S0167715200000389. 1.2.3, 1.3.4, 4.3.2

[12] S. N. Majumdar, A. Rosso, and A. Zoia, "Time at which the maximum of a random acceleration process is reached," J. Phys. A **43**, 115,001 (2010). URL http://iopscience.iop.org/article/10.1088/1751-8113/43/11/115001/pdf. 1.2.3, 1.2.5

[13] H. J. O. Boutcheng, T. B. Bouetou, T. W. Burkhardt, A. Rosso, A. Zoia, and K. T. Crepin, "Occupation time statistics of the random acceleration model," J. Stat. Mech.: Theory and Experiment **2016**(5), 053,213 (2016). URL http://stacks.iop.org/1742-5468/2016/i=5/a=053213. 1.2.3

[14] J.-P. Bouchaud and A. Georges, "Anomalous diffusion in disordered media: statistical mechanisms, models and physical applications," Phys. Rep. **195**, 127–293 (1990). URL http://www.sciencedirect.com/science/article/pii/037015739090099N. 1.2.4

[15] J. Chuang, Y. Kantor, and M. Kardar, "Anomalous dynamics of translocation," Phys. Rev. E **65**, 011,802 (2001). URL http://link.aps.org/doi/10.1103/PhysRevE.65.011802. 1.2.4

[16] I. M. Sokolov and J. Klafter, "From diffusion to anomalous diffusion: A century after Einstein's Brownian motion," Chaos: An Interdisciplinary Journal of Nonlinear Science **15**(2) (2005). URL http://arxiv.org/pdf/cond-mat/0411032.pdf. 1.2.4

[17] A. Amitai, Y. Kantor, and M. Kardar, "First-passage distributions in a collective model of anomalous diffusion with tunable exponent," Phys. Rev. E **81**, 011,107 (2010). URL http://journals.aps.org/pre/pdf/10.1103/PhysRevE.81.011107. 1.2.4, 1.3.2

[18] S. N. Majumdar, A. Rosso, and A. Zoia, "Hitting Probability for Anomalous Diffusion Processes," Phys. Rev. Lett. **104**, 020,602 (2010). URL http://link.aps.org/doi/10.1103/PhysRevLett.104.020602. 1.2.4, 2.3.3

[19] Y. G. Sinai, "Self-Similar Probability Distributions," Theory Probab. Appl. **21**(1), 63–80 (1976). URL http://epubs.siam.org/doi/abs/10.1137/1121005. 1.2.4

[20] J. Krug, "Origins of scale invariance in growth processes," Advances in Physics **46**, 139–282 (1997). 1.2.4

[21] B. B. Mandelbrot, "How Long Is the Coast of Britain? Statistical Self-Similarity and Fractional Dimension," Science **156**, 636–638 (1967). URL http://science.sciencemag.org/content/156/3775/636. 1.2.4

[22] B. B. Mandelbrot, *The fractal geometry of nature* (1983). 1.2.4

[23] E. Gumbel, *Statistics of Extremes* (Dover, 1958). 1.2.5

[24] J.-P. Bouchaud and M. Mézard, "Universality classes for extreme-value statistics," J. Phys. A **30**, 7997–8015 (1997). URL http://iopscience.iop.org/0305-4470/30/23/004. 1.2.5

[25] P. Le Doussal and K. J. Wiese, "Driven particle in a random landscape: Disorder correlator, avalanche distribution, and extreme value statistics of records," Phys. Rev. E **79**, 051,105 (2009). URL http://link.aps.org/doi/10.1103/PhysRevE.79.051105. 1.2.5

[26] G. Schehr and P. L. Doussal, "Extreme value statistics from the real space renormalization group: Brownian motion, Bessel processes and continuous time random walks," J. Stat. Mech. **2010**(01), P01,009 (2010). URL http://stacks.iop.org/1742-5468/2010/i=01/a=P01009. 1.2.5

[27] B. Derrida and H. Spohn, "Polymers on disordered trees, spin glasses, and traveling waves," J. Stat. Phys. **51**(5), 817–840 (1988). URL http://dx.doi.org/10.1007/BF01014886. 1.2.5

[28] S. N. Majumdar and P. L. Krapivsky, "Extremal paths on a random Cayley tree," Phys. Rev. E **62**, 7735–7742 (2000). URL http://link.aps.org/doi/10.1103/PhysRevE.62.7735. 1.2.5

[29] D. S. Dean and S. N. Majumdar, "Extreme-value statistics of hierarchically correlated variables deviation from Gumbel statistics and anomalous persistence," Phys. Rev. E **64**, 046,121 (2001). URL http://link.aps.org/doi/10.1103/PhysRevE.64.046121. 1.2.5

[30] C. A. Tracy and H. Widom, "Level-spacing distributions and the Airy kernel," Communications in Mathematical Physics **159**, 151–174 (1994). hep-th/9211141, URL http://dx.doi.org/10.1007/BF02100489. 1.2.5

[31] S. N. Majumdar and G. Schehr, "Top eigenvalue of a random matrix: large deviations and third order phase transition," J. Stat. Mech. **2014**(1), P01,012 (2014). URL http://iopscience.iop.org/article/10.1088/1742-5468/2014/01/P01012/pdf. 1.2.5

[32] C. Texier, "Individual energy level distributions for one-dimensional diagonal and off-diagonal disorder," J. Phys. A **33**(35), 6095 (2000). URL http://stacks.iop.org/0305-4470/33/i=35/a=303. 1.2.5

[33] C. Texier and C. Hagendorf, "The effect of boundaries on the spectrum of a one-dimensional random mass Dirac Hamiltonian," J. Phys. A **43**(2), 025,002 (2010). URL http://stacks.iop.org/1751-8121/43/i=2/a=025002. 1.2.5

[34] S. N. Majumdar, "Persistence in nonequilibrium systems," Curr. Sci. **77**, 370 (1999). URL http://arxiv.org/abs/cond-mat/9907407. 1.2.5, 1.2.5

[35] A. J. Bray, S. N. Majumdar, and G. Schehr, "Persistence and first-passage properties in nonequilibrium systems," Advances in Physics **62**(3), 225–361 (2013). URL http://dx.doi.org/10.1080/00018732.2013.803819. 1.2.5

[36] F. Aurzada and T. Simon, "Persistence probabilities & exponents," ArXiv: **1203.6554** (2012). URL http://arxiv.org/abs/1203.6554. 1.2.5

[37] B. Derrida, V. Hakim, and R. Zeitak, "Persistent Spins in the Linear Diffusion Approximation of Phase Ordering and Zeros of Stationary Gaussian Processes," Phys. Rev. Lett. **77**, 2871–2874 (1996). URL http://link.aps.org/doi/10.1103/PhysRevLett.77.2871. 1.2.5

[38] B. Derrida, V. Hakim, and V. Pasquier, "Exact First-Passage Exponents of 1D Domain Growth: Relation to a Reaction-Diffusion Model," Phys. Rev. Lett. **75**, 751–754 (1995). URL http://link.aps.org/doi/10.1103/PhysRevLett.75.751. 1.2.5

[39] M. Ding and W. Yang, "Distribution of the first return time in fractional Brownian motion and its application to the study of on-off intermittency," Phys. Rev. E **52**, 207–213 (1995). URL http://link.aps.org/doi/10.1103/PhysRevE.52.207. 1.2.5

[40] J. Krug, H. Kallabis, S. N. Majumdar, S. J. Cornell, A. J. Bray, and C. Sire, "Persistence exponents for fluctuating interfaces," Phys. Rev. E **56**, 2702–2712 (1997). URL http://journals.aps.org/pre/pdf/10.1103/PhysRevE.56.2702. 1.2.5, 1.3.1, 1.3.2

[41] J. Bertoin, "The inviscid Burgers equation with Brownian initial velocity," Commun. Math. Phys. **193**, 397–406 (1998). URL link.springer.com/content/pdf/10.1007/s002200050334.pdf. 1.2.5, 1.4.1

[42] C. Sire, S. N. Majumdar, and A. Rüdinger, "Analytical results for random walk persistence," Phys. Rev. E **61**, 1258–1269 (2000). URL http://link.aps.org/doi/10.1103/PhysRevE.61.1258. 1.2.5, 2.2.1

[43] C. Sire, "Probability Distribution of the Maximum of a Smooth Temporal Signal," Phys. Rev. Lett. **98**, 020,601 (2007). URL http://link.aps.org/doi/10.1103/PhysRevLett.98.020601. 1.2.5, 1.3.5

[44] C. Sire, "Crossing intervals of non-Markovian Gaussian processes," Phys. Rev. E **78**, 011,121 (2008). URL http://link.aps.org/doi/10.1103/PhysRevE.78.011121. 1.2.5, 1.3.5

[45] G. Molchan, "Survival exponents for some Gaussian processes," ArXiv: **1203.2446** (2012). URL http://arxiv.org/pdf/1203.2446v1.pdf. 1.2.5

[46] J. Krug, "Records in a changing world," J. Stat. Mech.: Theory and Experiment **2007**(07), P07,001 (2007). URL http://stacks.iop.org/1742-5468/2007/i=07/a=P07001. 1.2.5

[47] S. N. Majumdar and R. M. Ziff, "Universal Record Statistics of Random Walks and Lévy Flights," Phys. Rev. Lett. **101**(5), 050,601 (2008). URL http://journals.aps.org/prl/pdf/10.1103/PhysRevLett.101.050601. 1.2.5

[48] J. Franke, G. Wergen, and J. Krug, "Correlations of Record Events as a Test for Heavy-Tailed Distributions," Phys. Rev. Lett. **108**(6), 064,101 (2012). URL http://journals.aps.org/prl/pdf/10.1103/PhysRevLett.108.064101. 1.2.5

[49] G. Wergen, D. Volovik, S. Redner, and J. Krug, "Rounding Effects in Record Statistics," Phys. Rev. Lett. **109**(16), 164,102 (2012). 1206.4432, URL http://journals.aps.org/prl/pdf/10.1103/PhysRevLett.109.164102. 1.2.5

[50] G. Wergen, A. Hense, and J. Krug, "Record occurrence and record values in daily and monthly temperatures," Climate Dynamics **42**, 1275–1289 (2014). URL http://link.springer.com/content/pdf/10.1007/s00382-013-1693-0.pdf. 1.2.5

[51] A. Dieker, "Simulation of fractional Brownian motion," Ph.D. thesis, University of Twente (2004). 1.2, 1.3.3, 1.3, 2.4

[52] B. Mandelbrot and J. Van Ness, "Fractional Brownian Motions, Fractional Noises and Applications," SIAM Review **10**(4), 422–437 (1968). URL http://dx.doi.org/10.1137/1010093. 1.3.1, 1.3.2

[53] B. Duplantier, R. Rhodes, S. Sheffield, and V. Vargas, "Log-correlated Gaussian fields: an overview," ArXiv e-prints (2014). 1407.5605. 1.3.1

[54] Y. V. Fyodorov and P. Le Doussal, "Moments of the Position of the Maximum for GUE Characteristic Polynomials and for Log-Correlated Gaussian Processes," Journal of Statistical Physics **164**(1), 190–240 (2016). URL http://dx.doi.org/10.1007/s10955-016-1536-6. 1.3.1

[55] Y. Sinai, "Distribution of the maximum of a fractional Brownian motion," Russian Mathematical Surveys **52**(2), 359 (1997). URL http://stacks.iop.org/0036-0279/52/i=2/a=R12. 1.3.1

[56] G. Molchan, "Maximum of a Fractional Brownian Motion: Probabilities of Small Values," Communications in Mathematical Physics **205**(1), 97–111 (1999). URL `http://dx.doi.org/10.1007/s002200050669`. 1.3.1, 2.3.1, 2.3.1

[57] I. Nourdin, *Selected Aspects of Fractional Brownian Motion* (Bocconi & Springer Series, 2012). 1.3.1, 2.3.4

[58] J. Krug, "Persistence of non-Markovian Processes Related to Fractional Brownian Motion," Markov Processes And Related Fields **4**(4), 509–516 (1998). URL `http://math-mprf.org/journal/articles/id825/`. 1.3.1

[59] F. Aurzada, "On the one-sided exit problem for fractional Brownian motion," Electron. Commun. Probab. **16**, no. 36, 392–404 (2011). URL `http://ecp.ejpecp.org/article/view/1640`. 1.3.1, 2.3.1

[60] F. Aurzada and C. Baumgarten, "Persistence of fractional Brownian motion with moving boundaries and applications," J. Phys. A Math. G. **46**(12), 125,007 (2013). URL `http://iopscience.iop.org/article/10.1088/1751-8113/46/12/125007/pdf`. 1.3.1

[61] A. N. Kolmogorov, "Wienersche Spiralen und einige andere interessante Kurven im. Hilbertschen Raum," Acad. Sci. URSS **26**(2), 115–118 (1940). 1.3.2

[62] H. E. Hurst, "Long term storage capacity in reservoirs," Trans. Amer. Soc. civil Eng. **116**, 770–799 (1951). 1.3.2

[63] P. L. Krapivsky, K. Mallick, and T. Sadhu, "Large Deviations in Single-File Diffusion," Phys. Rev. Lett. **113**, 078,101 (2014). URL `http://link.aps.org/doi/10.1103/PhysRevLett.113.07810`. 1.3.2

[64] P. L. Krapivsky, K. Mallick, and T. Sadhu, "Tagged Particle in Single-File Diffusion," J. Stat. Phys. **160**(4), 885–925 (2015). URL `http://dx.doi.org/10.1007/s10955-015-1291-0`. 1.3.2

[65] P. L. Krapivsky, K. Mallick, and T. Sadhu, "Dynamical properties of single-file diffusion," arXiv:**1505.01287** (2015). URL `http://arxiv.org/abs/1505.01287`. 1.3.2

[66] V. Kukla, J. Kornatowski, D. Demuth, I. Girnus, H. Pfeifer, L. Rees, S. Schunk, K. Unger, and J. Karger, "NMR studies of single-file diffusion in unidimensional channel zeolites," Science **272**, 702–704 (1996). URL `http://science.sciencemag.org/content/272/5262/702`. 1.3.2

[67] Q.-H. Wei, C. Bechinger, and P. Leiderer, "Single-File Diffusion of Colloids in One-Dimensional Channels," Science **287**, 625–627 (2000). URL `http://science.sciencemag.org/content/287/5453/625`. 1.3.2

[68] D. Panja, "Probabilistic phase space trajectory description for anomalous polymer dynamics," Journal of Physics: Condensed Matter **23**(10), 105,103 (2011). URL `http://stacks.iop.org/0953-8984/23/i=10/a=105103`. 1.3.2

[69] J.-C. Walter, A. Ferrantini, E. Carlon, and C. Vanderzande, "Fractional Brownian motion and the critical dynamics of zipping polymers," Phys. Rev. E **85**, 031,120 (2012). URL `http://journals.aps.org/pre/pdf/10.1103/PhysRevE.85.031120`. 1.3.2

[70] S. Gupta, A. Rosso, and C. Texier, "Dynamics of a Tagged Monomer: Effects of Elastic Pinning and Harmonic Absorption," Phys. Rev. Lett. **111**, 210,601 (2013). URL http://link.aps.org/doi/10.1103/PhysRevLett.111.210601. 1.3.2, 1.3.2

[71] A. Zoia, A. Rosso, and S. N. Majumdar, "Asymptotic Behavior of Self-Affine Processes in Semi-Infinite Domains," Phys. Rev. Lett. **102**(12), 120602 (2009). URL http://link.aps.org/abstract/PRL/v102/e120602. 1.3.2

[72] J. Dubbeldam, V. Rostiashvili, A. Milchev, and T. Vilgis, "Fractional Brownian motion approach to polymer translocation: The governing equation of motion," Phys. Rev. E **83**, 011,802 (2011). URL http://link.aps.org/doi/10.1103/PhysRevE.83.011802. 1.3.2

[73] V. Palyulin, T. Ala-Nissila, and R. Metzler, "Polymer translocation: the first two decades and the recent diversification," Soft Matter **10**, 9016–9037 (2014). URL http://dx.doi.org/10.1039/C4SM01819B. 1.3.2

[74] N. J. Cutland, P. E. Kopp, and W. Willinger, "Stock Price Returns and the Joseph Effect: A Fractional Version of the Black-Scholes Model," in *Seminar on Stochastic Analysis, Random Fields and Applications*, E. Bolthausen, M. Dozzi, and F. Russo, eds., vol. 36 of *Progress in Probability*, pp. 327–351 (Birkhäuser Basel, 1995). URL http://dx.doi.org/10.1007/978-3-0348-7026-9_23. 1.3.2

[75] L. C. G. Rogers, "Arbitrage with fractional Brownian motion," Mathematical Finance **7**(1), 95–105 (1997). 1.3.2

[76] S. Rostek and R. Schöbel, "A note on the use of fractional Brownian motion for financial modeling," Economic Modelling **30**, 30 – 35 (2013). URL http://www.sciencedirect.com/science/article/pii/S0264999312002787. 1.3.2

[77] N. Savy, "Mouvement Brownien fractionnaire, applications aux télécomunication," Ph.D. thesis, Université de Rennes 1 (2003). 1.3.2

[78] A. L. Sellerio, D. Mari, and G. Gremaud, "Fractional Brownian motion and anomalous diffusion in vibrated granular materials," J. of Stat. Mech. **2012**(01), P01,002 (2012). URL http://stacks.iop.org/1742-5468/2012/i=01/a=P01002. 1.3.2

[79] B. B. Mandelbrot and J. R. Wallis, "Noah, Joseph, and Operational Hydrology," Water Resources Research **4**(5), 909–918 (1968). URL http://dx.doi.org/10.1029/WR004i005p00909. 1.3.2

[80] F. Molz, H. Liu, and J. Szulga, "Fractional Brownian motion and fractional Gaussian noise in subsurface hydrology: A review, presentation of fundamental properties, and extensions," Water Resources Research **33**(10), 2273–2286 (1997). 1.3.2

[81] A. B. Dieker and M. Mandjes, "On spectral simulation of fractional Brownian motion," Proba. in the Engineering and Informational Sciences **17**, 417–434 (2003). URL http://journals.cambridge.org/article_S0269964803173081. 1.3.3

[82] L. B. G. Andersen and V. I. Piterbarg, *Interest Rate Modeling. Volume 1: Foundations and Vanilla Models* (Atlantic Financial Press, 2010). 1.3.4

[83] A. W. Van der Vaart, *Asymptotic Statistics*, Cambridge Series in Statistical and Probabilistic Mathematics (Cambridge University Press, 1998). 1.3.4

[84] V. I. Piterbarg, *Asymptotic Methods in the Theory of Gaussian Processes and Fields*, Memoirs of the AMS (American Mathematical Society, 1996). 1.3.5, 1.3.5, 1.3.5, 5.4

[85] J. Pickands, "Maxima of stationary Gaussian processes," Zeitschrift für Wahrscheinlichkeitstheorie und Verwandte Gebiete **7**(3), 190–223 (1967). URL `http://link.springer.com/article/10.1007/BF00532637`. 1.3.5

[86] C. Borell, "The Brunn-Minkowski inequality in Gauss space," Invent. Math. **30**, 207–216 (1976). URL `http://link.springer.com/content/pdf/10.1007/bf01425510.pdf`. 1.3.5, 2.3.4

[87] J. Rambeau, S. Bustingorry, A. Kolton, and G. Schehr, "Maximum relative height of elastic interfaces in random media," Phys. Rev. E **84**, 041,131 (2011). URL `http://link.aps.org/doi/10.1103/PhysRevE.84.041131`. 1.3.5

[88] V. I. Piterbarg, "Discrete and Continuous Time Extremes of Gaussian Processes," Extremes **7**(2), 161–177 (2004). URL `http://dx.doi.org/10.1007/s10687-005-6198-8`. 1.3.5

[89] Z. Michna, "Remarks on Pickands theorem," ArXiv: **0904.3832** (2009). URL `http://arxiv.org/abs/0904.3832`. 1.3.5

[90] K. Dębicki, E. Hashorva, L. Ji, and K. Tabiś, "Extremes of vector-valued Gaussian processes: exact asymptotics," ArXiv: **1505.06461** (2015). URL `http://arxiv.org/abs/1505.06461`. 1.3.5

[91] K. Dębicki, S. Engelke, and E. Hashorva, "Generalized Pickands constants and stationary max-stable processes," ArXiv: **1602.01613** (2016). URL `http://arxiv.org/abs/1602.01613`. 1.3.5

[92] A. J. Harper, "Pickands' constant H_α does not equal $1/\Gamma(1/\alpha)$, for small α," ArXiv: **1404.5505** (2014). URL `http://arxiv.org/abs/1404.5505`. 1.3.5

[93] K. Burnecki and Z. Michna, "Simulation of Pickands constants," Proba. and Math. Stat. **22**(1) (2002). 1.3.5

[94] A. Dieker and B. Yakir, "On asymptotic constants in the theory of extremes for Gaussian processes," Bernoulli **20**, 1600–1619 (2014). `arXiv:1206.5840v3`, URL `http://www.columbia.edu/~ad3217/publications/BEJ534.pdf`. 1.3.5, 5.3.2, 5.1, 5.2

[95] A. Dobrinevski, "Field theory of disordered systems – Avalanches of an elastic interface in a random medium," Ph.D. thesis, Université Pierre et Marie Curie (2013). URL `http://arxiv.org/pdf/1312.7156v1.pdf`. 1.4.1, 1.4.4, 6.2.2

[96] H. Barkhausen, "Zwei mit Hilfe der neuen Verstärker entdeckte Erscheinungen," Phys. Ztschr. **20**, 401–403 (1919). 1.4.2

[97] S. Zapperi, P. Cizeau, G. Durin, and H. Stanley, "Dynamics of a ferromagnetic domain wall: Avalanches, depinning transition, and the Barkhausen effect," Phys. Rev. B **58**, 6353–6366 (1998). URL `http://prola.aps.org/abstract/PRB/v58/i10/p6353_1`. 1.4.2, 1.4.4

[98] G. Durin and S. Zapperi, "Scaling Exponents for Barkhausen Avalanches in Polycrystalline and Amorphous Ferromagnets," Phys. Rev. Lett. **84**(20), 4705–4708 (2000). URL `http://dx.doi.org/10.1103/PhysRevLett.84.4705`. 1.4.2

[99] G. Bertotti, *Hysteresis in magnetism: for physicists, materials scientists, and engineers* (Academic Press, 1998). 1.4.2

[100] P. L. Doussal, K. J. Wiese, S. Moulinet, and E. Rolley, "Height fluctuations of a contact line: A direct measurement of the renormalized disorder correlator," EPL **87**, 56,001 (2009). URL http://www.phys.ens.fr/~wiese/pdf/contact4Delta.pdf. 1.4.2

[101] D. Bonamy, S. Santucci, and L. Ponson, "Crackling Dynamics in Material Failure as the Signature of a Self-Organized Dynamic Phase Transition," Phys. Rev. Lett. **101**(4), 045,501 (2008). URL http://link.aps.org/abstract/PRL/v101/e045501. 1.4.2, 6.3.3

[102] J. Antonaglia, W. Wright, X. Gu, R. Byer, T. Hufnagel, M. LeBlanc, J. Uhl, and K. Dahmen, "Bulk Metallic Glasses Deform via Slip Avalanches," Phys. Rev. Lett. **112**, 155,501 (2014). URL http://link.aps.org/doi/10.1103/PhysRevLett.112.155501. 1.4.2

[103] D. S. Fisher, "Collective transport in random media: From superconductors to earthquakes," Phys. Rep. **301**, 113–150 (1998). URL http://dx.doi.org/10.1016/S0370-1573(98)00008-8. 1.4.2

[104] S. Papanikolaou, F. Bohn, R. Sommer, G. Durin, S. Zapperi, and J. Sethna, "Universality beyond power laws and the average avalanche shape," Nature Physics **7**, 316–320 (2011). URL http://dx.doi.org/10.1038/nphys1884. 1.4.2

[105] K. Dahmen and J. Sethna, "Hysteresis, avalanches, and disorder-induced critical scaling: A renormalization-group approach," Phys. Rev. B **53**, 14,872–14,905 (1996). URL http://prb.aps.org/pdf/PRB/v53/i22/p14872_1. 1.4.2

[106] T. Nattermann, S. Stepanow, L.-H. Tang, and H. Leschhorn, "Dynamics of interface depinning in a disordered medium," J. Phys. II (France) **2**, 1483–8 (1992). URL http://jp2.journaldephysique.org/articles/jp2/pdf/1992/08/jp2v2p1483.pdf. 1.4.3

[107] O. Narayan and D. S. Fisher, "Threshold critical dynamics of driven interfaces in random media," Phys. Rev. B **48**, 7030–42 (1993). URL http://journals.aps.org/prb/pdf/10.1103/PhysRevB.48.7030. 1.4.3, 6.3.4

[108] K. J. Wiese and P. Le Doussal, "Functional Renormalization for Disordered Systems, Basic Recipes and Gourmet Dishes," Markov Processes Relat. Fields **13** (2006). URL http://arxiv.org/abs/cond-mat/0611346v1. 1.4.3, 1.4.3

[109] P. Chauve, P. L. Doussal, and K. J. Wiese, "Renormalization of pinned elastic systems: How does it work beyond one loop?" Phys. Rev. Lett. **86**, 1785–1788 (2001). 1.4.3

[110] P. Le Doussal and K. J. Wiese, "Size distributions of shocks and static avalanches from the Functional Renormalization Group," Phys. Rev. E **79**, 051,106 (2009). URL http://www.phys.ens.fr/~wiese/pdf/shockArXive.pdf. 1.4.3, 6.7, 6.B, 6.B

[111] P. Le Doussal, "Exact results and open questions in first principle functional RG," Annals of Physics **325**, 49–150 (2009). 1.4.3

[112] P. Le Doussal and K. J. Wiese, "First-principle derivation of static avalanche-size distribution," Phys. Rev. E **85**, 061,102 (2011). URL http://journals.aps.org/pre/pdf/10.1103/PhysRevE.85.061102. 1.4.3, 1.4.4, 6.3.1, 6.6, 6.6

[113] T. Thiery, P. Le Doussal, and K. J. Wiese, "Universal correlations between shocks in the ground state of elastic interfaces in disordered media," ArXiv: **1604.05556** (2016). URL http://arxiv.org/pdf/1604.05556v1.pdf. 1.4.3

[114] T. Thiery and P. Le Doussal, "Universality in the mean spatial shape of avalanches," ArXiv: **1601.00174** (2016). URL http://arxiv.org/pdf/1601.00174.pdf. 1.4.3

[115] P. Le Doussal and K. J. Wiese, "Distribution of velocities in an avalanche," EPL **97**, 46,004 (2012). URL http://dx.doi.org/10.1209/0295-5075/97/46004. 1.4.4, 1.4.4, 6.3.1, 2, 6.7

[116] A. Dobrinevski, P. Le Doussal, and K. Wiese, "Non-Stationary Dynamics Of The Alessandro-Beatrice-Bertotti-Montorsi Model," Phys. Rev. E **85**, 031,105 (2012). URL http://dx.doi.org/10.1103/PhysRevE.85.031105. 1.4.4, 1.4.4, 6.2.1, 6.2.2, 6.2.3, 6.2.3, 6.3.1, 2, 6.6, 6.7, 6.H

[117] P. Le Doussal and K. J. Wiese, "Avalanche dynamics of elastic interfaces," Phys. Rev. E **88**, 022,106 (2013). URL http://link.aps.org/doi/10.1103/PhysRevE.88.022106. 1.4.4, 1.4.4, 6.2.1, 6.2.2, 6.2.3, 6.3.1, 6.3.2, 6.4.1, 2, 6.7, 6.B, 6.J

[118] B. Alessandro, C. Beatrice, G. Bertotti, and A. Montorsi, "Domain-wall dynamics and Barkhausen effect in metallic ferromagnetic materials. I. Theory," J. Appl. Phys. **68**, 2901 (1990). 1.4.4

[119] B. Alessandro, C. Beatrice, G. Bertotti, and A. Montorsi, "Domain-wall dynamics and Barkhausen effect in metallic ferromagnetic materials. II. Experiments," J. Appl. Phys. **68**(6), 2908 (1990). URL http://dx.doi.org/10.1063/1.346424. 1.4.4

[120] F. Colaiori, "Exactly solvable model of avalanches dynamics for Barkhausen crackling noise," Advances in Physics **57**, 287 (2008). URL http://www.tandfonline.com/doi/pdf/10.1080/00018730802420614. 1.4.4

[121] A. Middleton, "Asymptotic Uniqueness Of The Sliding State For Charge-Density Waves," Phys. Rev. Lett. **68**, 670–673 (1992). URL http://journals.aps.org/prl/pdf/10.1103/PhysRevLett.68.670. 1.4.4, 6.2.1

[122] T. Thiery, P. L. Doussal, and K. J. Wiese, "Spatial shape of avalanches in the Brownian force model," J. Stat. Mech. **2015**, P08,019 (2015). URL http://iopscience.iop.org/article/10.1088/1742-5468/2015/08/P08019/pdf. 1.4.4, 6.3.1

[123] M. Delorme and K. Wiese, "The maximum of a fractional Brownian Motion: Analytic Results from Perturbation Theory," Phys. Rev. Lett. **115**, 210,601 (2015). URL http://journals.aps.org/prl/abstract/10.1103/PhysRevLett.115.210601. 2.1, 5.3.1

[124] M. Delorme and K. J. Wiese, "Perturbative expansion for the maximum of fractional Brownian motion," Phys. Rev. E **94**, 012,134 (2016). URL http://link.aps.org/doi/10.1103/PhysRevE.94.012134. 2.1, 3.1

[125] K. J. Wiese, S. N. Majumdar, and A. Rosso, "Perturbation Theory for Fractional Brownian Motion in Presence of Absorbing Boundaries," Phys. Rev. E **83**, 061,141 (2011). URL http://journals.aps.org/pre/pdf/10.1103/PhysRevE.83.061141. 2.1, 2.2.1, 2.2.1, 2.2.1, 2.2.3, 2.3.6, 2.A, 2.B, 2.B, 2.B, 3.A, 3.A, 4.4.2, 5.3.1, 5.B

[126] S. N. Majumdar and C. Sire, "Survival Probability of a Gaussian Non-Markovian Process: Application to the $T = 0$ Dynamics of the Ising Model," Phys. Rev. Lett. **77**, 1420–1423 (1996). URL http://link.aps.org/doi/10.1103/PhysRevLett.77.1420. 2.2.1

[127] K. Oerding, S. Cornell, and A. Bray, "Non-Markovian persistence and nonequilibrium critical dynamics," Phys. Rev. E **56**, R25–R28 (1997). URL http://link.aps.org/doi/10.1103/PhysRevE.56.R25. 2.2.1

[128] J.-F. Coeurjolly, "Simulation and identification of the fractional Brownian motion: a bibliographical and comparative study," Journal of Statistical Software **05**(i07), i07 (2000). URL http://EconPapers.repec.org/RePEc:jss:jstsof:05:i07. 2.4

[129] J. Bertrand, "Solution d'un problème," Comptes Rendus de l'Académie des Sciences, Paris **105**, 369 (1887). 1

[130] M. Delorme and K. J. Wiese, "Extreme-Value Statistics of Fractional Brownian Motion Bridges," ArXiv: **1605.04132** (2016). 4.1

[131] T. S. Dario Gasbarra and E. Valkeila, "Gaussian bridges," Abel Symposium (2005). URL http://abelsymposium.no/symp2005/preprints/valkeila.pdf. 4.2

[132] N. H. Abel, "Auflösung einer mechanischen Aufgabe," Journal für Die Reine und Angewandte Mathematik **1**, 153–157 (1826). 4.B

[133] R. Bracewell, *The Fourier Transform and its Applications* (McGraw-Hill, New York, 1965). 4.B

[134] M. Delorme, P. Le Doussal, and K. J. Wiese, "Distribution of joint local and total size and of extension for avalanches in the Brownian force model," Phys. Rev. E **93**, 052,142 (2016). URL http://link.aps.org/doi/10.1103/PhysRevE.93.052142. 6.1

[135] A. Larkin, Sov. Phys. JETP **31**, 784 (1970). 6.6

[136] I. Dornic, H. Chaté, and M. Muñoz, "Integration of Langevin Equations with Multiplicative Noise and the Viability of Field Theories for Absorbing Phase Transitions," Phys. Rev. Lett. **94**, 100,601 (2005). URL http://link.aps.org/doi/10.1103/PhysRevLett.94.100601. 6.H

[137] M. Abramowitz and A. Stegun, *Pocketbook of Mathematical Functions* (Harri-Deutsch-Verlag, 1984). 6.I

[138] P. L. Krapivsky, K. Mallick, and T. Sadhu, "Dynamical properties of single-file diffusion," J. Stat. Mech. **2015**(9), P09,007 (2015). URL http://stacks.iop.org/1742-5468/2015/i=9/a=P09007.

[139] O. Narayan and D. Fisher, "Nonlinear fluid flow in random media: critical phenomena near threshold," Phys. Rev. B **49**, 9469–502 (1993). URL http://journals.aps.org/prb/pdf/10.1103/PhysRevB.49.9469.

[140] Y. V. Fyodorov, P. Le Doussal, and A. Rosso, "Statistical Mechanics of Logarithmic REM: Duality, Freezing and Extreme Value Statistics of $1/f$ Noises generated by Gaussian Free Fields," J Stat. Mech. p. P10005 (2009). URL http://arxiv.org/pdf/0907.2359v2.pdf.

[141] P. L. Doussal and K. J. Wiese, "An exact mapping of the stochastic field theory for Manna sandpiles to interfaces in random media," Phys. Rev. Lett. **114**, 110,601 (2014). URL http://journals.aps.org/prl/pdf/10.1103/PhysRevLett.114.110601.

[142] O. Benichou, P. L. Krapivsky, C. Mejia-Monasterio, and G. Oshanin, "Temporal correlations of the running maximum of a Brownian trajectory," ArXiv: **1602.06770** (2016). URL http://arxiv.org/pdf/1602.06770.pdf.

[143] I. Blake and W. Lindsey, "Level-crossing problems for random processes," IEEE Trans. Inf. Th. **19**(3), 295–315 (1973). URL http://ieeexplore.ieee.org/stamp/stamp.jsp?tp=&arnumber=1055016.

[144] P. W. Anderson, "Absence of Diffusion in Certain Random Lattices," Phys. Rev. **109**, 1492–1505 (1958). URL http://journals.aps.org/pr/abstract/10.1103/PhysRev.109.1492.

[145] E. Ben-Naim, L. Frachebourg, and P. L. Krapivsky, "Coarsening and persistence in the voter model," Phys. Rev. E **53**, 3078–3087 (1996). URL http://link.aps.org/doi/10.1103/PhysRevE.53.3078.

[146] S. Atis, S. Saha, H. Auradou, D. Salin, and L. Talon, "Self-Sustained Reaction Fronts in Porous Media," ArXiv: **1210.3518** (2012).

[147] S. N. Majumdar, C. Sire, A. J. Bray, and S. J. Cornell, "Nontrivial Exponent for Simple Diffusion," Phys. Rev. Lett. **77**, 2867–2870 (1996). URL http://link.aps.org/doi/10.1103/PhysRevLett.77.2867.

[148] S. N. Majumdar, A. J. Bray, S. J. Cornell, and C. Sire, "Global Persistence Exponent for Nonequilibrium Critical Dynamics," Phys. Rev. Lett. **77**, 3704–3707 (1996). URL http://link.aps.org/doi/10.1103/PhysRevLett.77.3704.

[149] S. N. Majumdar, "Universal first-passage properties of discrete-time random walks and Lévy flights on a line: Statistics of the global maximum and records," Physica A Stat. Mech. **389**, 4299–4316 (2010).

[150] B. Yakir, *Extremes in Random Fields: A Theory and its Applications*, Wiley Series in Probability and Statistics, 1st ed. (Wiley, 2013).

[151] P. M. Centres and S. Bustingorry, "Effective Edwards-Wilkinson equation for single-file diffusion," Phys. Rev. E **81**, 061,101 (2010). URL http://link.aps.org/doi/10.1103/PhysRevE.81.061101.

Résumé

Dans cette thèse, on étudie des processus stochastiques issus de la physique statistique. Le mouvement Brownien fractionnaire, objet central des premiers chapitres, généralise le mouvement Brownien aux cas où la mémoire est importante pour la dynamique. Ces effets de mémoire apparaissent par exemple dans les systèmes complexes et la diffusion anormale. L'absence de la propriété de Markov rend difficile l'étude probabiliste du processus. On développe une approche perturbative autour du mouvement Brownien pour obtenir de nouveaux résultats, sur des observables liées aux statistiques des extrêmes. En plus de leurs applications physiques, on explore les liens de ces résultats avec des objets mathématiques, commes les lois de Lévy et la constante de Pickands.

Dans un deuxième temps, le modèle phénoménologique d'interfaces élastiques en milieu désordonné est étudié, dans le cas d'un désordre Brownien. On s'intéresse aux avalanches, c'est-à-dire à la réponse du système à une impulsion, et plusieurs distributions d'observables sont calculées exactement. Ces résultats nouveaux sont obtenus en résolvant une équation d'instanton déterministe mais non-linéaire qui encode les propriétés statistiques du modèle.

Mots Clés

Mouvement Brownien, Mouvement Brownien fractionnaire, Processus Non-Markovien, Invariance d'échelle, Intégrales de chemin, Desordre gelé, Interfaces, Avalanches.

Abstract

In this thesis, we study stochastic processes appearing in different areas of statistical physics: Firstly, fractional Brownian motion is a generalization of the well-known Brownian motion to include memory. Memory effects appear for example in complex systems and anomalous diffusion, and are difficult to treat analytically, due to the absence of the Markov property. We develop a perturbative expansion around standard Brownian motion to obtain new results for this case. We focus on observables related to extreme-value statistics, with links to mathematical objects: Levy's arcsine laws and Pickands' constant.

Secondly, the model of elastic interfaces in disordered media is investigated. We consider the case of a Brownian random disorder force. We study avalanches, i.e. the response of the system to a kick, for which several distributions of observables are calculated analytically. To do so, the initial stochastic equation is solved using a deterministic non-linear instanton equation. Avalanche observables are characterized by power-law distributions at small-scale with universal exponents, for which we give new results.

Keywords

Brownian motion, fractional Brownian motion, Non-Markovian processes, Scale invariance, Path Integrals, Quenched disorder, Interfaces, Avalanches.

Numéro national de thèse:
xxxxx